Effects of Obstacle Separation Distance on Gas Explosions

Abdulmajid Muhammed Na'inna, MSc, B.Eng., AIFireE

Submitted in accordance with the requirements for the degree of
Doctor of Philosophy

The University of Leeds
Energy Research Institute
School of Process, Environmental and Materials Engineering

November, 2013

The candidate confirms that the work submitted is his own, except where work which has formed part of jointly-authored publications has been included. The contribution of the candidate and the other authors to this work has been explicitly indicated below. The candidate confirms that appropriate credit has been given within the thesis where reference has been made to the work of others.

List of Publications and Award

This thesis has led to the publications of papers in a reputable journal and conferences.

Journal publication:

1. NA'INNA A.M., H.N. PHYLAKTOU and G.E. ANDREWS. 2013. The acceleration of flames in tube explosions with two obstacles as a function of obstacle separation distance. *Journal of Loss Prevention in the Process Industries,* **26**(6), pp. 1597-1603.
   (This publication is part of Chapter 5 of this thesis)
   - The experimental work, data collection, results analysis and write-up of this journal was done by the main author.
   - The co-authors also contributed in the interpretation of the results and checking the paper contents.

Conference Publications:

2. NA'INNA A.M., H.N. PHYLAKTOU and G.E. ANDREWS. 2013. The acceleration of flames in tube explosions with two obstacles as a function of obstacle separation distance: The influence of mixture reactivity. In: *Proc. of the Seventh International Seminar on Fire & Explosion Hazards (ISFEH7)*, pp.627–636,Providence,USA.
   http://rpsonline.com.sg/proceedings/9789810759360/html/097.xml
   (This publication is part of Chapter 5 of this thesis)
   - The experimental work, data collection, results analysis and write-up of this paper was done by the main author.
   - The co-authors also contributed in the interpretation of the results and checking the paper contents.
3. NA'INNA A.M., H.N. PHYLAKTOU and G.E. ANDREWS. 2012. The acceleration of flames in tube explosions with two obstacles as a function of obstacle separation distance. In: *IX International Symposium on Hazards, Prevention, and Mitigation of Industrial Explosions*. Krakow, Poland.
   (This publication is part of Chapter 5 of this thesis)

- The experimental work, data collection, results analysis and write-up of this conference paper was done by the main author.
- The co-authors also contributed in the interpretation of the results and checking the paper contents.

Accepted for Publication

4. NA'INNA A.M., G. SOMUANO-BALLESTEROS, H.N. PHYLAKTOU and G.E. ANDREWS. 2014. Flame Acceleration in Tube Explosions with Three Flat-bar Obstacles with Variable Obstacle Separation Distance. To appear in: *X International Symposium on Hazards, Prevention, and Mitigation of Industrial Explosions, ISHPMIE.* Bergen, Norway.
   (This accepted paper is part of Chapter 5 of this thesis)
   - The experimental work was carried out by the first two authors. However, data collection, results analysis and write-up of this paper was done by the main author.
   - The co-authors (Phylaktou and Andrews) also contributed in the interpretation of the results and checking the paper contents.

Submitted for Publication

5. NA'INNA A.M., H.N. PHYLAKTOU and G.E. ANDREWS. 2014. The Influence of Obstacle Blockage Ratio and Separation Distance on Gas Explosions in a Tube. *Journal of Loss Prevention in the Process Industries.*
   (This submitted article is part of Chapter 5 of this thesis)
   - The experimental work, data collection, results analysis and write-up of this journal was done by the main author.
   - The co-authors also contributed in the interpretation of the results and checking the paper contents.
6. NA'INNA A.M., H.N. PHYLAKTOU and G.E. ANDREWS. 2014. Explosion Flame Acceleration over Obstacles: Effect of Separation Distance for a Range of Scales. To appear in: *35th International Symposium on Combustion.* San Francisco, USA.
   (This submitted paper is part of Chapter 5 of this thesis)
   - The experimental work, data collection, results analysis and write-up of this symposium paper was done by the main author.

- The co-authors also contributed in the interpretation of the results and checking the paper contents.

Award

The author won the "Best Paper Award at IX ISHPMIE 2012 in Krakow, Poland" . The paper which formed part of Chapter 5 of this thesis was "felt to be outstanding among all submissions and deserved recognition because of the quality of its scientific content and the clarity of the presentation". For more information, visit: http://www.engineering.leeds.ac.uk/faculty/news/2012/research-student-receives-best-paper-award.shtml

Acknowledgements

The author wishes to express his sincere gratitude to his supervisors, Dr H.N. Phylaktou and Professor G.E. Andrews for their guidance, invaluable advice and encouragement during the course of this research. Also, the technical assistance received from Mr Robert Boreham during the experimental work of this thesis is gratefully acknowledged.

The granting of FLACS (CFD) license by Gexcon Company in Norway to the author is duly acknowledged. Most importantly, the useful discussions with Helene Pedersen are highly appreciated.

In addition, the author is grateful to his fellow research group members in gas and dust explosions; Bala Fakandu, Hamed Sattar, Clara Huescar and David Slater for their kind supports both in the laboratory and in the office.

The financial support by the Nigerian Government provided through Petroleum Technology Development Fund (PTDF) is highly appreciated. Without this support, the present work would not have been possible.

The author is obliged to his wife Maryam for her love, support, patience and encouragement throughout the period of this research work. Also, your forbearance with looking after my children, Muhammad and Ummul-Khair is really remarkable.

Finally, I would like to express my appreciations to my father, mother, brothers, sisters, family members and well-wishers for their prayers and encouragements at all times to see that I achieve my objective (PhD award). My thoughts and prayers are with my late sisters; Ummul-Khair, Sara and Safiya who passed away while I am undergoing this PhD work. May you all rest in peace!

Abstract

The separation distance (pitch) between obstacles is an area that has not received adequate attention by gas explosion researchers despite general recognition of the important role it plays in determining the explosion severity. Either too large or too small a separation distance between the obstacles would lead to lower explosion severity. Therefore obstacles would need to have "optimal" separation distance to produce the worst case explosions overpressures and flame speeds. Most studies to date with multi-obstacles had the obstacles too closely packed resulting in data that most likely do not represent the worst case scenarios.

The major objective of this project was to investigate the influence of spacing between obstacles in gas explosions by systematically varying the distance in order to determine the worst case separation that will produce the maximum explosion severity. A long vented cylindrical vessel 162 mm internal diameter with an overall length to diameter ratio (L/D) of 27 was used in the experimental study. The vessel was closed at the ignition end and its open end connected to a large cylindrical dump-vessel with a volume of 50 m^3. The spacing between the obstacles in the test vessel was systematically varied from 0.25 m to 2.75 m. The influence of obstacle spacing was studied with obstacles of different blockage ratios, shapes, number and scale. Tests were carried out with methane, propane, ethylene and hydrogen mixtures with air.

A correlation was developed and applied in this research to predict the position to maximum intensity of turbulence downstream of an obstacle, x_{max} dimensionalised with obstacle scale, b as a function of obstacle blockage ratio, BR, using steady state experiments from the limited available data in the literature as,

$$(x/b)_{max} = 2.77BR^{-1.55} \text{ for } t/d < 0.6 \text{ (thin/sharp obstacles)}$$

A clearly defined separation distance which gave the most severe explosions in terms of both maximum flame speed and overpressure was found in this research. The profile of effects with separation distance agreed with the cold flow turbulence profile determined in cold flows by other researchers. However, the present results showed that the maximum effect in explosions is experienced further downstream than the position of maximum turbulence determined in the cold flow studies. It is

suggested that this may be due to the convection of the turbulence profile by the propagating flame, after the flame has moved passed the obstacle. The predicted model on position to maximum intensity of turbulence from cold flow data agreed with the worst case obstacle separation distance in the current research if multiplied by a factor of three.

Turbulence parameters were estimated from pressure differential measurements and geometrical obstacle dimensions. This enabled the calculation of the explosions induced gas velocities, r.m.s turbulent velocity, turbulent Reynolds number and Karlovitz number. By expressing these parameters in terms of turbulent combustion regimes, the bulk of the tests in this study was shown to be within the thickened-wrinkled flames regime.

Turbulent burning velocity, S_T models with dependence on obstacle scale, ℓ higher than the ones in the existing gas explosion scaling techniques were obtained as,

$$\frac{S_T}{S_L} = 2.99 R_\ell^{0.36} \qquad \text{for single hole-obstacles}$$

$$\frac{S_T}{S_L} = 7.36 R_\ell^{0.27} \qquad \text{for single flat-bar obstacles}$$

From the newly obtained S_T correlation for single flat-bar obstacles, an overpressure correlation, P for scaling relationship was derived and validated against both small and large scale experimental data and the results were encouraging.

$$P \propto \left[\left(C_T\sqrt{K}\right)^{0.54} \ell^{0.54}\right]\left[E^{2.54} S_L^{2.54} v^{-0.54}\right]$$

In planning the layout of new installations, it is appropriate to identify the relevant worst case obstacle separation in order to avoid it. In assessing the risk to existing installations and taking appropriate mitigation measures it is important to evaluate such risk on the basis of a clear understanding of the effects of separation distance and congestion. The present research would suggest that in many previous studies of repeated obstacles the separation distance investigated might not have included the worst case set up, and therefore existing explosion protection guidelines may not correspond to worst case scenarios.

Table of Contents

List of Tables

List of Figures

Chapter 1
Gas Explosions - Overview

1.1 Introduction and Motivation

In general, a gas explosion (caused by the ignition of flammable gas or vapour mixture with air) is associated with a sudden increase in temperature and pressure capable of causing damage to life and property. Gas explosions can happen within process vessels and equipment, transport systems such as pipelines, in open/unconfined process areas, in residential/commercial buildings and in offshore structures.

Flammable gases may be released as a result of a failure from gasket, pipe or vessel rupture. During and after the release, the flammable gas will mix with air and produce an explosible cloud. In the absence of continuous release and of an ignition source the flammable gas cloud will eventually disperse and dilute to below its flammable range. In the presence of an ignition source and depending on its relative position to the release and its timing the release may be ignited instantly after a short or long delay. In case of an immediate ignition a jet fire will occur. If ignition is delayed and the gas forms a flammable cloud then an explosion will occur. A more dangerous situation will occur if large quantity of combustible premixed fuel-air cloud is formed and ignites. The duration from release start to ignition and the amount of fuel released ranges from a few seconds to several minutes and a few kilograms to a number of tons respectively (Bjerketvedt *et al.* 1997).

The severity of explosions is mostly expressed in terms of the overpressure generated because it determines the level of damage. Other effects of gas explosions include shrapnel, temperature and radiation. The level of damage in gas explosions in terms of overpressure was given by Clancey (1975) and this is reproduced in Table 1.1. As shown, small overpressures could lead to a significant damage with an overpressure of 0.1 bar capable of causing serious structural damage.

The generated overpressure in gas explosions is dependent upon number of factors which make it a difficult task to estimate the consequences of gas explosions. These factors are:

- Fuel type,
- Stoichiometry of fuel,
- Obstacles,

- Ignition source type and location,
- Confinement and venting (location and size of vents),
- Initial turbulence level in the plant and
- Scale of event/equipment.

Table 1.1 Damage produced by overpressure (Clancey 1975).

Overpressure (bar)	Damage
0.002	Large glass windows under strain smashed.
0.003	Loud sound. Sonic boom glass failure.
0.01	Usual pressure for glass failure.
0.02	Possibility of no severe damage up to 95%.
0.03-0.07	Large and small windows generally shattered.
0.05	Trivial damage to house structures.
0.07	Incomplete destruction of houses, unfit for habitation.
0.09	Slightly distortion of steel frame of clad building.
0.14-0.2	Shattering of non-reinforced concrete or cinder walls.
0.16	Lesser limit of serious structural damage.
0.20	Steel frame building distorted and pulled from foundation.
0.20-0.28	Rupture of oil storage tanks.
0.34	Wooden utility poles shattered.
0.34-0.5	Almost full destruction of houses.
0.5	Loaded train wagons upturned.
0.6	Loaded train boxcars entirely destroyed.
0.7	Possible total damage of buildings.

Many enclosures in onshore and offshore industrial sites in which gas explosions occur are likely to have obstructions in the form of process equipment, pipes, machinery, heat exchanger tubes and alike. These are known to increase the explosion severity. Recently, trees and undergrowth have also been considered by Newton (2008) to enhance flame acceleration. In the present perspective, obstacle

should be considered as any object hindering and disturbing a flow field ahead of the flame front. Such obstacles are the most recognised means of increasing the violence of explosions (Hjertager 1984).

Obstacles tend to wrinkle the propagating flame and make it more turbulent thereby increasing the reaction front area and the burning rate and hence the expansion rate and overpressure.

As will be discussed with more details in the literature review chapter, there are other mechanisms of flame acceleration including self-acceleration, Rayleigh-Taylor instabilities, pressure-wave/flame interactions etc. This work concentrates on the effects of physical obstacles on the explosion severity.

1.2 Historical Losses due to Gas Explosions

The risk of gas explosions has always been associated with the extraction and utilisation of fuels and this has increased substantially with the commencement of industrial scale petroleum and chemical operations.

Up to 1950s, losses from explosions and other hazards such as fires, in the petroleum and chemical industries were insignificant. This was due to the small scale facilities and the small volume of oil, gas and chemicals produced and used. Until 1950, no loss of more than $ 5 million had occurred in the US as a result of fire or explosions incidents. After 1950 the capital intensive offshore oil exploration and production was just commencing. The expenditure in petroleum safety features was usually only the absolute minimum required by the government regulations. The improvement of loss prevention attitudes and practices was not established within the industry until the tragic and financially significant incidents of the 1980s and 1990s (Nolan 2011).

An analysis of industrial accidents with harmful substances from 1974 to 2002 was performed by Carol *et al.* (2002). The analysis was based on a study of 1,694 incidents and the severity of the event was characterised by the number of deaths. The study facilitated the quantification of the possible number of fatalities that will result from an accident relating hazardous substances, as a function of a number of factors including the type of hazard (e.g. explosion, fire or toxic release). Whilst the probability of explosion incidents can be worked out from their data to be 0.15

compared to 0.58 for fires and 0.27 for toxic releases, the authors showed that explosions carried the higher probability of deaths per incident and therefore explosions are the most serious events (in terms of fatalities) followed by fires and toxic substances respectively.

Knowing the history of the previous gas explosion incidents in both onshore and offshore is crucial in targeting appropriate research into this hazard. In this introduction it is worth reviewing some of the most important incidents that have driven industrial and academic researchers into seeking greater understanding and quantification of the parameters influencing the explosion severity and hence improving the design of handling systems and the safety precautions against these incidents.

Table 1.2 shows the summary of some previous gas explosions events.

Table 1.2 An overview of some notable previous gas explosions.

S/N	Location	Date and Time	Background	Explosions consequences
1	Cleveland, Ohio, USA (ERM 2010).	20 October 1944, 2:30 p.m.	Release of about 2000 m^3 of LNG into dams, streets and sewers from the bottom of a cracked tank 4. The vaporised mixture with air was later ignited from the ignition sources nearby.	About 130 people killed, 200 injured. Over 600 people left homeless. Individual and industrial losses were estimated to be $7 to $14 million.
2	Port Hudson, Missouri, USA (Knudsen 2006).	9 December 1970	The event was due to the rupture of a pipeline that conveyed liquefied propane. The fuel was released in large quantity into the open atmosphere to form a flammable cloud and later flowed into a valley. The mixture was ignited 20 minutes after the release thereby leading to a violent unconfined gas explosions.	Severe damage of houses within 3.2 km radius was experienced.
3	Flixborough, Linconshire, UK (HSE 1974).	1 June 1974, 4:33 p.m.	Complete destruction of a major chemical plant through explosion of flammable cyclohexane-air mixtures.	28 fatalities and 36 injuries were recorded during this accident because it was on Sunday. Normally, many people would be on site and would have died.
4	Piper Alpha, North sea, UK (E-Scotland 2013).	6 July 1988	Release of gas as a result of leaking gas valve which was not properly sealed. Also the conversion of the platform from oil to gas contributed to the disaster. The safety measures were for fire and not explosions.	A total number of 167 people had died in the accident making it the world's worst offshore oil disaster. Most of the victims choked in toxic smoke. The accident caused a total insured loss of about £ 1.7 billion.

Table 1.2 Cont'd

S/N	Location	Date and Time	Background	Explosions consequences
5	Ufa, Russia (Makhviladze and Yakush 2002).	4 June 1989	The accident was as a result of the release of liquefied oil products caused by rupture of a large pipeline that connected Siberia to large chemical plants in Russia. The pipeline cracked close to the head of the valley about 900 m from the railway tracks. The flammable mixtures were later ignited by two passenger trains passing each other.	Out of the 1,284 passengers in both trains, 1,224 died or were severely injured. Majority of the injured victims suffered from strong heat radiation.
6	Saint Herblain, France (ARIA 2006).	7 October 1991, 4:20 a.m.	Leak of gasoline fuel from a transfer line into bund led to the formation of a flammable cloud of about 25,000 m^3. Twenty minutes later, the mixture was ignited near the car parking lot.	One person died and two others seriously injured. Structural damage of up to 100 m was observed. In this explosion, faster flame acceleration and hence higher generated overpressures were attained due to the series of repeat of obstacles formed by the trucks positioned diagonally.
7	BP Refinery, Texas City, USA (CSB 2007).	23 March 2005, 1:20 p.m.	The release of the flammable fuel was as a result of overfilling and overheating of a key piece of refining plant. The most possible source of ignition was the fireback from idling pickup truck situated 7.6 m away from plant.	15 people were killed while about 150 sustained injuries. Also, the incident caused a financial loss of over $1.5 billion dollars.

Table 1.2 Cont'd

S/N	Location	Date and Time	Background	Explosions consequences
8	Buncefield, Hertfordshire, UK (Newton 2008).	11 December 2005, 6:01 a.m.	An overfilling of a large petrol storage tank (Tank 912) led to the development of flammable vapour cloud which spread off site and eventually ignited with great severity. Subsequently, the explosion was followed by fire which consumed 23 storage tanks.	Luckily, there was no loss of life; however, 43 people were injured. The overall economic impact of the incident was about £1 billion pounds. Also, nearly 2000 persons were evacuated from their homes.
9	Toronto LPG, Toronto, Canada (Sidhu 2010).	10 August 2008, 3:50 a.m.	The explosion was due to a prohibited tank-to-tank transfer along with a gas hose leak.	Two fatalities were recorded and some people injured. Large pieces of metals from the affected tanks were expelled onto immediate streets. Also, many homes and offices were severely destroyed.
10	Jaipur India (Tony 2011).	29 October 2009, 7:30 p.m.	The event happened as a result of a huge leak of petroleum product from a valve on the delivery line of Indian Oil Corporation, IOC. An ignition source initiated the explosion after about 75 minutes.	12 people were reported dead and over 200 injured. Financial loss of about 280 Indian Crore ($42 million) was realised.

Table 1.2 Cont'd

S/N	Location	Date and Time	Background	Explosions consequences
11	Connecticut, USA (CSB 2010).	7 February 2010, 11:17 a.m.	The incident happened in a power generation room when natural gas was being blown from an open-ended pipe between two big structures. The outer part of the building was congested by the nearby power generation equipment. Several sources of ignition exist both within and outside the building.	Six people were killed and at least 50 injured.
12	Deep Water Horizon, Gulf of Mexico (BP 2010).	10 April 2010	The mishap was as a result of methane gas bubbles which escaped from the well and shot up the drill column, expanding quickly as it burst through several barriers and seals before exploding.	Eleven people died and several others injured. Over $14 billion was spent on response activities. Currently, long-term independent scientific investigation is on-going.
13	Nanjing, China (Xinhua 2010).	28 July 2010, 10:11 a.m.	Leakage of propylene gas and subsequent ignition was the main cause of the event. The leak was as a result of damaging an underground propylene pipeline by the workers during excavation process.	Thirteen people were reported dead while 120 injured.

1.3 Gas Explosion Theory and Current Understanding

1.3.1 Burning Velocities, Flame Speeds and Gas Velocities

There are three basic velocities associated with gas explosions and these are: flame speed, S_f, burning velocity, S_u and induced gas velocity, S_g. The S_f is defined as the rate of flame propagation relative to a fixed reference point. The S_u is defined as the rate of flame propagation with respect to the unburnt gas velocity ahead of it. This can be either laminar, S_L, or turbulent, S_T as the case may be. S_g is the velocity of the unburnt gas ahead of the flame (relative to an external observer).

Assuming a 1-D flame propagation (spherical or planar flame moving for example from the closed ignition end of the tube towards the open end of the tube), the flame speed is greater than the burning velocity, S_u due to the expansion of the burnt gases behind the flame front as shown by the equation,

$$S_f = ES_u \tag{1.1}$$

where E is the expansion factor or volume ratio of the burnt (subscript b) to unburned (subscript u) gases arising mainly from the increase in temperature of the burnt gases as shown by the equation,

$$E = \frac{V_b}{V_u} \tag{1.2}$$

Assuming that the burnt and unburned gases are at equal pressure, from an ideal gas law, the volume ratio, E will be,

$$\frac{V_b}{V_u} = \frac{n_b T_b}{n_u T_u} \tag{1.3}$$

The mole ratio n_b/n_u is the effective ratio of moles of products to moles of reactants which is approximately 1 for most hydrocarbon fuels. The adiabatic flame temperature, T_b is within a range of 2,100 K – 2,400 K for the majority of hydrocarbon flames. The initial gas temperature, T_u is typically around 300 K. Inputting these values in Eq.1.3 the volume ratio or expansion factor, E is of the order of 7-8.

Conversely, the expanding spherical or planar flame pushes unburned gas away from the flame surface at a gas velocity, S_g sometimes known as the explosion induced wind given as,

$$S_g = S_f - S_u \tag{1.4}$$

Combining Eqs. 1.1 and 1.4, gas velocity, S_g can be re-written as,

$$S_g = S_u(E-1) = S_f(1-\frac{1}{E}) = 0.8667 S_f \tag{1.5}$$

1.3.2 Obstacles and Flame Acceleration

Gas explosions can be divided into two types namely: deflagrations and detonations.

In a deflagration, the flame front propagates at subsonic velocity in the unreacted medium. This is associated with flame speed varying from the order of 1 m/s up to 500-1000 m/s resulting to explosion pressures between a few mbar up to 8 bar. This type of combustion is accountable for most of the uncontrolled gas explosion events (Bjerketvedt *et al.* 1997).

In a detonation, by contrast, the flame front propagates at supersonic velocity in the unreacted medium. A detonation velocity of up to 2000 m/s and maximum pressures closed to 20 bar could be achieved for fuel-air mixtures at ambient pressure. A detonation can either be set off directly by detonating a high charge explosive or be formed when a deflagration speeds up in a confined and congested medium and transits to detonation (Bjerketvedt *et al.* 1997).

For a sluggish laminar flame with a velocity in the order of 3 m/s, the flame is not likely to accelerate to velocities of greater than around 20 m/s with an insignificant overpressure if the flammable cloud is truly unconfined and obstacle free i.e. no equipment or other structures are consumed by the cloud. The acceleration of the flame under these circumstances is mainly due to flame instabilities, generated turbulence in the atmosphere by wind and by the flame itself at the ground surface.

In a closed vessel i.e. totally confined situation with no or very little venting, a high flame velocity is not a requirement for generation of pressure. As such, even a slow combustion will generate pressure.

In a partially confined area with obstacles such as piping, process equipment etc. the flame acceleration in gas explosion may rise up to numerous hundred meters per second. The mechanisms producing the improved burning rate in turbulent deflagrations are the wrinkling of the flame front by large eddies and the turbulent transport of heat and mass at the reaction front. This turbulence is predominantly affected by the interaction of the flow with structures, pipe racks etc.

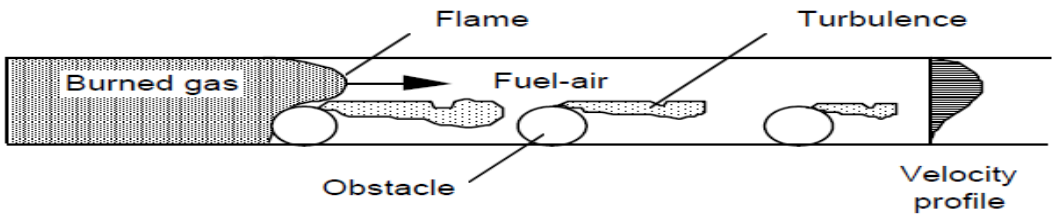

Figure 1.1 Turbulence generation in a channel due to repeated obstacles in gas explosions (Bjerketvedt *et al.* 1997).

Figure 1.1 shows how turbulence is generated in the wake of obstacles in a channel. As the unburnt gas pushed ahead of the moving flame passes an obstacle, turbulence will be created. The flame speed in a turbulent flow is much higher than the laminar flame speed. The turbulence wrinkles the flame, producing a much greater surface area for reaction. Thus, the flame burns faster when it reaches the turbulent region downstream of the obstacles. This faster burning in turns generates faster flow and so a higher level of turbulence downstream of the subsequent set of obstacles. The more the intense is turbulence, the more it results in even faster burning, and so on. This process is known as Shchelkin mechanism (Shchelkin 1940) and this is summarised by the positive feedback loop shown in Fig. 1.2 When a deflagration propagates through a region of obstacles and then terminates in an unobstructed region the flame speed will normally reduce to much lower flame speeds corresponding to those achievable in an open region.

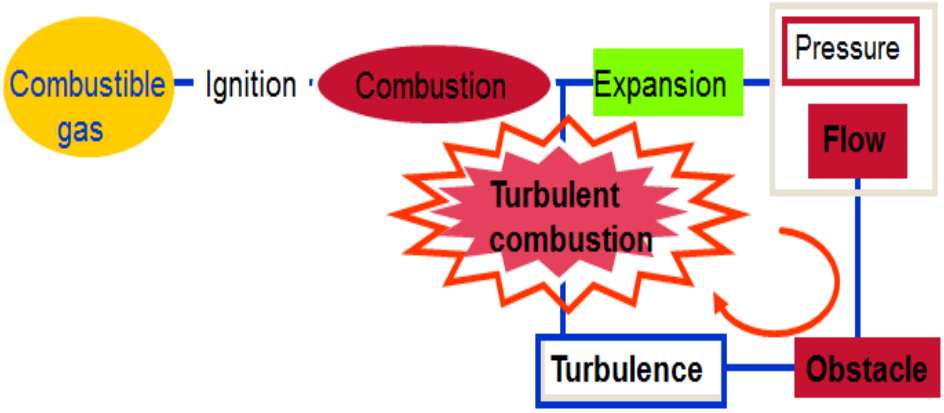

Figure 1.2 Positive feedback system on gas explosions in the presence of obstacles.

1.3.3 Overpressure Generation

For a deflagration there are two mechanisms leading to the pressure build-up in partially confined gas clouds, namely:

- Flame acceleration due to turbulence produced by flow past obstacles i.e. volumetric rate of hot gas generation.
- Venting providing pressure relief or decreasing the effect of the feedback mechanism i.e. volumetric rate of discharge through the vent.

These mechanisms have competing effects. The acceleration of flame due to turbulence will escalate explosion pressure, whereas venting will lessen the pressure. It is the balance between these two that is guiding the pressure build-up.

For an unconfined and congested explosion (vapour cloud explosion), a different mechanism is accountable for pressure generation. The absence of confinement enables free volume expansion as gas is consumed. The flame effectively behaves like a porous piston that generates a pressure wave because of the inertia of the unburnt gas immediately ahead of the flame. The level of the pressure produced is associated with the flow velocity of the unburnt gas and therefore to the speed of flame propagation through the gas cloud (Harris and Wickens 1989). This relationship is shown diagrammatically in Fig.1.3. In this scenario, the overpressure, P is assumed to be proportional to the square of the flame speed, S_f i.e. $P \propto S_f^2$. *This mode of pressure generation is used in the current research as discussed later.*

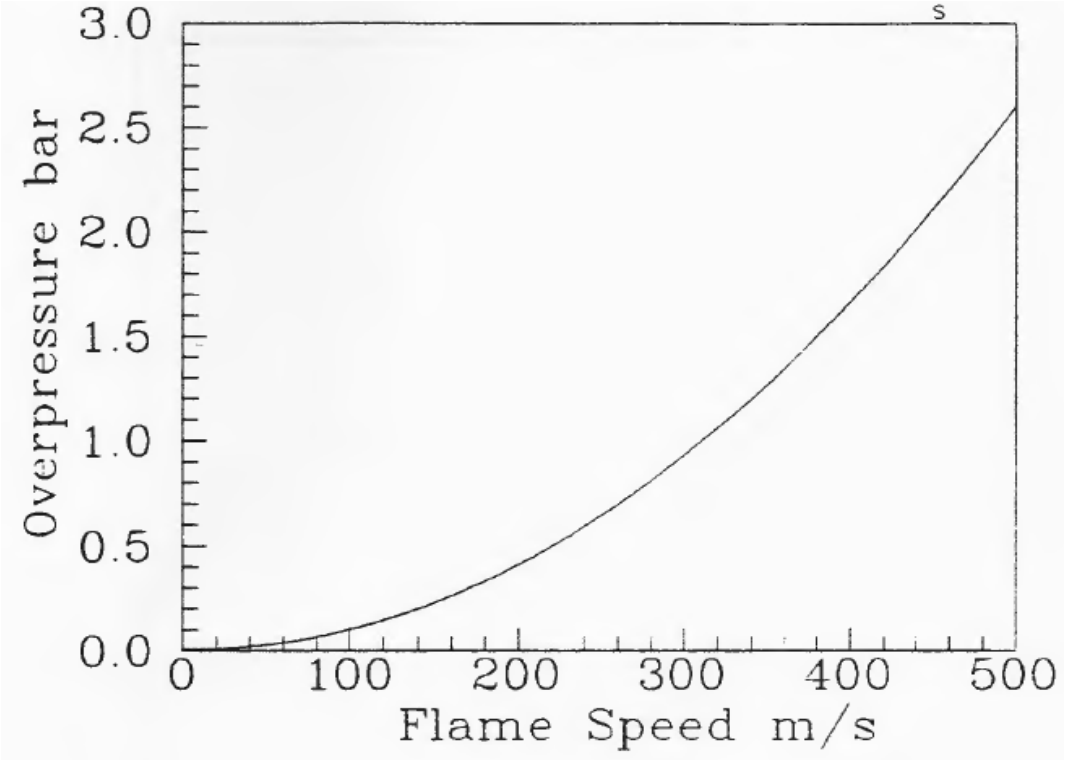

Figure 1.3 Relationship between flame speeds and overpressures (Harris and Wickens 1989).

1.4 Obstacles Parameters Affecting the Explosion Severity

Many research investigations over the last 4 decades which will be reviewed in detail in Chapter 3 have identified a number of important obstacle variables that affect the severity of gas explosions in a congested region (in addition to combustion chemistry). These obstacle properties include:

- Blockage ratio,
- Size,
- Shape,
- Scale,
- Location of obstacles,
- Number of obstacles (for a given blockage ratio) and
- Spacing between the obstacles.

It will be shown in Chapter 3 that although many researchers have investigated the effect of multi-obstacles, the separation distance between obstacles has received little methodical investigation despite the general recognition of the significant role it plays in determining the explosion severity.

1.5 Aim of this Work

This work aims to determine the influence of spacing between obstacles in gas explosions by systematically varying the distance in order to determine the worst case separation that will produce the maximum explosion severity (overpressure).

Chapter 2

Grid Plate Turbulence in Cold Flows

2.1 Introduction to Turbulence

2.1.1 Characteristics of Turbulent Flow

2.1.2 Range of Scales and Turbulent Reynolds Numbers

2.1.3 Energy Production and Dissipation

2.2 Generation of Turbulence

2.2.1 Fluid Flow Theory

2.2.1.1 Jet flow

2.2.1.2 Orifice flow

2.2.2 Turbulent Length Scale

2.2.3 Intensity of Turbulence

2.2.3.1 Maximum Intensity of Turbulence of Grid Plates

2.2.3.2 Distance to Maximum Intensity of Turbulence of Grid Plates

2.2.3.3 Relationship between $(u'/U)_{max}$ and $(x/b)_{max}$

2.2.3.4 Maximum Intensity of Turbulence and its Position for Baffle Obstacles

2.2.3.5 Position of Maximum Intensity of Turbulence of Grid Plates and Free Jet Theory

2.3 Application of Cold Flow Turbulence to Present Research

2.1 Introduction

As outlined in the previous chapter - and as will be elaborated extensively throughout the Thesis - turbulence in the unburnt gas flow ahead of the flame, induced by the interaction of the flow with the solid flow boundaries and obstructions in the path of the flow, plays a major role in the acceleration of the flame and increased severity of the explosion. In its simplest representation we have a reaction front interacting with the cold flow turbulent field generated ahead of the reaction front. Therefore understanding and quantifying the turbulent cold flow characteristics is an essential step in understanding and quantifying the acceleration of the reaction front as it burns through this flow field. In this chapter the important characteristics of the turbulent flow induced by cold flow and obstructions will be reviewed and related to the anticipated effects on a propagating flame.

Fluid flow is characterised by the Reynolds number, Re. Mathematically, Re is expressed as UL/v where U and L are characteristic velocity and length scales of the mean flow respectively and v is the kinematic viscosity of the fluid. For low Re (typically below 2300) the flow is laminar and above 4000 the flow is turbulent. Transitional flow between laminar and turbulent flows occurs at a R_e in between 2300 to 4000 (Cengel and Cimbala 2010).

An example of the velocity of a turbulent flow as function of time, $u(t)$, is shown in Fig. 2.1 being represented by a steady mean flow velocity U and a superimposed velocity fluctuation $u'(t)$. It is thus expressed as,

$$u(t) = U + u'(t) \tag{2.1}$$

The intensity of turbulence is given as the quotient of the root mean square (r.m.s) of $u'(t)$ to the mean velocity of the flow U (Bearman and Morel 1983).

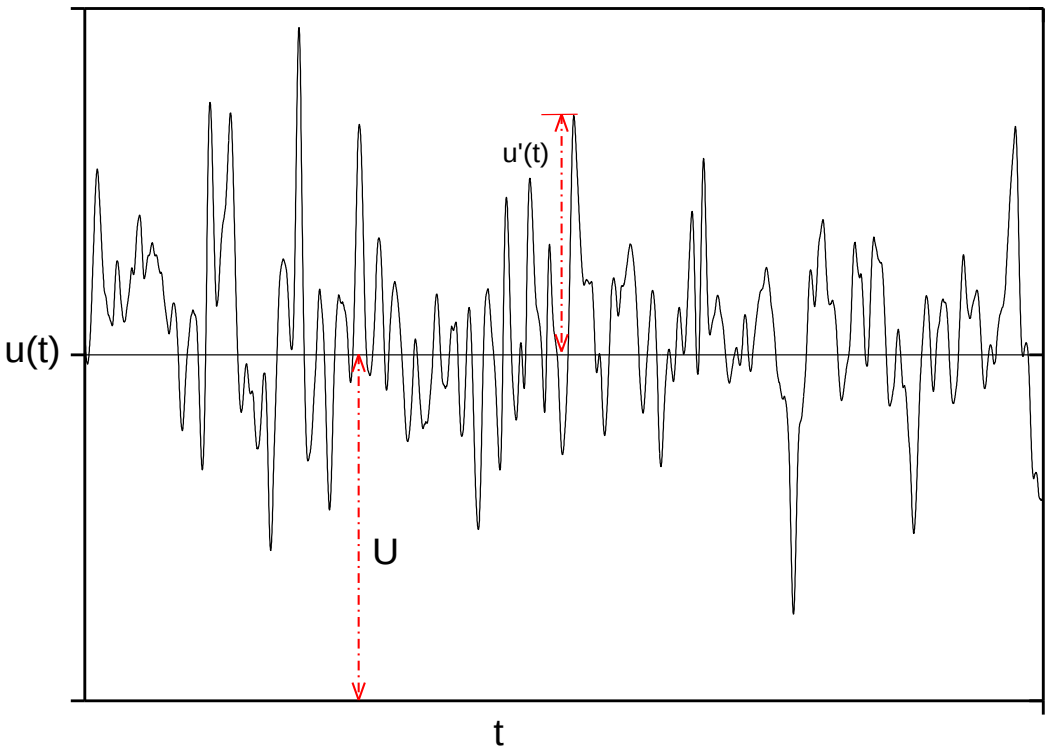

Figure 2.1 Velocity measurement in turbulent flow adapted from Versteeg and Malalasekera (2007).

2.1.1 Characteristics of Turbulent Flows

Turbulence and turbulent flows have the following general characteristics:

- Irregularity or randomness: Turbulent flow is regarded as an irregular condition of flow where several quantities like pressure and velocity components demonstrate a random variation with time and space. Therefore, statistical approach is required to quantitatively express these quantities.
- Diffusivity: As a result of the diffusive behaviour of turbulence, the rates of transfer of mass and momentum are higher than laminar flow thereby augmenting the mixing of chemical and/or physical properties within a flow.
- Large Reynolds number, Re: Turbulent flows are characterised with large Re, a flow with a value of over 4000 is considered to be turbulent.
- 3-D vorticity fluctuations (eddies): Turbulent flow visualisations disclosed the presence of rotational flows structure named turbulent eddies. The turbulent eddies are of various sizes which are in continuous interaction with each other. The largest eddy size is referred to as the integral length scale, ℓ,

the intermediate and smallest sizes of eddies are called Taylor, λ and Kolmogorov, η length scales respectively.

- Dissipation: Kinetic energy of flow is transferred into turbulent motion by the action of viscous forces, the turbulence then dissipates rapidly through a cascade of decreasing size eddies as internal energy of the fluid and lost heat from the system. Due to the dissipative nature of turbulence, constant supply of energy is required in order to sustain the turbulence.

2.1.2 Range of Scales and Turbulent Reynolds Numbers

There are several types of length scale in turbulence flow; however, only three are generally used with each being relevant to a different category of physical problem. These are the integral length scale,ℓ, the Taylor microscale, λ and the Kolmogorov length scale, η.

The integral length scale, ℓ, physically represents the average size of the largest eddies in turbulent flow. These eddies are characterised with the energy production. In practice, ℓ can be measured by integrating the correlation coefficient for the fluctuating velocities obtained as a function of the distance between two points (Turns 1996). The integral length scale is always smaller than L (the characteristic size of the geometry), but is of the same order of magnitude (Turns 1996). The arrangement of the largest eddies is anticipated to be greatly anisotropic owing to the variation of turbulent fluctuations in different directions (Versteeg and Malalasekera 2007). Mathematically, the turbulent producing eddies i.e. integral length scale is expressed in terms of the turbulent kinetic energy, κ, and turbulent dissipation, ε as,

$$\ell = \frac{\kappa^{3/2}}{\varepsilon} \tag{2.2}$$

The Kolmogorov length scale η is the smallest of all types of length scale associated with a turbulent flow. This scale is related to the energy-dissipating eddies where turbulent kinetic energy is converted into heat. The influence of kinematic viscosity is significant on the η. Mathematically, η is defined based on the relationship between the kinematic viscosity, v and the rate of dissipation of turbulent energy, ε as,

$$\eta = \left(\frac{v^3}{\varepsilon}\right)^{1/4} \tag{2.3}$$

The lowest eddies in turbulent flow are considered isotropic (similar turbulent fluctuations in all directions) (Versteeg and Malalasekera 2007).

The Taylor microscale, λ is an intermediate length scale between the integral and Kolmogorov length scales. The λ, is weighted more towards the smaller scales.

Alternative turbulent Reynolds numbers can be used to describe turbulent flow, based on the three length-scales of turbulence given as,

$$R_\ell = \frac{u'\ell}{\nu} \tag{2.4}$$

$$R_\lambda = \frac{u'\lambda}{\nu} \tag{2.5}$$

$$R_\eta = \frac{u'\eta}{\nu} \tag{2.6}$$

According to dimensional analysis given by Nichols (2012), the large scale eddies have time scales of the order of,

$$T = \kappa/\varepsilon \tag{2.7}$$

At the Kolmogorov scale, the dissipative eddies have a time scale specified as,

$$\tau = \left(\frac{\nu}{\varepsilon}\right)^{1/2} \tag{2.8}$$

By substituting Eq. 2.2 into 2.4 the turbulent Reynolds number given by Nichols (2012) is,

$$R_\ell = (k^2/v\varepsilon) \tag{2.9}$$

The ratio of the smallest to largest eddy length scales i.e. Eq. 2.3 to 2.2 is given as,

$$\frac{\eta}{\ell} = R_\ell^{-3/4} \tag{2.10}$$

Also, the ratio of the smallest to largest time scales i.e. Eq. 2.8 to 2.7 is given as,

$$\frac{\tau}{T} = R_{\ell}^{-1/2} \tag{2.11}$$

The implication of Eq. 2.10 is that as the turbulent Reynolds number increases the scale ratio (largest to smallest) also increases (Gardner 1998). From a computational point of view, the length scales of turbulence are greatly smaller than the physical scales such as channel height or wing chord. The quantification of the highest and lowest eddy length and time scales can be utilized in spacing for computational grid and choosing the suitable time step for a specified scenario respectively (Nichols 2012). Therefore, it is simple to realize that a large number of grid points would be needed to simulate accurately a high Reynolds number turbulent flow (Nichols 2012).

2.1.3 Energy Production and Dissipation

Figure 2.2 shows a universal spectrum of turbulent kinetic energy, κ. The profile shows how κ is partitioned among the various size of eddies. The κ, is given as $2\pi/n$, where n is the wavelength of eddies. For a given frequency, f, the n is expressed as $2\pi f/U$ (Versteeg and Malalasekera 2007). The wavenumber increases with decrease in turbulent length scale with most κ situated in the low wavenumbers (large turbulent scales). In the energy production section, the large scale eddies obtain their kinetic energy from the mean flow. The energy production is related to the generation of turbulence induced by the obstacles in the present research. In the inertial range, smaller eddies are reliant upon the larger energy producing eddies. Here, the turbulence is basically in equilibrium and energy transfer by inertial forces is the main process. For the smallest scale (high wavenumbers) of the turbulent spectrum, the eddies turn out to be so small that viscous dissipation changes kinetic energy into heat (Nichols 2012).

As seen in Fig. 2.2, the turbulent length scales are measures normally used to define the numerous portions, or the entire power spectrum of turbulent fluctuations.

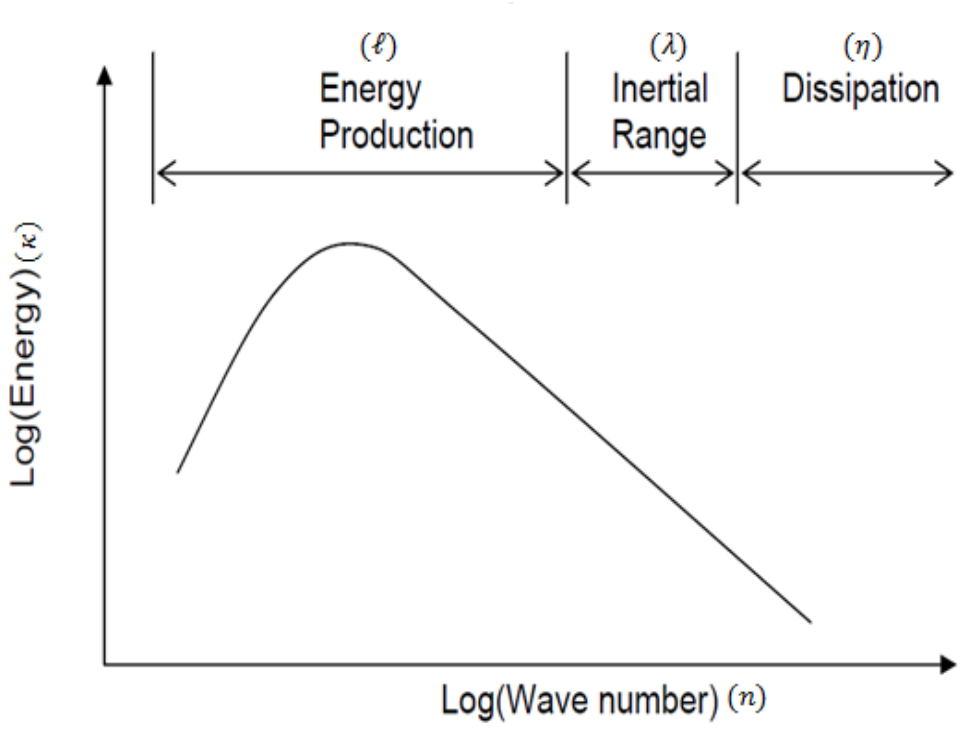

Figure 2.2 Modified turbulent energy spectrum from Nichols (2012).

2.2 Generation of Turbulence

Turbulence can be generated by either frictional forces at the confining solid walls or by the flow of layers of fluids with different velocities over one another. Also, it can be initiated due to the presence of an obstacle such as a grid in the flow path. The generated turbulence leads to continuous velocity fluctuations which result in variations in scalar properties such as density, temperature, and mixture composition.

The interaction of unburnt gas flow induced in an explosion with an obstacle results in the production of turbulence downstream of the obstacle and the acceleration of the flame when it reaches this turbulence. The turbulence level created is dependent upon the flow velocity and the geometry of confining boundaries.

Currently, there are inadequate experimental measurements of these turbulent flows in gas explosions due to transient nature of explosion flows and the connected harsh conditions. Therefore, the bulk of measurements of intensity of turbulence downstream of obstacles have involved steady-state flows in large wind tunnels such as Baines and Peterson (1951) among others. This has been recognised by Phylaktou and Andrews (1994) who presented a method to estimate the maximum intensity of

turbulence behind a grid plate obstacle by an explosion-induced flow in terms of steady-state theory. Also, Cates and Samuels (1991) applied steady state flows to perform a simple assessment methodology for vented explosions.

The turbulence generation is usually expressed in a non-dimensional form as either discharge coefficient, C_d or the pressure loss coefficient, K. The C_d and K parameters were applied by Cates and Samuels (1991) and Phylaktou and Andrews (1994) respectively. However, K is preferable because it governs the turbulence while C_d is associated to the forces induced on the structures by the explosion (Phylaktou and Andrews 1994). Nonetheless, the C_d influence is incorporated into Shell Research Ltd models such as SCOPE (Shell Code for Overpressure Prediction in gas Explosions) (Puttock 1999).

2.2.1 Fluid Flow Theory

In most processes fluids have to be moved from one point to another. So, study of fluid flow is imperative in the present experiments especially with regard to the interaction of the explosion induced flow with grid plate obstacles. It is considered necessary to briefly review the basic features of jet flows and orifice plate flows. It should be borne in mind that the review on such flows relates to steady state; whereas the flow induced in the present experiments are transient in nature. Nevertheless, experimental evidence of the previous researchers like Phylaktou (1993) and Gardner (1998) showed that steady state flow theories can be applied to the current conditions successfully.

2.2.1.1 Jet Flow

Jet flows are categorised as completely separated flows because, after separation from solid surfaces, the solid surfaces no longer play an important role in the jet development. Fluid emerging from a nozzle into a totally unconfined region is the simplest form of a jet as shown in Fig. 2.3. Immediately downstream the nozzle is a region called the potential core characterised with unchanged fluid velocity and concentration of the nozzle. After this region a free boundary layer propagates in which the momentum and mass is transported perpendicular to the direction of flow. The fully established region of the jet is preceded by a transition region. The lengths of the potential core and transition regions are 4 to 5 and 10 nozzle diameters respectively (Beer and Chigier 1983).

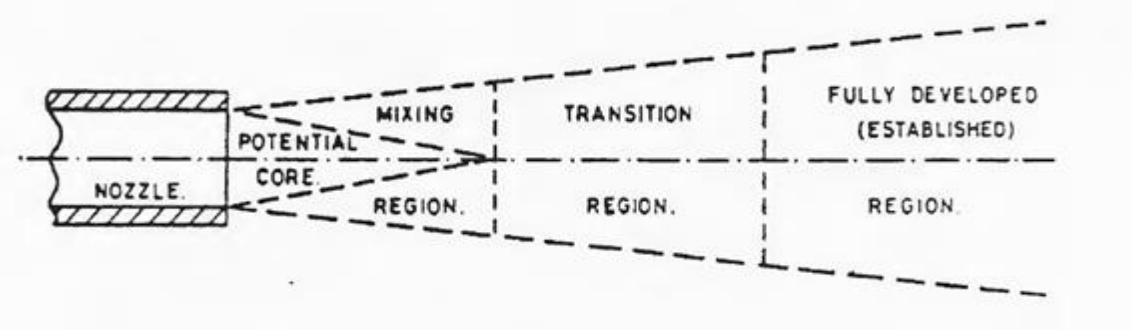

Figure 2.3 Free jet flow regions (Beer and Chigier 1983).

Fluid is entrained from the environments across the boundaries of the jet due to the consequence of momentum exchange between the jet and the surroundings. The fluid entrainment is as a result of friction which depends upon the velocity gradient and exchange coefficient. In case of a jet in an enclosed space, the free supply of ambient fluid for entrainment is seized. If the surrounding fluid is lesser than which the jet can entrain then the fluid entrained in the region close to the nozzle initiates from the edge of the jet farther downstream. Thus, jet starts to entrain its own fluid and a recirculating flow is established. The essentials of recirculating flow are of significant concern to combustion engineers as the size and strength of the recirculation eddy influence the stability of the combustion and the length of the flame.

2.2.1.2 Orifice Flow

Orifice plates in their simplest form are thin flat plates with a single-hole in the middle and this description could be applied to the single-hole obstacles used in the present work. Orifice plates are commonly used as differential-pressure flow-metering devices at high Re in accordance to British Standard, BS 5167-2 (2003). Due to the flow metering applications the induced pressure distribution by orifice plates is well predictable. It is for this reason that in the present experiments it was possible to use differential pressure measurements across the obstacle to quantify the velocity of the explosion induced flow.

For flow metering application, the mass flow rate, $\dot{m}$ through an orifice can be given as,

$$\dot{m} = EA_1\sqrt{2\rho\Delta P_s} \tag{2.12}$$

where ΔP_s is the static pressure difference between two points, E is the velocity approach factor, A_1 is area of the orifice, and ρ is the fluid density .

Pressure loss characteristics in ducts with constrictions have been the subject of many theoretical and experimental studies with a comprehensive review specified by Ward Smith (1971; 1980) especially for single-hole sharp-edged orifices under incompressible, high Re conditions. Smaller numbers of studies on multi-hole grid plates have been conducted and it is largely assumed that they act as single-hole orifices of similar area. Perforated plates are used in a range of industrial application such as flow straighteners, in boundary layer control, in distillation columns, flame stabilisers in combustion systems and turbulence promoters.

As the flow in a pipe with an area, A_2 passes through an orifice plate it separates from upstream face of the orifice to form a discrete jet, which contracts to a minimum cross-sectional area downstream of the orifice. This area is also known as the vena contracta, A_{vc}. Usually, the vena contracta plane arises at an axial distance of half-pipe diameters (0.5D) downstream. The coefficient of the jet contraction, C_c is given as,

$$C_c = \frac{A_{vc}}{A_1} \tag{2.13}$$

Extensive review of flow through an orifice in a pipe detailing pressure drop across an orifice, ΔP_s and total pressure loss, P_T was performed by Phylatou and Andrews (1994).

The P_T is a function of the obstacle geometry and the flow velocity, U, and it is normally expressed in a dimensionless form as the pressure loss coefficient; K. This is defined as,

$$K = \frac{\Delta P_T}{\frac{1}{2}\rho U^2} \tag{2.14}$$

In terms of fractional obstacle blockage ratio (BR = 1- A_1/A_2), K according to Ward Smith (1980) can be expressed as,

$$K = \left(\frac{1}{C_c(1-BR)} - 1\right)^2 \tag{2.15}$$

The value for C_c is 0.61 for sharp edged obstacle of higher blockage ratio, but its real value is dependent on the obstacle blockage and aspect ratio (t/d).

In order to express K independent of C_c and only dependent upon the porosity ratio, p and geometrical characteristics of the obstacle, Ward Smith (1971) correlated an empirical data of C_c and combined with Eq. 2.15 to give a new value of K based on either thin/sharp edged obstacle ($0 < t/d < 0.6$) or thick/round edged obstacle ($t/d > 1$) as Eqs. 2.16 and 2.17 respectively.

$$K = \left[\frac{1}{0.608p(1-p^{2.6})\left[1+\left(\frac{t}{d}\right)^{3.5}\right]+p^{3.6}} - 1\right]^2 \tag{2.16}$$

$$K = \left[\frac{1}{p\left[0.872-0.015\left(\frac{t}{d}\right)-0.08(d/t)\right](1-p^{3.3})+p^{4.3}[1+0.134(t/d)^{0.5}]^{-1}} - 1\right]^2 \tag{2.17}$$

The implication of the above two equations is that flow separation and reattachment occurs at the entry edge of the orifice depending on the orifice geometry. Eq. 2.16 indicates that the jet formed downstream of the orifice plate entry remains separated from the orifice wall and reattaches to the pipe wall. This condition is known as a fully separated flow regime and no pressure is lost in this case. However, Eq. 2.17 implies that the jet formed downstream of the orifice plate entry reattaches to both the orifice and pipe walls. This condition is known as a fully reattached flow regime and this reduced the baffle-pressure characteristics. For data within the range of $0.6 < t/d < 1$, uncertainly arises because the flow may reattach or not (marginally reattached flow) and hence omitted from the correlation (Ward Smith 1971).

2.2.2 Turbulent Length Scale

The integral length-scale ℓ is the scale of concern in the present study. It is this physical dimension that governs the initial scale of turbulence and can itself be associated to the geometrical scale of the turbulence generating obstacles, b. The interaction between a stream of gas and a confining boundary like an obstacle will lead to a rotating, mixing eddies of a mean size equivalent to ℓ.

Based on the calculation of ℓ at the position of maximum intensity of turbulence, Phylaktou (1993) assumed that integral length scale, ℓ at such position be taken as half the size of the characteristics obstacle scale, b. This relationship was found to be promising when tested by the author in his turbulent combustion model.

$$\text{i.e. } \ell = 0.5\text{b} \tag{2.18}$$

Uncertainty on the influence of length scale on turbulent combustion arises mostly due to the absence of no systematic investigation of the parameter. In most studies, the variation of the turbulent length scale has been an unintentional side-effect of altering other variables. For instance Bradley *et al.* (2011) in their turbulent combustion chamber used rotating fans with a fixed width (length scale in this case) and vary only the intensity of the flow by increasing the speed of the fan.

Typically each study of turbulent combustion has been performed in a fixed geometry rig generating a characteristic length scale with small variation (reliant upon the condition). Some variation of scale is attained by comparison of various studies. But considering the various measuring techniques employed by different research groups and the uncertainties related with the measurements of turbulence levels, turbulent and laminar burning velocities, etc., it is obviously very problematic to isolate the influence of length scale. This problem arose due to the fact that most of the studies have been accomplished in similarly small scale rigs where the characteristic length scale hardly go beyond 40 mm and in the majority of cases it was lower than 10 mm (Abdel-Gayed and Bradley 1981). The insufficiency of the scale of these studies is immediately obvious when associated to typical industrial scales with variety from several tens of millimetres to several meters.

2.2.3 Intensity of Turbulence

2.2.3.1 Maximum Intensity of Turbulence of Grid Plates

Since ΔP_T needs to seem as turbulent energy before it dissipates as molecular motion, therefore, ΔP_T can be linked to the isotropic turbulent kinetic energy as in Eq. 2.19 (Swithenbank 1974; Al-Dabbagh and Andrews 1984).

$$\Delta P_T = \frac{3}{2}\rho u'^2 \tag{2.19}$$

Relating Eqs. 2.14 and 2.19 yields an equation for the turbulence intensity specified as,

$$u'/U = C_T\sqrt{K} \tag{2.20}$$

where C_T is a constant with a value of 0.58 in theory, but in practice it is lower than that since not all pressure loss through a constriction is transformed to isotropic, turbulent, kinetic energy. In order to determine the validity of Eq. 2.20 and assess the practical value of the constant, C_T, existing experimental data need to be considered (Phylaktou and Andrews 1994).

The turbulence intensity and its spatial distribution downstream of the obstacle are the responsible factors of the severity of the explosion and speed of flame acceleration. The extent of turbulence created is reliant upon the flow velocity and the geometry of the confinement. There is very limited data on the turbulence generated in transient flows so reliance on data from steady state non-reacting flow studies becomes imperative.

However, most turbulent measurements induced by obstacle (generally grid plates) have been made far behind the obstacle, in the turbulent decay region, where the turbulence is isotropic i.e. 40-50 hole diameters downstream of the grid (Comte-Bellot *et al.* 1966). This is well away from the region of concern in the explosion hazards field since the maximum combustion rate generally takes place within a distance of 3 to 20 obstacle-hole diameters after the obstacle (Phylaktou and Andrews 1991).

Measurements of the turbulence intensity, u'/U, in the region immediately downstream of the grid are scant and only limited data could be found from cold flow wind tunnel/steady state studies from Baines and Peterson (1951); Robinson and Kovitz (1975); Checkel (1981) etc.

An example of these near grid measurements of turbulence is reproduced in Fig. 2.4 from the work of Baines and Peterson (1951). This is a plot of the turbulence intensity (measured on the centre-line of the grid holes) as a function of the axial distance normalised by the characteristic grid-scale b (b is defined as the width of the solid material between the grid holes). It is shown that the turbulence intensity

increases downstream of the grid, it reaches a maximum value (about unity for 75% BR) some distance after it (at five obstacle scales), and it then begins to decay at a more or less steady rate over a relatively long distance.

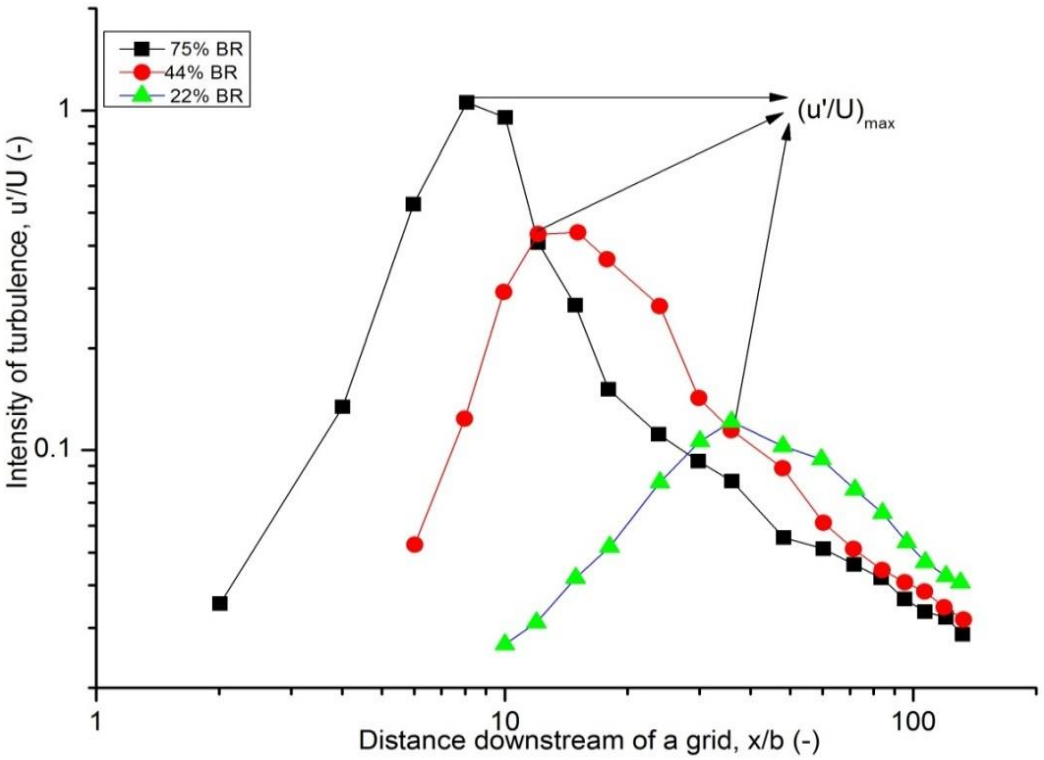

Figure 2.4 Turbulence intensity downstream of grid-plates of various obstacle blockages (Baines and Peterson 1951).

Phylaktou and Andrews (1994) obtained the value of C_T as 0.225 and 0.075 for thin/sharp edged obstacle and thick/round edged obstacles respectively as shown in Fig. 2.5. The authors' correlation was based on maximum intensity of turbulence, u'/U immediately downstream of the grid (to produce maximum severity of explosion) using scanty steady state data from Baines and Peterson (1951); Robinson and Kovitz (1975) and Checkel (1981).

In the present work, additional works on measuring maximum intensity of turbulence behind a grid were sourced despite data insufficiency. These include the work performed by Tan-Atichat *et al*. (1982), Groth and Johansson (1988), DeOtte Jr *et al.* (1991) and Zhou and Lee (2004).

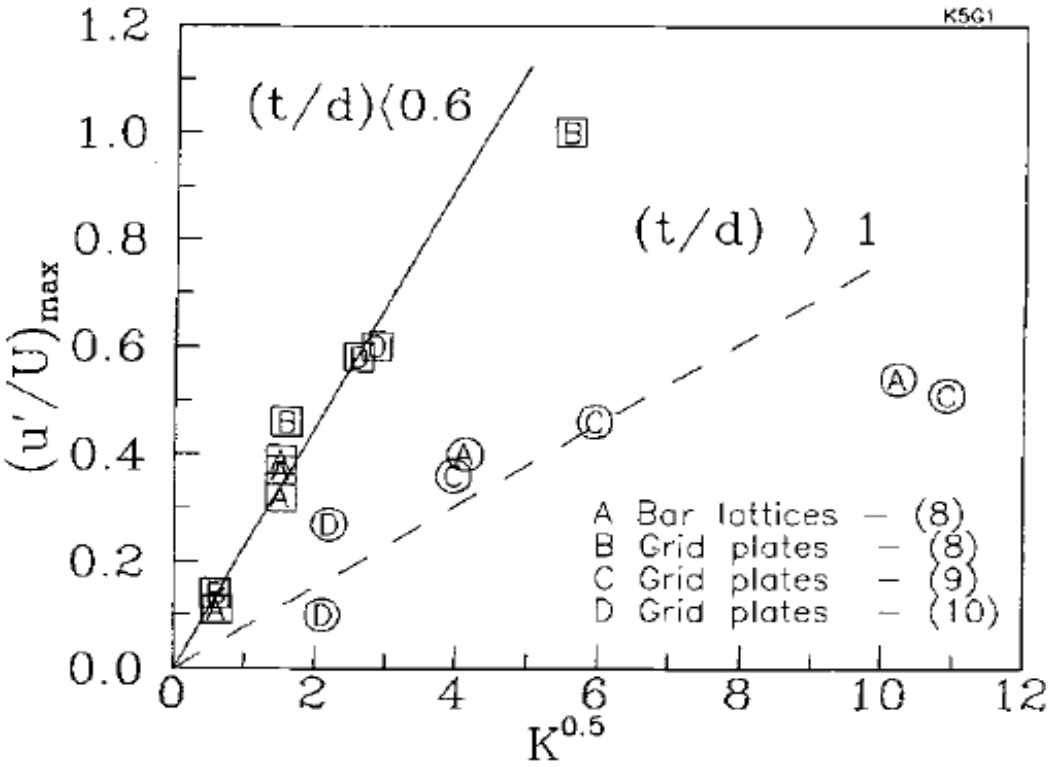

Figure 2.5 Maximum intensity of turbulence against pressure loss coefficient from steady state flow (Phylaktou and Andrews 1994).

Figure 2.6 and 2.7 show a plot of maximum intensity of turbulence against obstacle blockage ratio with the data separated into thin/sharp and thick/round geometries respectively. The acronyms BL, PP and SM stand for bi-plane lattice, perforated plate and square mesh respectively. For each geometry type, a strong dependence of the maximum u'/U on BR is indicated. The equations of the exponential correlations are given below as,

$$t/d < 0.6$$

$$(u'/U)_{max} = 0.042e^{4.23BR} \quad (2.21)$$

$$t/d > 1$$

$$(u'/U)_{max} = 0.018e^{3.90BR} \quad (2.22)$$

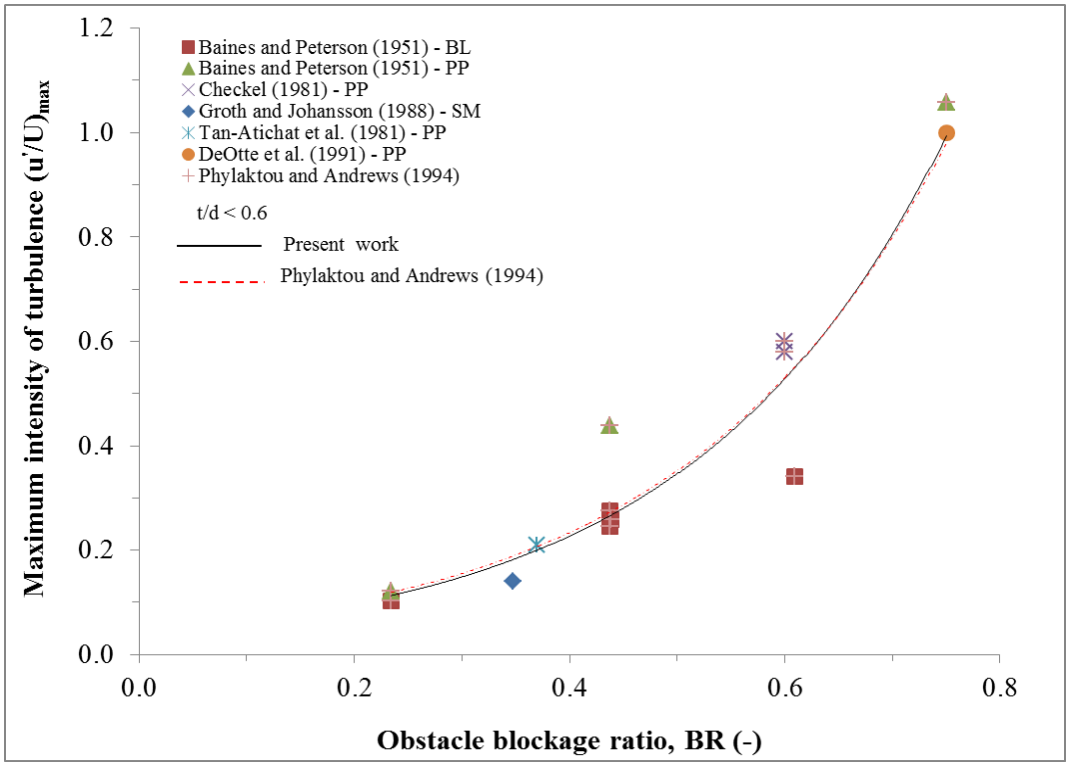

Figure 2.6 Maximum intensity of turbulence against obstacle blockage from cold flow turbulence for t/d < 0.6.

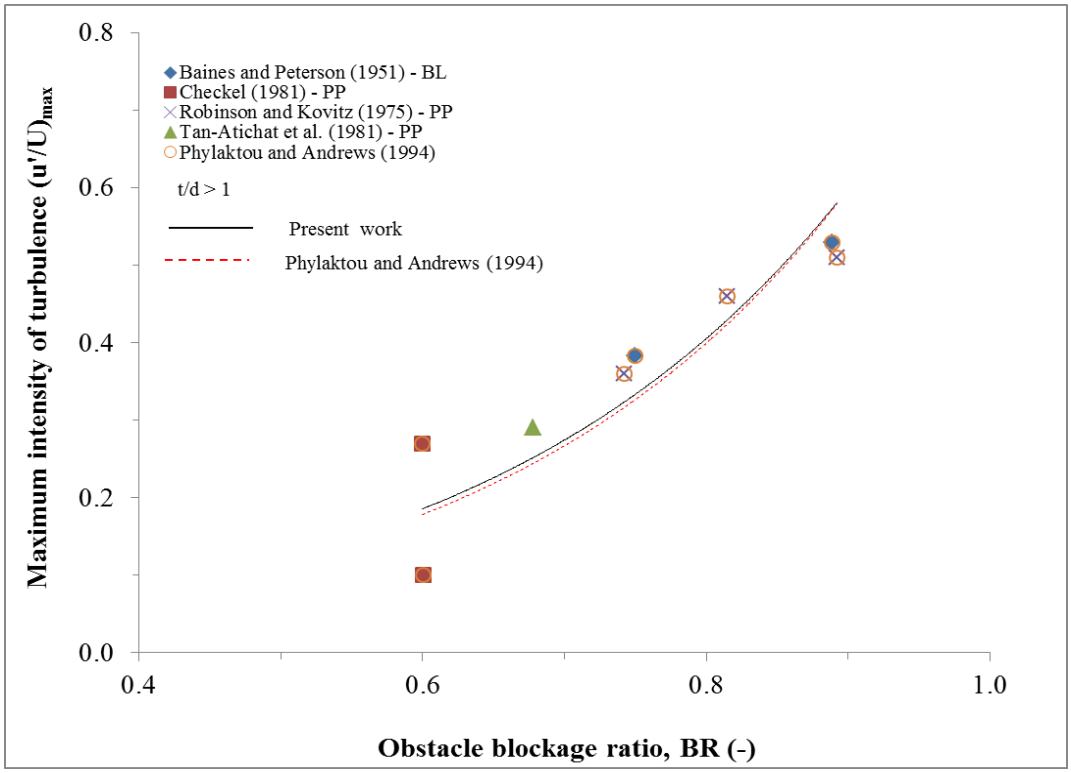

Figure 2.7 Maximum intensity of turbulence against obstacle blockage from cold flow turbulence for t/d > 1.

2.2.3.2 Distance to Maximum Intensity of Turbulence of Grid Plates

From Fig 2.4, it is evident that there is an "optimum" spacing for obstacles where each successive obstacle is placed just after position of peak turbulence so that it "sees" the maximum flame speed. This would in turn be expected to cause the maximum possible turbulence downstream of that obstacle and therefore overall would cause the fastest possible acceleration to the highest possible flame speed and hence highest overpressure. Conversely if the obstacle spacing is larger or smaller than the optimum, then flame acceleration would not be as severe as it should and the limit cases (too near or too far) the effect of repeat obstacles would be minimal.

The position to maximum intensity of turbulence, x_{max} has been correlated using steady state experiments from the few works of Baines and Peterson (1951); Robinson and Kovitz (1975); Checkel (1981); Tan-Atichat *et al*. (1982), Groth and Johansson (1988), DeOtte Jr *et al.* (1991) and Zhou and Lee (2004).

Figure 2.8 shows the relationship between the dimensionless distances to peak intensity, $(x/b)_{max}$ behind the grid against an obstacle blockage with an aspect ratio (t/d) of less than 0.6. The $(x/b)_{max}$ was found to increase with decrease in obstacle blockage. A power fit equation to the data is given as,

$$(x/b)_{max} = 2.77BR^{-1.55} \tag{2.23}$$

The relation between the $(x/b)_{max}$ and obstacle blockage for grid plates with t/d > 1 is presented in Fig. 2.9 with a similar trend found with that of Fig. 2.8. With the exception of data of Robinson and Kovitz (1975); the scanty data were fitted with a power fit equation applicable to an obstacle blockage of 0.6 to 0.9 as,

$$(x/b)_{max} = 3.10BR^{-2.40} \tag{2.24}$$

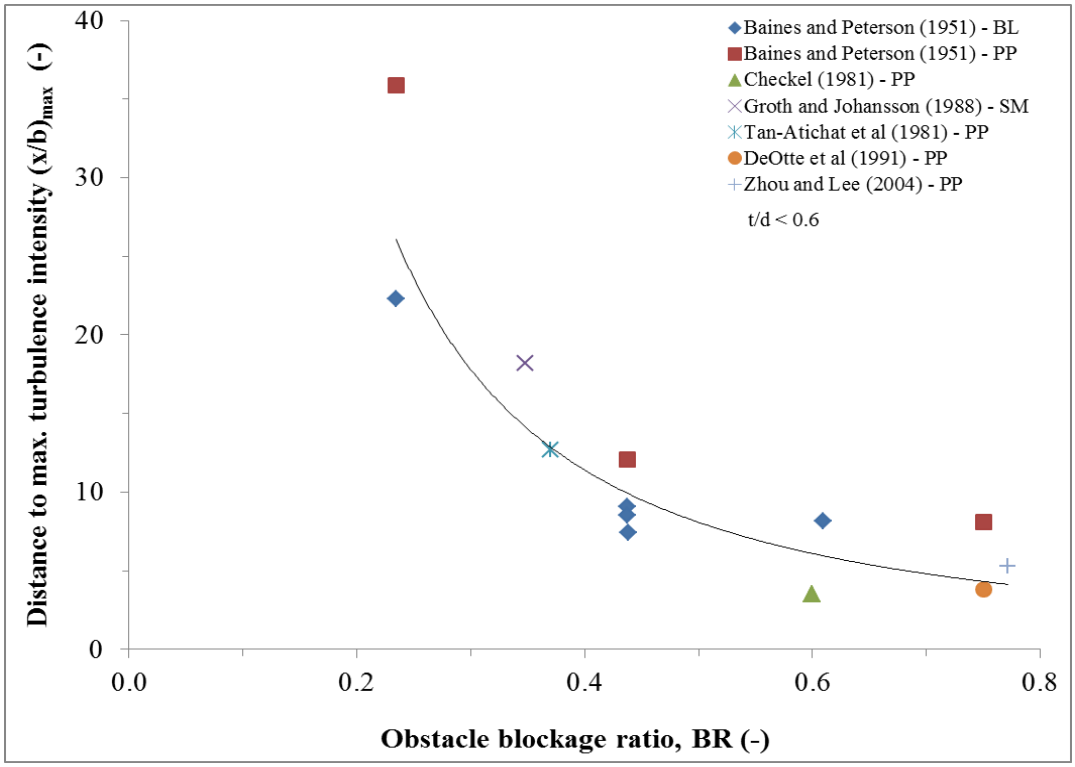

Figure 2.8 Position to $(u'/U)_{max}$ against obstacle blockage for grids of t/d < 0.6.

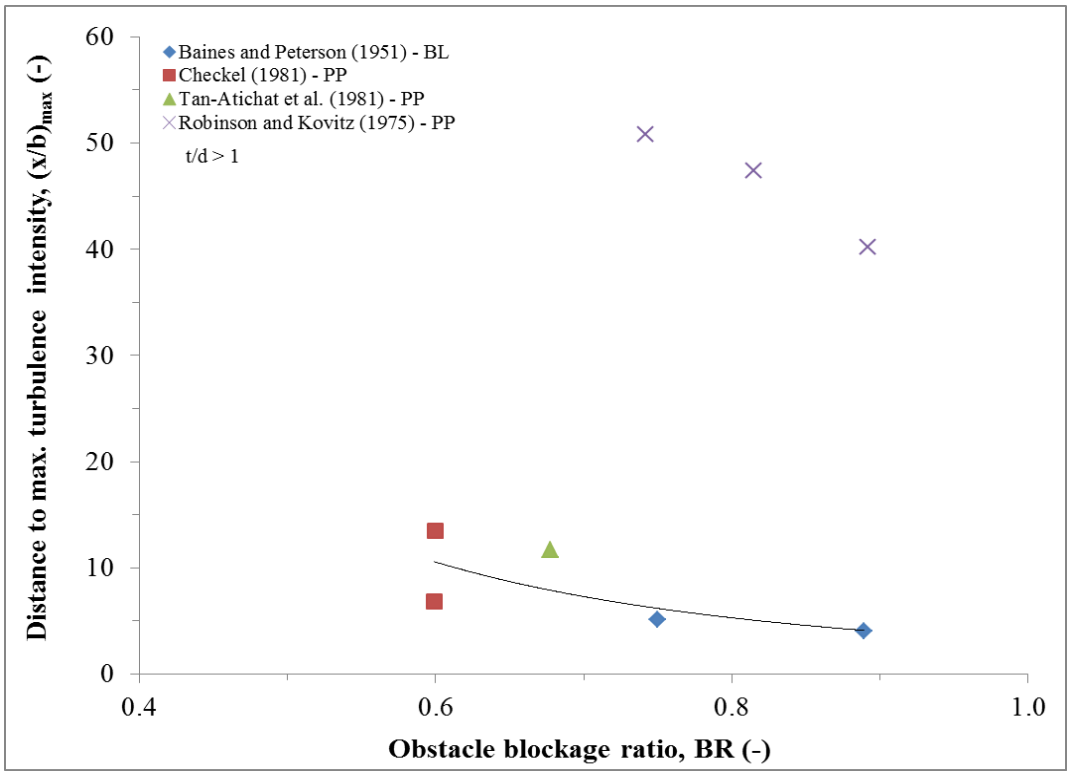

Figure 2.9 Position to $(u'/U)_{max}$ against obstacle blockage for grids of t/d > 1.

2.2.3.3 Relationship between $(u'/U)_{max}$ and $(x/b)_{max}$

The region of major concern in explosion hazards is the region of maximum turbulence that is shown in Fig. 2.4 to occur at some distance behind the grid. In an explosion situation, the highest burning rate (and hence peak rate of generation of overpressure) will transpire at the position of maximum turbulence intensity, and it is therefore this region that should guide the protection and mitigation requirements in a system.

The position to maximum u'/U is of great concern in multi-obstacle explosions. This would determine the spacing between the obstacles in order to determine the utmost severity of explosions. From the existing data of turbulence measurement immediately behind a grid, a correlation between dimensionless distance to maximum intensity and the maximum intensity of turbulence was formed for thin/sharp and thick/round obstacles as shown in Figs 2.10 and 2.11 respectively. The $(u'/U)_{max}$ with dependence on obstacle BR would be obtained from either Eq. 2.21 or 2.22. The equations best fitted for the correlations are given as,

$$(x/b)_{max} = 3.87 \left(\frac{u'}{U}\right)_{max}^{-0.77} \quad \text{for } \frac{t}{d} < 0.6 \tag{2.25}$$

$$(x/b)_{max} = 18.65\, e^{-2.94\left(\frac{u'}{U}\right)_{max}} \quad \text{for } \frac{t}{d} > 1 \tag{2.26}$$

The implication of Eqs. 2.25 and 2.26 is that in real multi-obstacle explosions, both the u'/U_{max} and its corresponding x/b can be predicted and compared with the actual values given in the experiments to ascertain whether maximum severity of explosions is achieved or not.

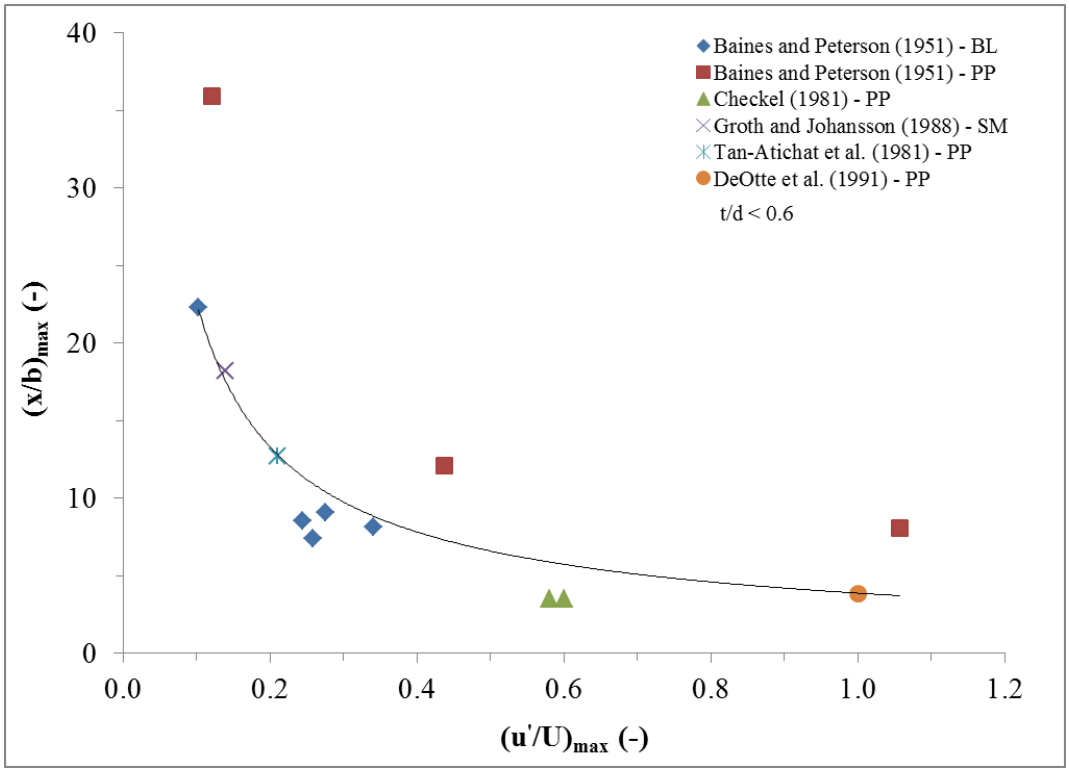

Figure 2.10 Correlation between maximum intensity of turbulence and its distance for grid plates with t/d < 0.6.

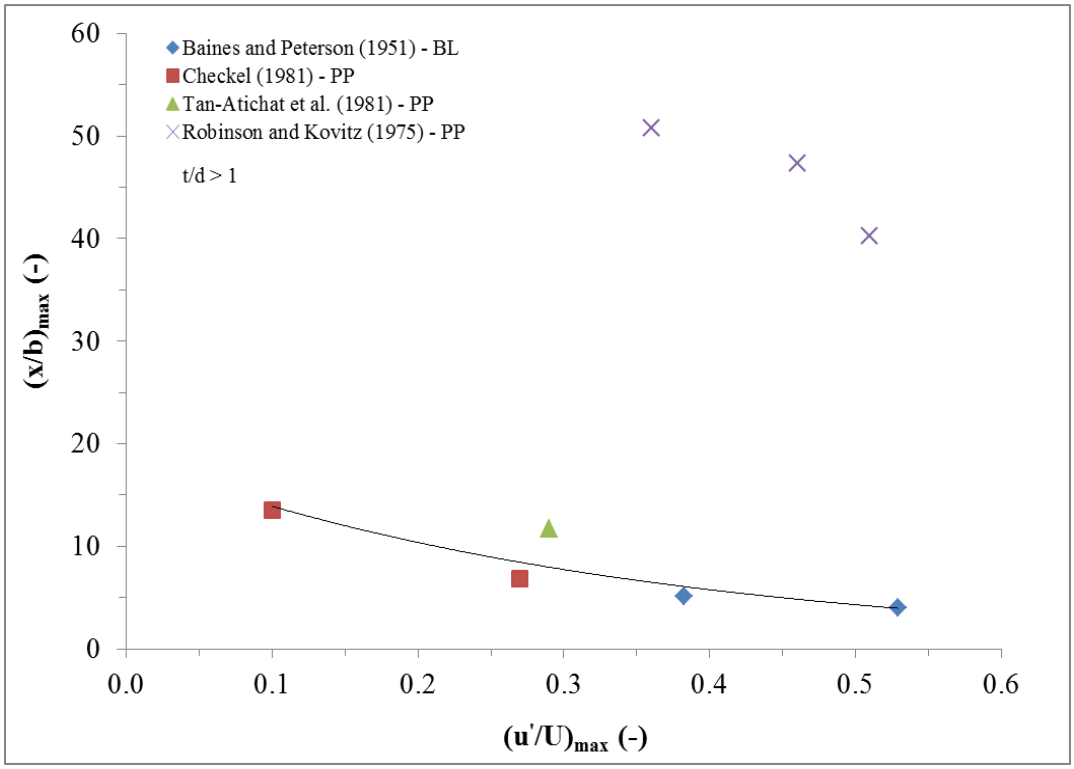

Figure 2.11 Correlation between maximum intensity of turbulence and its distance for grid plates with t/d > 1.

2.2.3.4 Maximum Intensity of Turbulence and its Position for Baffle Obstacles

As reviewed in Chapter 3, most investigators in gas explosions have considered obstacles such as orifice plates, flat-bar and wire-mesh etc. (grid plate obstacles) whose interval, blockage ratio and number have effects on flame propagation. Even though some suitable conclusions were acquired and they could aid to prevent disaster of flammable gas explosive, however, obstacles in the path of a propagating flame usually have solid structure. Thus there is the need to investigate the influence of solid obstacles referred to as baffles on gas explosions. This will be more useful in preventing gas explosions and providing reference for industry safety design (Yibin *et al.* 2011).

Similar to grid plate obstacles, there are limited data available in the literature (from cold flow turbulence) that measured the maximum intensity of turbulence and its corresponding distance. This comes from Chun and Sung (1996) , Taylor and Whitelaw (1984), Durao *et al.* (1979), Bradbury (1976), Etheridge and Kemp (1978) and Fuji *et al.* (1978). The acronyms for the authors name and baffle types are: CS – BFS: Chun and Sung – Backward Facing Step; TW – disk/cone: Taylor and Whitelaw – disk/cone; B – FP: Bradbury: flat plate; DW-disk: Durao and Whitelaw – disk; EK – BFS: Etheridge and Kemp - Backward Facing Step and F – BB: Fuji – Bluff Body.

Figure 2.12 shows a plot of the maximum intensity of turbulence $(u'/U)_{max}$ against obstacle blockage ranging from close to 0.1 to 0.6. Unlike the grid plates (see Fig. 2.6), there is a considerable data scatter in the baffles. This could be attributed to the fact that the baffles used are of different shapes resulting to different aerodynamic flow. However, the u'/U_{max} for the baffle obstacles is found to be higher than that of a grid plate having similar obstacle BR.

The corresponding distance to $(u'/U)_{max}$ against blockage is presented in Fig. 2.13. The dimensionless distance in baffle is shorter when compared with grid plate obstacles of similar blockage. The data with the exception of Etheridge and Kemp (1978) and Fuji *et al.* (1978) was fitted well with a logarithmic correlation as,

$$\left(\frac{x}{b}\right)_{max} = -1.22\ln(BR) - 0.06 \qquad (2.27)$$

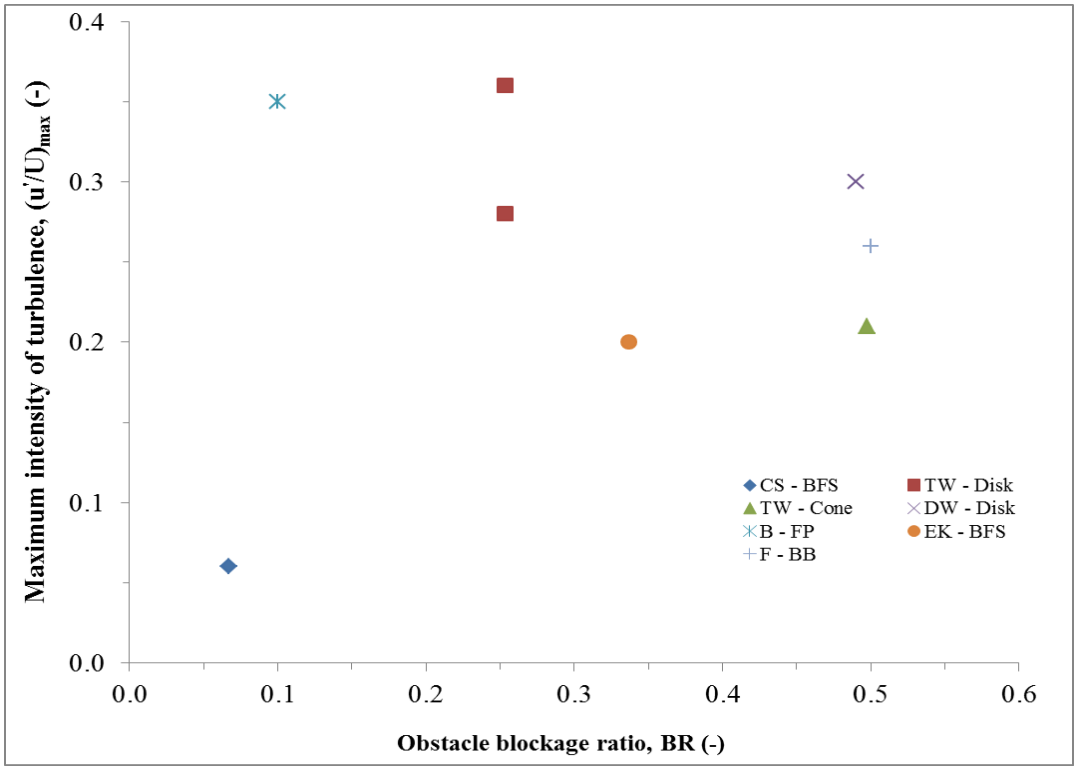

Figure 2.12 Maximum intensity of turbulence against blockage ratio for baffle obstacles.

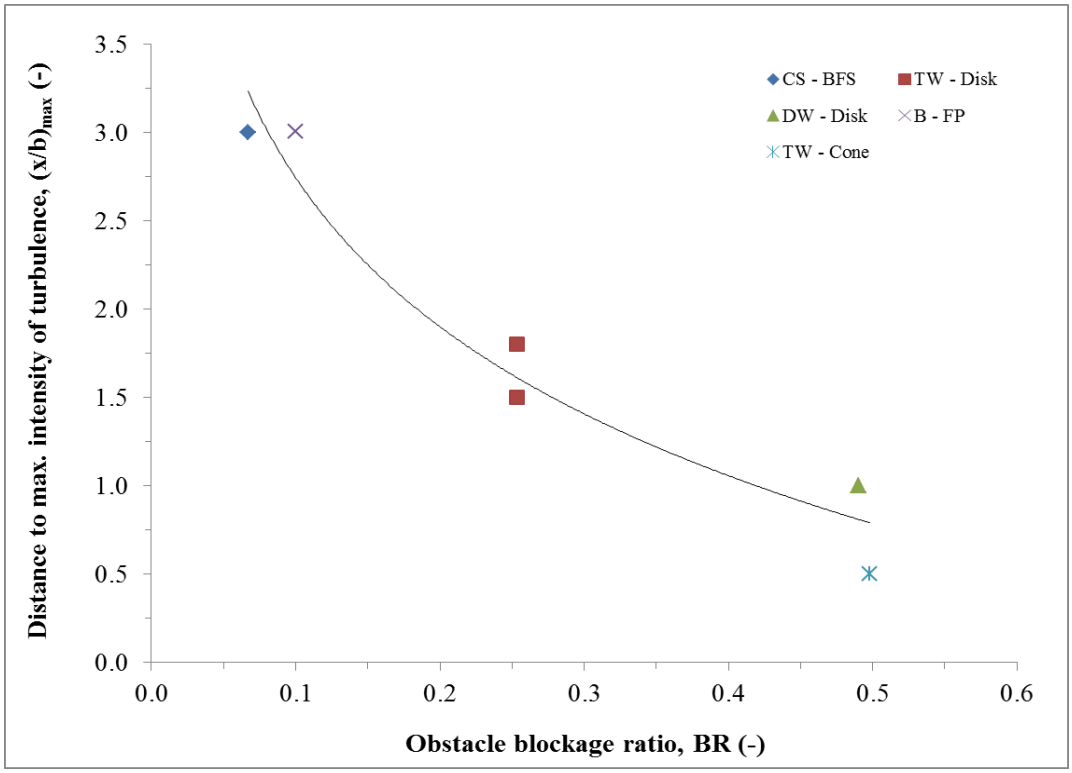

Figure 2.13 Distance to maximum intensity of turbulence against blockage for baffle obstacles.

2.2.3.5 Position of Maximum Intensity of Turbulence of Grid Plates and Free Jet Theory

From free jet theory, the greatest intensity of turbulence on the centreline of an orifice plate was anticipated to occur after the completion of the jet potential core where the interior edges of the surrounding shear region meet (Beer and Chigier 1983). The length of the potential core was expressed in terms of jet diameter, d_{jet}. The jet diameter of a flow through an orifice is the diameter of the vena contracta from Eq. 2.13 which is dependent on the open flow diameter of an obstacle, d and the coefficient of contraction, C_c. Prior to obtaining d_{jet}, the values of K for the geometries in Fig. 2.8 were calculated using Eq. 2.16 followed by determining the appropriate value of C_c for each geometry using Eq. 2.15. Figure 2.14 shows a plot of the position of maximum intensity of turbulence as a function of the jet diameter, x_{max}/d_{jet} against the obstacle blockage ratio, BR. It was observed that the, x_{max}/d_{jet} is independent of the obstacle blockage and hence the intensity of turbulence. The whole data used in the plot fell within a region of 3 to 10 jet diameters with the majority been between 3 to 6 jet diameters. The average position of u'/U_{max} for all the data points shown as a solid line is five and this agrees well with the expectancy of peak turbulence intensity been at or subsequent to the completion of the potential core generally taken to be 4-5 jet diameters long. The dotted lines at 3 and 20 d_{jet} indicate the range at which the maximum flame speed occurred downstream of the obstacle in a series of explosion test in tubes with grid plates (Phylaktou and Andrews 1991).

To further substantiate the relationship between the position of maximum intensity of turbulence and the free jet theory, the length of the potential core (4.5 d_{jet}) could be equated to the distance to $(u'/U)_{max}$. Figure 2.15 shows the ratio of x_{max}/L_{core} against the obstacle blockage for all the geometries in Fig. 2.8. The ratio x_{max}/L_{core} was found to be independent of the blockage just like x_{max}/d_{jet}. The entire data points are situated within a range of x_{max}/L_{core} of 0.6 to 2.4 with the majority been between 0.6 to 1.2. The solid line shown in the plot is the average of the x_{max}/L_{core} for all the data points and it was obtained to be around unity. This suggests that the position to $(u'/U)_{max}$ could be ascertained using free jet theory by obtaining the length of the potential core.

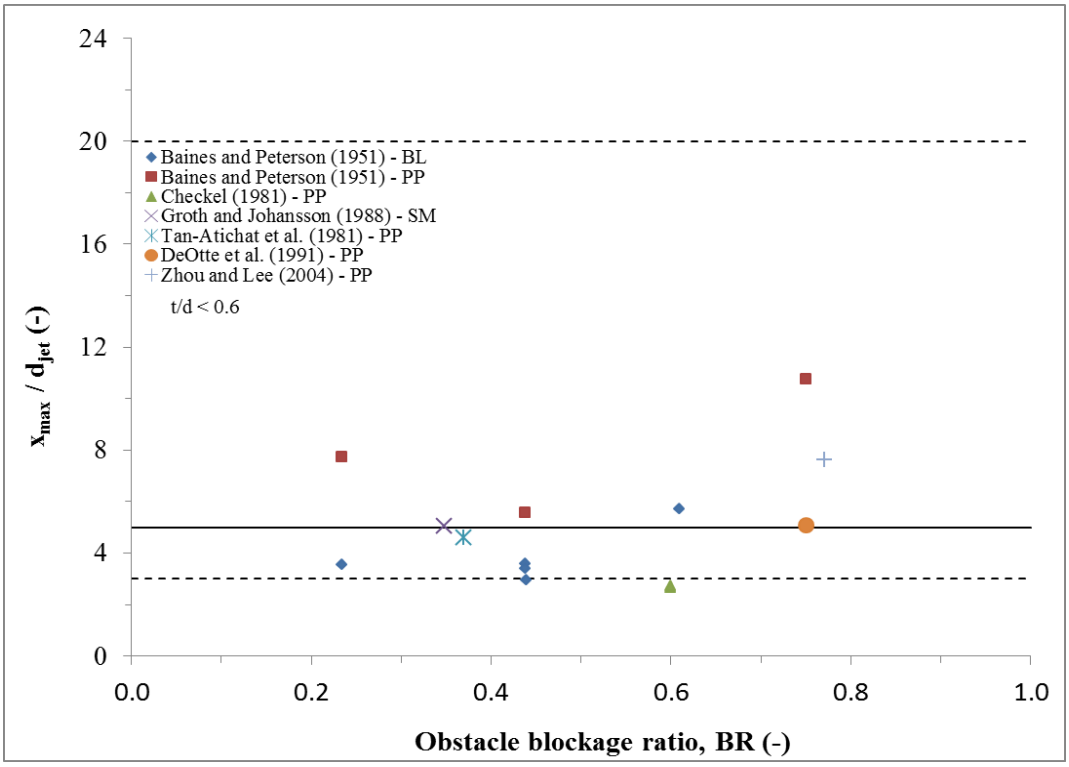

Figure 2.14 Distance to $(u'/U)_{max}$ expressed in terms of jet diameter versus obstacle blockage.

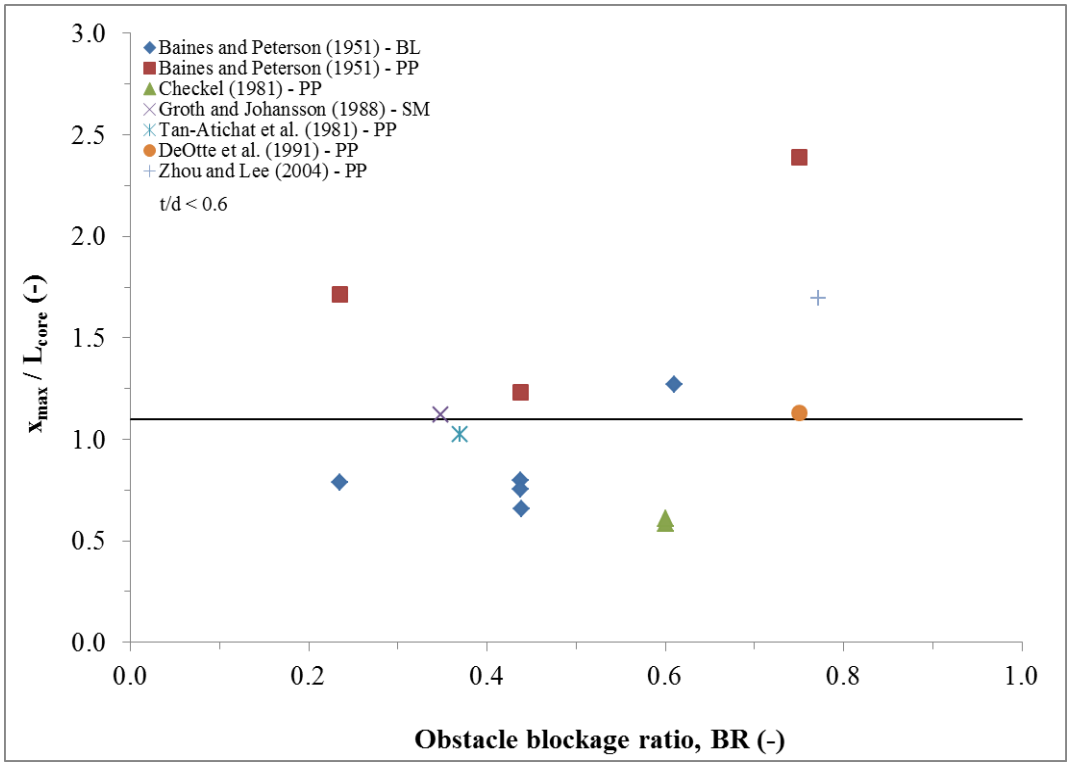

Figure 2.15 x_{max} to L_{core} relationship against obstacle blockage.

2.3 Application of Cold Flow Turbulence to Present Research

The interaction of the explosion-induced unburnt gas flow with an obstacle results in the generation of turbulence behind the obstacle and the acceleration of the flame when it reaches this turbulence. This mechanism leads to the generation of very fast explosions flames thereby giving rise to severe overpressure. Estimation of these phenomena is of great concern to process industries in order to enhance safety.

In practice, many obstacles can be treated as grid-plate obstacles, and there have been several explosion studies using grid plates. However, the outcomes from these works are of restricted application due to the fact that the data are not offered in terms of fundamental turbulent flow and combustion parameters, as these factors are mostly hard to measure under harsh transient conditions.

As reviewed previously, the bulk of measurements of intensity of turbulence immediately downstream of obstacles was based on steady-state flows by a small number researchers. These data were shown to be valid and usable in explosion induced transient flows by Cates and Samuels (1991) and Phylaktou and Andrews (1994) .

In the present research, the two developed models for the prediction of the explosion-induced maximum turbulent intensity and its corresponding position downstream of an obstacle respectively could be quantified. In combination with a turbulent burning velocity correlation, the first model could be applied to predict the highest overpressures generated in explosions while the second model would be useful to guide the spacing between obstacles that would lead to maximum intensity of turbulence and thus severe explosion overpressures.

Chapter 3

Review of the Effects of Obstacles on Gas Explosions, Gas Explosion Scaling and CFD Modelling

3.1 Introduction

In the previous chapter the literature and available data on turbulence generated by grid plates in steady state, non-reacting flows were reviewed. It was postulated that the cold flow turbulence could be related to transient gas explosions with obstacles. Also, two correlations were developed based on steady state flow to predict the maximum intensity of turbulence and its relative position downstream of an obstacle. These data and relationships were used to guide the design of experiments for this project.

This chapter is concerned with the transient nature of turbulent flow as applicable to congested gas explosions. Since the pioneering work of Chapman and Wheeler (1926), there have been numerous investigations into gas explosions in the presence of obstacles. The most important multi-obstacle studies that have been used in formulating safety guidelines and standards will be reviewed here and this will be split into studies with fixed obstacle spacing and studies with variable spacing.

The integral length scale, ℓ is considered an important parameter in scaling gas explosions from small scale tests (as in the present research) to full scale applications. The review in this chapter will therefore focus on the turbulent burning velocity models which show a dependence on ℓ and form the basis for scaling applications.

Nowadays, simulations from Computational Fluid Dynamics, CFD are performed in order to offer better understanding into turbulent flow behaviour. A CFD code, FLACS (Flame Accelerator Simulator) will be used in this research to study the effect of obstacle spacing in gas explosions. The results from the model will be validated from the current experimental work. A brief introduction to explosion CFD modelling and in particular the FLACS code will also be given in this chapter.

3.2 Multi-Obstacle Tests with Fixed Obstacle Spacing

Most researchers conducted gas explosion experiments with multi-obstacle arrays but with no variation in obstacle separation distance. Examples of these works include that of: Chapman and Wheeler (1926); Kirkby and Wheeler (1931); Robinson and Wheeler (1933); Eckhoff *et al.* (1984); Lee *et al.* (1984); Hjertager *et al.* (1988a); Moen *et al.* (1988); Peraldi *et al.* (1988); Chan and Greig (1989);

Mackay *et al.* (1989); Phylaktou (1993); Sakthitharan (1995); Chan and Dewit (1996); Dorofeev *et al.* (1996); Gardner (1998); Alekseev *et al.* (2001); Kuznetsov *et al.* (2002a); Lowesmith *et al.* (2011); Dong *et al.* (2012) and Gamezo *et al.* (2013). The detail of these studies is presented in Table 3.1. For each study, the obstacle parameters such as blockage ratio (BR), scale (b), spacing (x) and types are listed.

The influence of obstacle separation distance on gas explosion severity from the above experiments could not be quantified because of the fixed pitch that was used within each set of experiments.

With the exception of Phylaktou (1993) and Gardner (1998), the pitch in all of the above studies was varied just from 1.2 to 8.8 characteristic obstacle scales as shown in Fig. 3.1. However, this is not within the range of 3 to 20 characteristic obstacle scales downstream of the grid where the maximum combustion rate usually occurs as given by Phylaktou and Andrews (1991).

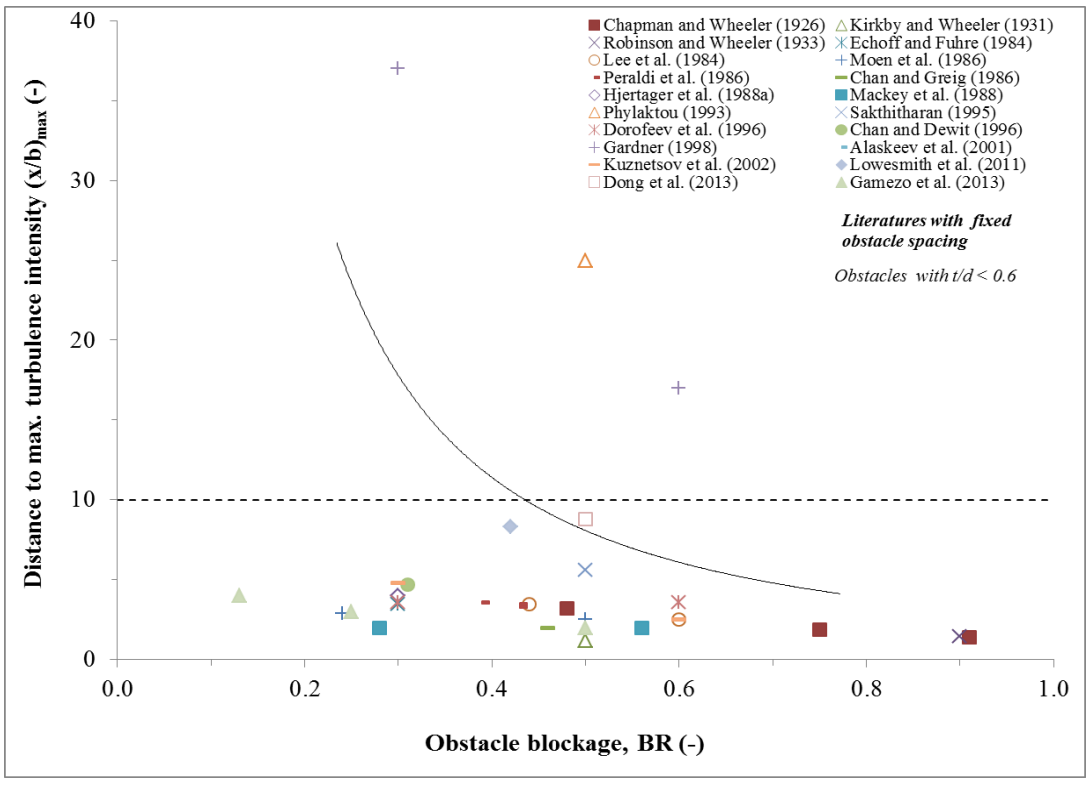

Figure 3.1 Relationship between gas explosions from literature with fixed obstacle spacing and optimum distance to maximum intensity from cold flow turbulence.

Table 3.1 Review of multi-obstacle experimental studies with constant obstacle spacing.

Reference	Experimental conditions	Obstacle Type	BR (-)	Obstacle scale, b (m)	Obstacle spacing, x (m)	x/b (-)	P_{max} (bar)	S_{fmax} (m/s)	Conclusion	Comment
Chapman and Wheeler (1926)	Geometry: Brass tube opened at both ends with quartz section for visual aids. Dimension: 5 cm diameter and 240 cm long. Mixture: Methane-air 9.5-10% by vol. Ignition: At one end of the tube.	20 orifice plates	0.91	0.036	0.05	1.4	-	420	Flame speeds were enhanced in the presence of obstacles with about 420 m/s compared to single and no obstacle (6 m/s) tests.	Overpressure was not reported.
			0.75	0.026		1.9				
			0.48	0.016		3.2				
Kirkby and Wheeler (1931)	Geometry: Explosion tube closed at both ends with quartz section for visual aids Dimension: 100 mm diameter and 1.714 m long Mixture: Methane-air 10% by vol. Ignition: Ignition plug at one end.	10 orifice plates	0.5	0.033	0.04	1.21	4.8	-	The maximum overpressure occurred at about 0.09 seconds after ignition. The total explosion time (0.17 seconds) was 2.4 times lesser than obstacle free tests.	The first 65.7 cm from ignition was unrestricted followed by 40 cm with 10 orifice plates. The remaining length of the tube was unobstructed.
Robinson and Wheeler (1933)	Geometry: Elongated steel tube opened at both ends. Dimension: 32.3 m long and 30.5 cm diameter. Mixture: Methane-air 9.8-10% by vol. Ignition: At one end of the tube.	11 orifice plates with first one placed 13.4 m after spark.	0.89	0.208	0.305	1.47	-	600	Flame speed of 454 m/s was attained at the restricted zone prior to its decrease to 300 m/s and later rose to a maximum value of 600 m/s at the end of the tube.	Abundant tube length would enable the flame to propagate fully downstream of the orifice even for smaller number of orifice plates. Comparing this work with that of Chapman and Wheeler (1926) proved this.

Table 3.1 Cont'd

Reference	Experimental conditions	Obstacle Type	BR (-)	Obstacle scale, b (m)	Obstacle spacing, x (m)	x/b (-)	P_{max} (bar)	S_{fmax} (m/s)	Conclusion	Comment
Echoff and Fuhre (1984)	Geometry: 4.5 m long and 0.5 m diameter jet generation tube (with obstacles) attached to 50 m^3 main explosion chamber fully opened at one end. Mixture: Stoichiometric propane-air mixtures. Ignition: 100 J electrically activated match.	Up to 12 hexagonal perforated steel plates	0.3	0.103	0.36	3.5	18	-	The maximum overpressure was close to six times higher than the one generated in the main chamber. Full detonation could occur under optimal geometric and turbulence conditions.	The data from these experiments were used by CMI to generate a database for vented explosions under non-quiescent conditions.
Lee *et al.* (1984)	Geometry: Steel tube of 5 cm diameter and 11 m long (3 m section housed the obstacles). Mixture: Hydrogen-air 10-45% by vol. Ignition: Glow wire igniter at the end of the tube.	Repeat obstacles of spiral and orifice types.	0.44 spiral	0.014	0.05	3.6	15	2000	Detonation speeds occurred at about 10-40 tube diameters. Orifice plates were more efficient in terms flame acceleration rate than spiral obstacles for similar BR. H_2 –air 13% by vol. was the limit from which transition to detonation occurred.	The results showed concern in hydrogen explosions in view of the concern of hazards in nuclear reactor due to likelihood of hydrogen leaks.
			0.44 orifice	0.014		3.6				
			0.6 orifice	0.020		2.5				

Table 3.1 Cont'd

Reference	Experimental conditions	Obstacle Type	BR (-)	Obstacle scale, b (m)	Obstacle spacing, x (m)	x/b (-)	P_{max} (bar)	S_{fmax} (m/s)	Conclusion	Comment
Moen *et al.* (1986)	Geometry: Top vented channel of 1.8 m by 1.8 m cross section and 15.5 m long. Mixture: Acetylene, propane and hydrogen-sulphide-air mixtures at different concentrations. Ignition: Four sparks at the end of the tube.	Circular obstacles of 0.5 m and 0.22 m diameters	0.5	0.5	1.27	2.5	0.16	435	Near stoichiometric acetylene-air, flame produced the highest flame speed and overpressure with onset to detonation. But severity of the flame in lean acetylene-, propane- and hydrogen sulphide-air mixtures was much less intense.	The chance of flame acceleration to detonation in the more open areas in chemical industries is much smaller than confined areas. However, the presence of obstacles in open areas shows that the potential for damaging explosions does exist.
			0.24	0.22	0.63	2.9				
Peraldi *et al.* (1986)	Geometry: Three tubes of 18 m long each with variable internal diameters of 5 cm, 15 cm and 30 cm closed at both ends. Mixture: hydrogen, acetylene, ethylene, propane and methane-air at various concentrations. Ignition: At one end of the tube using glow wire.	Orifice plates	0.43 ϕ5cm	0.015	0.05	3.3	-	2000	High speed and flame propagation with transition to detonation was attained in all the three obstacle laden tubes.	A criterion for the onset to detonation was obtained in this test as $\lambda/d \leq 1$ where λ is the characteristic cell size and d is the orifice diameter.
			0.39 ϕ15cm	0.042	0.15	3.6				
			0.43 ϕ30cm	0.085	0.30	3.5				
Chan and Greig (1988)	Geometry: 6 m long tube with 90 mm by 90 mm cross section. Mixture: H_2-O_2 mixtures. Ignition: End of the tube.	Baffle-types	0.46	0.038	0.076	2	-	2500	Flame accelerated very rapidly down the channel thereby leading to quasi DDT.	Obstacles in a tube influenced fast deflagrations and DDT.

Table 3.1 Cont'd

Reference	Experimental conditions	Obstacle Type	BR (-)	Obstacle scale, b (m)	Obstacle spacing, x (m)	x/b (-)	P_{max} (bar)	S_{fmax} (m/s)	Conclusion	Comment
Hjertager *et al.* (1988a)	Geometry: 10 m long tube and 2.5 m diameter opened at one end and closed at the other. Mixture: Propane and methane-air mixtures at different concentrations. Ignition: Planar and point ignition at the closed end of the tube.	6 Orifice plates	0.3	0.505	2	3.96	9	900	Fuel concentration increased the flame speed and overpressure for both fuels with propane higher than methane. Planar ignition produced maximum overpressure twice that of point ignition.	The experimental data presented were used in further testing and development of the FLACS gas explosion simulation model.
Mackay *et al.* (1988)	Geometry: Steel tube 7.8 m long and 0.9 m diameter. One end closed and the other open to a cylindrical bag of 20.4-36.2 m^3 with partially central circular disc of either 0.43 m or 0.58 m in diameter. Mixture: Acetylene, ethylene, propane and vinyl chloride.	Circular obstacles	0.28 0.56	0.25 0.5	0.5 1	2 2	15	2000	DDT was witnessed in the bag for acetylene-air mixtures under range of geometric conditions. However this was not observed with the other fuel-air systems. But it was found that a significant explosion does occur.	The flame jet velocity which emerged at the end of the tube due to the presence of central circular disc played an important role in the DDT.
Phylaktou (1993)	Geometry: An elongated tube of 76 mm diameter with an L/D of 21.6 closed at both ends. Mixture: methane-air mixtures at 10% by vol. Ignition: Spark ignition at one end of the tube.	2 Orifice plates	0.5	0.022	0.55	25	Over 9	240	The combined effect of the obstacles resulted in an intense explosions overpressure signifying a probable occurrence of short lived detonation.	The flame speeds (240 m/s) were much lower than detonation speeds.

Table 3.1 Cont'd

Reference	Experimental conditions	Obstacle Type	BR (-)	Obstacle scale, b (m)	Obstacle spacing, x (m)	x/b (-)	P_{max} (bar)	S_{fmax} (m/s)	Conclusion	Comment
Sakthitharan (1995)	Geometry: Flame tube of 10 m long and 72 mm x 34 mm cross section. Mixture: Stoichiometric methane-air. Ignition: Spark ignition at the end of the tube.	4 flat plates	0.5	0.036	0.2	5.6	3	633	The severity of the event is mainly due to the localised explosions occurring behind the obstacles and not due to the accelerating flow ahead.	The obstacles were positioned in a staggered form.
Dorofeev *et al.* (1996)	Geometry: 34.6 m long and 2.3 m by 2.5 m cross section Mixture: Hydrogen-air at 9.8-14% by vol. Ignition: Electric spark at the end of the channel.	Concrete types	0.3	0.69	2.5	3.6	14.2	1690	A minimum of 12.5% of hydrogen was established to be essential for DDT.	Flame propagation, pressure build up and DDT depend on mixture composition, turbulence generation and geometrical scale.
			0.6	1.38	5	3.6				
Chan and Dewit (1996)	Geometry: 6.4 m long, 0.28 m diameter closed at both ends. Mixture: Hydrogen-steam mixture at different concentrations. Ignition: Spark igniter at the end of the tube.	Baffle types	0.31	0.06	0.28	4. 7	90	-	The overpressure was greatly higher than the normal CJ detonation pressure. This is due to the fact that DDT transpired in the precompressed region produced by the reflection of the precursor shock wave off the end plate.	Even in the precompressed end gas region, slight change in mixture reactivity can inhibit the onset of detonation.

Table 3.1 Cont'd

Reference	Experimental conditions	Obstacle Type	BR (-)	Obstacle scale, b (m)	Obstacle spacing, x (m)	x/b (-)	P_{max} (bar)	S_{fmax} (m/s)	Conclusion	Comment
Gardner (1998)	Geometry: An elongated tube of 162 mm diameter with an L/D of 26.1 closed at one end. The opened end was connected to 50 m^3 cylindrical dump vessel. Mixture: 10% CH_4 by vol. Ignition: Spark ignition at the end of the closed tube.	2 orifice plates	0.3	0.027	1	37	3.38	420	In comparison with single obstacles, the overall effect of doubling the number of obstacles for 0.3 and 0.6 BR was doubled and 1.3 maximum overpressure respectively.	This experimental set up was maintained in the present research to study the influence of obstacle spacing.
			0.6	0.060		17				
Aleskeev *et al.* (2001)	Geometry: Two transverse vented tubes of 92 mm and 46 mm internal diameters corresponding to 5.8 m and 2.9 m long. Mixture: H_2-air (9-70% by vol.) and H_2-O_2. Ignition: Weak electrical spark at the end of the closed tube.	Orifice plates	0.6 ϕ92mm	0.037	0.092	2.5	-	1700	Significant flame acceleration was influenced in the test as a result of venting. The vent ratio was proportional to the reactive mixture necessary for the development of fast flames.	The critical conditions for detonation onset in vented tubes with BR=0.6 were found to be very close to those in closed tubes with the same obstacle configuration.
			0.6 ϕ46mm	0.018	0.046	2.6				

Table 3.1 Cont'd

Reference	Experimental conditions	Obstacle Type	BR (-)	Obstacle scale, b (m)	Obstacle spacing, x (m)	x/b (-)	P_{max} (bar)	S_{fmax} (m/s)	Conclusion	Comment
Kuznetsov *et al.* (2002a)	Geometry: Two explosion tubes of 174 mm and 520 mm internal diameters corresponding to 12 m and 34.5 m long. Mixture: Methane, propane and ethylene –air mixtures at different concentrations Ignition: Weak electrical spark at the end of the closed tube.	Orifice plates	0.6 ϕ174mm	0.070	0.174	2.5	9	2220	In lean mixtures, the critical compositions for the development of fast flames were not dependent on the tube size and vice-versa on the rich side with 520mm tube higher than 174mm tube.	This work provided surplus data for mixtures of hydrocarbon fuels in air by identifying the onset between slow and fast deflagrations in these mixtures.
			0.3 ϕ174mm	0.036	0.174	4.8				
			0.6 ϕ520mm	0.208	0.520	2.5				
			0.3 ϕ520mm	0.107	0.520	4.9				
Lowesmith *et al.* (2011)	Geometry: Open congested region of 3 m x 3 m x 18 m long after an enclosed region. Mixture: Hydrogen-methane mixtures of different concentrations. Ignition: Low spark energy at variable locations.	Plastic pipes	0.42	0.18	1.5 per rack	8.3	6.5	Over 800	The behaviour of a CH_4/H_2 mixture with<30% H_2 is likely to be similar to pure CH_4. However, 40% H_2 mixture or more presented a significant risk of generating damaging overpressure and DDT.	This work was part of the EC-funded project NATURALHY, aimed at studying the potential for the present natural gas pipeline networks to convey hydrogen from manufacturing sites to hydrogen users.

Table 3.1 Cont'd

Reference	Experimental conditions	Obstacle Type	BR (-)	Obstacle scale, b (m)	Obstacle spacing, x (m)	x/b (-)	P_{max} (bar)	S_{fmax} (m/s)	Conclusion	Comment
Dong *et al.* (2012)	Geometry: 104 mm ID and 2.4 m long pipe closed at both ends. Mixture: Methane-air / Methane-Coal-Air mixtures ranging from 6-12% by vol. Ignition: Spark plug at one end of the tube.	Up to 7 Orifice plates	0.5	0.034	0.3	8.8	7	-	The explosion pressure increased slightly when the deposited coal dust and repeated obstacles were set in the pipe.	Thorough dispersion process of deposited coal dust and combustion cannot be understood completely, for the transient process is complicated in the co-presence of gas and deposited dust.
Gamezo *et al.* (2013)	Geometry: Elongated detonation tube of 105 cm ID and 73.2 m long open at one end and closed at the other. Mixture: NG-air mixture of 5.1-15% by vol. Ignition: Weak electric match 0.5 m away from the closed end.	Up to 16 baffle types	0.13	0.379	1.52	4.0	76	2773	DDT and sustained detonations were observed over the composition range 8.0 to 10.8%.	According to US regulations on Coal mine safety, mine seals are required to resist an explosion pressure-time curve that increases rapidly to 0.8 MPa and stays at that level for 4 seconds.
			0.25	0.525		2.9				
			0.5	0.742		2.1				

3.3 Multi-Obstacle Tests with Variable Obstacle Spacing

The separation distance (pitch) between obstacles is an area that has not received adequate attention by explosion researchers despite the general recognition of the important role it plays in determining the explosion severity. With reference to Fig. 2.4, it is discernible that either too large or too small separation distance between the obstacles would lead to lower intensity of turbulence and hence explosion severity. According to Lee and Moen (1980), sustained flame acceleration could not be attained for large pitch due to decay of turbulence in between obstacles while for small pitch the pocket of unburned gas between the obstacles would be too small to allow for the flame to accelerate before reaching the next obstacle. In compliance with the ATEX directive (ATEX 1994), the worst case scenarios need to be used in assessing the severity of the hazard posed by gas explosions in process plant. Therefore an optimum obstacle spacing corresponding to maximum explosion overpressure should be used in the general assessment of these phenomena.

A number of experimental explosion studies have demonstrated the effect of obstacle separation distance as part of wider assessment of the effects of congestion. These include the works of: Moen *et al.* (1980); Moen *et al.* (1982); Chan *et al.* (1983); Harrison and Eyre (1987); Lindstedt and Michels (1989); Teodorczyk *et al.* (1989); Mercx (1992); Beauvais *et al.* (1993); Obara *et al.* (1996); Mol'kov *et al.* (1997); Yu *et al.* (2002); Cicarelli *et al.* (2005); Teodorczyk *et al.* (2009); Rudy *et al.* (2011); Vollmer *et al.* (2011); Pang *et al.* (2012); Boeck *et al.* (2013) and Porowski and Teodorczyk (2013).

As shown in Fig 3.2, the bulk of the spacing between obstacles of different blockage was within a range of 1.3 to 10 obstacle scales. The systematic reviews of these experimental works are given in Table 3.2.

In most cases many repeat obstacles were used over a short distance (and in some tests the pitch was varied over a limited range) for example the studies from Chan *et al.* (1983) ; Lindstedt and Michels (1989); Mercx (1992) and Vollmer *et al.* (2011). Also, there have been a number of investigations in explosions in obstacle-laden tubes where the separation distance of the multi-obstacles was also partially explored. For instance, Beauvais *et al.* (1993); Obara *et al.* (1996); Yu *et al.* (2002); Rudy *et al.* (2011); Vollmer *et al.* (2011) and Porowski and Teodorczyk (2013). In most of the tests, the

explosion geometry was filled completely with obstacles thereby leading to deflagration to detonation transition, DDT.

Most of the industrial explosion incidents involved deflagrative rather than detonative propagation, and it is important therefore to explore the influence of obstacle separation in scenarios where the combustion remains in the deflagration regime without transition to detonation. The present research addressed the effects of systematic obstacle spacing within deflagration combustions.

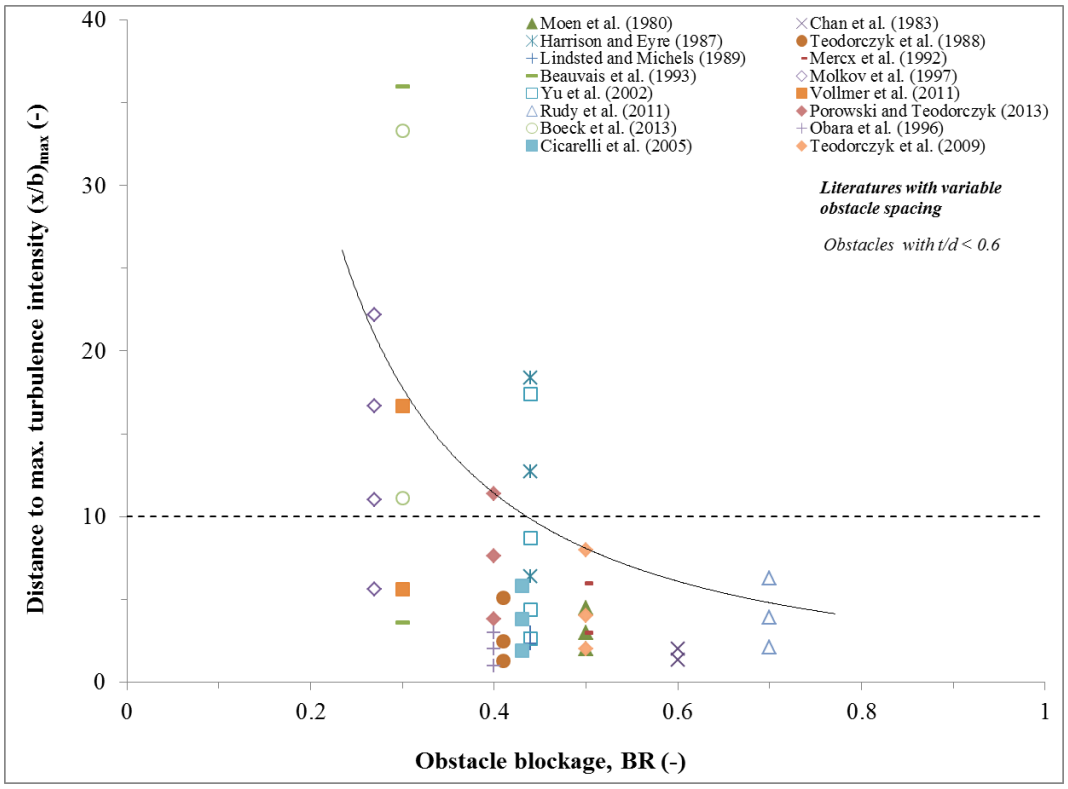

Figure 3.2 Relationship between gas explosions from literature with variable obstacle spacing and optimum distance to maximum intensity from cold flow turbulence.

Table 3.2 Review of multi-obstacle experimental studies with variable obstacle spacing.

Reference	Experimental conditions	Obstacle Type	BR (-)	Obstacle scale, b (m)	Obstacle spacing, x (m)	x/b (-)	P_{max} (bar)	S_{fmax} (m/s)	$(x/b)_{max}$ (-)	Conclusion	Comment
Moen *et al.* (1980)	Geometry: Cylindrical chamber of 61 cm diameter with top and bottom walls. Mixture: Stoichiometric methane-air. Ignition: At the centre.	Spiral	0.5	0.0064	0.029	4.5	-	50	4.5	With repeated obstacles of suitable sizes and spacing, flame speeds of about 50 m/s for 2.92 cm pitch was attained. This flame speeds doubled that of the 1.27 cm obstacle spacing.	Flame speeds were found to increase to 130 m/s when the obstacle scale and pitch were increased to 1.27 cm and 3.81 cm respectively.
					0.019	3.0					
					0.013	2					
Moen *et al.* (1982)	Geometry: 10 m long tube and 2.5 m diameter opened at one end and closed at the other. Mixture: Stoichiometric methane-air mixtures. Ignition: Planar ignition at the closed end of the tube.	Orifice plates	0.16	0.32	1-2.5	3-8 for 0.16 BR	8.8	-	-	Repeated obstacles of 0.16 BR had an intense influence on the violence of the explosion, generating explosion overpressures higher than 1 bar in the tube.	The obstacles' spacing was not systematic i.e. no array of obstacles of similar BR was spaced for more than one pitch.
			0.3	0.51							
			0.5	0.82							
			0.84	1.55							
Chan *et al.* (1983)	Geometry: 1.22 m long channel and 127 mm x 203 mm cross section closed at one end and open at the other with variable degree of confinement at the top Mixture: CH_4 –air 9.5% by vol. Ignition: Spark at the closed end.	Repeat baffles	0.6	0.076	0.101	1.33	-	160	1.33	Obstacle spacing had little effect on the flame acceleration for a slight degree of venting provided by the top plate but the reverse was the case for the fully confined configuration.	Limited obstacle pitch was used by the authors.
					0.152	2					

Table 3.2 Cont'd

Reference	Experimental conditions	Obstacle Type	BR (-)	Obstacle scale, b (m)	Obstacle spacing, x (m)	x/b (-)	P_{max} (bar)	S_{fmax} (m/s)	$(x/b)_{max}$ (-)	Conclusion	Comment
Harrison and Eyre (1987)	Geometry: Unconfined wedge-shaped rig of about 60 m diameter and 10 m high. Mixture: Natural gas-air mixtures at different concentrations. Ignition: At the end of geometry.	3 grids of 10 pipes each	0.44	0.315	2	6.4	0.063	Over 100	12.7	Obstacle arrays typical of those encountered in industrial plant can lead to the production of damaging overpressures. The severity dropped once flame was out of the congested region.	The initial spacing i.e.2 m was based on Baines and Peterson (1951) however, the mixture concentration was not kept constant for the different spacing explored with the obstacles.
					4	12.7					
					5.8	18.4					
Teodorczyk *et al.* (1988)	Geometry: 1.5 m long channel with 61.8 mm by 61.8 mm cross-section. Mixture: H_2-O_2, C_2H_4-O_2 and C_3H_8 –O_2 mixtures. Ignition: Electric spark at the end of the channel.	Baffles	0.41	0.0254	0.032	1.3	-	2600	1.3	The propagation of flame at high speed deflagrations in the choking regime, and the leading shock and its reflections from the wall played a trivial role. However, a complex flame obstacle interaction is controlling combustion mechanism for the wave propagation.	The obstacle spacing was established to represent an effective reaction zone length (or cell length) of the quasi-detonation.
					0.064	2.5					
					0.128	5.0					
Lindsted and Michels (1989)	Geometry: Explosion tube of 11 m long and 5.08 cm ID. Mixture: Ethane-air. Ignition: Spark igniter.	Orifice and spiral	0.44	0.015	0.035	2.3	-	1800	-	It was demonstrated that the condition for detonation in repeated orifice obstacles $(\lambda/d \leq 1)$ is not sufficiently applicable to conventional Shchelkin spirals.	The influence of obstacle spacing for a given condition was not explicit in this work.
					0.045	3					

Table 3.2 Cont'd

Reference	Experimental conditions	Obstacle Type	BR (-)	Obstacle scale, b (m)	Obstacle spacing, x (m)	x/b (-)	P_{max} (bar)	S_{fmax} (m/s)	$(x/b)_{max}$ (-)	Conclusion	Comment
Johnson *et al.* (1991)	Geometry: 9 m long and 0.6 m by 0.6 m cross-section. Mixture: Natural gas with O_2 enrichment Ignition: end of the confined region.	Pipe obstacles	0.21-0.63	0.02-0.063	0.15-0.5	7.5- 8	Over 6	-	-	The spacing between obstacles led to increase in the severity of gas explosions.	The obstacle spacing was not studied systematically.
Mercx *et al.* (1992)	Geometry: Rectangular geometry of 25.4 m x 12.7 m x 12.7 m. Mixture: Stoichiometric methane-air mixtures. Ignition: Central ignition	Mild steel pipes	0.5	0.5	1.5 3	3 6	1.16	439	3	Flame speeds and overpressures in this scale were greater in magnitude than those from a small scale tests with a scale factor of 6.35. However, similar trend on blockage, reactivity and pitch were similar in both scales.	Limited obstacle spacing was used.
Mercx *et al.* (1992)	Geometry: Rectangular geometry of 25.4 m x12.7 m x 1 2.7 m. Mixture: Stoichiometric propane-air mixtures. Ignition: Central ignition.	Mild steel pipes	0.5	0.5	1.5 3	3 6	Over 25	575	3	The influence of higher mixture reactivity led to a transition to detonation.	Limited obstacle spacing was used.

Table 3.2 Cont'd

Reference	Experimental conditions	Obstacle Type	BR (-)	Obstacle scale, b (m)	Obstacle spacing, x (m)	x/b (-)	P_{max} (bar)	S_{fmax} (m/s)	$(x/b)_{max}$ (-)	Conclusion	Comment
Beauvais *et al.* (1993)	Geometry: Totally confined tube of 6 m long and 66 mm diameter. Mixture: H_2-air-Steam mixture of variable concentration and temperature. Ignition: Spark plug at one end of the tube.	Orifice plates	0.3 & 0.7	0.014 for 0.3	0.05-0.5	3.6-36	-	1800	3.6	Mixture potential for a turbulent flame acceleration increases when the initial temperature was raised but more effective turbulence inducing obstacles in the flame path were necessary to activate this potential.	The outcome of this work is applicable to explosion mitigation/prevention in a light water reactor where hydrogen is released in case of an accident.
Obara *et al.* (1996)	Geometry: Detonation tube of 3 m long and 25 mm by 30 mm cross-section closed at both end. Mixture: Stoichiometric oxygen -hydrogen mixtures diluted with N_2. Ignition: Spark at the tube end.	Baffle types	0.2-0.6	0.01 for 0.4 BR	0.01 0.02 0.03	1 2 3	-	3000	-	DDT transpired earlier when the obstacle was inserted near the ignition plug. In overall, the presence of obstacles was effective for the transition of the deflagration to detonation wave.	The influence of obstacle spacing for a given condition was not explicit in this work.
Molkov *et al.* (1997)	Geometry: Vented cylinder of 2 m diameter and 3.5 m long. Mixture: Propane-air mixture at 4.05% by vol. Ignition: Point ignition at the end of the vessel.	Metal rods	0.27	0.018	0.1 0.2 0.3 0.4	5.6 11 16.7 22.2	0.55	-	11	The reliance of explosion dynamics on the pitch between two arrays was established to be non-monotonic. The largest intensity was between 20-30 cm corresponding to peak u'/U i.e. 2-3 cell sizes.	This was one of the first set of quantifiable data on the turbulence factor for combustion in a big volume enclosure with obstacles in the form of a set of arrays.

Table 3.2 Cont'd

Reference	Experimental conditions	Obstacle Type	BR (-)	Obstacle scale, b (m)	Obstacle spacing, x (m)	x/b (-)	P_{max} (bar)	S_{fmax} (m/s)	$(x/b)_{max}$ (-)	Conclusion	Comment
Yu *et al.* (2002)	Geometry: Semi open tube 0.08 m diameter and 5 m long. Mixture: Water gas. Ignition: Electrical spark.	Orifice plates	0.3-0.6	0.023 for 0.44 BR	0.06	2.61	-	450	4.35	Spacing between obstacles played a role in influencing the rate of flame acceleration only rather than the final flame speed. The peak average flame speed was attained when the obstacle spacing was about equal to the inner diameter of flame tube.	The maximum terminal flame speed was achieved with the BR 0.3-0.4 in the low-speed combustion regime, whereas in the choking regime, the maximum flame speed was insensitive to the BR. In the detonation regime, the full flame speed and overpressure reduced with increasing BR.
					0.1	4.35					
					0.2	8.70					
					0.4	17.4					
Cicarelli *et al.* (2005)	Geometry: 3 m long tube with an internal diameter of 14 cm closed at both ends. Mixture: Stoichiometric propane-air mixture Ignition: Spark ignition at one end of the tube	Orifice plates	0.43-0.75	0.04 for 0.43 BR	0.076	1.9	9	890	-	Obstacle spacing has no much influence on flame acceleration for lower obstacle blockage ratios but does on higher. The shortest run up distance in the tests occurred at 7.6 cm obstacle spacing and 0.75 blockage ratio.	The effect of obstacle blockage and spacing reported in the work were focused only on the early stage of flame acceleration where flame folding is the main mechanism.
					0.15	3.8					
					0.23	5.8					

Table 3.2 Cont'd

Reference	Experimental conditions	Obstacle Type	BR (-)	Obstacle scale, b (m)	Obstacle spacing, x (m)	x/b (-)	P_{max} (bar)	S_{fmax} (m/s)	$(x/b)_{max}$ (-)	Conclusion	Comment
Teodorczyk *et al.* (2009)	Geometry: 2 m long channel with 0.08 m by 0.11 m cross-section closed at both ends Mixture: H_2-air mixture at various concentrations Ignition: Low electric spark at the end of the channel.	Flat bars	0.25-0.6	0.04 for 0.5 BR	0.08 0.16 0.32	2 4 8	-	2000	8	High obstacle BRs were destructive for the flame propagation (large momentum losses) and irrespective of the turbulizing effect they lessen the risk of DDT.	The present study was inspired by the latest advanced computer simulations of flame acceleration and DDT in hydrogen–air mixture in obstructed channels.
Vollmer *et al.* (2011)	Geometry: Confined rectangular geometry of 5.4 m long and 0.3 m by 0.06 m cross section. Mixture: Hydrogen-air mixture at 20% by vol. Ignition:	Flat plate	0.3 & 0.6	0.018 for 0.3 BR	0.1 0.3	5.6 16.7	-	2250	-	A DDT criterion of 7λ was established for obstacle-laden geometry with homogenous mixtures. However, this cannot be applied confidently on non-homogenous H_2 –air.	The work was aimed at achieving a comprehensive risk assessment in gas explosions in non-homogenous mixtures as typically found in industries.
Rudy *et al.* (2011)	Geometry: 6 m long tube with 140 mm ID closed at both ends Mixture: Stoichiometric H_2-air mixture Ignition: Weak electric spark at the one end of the tube.	Orifice plates	0.4-0.7	0.067 for 0.7 BR	0.14 0.24 0.42	2.1 3.6 6.3	30	2100	-	High obstacle BR of 0.6 and 0.7 showed a high influence of obstacle spacing of about 6 to 20% on detonation velocity while low obstacle 0.4 and 0.5 showed little influence on obstacle spacing of about 3-7%.	Separation distance between obstacles and BR value have very great effect on stability of detonation velocity.

Table 3.2 Cont'd

Reference	Experimental conditions	Obstacle Type	BR (-)	Obstacle scale, b (m)	Obstacle spacing, x (m)	x/b (-)	P_{max} (bar)	S_{fmax} (m/s)	$(x/b)_{max}$ (-)	Conclusion	Comment
Porowski and Teodorczyk (2013)	Geometry: Detonation tube of 6 m long and 140 mm ID closed at both ends. Mixture: $CH_4 - H_2$ mixtures with different CH_4 contents. Ignition: Weak electric spark at the end of the tube.	Orifice plates	0.4 -0.7	0.037 for 0.4 BR	0.14	3.8	30	2015	11.4	For the hybrid mixtures, DDT happened with BR from 0.6 to 0.4, with 0.4 BR occurring at 3D for mixtures up to 50% of methane contents in the mixtures. The 1D spacing resulted in quasi-detonation regime for mixtures comprising 30-50% CH_4	This work can be applied towards hydrogen economy in the future. This was due to the blend of $CH_4 - H_2$ mixtures. Previous work of Lowesmith et al. (2011) on this was on deflagration but the current work was on detonation.
					0.28	7.6					
					0.42	11.4					
Boeck *et al.* (2013)	Geometry: Closed explosion channel of 5.4 m long and 0.3 m by 0.06 m cross-section. Mixture: Non-homogenous H_2 - air mixture at different concentration. Ignition: Spark plug at one end of the channel.	Flat-bar	0.3	0.009	0.1	11.1	120	-	11.1	Concentration gradients of mixtures influenced the peak overpressures in gas explosions by shifting its occurrence towards lower average H_2 concentrations. In the experiments presented, the shift was about 2.5 %vol.	Pressure loads during explosive combustion of hydrogen-air mixtures with concentration gradients cannot be assessed by concepts that study a homogeneous mixture as worst-case scenario.
					0.3	33.3					

Table 3.2 Cont'd

Reference	**Experimental conditions**	**Obstacle Type**	**BR (-)**	**Obstacle scale, b (m)**	**Obstacle spacing, x (m)**	**x/b (-)**	**P_{max} (bar)**	**S_{fmax} (m/s)**	**$(x/b)_{max}$ (-)**	**Conclusion**	**Comment**
Present research	Geometry: An elongated tube of 162 mm diameter with an L/D of 27.7 closed at one end. The opened end was connected to 50 m^3 cylindrical dump vessel. Mixture: 10% CH_4 by vol. Ignition: Spark ignition at the end of the closed tube.	2 orifice plates	0.3	0.033	0.5-2.75	15-83	2.68	486	53	A worst case separation distance was found to be 1.75 m which produced close to 3 bar overpressure and a flame speed of about 500 m/s. These values were of the order of twice the overpressure and flame speed with a double obstacle separated 2.75 m apart.	The profile of effects with separation distance was shown to agree with the cold flow turbulence profile determined in cold flows by other researchers.

3.4 Gas Explosion Scaling

In order to replicate large-scale overpressure at small scale, it is required to reproduce the flame speeds at the same relative position in the rig since $P \propto S_f^2$ in VCE. Most gas explosion tests from inception were conducted in small scales. The relatively low costs and environmental impact of the reduced-scale experiments made them an attractive choice. It was shown by van Wingerden *et al.* (1994) that flame speeds and overpressures generated in undersized-scale experimentations were lower than those produced on a large scale tests. This was as a result of the presence of hydrodynamical instabilities which influenced the initial flame speed propagation on large scale and also due to the effect of turbulent length scale on the burning rate.

As a consequence, scaling techniques are needed to relate small-scale test results with those that would be expected from the actual geometry. The effects of smaller scales can be compensated by increasing the reactivity of the mixture used at small scale either by using a more reactive fuel such as ethylene instead of methane (Taylor and Hirst 1989) or by oxygen enrichment of the gas-air mixture (Catlin and Johnson 1992).

The accuracy of these scaling techniques depends on the turbulent combustion models which were derived from small-scale experiments. The techniques apply only to the fast flames propagating through obstacle arrays. It could be applied to vented explosions but not to the propagation of deflagration to detonation transition (Taylor and Hirst 1989). A thorough review on the gas explosion scaling techniques and their applications to turbulent models was performed by Phylaktou and Andrews (1995).

Until now, there exist several experimental and theoretical methods in the literature on turbulent burning velocity models by a number of researchers. Among all the parameters that influence turbulent burning velocity (such as u', S_L, L_e, v, ℓ etc.), ℓ is the main determining factor in gas explosion scaling (Phylaktou 1993). Therefore scale of importance in turbulent combustion is not the whole size of the rig but rather the size of the turbulent generator as this determines the length scale, ℓ. In explosions the turbulence initiators are the obstacles and for grid plate obstacle or

similar the dimension that defines ℓ is the width of the solid materials between the holes (Baines and Peterson 1951). For a significant interpretation of results by most researchers from small scale tests and for application to actual size explosion hazards, the understanding of the influence of scale is necessary.

However, the information on the effect of scale is rare since most turbulent combustion studies have been performed in a fixed-size equipment (Phylaktou 1993). Also, experimental data of S_T operating in regimes of very high turbulence akin to gas turbines and explosions are scarce. This is due to the fact that tests at these conditions are not easy to perform in many aspects such as expensive equipment, high operating costs, intricate experimental arrangements and complex analyses methods. Furthermore, the turbulence-chemistry interactions at these conditions are very harsh and damaging to sensitive measuring equipment (which by intention have to be as non-intrusive as possible as otherwise they affect the measurements they are trying to make) and hence difficult to investigate. In order to resolve these problems, correlations for S_T based on less pricy experiments accomplished at reduced operating conditions with lower pressure, temperature and lean fuel concentrations are developed (Siewert 2006).

3.4.1 Review of S_T Models with Dependence on Scale, ℓ

Turbulence combustion models with dependence on scale, ℓ were reported by the following researchers: Ballal and Lefebvre (1975); Gouldin (1987); Bray (1990); Bradley *et al.* (1992); Phylaktou and Andrews (1995); Kobayashi *et al.* (1997); Zimont *et al.* (1998); Peters (1999); Shy *et al.* (2000); Filatyev *et al.* (2005); Dorofeev (2008); Driscoll (2008); Muppala *et al.* (2009) and Daniele and Jansohn (2012).

Table 3.3 shows an overview of the turbulent burning velocities models from the above researchers with dependendce on the characteristics length scale, ℓ. The dependence on ℓ exponent from the models ranged from 0.15 to 0.61. Even though, the variation is small in absolute terms, the resultant estimates, mostly overpressures are significantly different and could make a barrier between safe and unsafe design. The comparative increase in flame speed and overpressure estimated by the reviewed S_T models for a given factor (e.g. 30 fold) increase in scale was demonstrated in Chapter 7.

Table 3.3 A review on turbulent burning velocity models with dependence on integral length scale.

Reference	Methodology	Equation	Conclusion	Comment
Balal and Lefevre (1975)	Geometry: Side-wall transparent combustion chamber of 30 cm by 10 cm by 10 cm. Grids positioned upstream of the combustion zone were used as turbulence generators. Mixture: Premixed flammable propane-air mixtures of different equivalent ratios, ϕ at atmospheric pressure and temperature.	$\frac{S_T}{S_L} = \left[1 + 0.125\left(\frac{u'\ell}{\delta_L S_L}\right)^2\right]^{1/2}$ [3.1]	From the analysis of the results obtained, three distinct regions (based on the level of turbulence with region one been the lowest and three highest) were identified each having different characteristics in regards to the effect of scale on turbulent burning velocity.	The criterion for S_T in Eq. 3.1 is for $u' < 2S_L$.
Gouldin (1987)	Based on a fractal depiction of the geometry of rough surfaces applied to flamelets in premixed turbulent combustion at low to moderate levels of turbulence reaction.	$\frac{S_T}{S_L} = R_\ell^{0.26}$ [3.2]	Equation 3.2 was tested and validated by the author against data from experimental source with high turbulence level of Re up to 40,000.	Taylor and Hirst (1989) implemented this essential model of turbulent combustion in the devising of a scaling technique relevant to gas explosions.
Bray (1990)	The S_T correlation was based on laminar flamelet model of premixed turbulence combustion based on Bray-Moss-Libby BML model of turbulent combustion.	$\frac{S_T}{S_L} = 1.8\left(\frac{u'}{S_L}\right)^{0.412}\left(\frac{\ell}{\delta_L}\right)^{0.196}$ [3.3]	The author pointed out that the studies of S_T by other investigators were equal to each other and were applicable to flames propagating into a uniform turbulent medium.	Currently, this correlation is incorporated into a CFD code called Flame Accelerator Simulator (FLACS) to model gas explosion.
Bradley *et al.* (1992)	The model was developed based on the correlation of huge set of experimental data from several origins as well as theoretical considerations of flame straining.	$\frac{S_T}{S_L} = 1.53 L_e^{-0.3}\left[\frac{u'}{S_L}\right]^{0.4} R_\ell^{0.15}$ [3.4]	Good agreement between predicted and measured value of S_T was achieved in the current method.	Catlin and Johnson (1992) applied this modelling technique to experimental scaling of gas explosions.

Table 3.3 Cont'd

Reference	Methodology	Equation	Conclusion	Comment
Phylaktou and Andrews (1995)	Geometry: Elongated confined vessels of 76 mm and 162 mm internal diameters corresponding to L/D of 22 and 26. Multi-hole grid plates were used to generate turbulence. Mixture: methane-air mixtures.	$\frac{S_T}{S_L} = 1 + 0.67\left(\frac{u'}{S_L}\right)^{0.47} R_\ell^{0.31} Le^{-0.46}\left(\frac{\nu}{\nu_a}\right)^{0.95}$ [3.5]	The model was validated against experimental data in the literature and it showed an outstanding agreement.	This is the pioneer turbulent model based on very high Reynolds number that is similar to real vapour cloud explosions.
Kobayashi *et al.* (1996)	Geometry: A nozzle-type burner of 20 mm outlet diameter installed in a high pressure chamber of 498 mm and 600 mm inner diameter and length respectively. Four perforated plates of 0.5 BR each but with variable hole diameters were used to generate turbulence. Mixture: A flammable methane/air mixture at ϕ of 0.9.	$\frac{S_T}{S_L} = R_\ell^{1/4}\left(\frac{u'}{S_L}\right)^{\frac{1}{2}} \sim \left(\frac{1}{p^{-1}}\right)^{1/4} . \left(\frac{1}{p^{-1/2}}\right)^{1/2} \sim p^0$ [3.6]	The S_T demonstrates that the turbulent flame speed is independent of pressure, or at least it is essentially a weak function of pressure if one takes into consideration that pressure exponent of laminar of laminar flame speed is not -0.5 precisely.	The authors examined the influence of elevated pressure up to 3.0 MPa on propagation and structure of turbulent premixed flames. Equation 3.6 was given by Siewert (2006).
Zimont *et al.* (1998)	The model was derived upon closed single transport equation using a model for turbulent flame speed Closure, TFC).	$\frac{S_T}{S_L} = Z.\, P_r^{1/4} R_\ell^{1/4}\left(\frac{u'}{S_L}\right)^{1/2}$ [3.7]	The constants P_r and Z are given as 0.71 and 0.52 respectively. The S_T model was found to be applicable to model flame propagation in laboratory (small scale geometry) as well as industrial burners.	Currently, the Zimont model is used in a CFD code FLUENT to model flame propagation in gas turbines.
Peters (1999)	G-equation approach followed by simplifications based on physically justified assumptions.	$\frac{S_T}{S_L} = \left(\frac{u'\ell}{S_L\delta_L}\right)^{1/2}$ [3.8]	Fair qualitative agreement was obtained when Eq. 3.8 was validated with the experimental work.	The discrepancy associated to this model was credited to both the experimental inaccuracy and scarce or imperfect theoretical assumptions (Siewert 2006).

Table 3.3 Cont'd

Reference	Methodology	Equation	Conclusion	Comment
Shy *et al.* (2000)	Geometry: The burner consisted of long vertical and horizontal vessels. The former provided a steady, downward-propagating premixed flame. The latter vessel was fitted with a couple of counter-rotating fans and perforated plates at each end to produce isotropic turbulence of high intensity. Mixture: Flammable methane and propane-air mixtures.	$\frac{S_T}{S_L} = 1 + 0.05\left(\frac{u'}{S_L}\right)^{0.39}\left(\frac{\ell}{\delta_L}\right)^{0.61} L_e^1$ [3.9]	Eq. 3.9 was based in terms of strain rates of turbulent premixed combustion over a broad range of Damkohler number, Da. The model is applicable to both corrugated flamelet to distributed regimes.	This model has the highest dependency on obstacle scale, ℓ reviewed in this research. The model is aimed to be useful to gasoline engines and atmospheric explosions.
Filatyev *et al.* (2005)	Geometry: Large 2D Bunsen burner. Mixture: Stoichiometric methane-air mixtures at atmospheric temperature and pressure.	$\frac{S_T}{S_L} = 1 + B_1\left[\left(\frac{u'}{S_L}\right) - B_2\left(\frac{u'}{S_L}\right)^2\right]^{1/2}\left[\frac{U}{S_L}\right]\left[\frac{\ell}{\delta_L}\right]^{1/2}\left[\frac{W}{\delta_L}\right]^{1/2}$ [3.10]	The constants, B_1 and B_2 in Eq. 3.10 are given as 0.002 and 0.16 respectively. The new properties were suitable for the prospect assessment of Direct Numerical Simulations, DNS and models.	The authors considered properties of S_T not reported previously, these properties include: local stretch rates, wrinkledness parameter, degree of flamelet extinction, reaction layer thicknesses, and Bunsen burner width, W.
Driscoll (2008)	Turbulent burning velocity was obtained using no modelling constants in Bunsen, spherical and V-flame geometries.	$\frac{S_T}{S_L} = 1 + 0.95 L_e^{-1}\left(\frac{u'}{S_L}\frac{\ell}{\delta_L}\right)^{0.5}$ [3.11]	Eq. 3.11 was based on the Bradley's correlation of S_T (1992) where the product of Karlovitz number and Lewis number was held constant.	The S_T model was aimed at determining realistic turbulent Re usually found in industries.
Dorofeev (2008)	The experimental set up was based on Kido *et al.* (2002).	$\frac{S_T}{S_L} = \left[\left(\frac{u'}{S_L}\right)^{1/2}\left(\frac{\ell S_L}{\nu}\right)^{1/6}\right]$ [3.12]	There exists a clear change in the S_T characteristics due to the addition of fuel between rich and lean mixtures.	This model improved the knowledge needed to predict the turbulent burning velocity in order to come up with a framework for appraising potential explosion hazards in hydrogen mixtures.

Table 3.3 Cont'd

Reference	Methodology	Equation	Conclusion	Comment
Muppala *et al.* (2009)	Geometry: Spherical-like chamber of 120 mm internal diameter with four obstacle-plates of 100 mm diameter each and positioned on each side of the geometry. A fan was situated behind each perforated plate. This is to ensure efficient mixing of gases. Mixture: The flammable mixtures for CH_4–H_2 and C_3H_8–H_2 were prepared in a way that similar S_L of 0.25 m/s was obtained for each hydrocarbon-hydrogen blends.	$S_T = S_L\left[1 + 0.46R_\ell^{0.25}\left(\frac{u'}{S_L}\right)^{0.3}\right]$ [3.13]	The S_T model validated the available experimental measurements.	This is one of the few studies that addressed the effect of the use of hydrogen.
Daniele and Jansohn (2012)	Geometry: Combustion chamber of 320 mm length and an inner diameter of 75 mm with optical access. Mixture: A flammable syngas-air and methane-air mixtures were used. The tests were performed at pressures up to 2.0 MPa and inlet temperatures up to 773 K.	$\frac{S_T^{0.05}}{S_{L,0}} = 337.5\left(\frac{u'}{S_{L,0}}\right)^{0.63}\left(\frac{L_T}{\delta_L}\right)^{0.58}\left(\frac{P}{P_R}\right)^{0.63}\left(\frac{T_0}{T_R}\right)^{-0.63}$ [3.14]	The experimental output showed that the ratio of S_T to S_L was found to rise with increasing hydrogen content in the fuel mixture and with pressure. Also, comparison between various syngas mixtures and methane noticeably displayed much higher S_T/S_L for the former fuel.	This model was due to clear lack of data and understanding of the behaviour of turbulent flames at elevated temperature and high pressure particularly regarding hydrogen comprising fuels.

3.5 CFD Modelling

Computational Fluid Dynamic, CFD is a computer-based simulation which involves the study of systems involving fluid flow, heat transfer and related phenomena such as chemical reactions. Complex flows are mostly turbulent in nature and can be tackled numerically with the aid of CFD methods. This method covers an extensive range of industrial and non-industrial applications such as: aerodynamics of aircraft and vehicles such as lift and drag, cooling of electrical and electronic equipment, distribution of pollutants and effluents, weather prediction, combustion in internal combustion engines and gas turbines, blood flows through arteries and veins, hydrodynamics of ships among others (Versteeg and Malalasekera 2007).

For a CFD model to be useful, it must have the following qualities: broad applicability, accurate, simple and economical to run (Bakker 2006).

Currently, there are many CFD-based explosion models in use. These include: FLACS, AutoReagas, EXSIM, CFX-4, COBRA, REACFLOW, NEWT etc. (Lea and Ledin 2002).

However in this research, FLACS code is used to model gas explosions in the presence of obstacles as usually found in process industries. The choice for this code is as a result of the partnership between the developers and our Research group.

3.5.1 Common Terminologies in CFD/FLACS

There are common terminologies used in CFD/FLACS and these include the following:

- Domain: this is sometimes called computational domain or analytical domain. It is a geometrical region within which a simulation is carried out.
- Grid/mesh: a process in which the computational domain is divided up (discretisation) into a number of cells or elements defining the discrete points at which the numerical solution is solved. The points are usually the cell centres or cell vertices.
- Finite volume method (FVM): a computational technique in which the computational domain is partitioned into a finite number of control volumes from which discretised governing equations are resolved.

- Governing equations: the mathematical equations that define the physics of the flow under study. These are the conservation equations of mass, momentum and energy.
- Navier-Stokes equations: the momentum equations for viscous flow.
- Reynolds Averaged Navier Stokes (RANS): a form of the Navier Stokes equations in which extra terms are involved to account for the time averaged effects of turbulence.
- Turbulence models: collections of equations that govern the transport of turbulence in the mean flow equations. They are established on theories about turbulent practices and normally need important empirical input in the form of constants or functions. The models simulate only the influence of turbulence on the mean flow behaviour and not the details of the turbulent motions (turbulent eddies). This is otherwise known as the RANS approach.
- Two-equation model: a turbulence model that applies two transport equations to simulate the influence of turbulence in the RANS equations.
- $\kappa - \varepsilon$ turbulence model: a two-equation turbulence model expressed by the theory of eddy-viscosity where the influence of turbulence is monitored by the turbulent kinetic energy, κ of the fluid and the rate of energy dissipation, ε.
- Sub-grid model: a model that is used to generate turbulence from sub-grid objects. For instance, when an obstacle in geometry is smaller than the size of a single grid cell.

3.6 Objectives of the Present Research

As stated in Chapter 1, gas explosions in the presence of obstacles produced higher overpressures (level of damage) compared to obstacle free explosions. The obstacles tend to wrinkle the propagating flame and make it more turbulent thereby increasing the reaction front area and the burning rate and hence the expansion rate and overpressure. In addition to combustion chemistry, obstacle blockage ratio, type, shape, number, location and spacing are the obstacle parameters affecting gas explosions severity. The spacing between obstacles was identified as a parameter that received less attention by gas explosion researchers despite its known existence.

It was shown in Chapter 2 that in practice, many obstacles can be treated as grid-plate obstacles, and there have been several explosion studies using grid plates. However, the outcomes from these works are of restricted application due to the fact that the data are

not offered in terms of fundamental turbulent flow and combustion parameters, as these factors are mostly hard to measure under harsh transient conditions. The limited data on measurements of intensity of turbulence immediately downstream of obstacles from a steady-state flows where maximum overpressure is expected to occur were shown to be valid and applicable to explosion induced transient flows by gas explosion researchers.

Based on the above hypothesis, a model was developed in this research to predict the explosion-induced maximum turbulent intensity and its relative position downstream of an obstacle.

The comprehensive review performed in this chapter on gas explosions studies with multi- obstacles having both fixed and variable spacing revealed that the bulk of the investigators spaced their obstacles at short distances of not more than ten obstacle scales. Most of the experiments reviewed with respect to obstacle spacing had not given any justification to the obstacle separation distance used. Also, no systematic studies of the influence of obstacle separation distance exist in the literature.

As a consequence this project addressed the effect of obstacle separation distance on gas explosions by varying the spacing between obstacles systematically in order to determine the worst case separation that will produce the maximum explosion severity (overpressure). The objectives of the project were as follows:

- To apply the correlations obtained from cold flow turbulence to guide the design of experiments for this project.
- To investigate the influence of obstacle separation distance on different types of obstacles (hole-grid, bar-grid and baffle disc), obstacle blockage ratio, obstacle scale and number of obstacles.
- To investigate the influence of mixture composition using methane, propane, ethylene or hydrogen with air on obstacle spacing.
- To develop an S_T correlation with dependence on ℓ from the experimental work of this research and validate it with the limited large scale data applicable to real industrial set-up.
- To use a CFD code FLACS (Flame Accelerator Simulator) to study the influence of obstacle spacing and to validate the results with that of the present experimental research.

Chapter 4

Experimental Set-up and Measurement Techniques

4.6.4 Ignition Failure of the Fuel-Air Mixtures

4.1 Gas Explosions Facilities

The venue for the explosion tests was Room B11 of energy building, and it was labelled “Explosion Hazards-High Pressure Test Facility”. In order to ensure optimum safety of the experimentalist and that of others, Room B11 was partitioned by concentre walls into two areas namely: Test room and Control room. Entrance between the two rooms was by means of an interlocked door which was an integral part of the safety system controlling the ignition circuit. The Test room housed the dump vessel, test vessels, instrumentation equipment and data logging hardware. The Control room accommodated a computer network which was linked to the data logger electronically.

The major pros of performing gas explosion experiments indoors compared to field scale tests are to prevent the former from adverse weather effects; save cost, protect the environment from pollution and to carry out small scale tests which can later be scaled to large industrial sizes. This technique of scaling was discussed in details in Chapter 7.

A test vessel of 162 mm in diameter was constructed from a 0.5 m flanged pipe sections separated by 3 mm thick asbestos fibre type gaskets having an L/D of 26.1. Previous researchers Phylaktou (1993) and Gardner (1998) used this geometry to carry out gas explosion tests with single obstacles of various configurations. The former researcher integrated an end plate at the vessel end opposite to the ignition point. The total vessel confinement caused a highly oscillatory waveform of large amplitude to be generated. This was as a result of the continuous reflection of pressure waves between the vessel end walls. The waves were superimposed on the major pressure records and impeded their successive analysis. The latter author used the geometry with an open-end opposite to the ignition source to allow free movement of gases towards the vent without hindrance to the generated flame speeds.

The present research was intended to investigate the effect of transient turbulent vented gas explosion in the presence of repeat of obstacles at regular interval as commonly found in industrial sites. The outcome of this research would be related to vapour cloud explosions where the initial pressure is near to atmospheric. Also, the current research represents gas explosions in large L/D end-vented vessels. The

results are expected to offer much needed data to be applied in formulating guidelines/standards aimed at industries dealing with flammable gas-air mixtures.

4.1.1 Test Vessel

The 162 mm internal diameter test vessel section was made up from eight existing pipe sections of 0.5 m long each. An extra pipe section of close to 0.25 m long of similar diameter was incorporated into the other pipe sections in order to have various options to obstacle spacing. All the pipe sections were originally manufactured by Vierod and Woods Ltd, Bradford. A shell wall thickness of about 3.4 mm was calculated so that the vessel could withstand any possible detonation combustion which is likely to occur in the presence of obstacles. In order to allow for instrumentation such as thermocouples, pressure transducers and other supportive equipment to be fixed, each pipe section was bored with a tapped bosses welded on at position axially. A detachable blind flange positioned near one end of the pipe sections was drilled and tapped centrally to enable a spark plug to be fitted. Figure 4.1 and Table 4.1 show the drawings of a pipe section and major dimension and pressure ratings respectively for the test vessel.

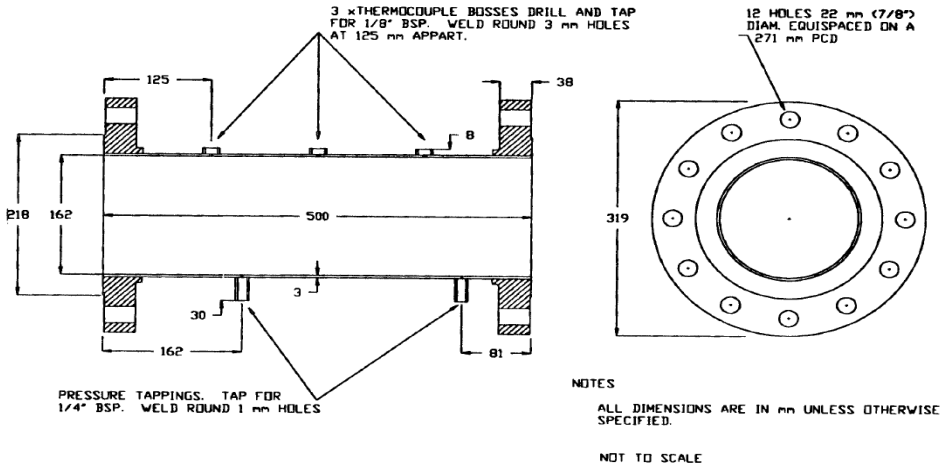

Figure 4.1 Scaled drawing of one pipe section (left) and a blind flange (right).

Two fixed fabricated frames made from mild steel were used to support the vessel. The test pipe sections rested on the V-shaped sections which were welded to threaded rod positioned in the tapped fittings on the support frame. This changeable arrangement enabled quick substitute of obstacles without main vessel disassembling. The open-end vented test vessel demanded a method of isolation

during mixture preparation with the aid of a closed pneumatically gate valve. The gate valve was fastened between the flange of the open-end test vessel and the flange of the dump vessel opening.

Table 4.1 Important design parameters for 162 mm internal diameter test vessel.

Design Detail	**Units**	**Value**
Pipe Sections		
Nominal internal diameter	mm	162
Nominal section length	mm	500
Number of sections	-	9
Wall thickness	mm	3.4
Design pressure	bar	35.5
Flanges		
Class	-	300
Flange thickness	mm	36.5
Number of bolts	-	12
Bolt-hole diameter	mm	22
Bolt-hole PCD	mm	269.9
Diameter of bolts	mm	19
Assembled test vessel		
Hydraulic pressure rating	baro	30
Length to diameter ratio, L/D	-	27.7
Test vessel volume, V_t	m^3	0.0925
Total system volume,V_T = V_d + V_t (V_d = dump vessel volume)	m^3	50.1
V_d / V_t	-	541

4.1.2 Dump Vessel

The test vessel was connected to an existing cylindrical dump vessel with dished ends. This was to ensure that harmless vented explosion of both burnt and unburned gases were conducted in the laboratory prior to vessel purging. The dump vessel was made up of two connected sections of various lengths and diameters. The bigger section had its nominal diameter and length as 2.5 m and 8 m respectively. The other

section was having a diameter of 1.6 m and a length of 6.3 m. This enabled the dump vessel to have a total volume of about 50 m^3. The dump vessel was initially designed locally, but, the final design, fabrication and commissioning was done by Hustlers of Yeadon Ltd, Leeds (Gardner 1998). Figure 4.2 shows a schematic diagram of the dump vessel.

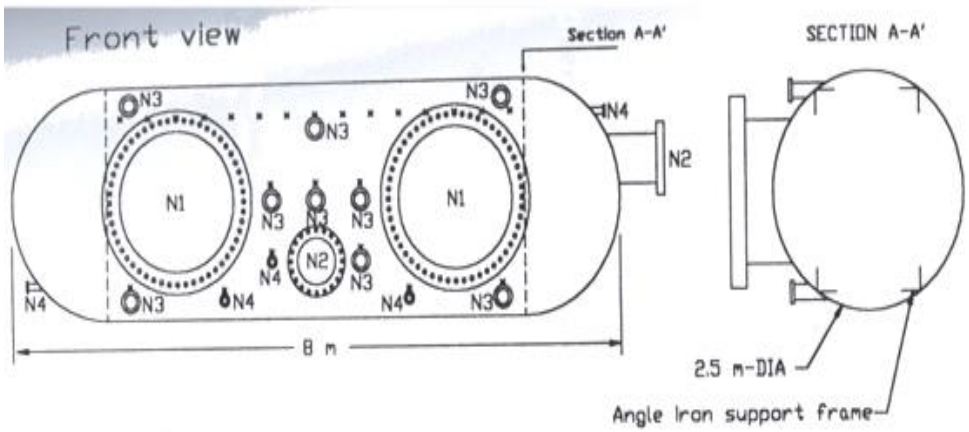

Figure 4.2 Schematic diagram of a dump vessel (Gardner 1998).

As shown in Fig. 4.2, the dump vessel was designed and provided with five different flange opening diameters (N1-N5). This would enable test vessels of various open-hole diameters to be connected to the dump vessel. Any flange opening not in use was fitted with blank end-plates for safety reasons.

For an efficient simulation of open-to-atmosphere gas explosion, the dump vessel had little or no influence on the explosion propagation in a test vessel. This was achieved as the internal diameter and length of the dump-vessel produced a volume much greater than that of the test vessel by a large factor of 541 as shown in Table 4.1. Table 4.2 gives the major design parameters of the dump vessel.

Table 4.2 Major design parameters for 50 cubic metres dump vessel.

Assembled structure	**Units**	**Value**
Design pressure Certified pressure (hydraulic test)	bar baro	9 11.25

Flanged openings						
Type	**Nominal bore (mm)**	**Neck thickness**	**Flange**	**Number of bolts**	**Bolt-hole PCD (mm)**	**Rating**
N1	1524 O/DIA	20 Plate	Special	52	1759	Special
N2	508 O/DIA	10 plate	RFSO	20	635	BS EN 1092-2
N3	162	SCH 40	RFSO	12	269.9	BS EN 1560 Class 300
N4	76	SCH 40	RFSO	8	168.3	BS EN1560 Class 300
N5	¼" BSP	COUPLING				Special

Figure 4.3 shows a complete experimental set-up where the test vessel was connected to a dump vessel. Also, shown is the thermocouples and pressure transducers instrumentation attached to both vessels. Gate valve is placed between the two vessels and opens only just prior to ignition.

(a)

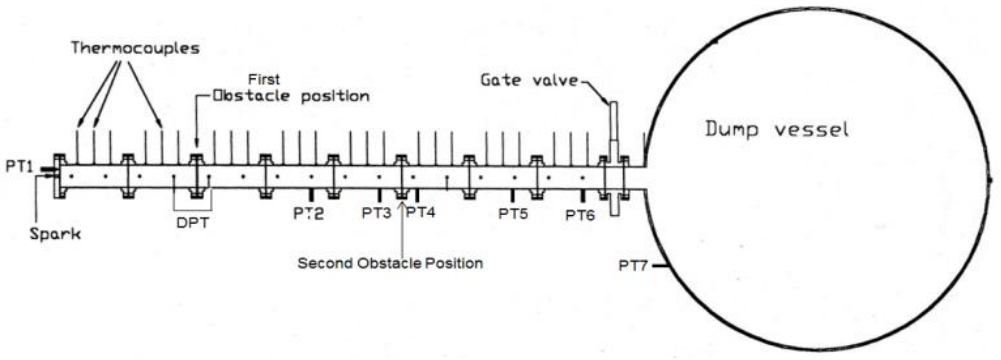

(b)

Figure 4.3 Experimental set-up (a) Photograph (b) Schematic diagram.

4.2 Obstacle Design

In the present research, obstacles were used to generate turbulence thereby increasing the mixing capacity of a given flow. For a constant test vessel size, the scale of any obstacle pattern is best described by its blockage ratio, a range which varies from zero for no screen at all to unity for a solid plate. By varying the obstacle blockage ratio and its shape, the turbulent length scale was varied. A repeat of obstacles having low blockage of up to 40% was used. The low blockage ratio obstacles where chosen in order to prevent detonation from occurring.

4.2.1 Hole-grid Plate

In its easiest appearance, an orifice plate is a thin flat plate with a single hole at the centre (concentric orifice). Single-hole plates are widely used in industries as flow straighteners and flame stabilisers in combustion systems. For a single-hole grid plate perpendicular to and facing towards the direction of flow, an obstacle blockage ratio, BR is defined as the ratio of the blocked area to the total flow area, A_2. Mathematically, blockage ratio is given as,

$$BR = 1 - {A_1}/{A_2} \tag{4.1}$$

where A_1 is the cross-sectional area of the orifice plate. Figure 4.4 gives the schematic diagram of a single-hole perforated plate.

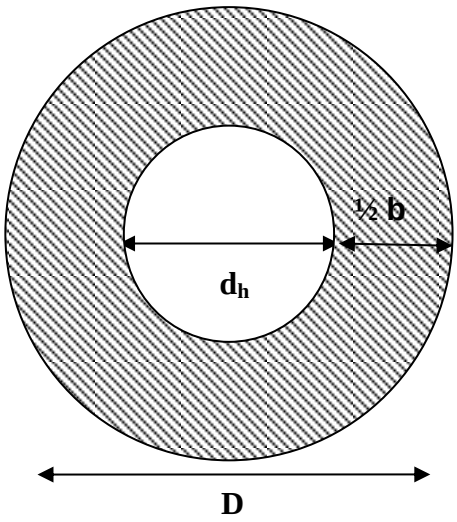

Figure 4.4 A simple diagram of an orifice plate.

In case of multi-hole diameter grid-plate with holes of equal diameter, its blockage ratio is,

$$BR = 1 - N_h\left(\frac{d_h}{D}\right)^2 \tag{4.2}$$

where N_h is the number of holes, d_h is the hole diameter and D is the diameter of the open flow area.

A single-hole orifice plate was considered as part of an imaginary larger array, the width of the solid material, b (obstacle scale) according to Baines and Peterson (1951) is specified as,

$$b = D - 0.95d_h \tag{4.3}$$

4.2.2 Flat-bar Grid Plates

Multi flat-bar plates represent a usual array of pipework mostly found in an offshore module spread all over an open region. A gas flow through such region would diverge and pass through into stream around individual obstacle. For the purpose of maintaining the blockage ratio of a bar type obstacle fixed, the width of the bar was decreased as the number of bars, N_b increased. The bar width was the characteristics obstacle scale, b and was equivalent to the solid width for a single-hole obstacle. This technique of altering the obstacle scale was used for blockage ratio of 20% only. Figure 4.5 shows a detailed diagram of single flat-bar obstacle.

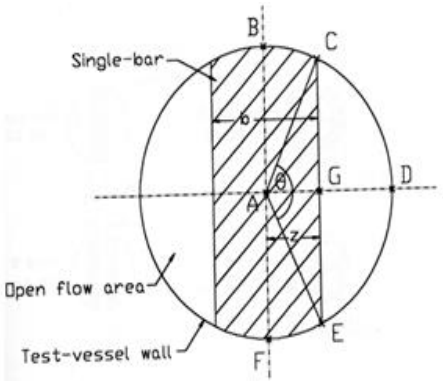

Figure 4.5 Detailed diagram of a single flat-bar obstacle (Gardner 1998).

As demonstrated by Gardner (1998), the computation of the bar width entailed an iterative procedure where the easiest calculation was for a single-bar obstacle of a given blockage ratio with indication to Fig. 4.5. Therefore, the width of the bar otherwise known as obstacle scale was given as,

$$b = 2z \tag{4.4}$$

4.2.3 Baffle Disc Obstacles

For a circular disc placed centrally across the flow area,

$$BR = d_d/D \tag{4.5}$$

where d_d is the disc diameter and represented the obstacle scale, b. Discs with a blockage ratio of 0.2 were tested for the test-vessel.

A simple method was used to insert the obstacles between two pipe sections of the test vessel without constraint to conform to the existing arrangements. The obstacle plate diameter was designed to be as big as the diameter of the circle formed by the inner edges of the flange bolt-holes (see Fig. 4.4). The test vessel was always used in the horizontal position and the following procedure was used to position the obstacle plates: The two pipe-section flanges between which the obstacle would be positioned were placed about 10 mm apart. They were then connected by two stainless steel pins having the exact diameter as the flange bolt holes. These pins were inserted through bolt holes at the bottom half of the flanges, one at each quarter. The hole-plate obstacle sandwiched with gasket (to minimise leakage) was inserted from the top and allowed to drop onto the locating pins, thus coming to rest at the exact position at which it should be secured. Bolts were then inserted through the other boltholes and tightened with nuts, bringing the flanges together and

securing the obstacle. The locating pins could then be replaced by bolts. This same procedure was applied to insert the flat-bar and disc baffle obstacles. However, the former was secured within two recess plates prior to sandwiching with two gaskets. Figure 4.6 shows all the obstacle configurations used in the current research.

For all tests in the present research, the first obstacle was positioned 1 m downstream of the spark while the second obstacle's position was varied from 0.25 m to 2.75 m downstream of the first obstacle in order to obtain the worst case obstacle spacing. For the triple obstacle tests, the first two obstacles were kept at the established worst case spacing and only the spacing between second and third obstacles was changed systematically.

(a) 1-16 hole

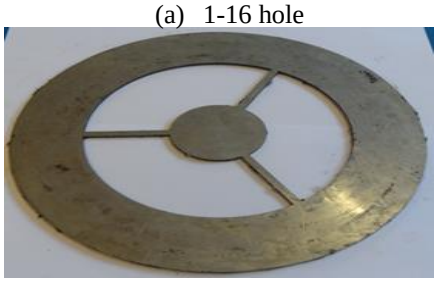

(b) Baffle-disc

(c) 1-4 flat-bar

Figure 4.6 Obstacle configurations used in the current research.

Table 4.3 summarises the designed obstacle parameters for hole, flat-bar and disc obstacles respectively. The metal thickness, t for all the obstacles was 3.2 mm. This

value was used in conjunction with the open flow area diameter to obtain an aspect ratio, t/d. The t/d was later used to determine the obstacle pressure loss coefficient, K for thin/sharp obstacle for t/d < 0.6 as given in Eq. 2.16.

Table 4.3 Basic design parameters for the obstacles used in this research.

Shape	**BR**	**N_b/N_h**	**t/d**	**K_{ob}**	**b**	**ℓ**
(-)	**(-)**	**(-)**	**(-)**	**(-)**	**(mm)**	**(mm)**
Hole-type	0.2	1	0.02	0.26	24.4	12.2
”	0.3	1	0.02	0.76	33.2	16.6
”	0.4	1	0.03	1.80	42.8	21.4
”	0.4	4	0.05	1.80	22.0	11.0
”	0.4	16	0.10	1.80	5.4	2.7
Flat-bar	0.2	1	0.05	0.26	25.6	12.8
”	0.2	2	0.11	0.26	12.8	6.4
”	0.2	4	0.17	0.26	6.4	3.2
”	0.3	1	0.05	0.76	38.5	19.3
Baffle-disc	0.2	-	0.03	0.26	58.2	29.1

4.3 Instrumentation and Data Acquisition

In gas explosions analysis, maximum overpressure, flame speed and rate of pressure rise are the most important parameters to be considered. The first parameter determined the level of damage caused by the explosion. The relative position of flame to a fixed observer and how fast the maximum overpressure is attained are determined by the second and last parameters respectively. Pressure transducers had been used by most researchers to measure the gas explosion pressure. Therefore, the present research made use of the transducers for the same purpose. Meanwhile, flame speed for a known distance had been calculated using flow visualisation technique with the aid of high speed camera (Starke and Roth 1989). Due to safety consideration, this practice was not feasible in the current research work because of high pressure expected to be generated. As such, thermocouples were used to measure the flame speed. The data from all the instrumentations were collected using a high speed data collection system for subsequent analysis.

4.3.1 Pressure Transducers

Explosion overpressures were measured in the present research using Keller type-PAA/11 piezo-resistive pressure transducers. These instruments were positioned in the drilled hole of the test and dump vessels via threaded bosses welded to it. Thus, the instruments became an essential part of the test apparatus and therefore subjected to the same internal pressure. This necessitated the transducers to be tough enough to survive explosion pressure without loss of sensitivity. The highly sensitive, stable and resistance to shock and water transducers had a 5 bar measurement range with a maximum pressure rating of about 10 bar.

The test vessel and dump vessel pressure histories were recorded using an array of 8 Keller-type pressure transducers - 7 gauge pressure transducers (PT1to PT7) and 1 differential (DPT), as shown in Fig. 4.3. Wall static pressure tapping measured by a differential pressure transducer (DPT) were located at 0.5D upstream and 1D downstream of the first obstacle as specified by BS5167-2 (2003). Pressure transducers, PT3 and PT4 were positioned 0.5D upstream and 1D downstream of the second obstacle and they were used to obtain the pressure differential across these obstacles. For the third obstacle tests, PT2 and PT5 (0.5D and 1D upstream and downstream respectively) were used to measure the pressure drop across such obstacles. These measured pressure drops enabled the calculation of the explosion induced gas velocity through each obstacle by treating the obstacle as an orifice flow meter. PT1 and PT6 pressure transducers were positioned permanently at the ignition position-end flange and end of the test vessel (25D from the spark) respectively. The pressure history in the dump vessel was measured using PT7 positioned as shown in Fig. 4.3.

4.3.2 Thermocouples

Exposed junction, mineral insulated type-K thermocouples were positioned in the course of a propagating flame in order to record the time of its arrival as a change in voltage potential across the junction. The flame arrival at each thermocouple triggered an abrupt increase in the thermocouple's temperature which was translated to a distinct change in the gradient of the output signal. The precise time of the flame arrival was then easily read off the computer screen with the aid of a digital readout cursor. From these time records and from the knowledge of the spacing

between the thermocouples, the average flame speed between any two thermocouples was calculated. It should be emphasised, however, that the aim was not to measure the flame temperature but rather to detect the change in temperature due to the flame arrival.

This method was validated by comparing with photographic records of explosions in a closed vessel by Herath (1986). Kumar *et al.* (1989) also applied this method to detect flame arrival in hydrogen explosions. It is perhaps the only technique for detecting hydrogen flames which have no ionisation and low luminosity.

The main body of the thermocouple had a diameter of 3 mm and positioned through the wall of the vessel so that the exposed 0.6 mm diameter conduction wires were on the test vessel centreline. This subjected the thermocouples to a high dynamic loads resulting from impact by high gas velocity flow prior to and after flame arrival. The test vessel was fitted with up to 24 thermocouples along its length with the aid of threaded Swage lock compression fittings to seal the units in tapped bosses. Also, support structures were fabricated into the vessel so as to prevent the thermocouples from bending and to preserve their exact positions.

Average flame speed allocated to the midway position between two thermocouples was obtained by dividing the distance between two thermocouples by the difference in time of flame arrival. However, this method of flame speed calculation was only possible for raw data from the thermocouples upstream of the obstacle (Gardner 1998) . Throughout this period, the speeds were little but, the reverse was the case downstream of an obstacle. The author pointed out that high levels of turbulence were assumed to have piloted to flame fragmentation. At a given position, downstream thermocouple recorded flame arrival at or prior to the time it was recorded at adjacent upstream thermocouples. Using the flame speed technique mentioned above, either high or negative flame speeds could be calculated at some points. In order to extract significant results, a smoothing technique was employed to exclude the excessive flame speed variations.

Figure 4.7 shows a plot of dimensionless flame position against time of flame arrival for a slightly rich methane-air (10% by vol.) mixtures using double 1-flat-bar obstacle of 0.2 BR spaced at 2.25 m. The data points were obtained from the thermocouple measurements between the obstacles and the test vessel exit (TC7-

TC24) where fast flame speeds were produced. The four data series shown signify the consecutive smoothed values using the technique given by Gardner (1998). Figure 4.8 shows a plot of flame speeds measured from the four data series against the flame position. A fluctuated flame speed and a maximum value of about 1,300 m/s were attained from the raw flame speeds data. In case of primary smooth data series, the calculated flame speeds followed similar trend as the raw flame speeds but with lower magnitude and less fluctuations between the neighbouring positions. This method of smoothing over the consecutive thermocouple positions was reiterated until the maximum resulting flame speed was lower than +/- 10% of the maximum calculated from the previous smoothed flame position data series. The third degree smooth data series in Fig. 4.7 gives the flame speed profile in Fig. 4.8 that satisfies this criterion for this specific test. As it will be seen in Chapter 5, the smoothed flame speeds from the above technique were used to predict an explosion overpressure and compared with that obtained from the experiment using a pressure transducer. Good agreement between the two sources of overpressure measurements was attained.

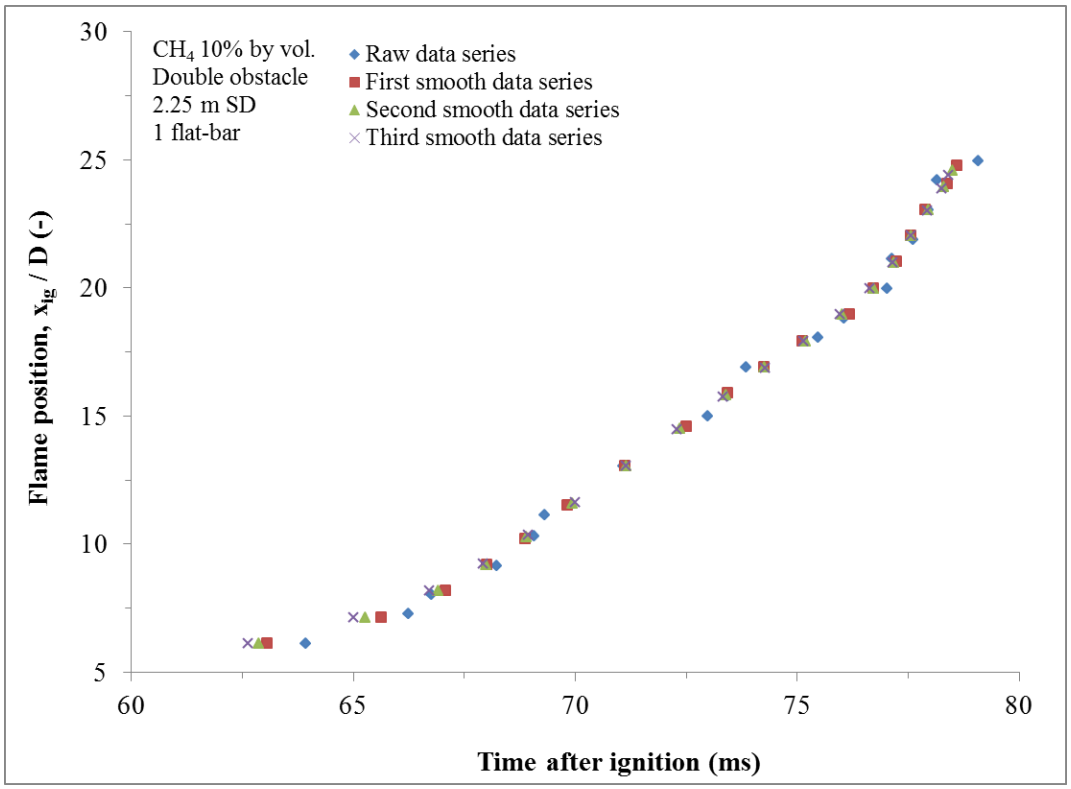

Figure 4.7 Flame position against time of flame arrival from the thermocouples for different smoothing levels.

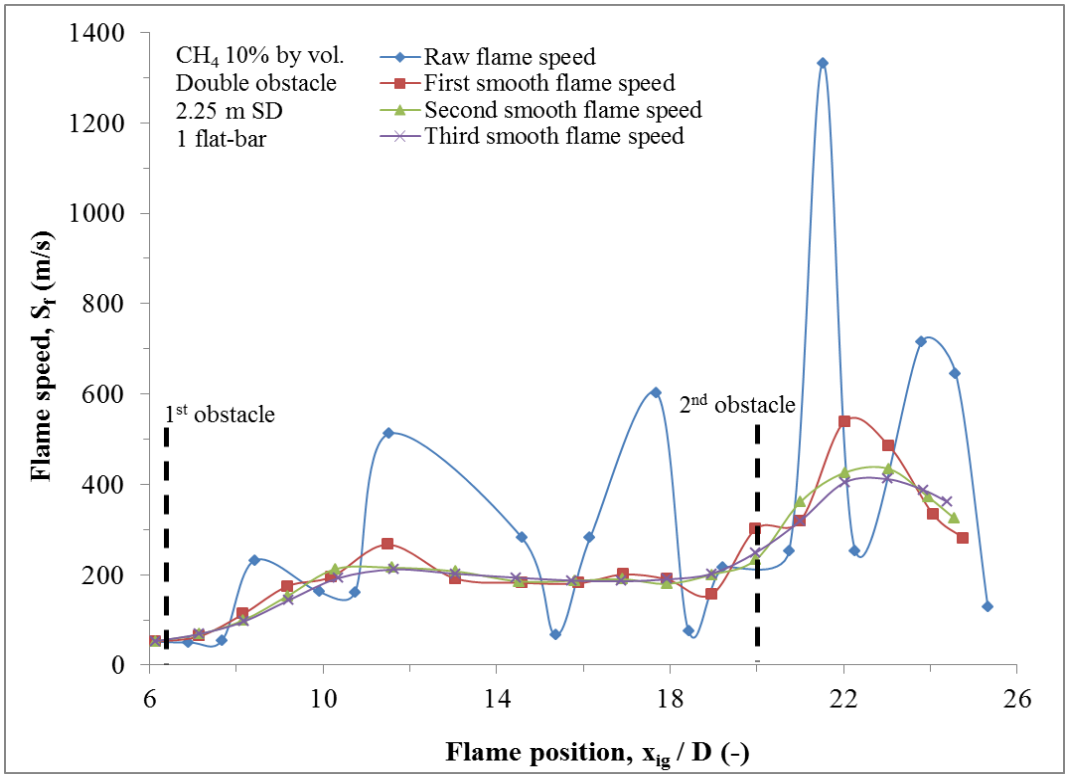

Figure 4.8 Measured flame speeds against flame positions for different smoothed flame speed levels.

4.3.3 Auxiliary Instruments

Auxiliary instruments were used before and after conducting the gas explosion tests. Some of the vital instruments belonging to this category include: pressure monitoring system, gate valve, vacuum pump, ignition system etc.

4.3.3.1 Pressure Monitoring System

The test vessel pressure during mixture preparation was monitored using an existing Diametric type 600 Barocel pressure sensor. In order to observe the mixture pressure at all times, its component were fitted into the test vessel filling line circuit. Its mode of operation, benefits and technical data were given by Boc Edwards (2013). The system was also linked to a Diametric type 1500 digital pressure display. This combination of both analogue and digital display enabled the mixture to be monitored with high accuracy, stability, over a broad range of input pressure. A standby pressure gauge of 0-2 bar parallel to the Barocel sensor was provided for safety concerns in case the main Barocel fails.

4.3.3.2 Vacuum Gate Valve

A pneumatically operated VAT Series 12.1 vacuum gate valve with shaft feed through was used to isolate the test vessel from dump vessel during the mixture preparation. The gate valve was made from a light aluminium metal. Its operation was controlled by a solenoid valve in the air supply line by means of on/off switch on the ignition panel.

4.3.3.3 Vacuum Pumps A and B

Vacuum pumps were used to evacuate flammable burnt and unburned mixtures for both test vessel (vacuum pump A, Edwards E1M18) and dump vessel (vacuum pump B, E2M175). The vacuum pump A is a single direct-drive revolving pump having a 340 L/min displacement rating. A completely covered fan-cooled motor was to provide a straight drive to the pump. An on/off switch situated on the pressure monitoring panel was used to control the pump. A vacuum pump B is an oil-sealed pump meant for dependable long term operation in both laboratory and industrial sites. The pump has a 2967 L/min displacement capacity. This is about 8.7 times higher than vacuum pump A. The pump is water cooled and it was powered by means of a mains isolation valve and soft-starter.

4.3.3.4 Recirculation Pump

An R95 EPM recirculation pump with 18 L/min capacity was used to circulate the mixture in order to ensure good mixing between the fuel gas and air. Since the volume of the test vessel accommodating the combustible mixture was about 93 litres, one volume air change occurred in about 5 minutes. Prior to ignition, the flammable fuel-air mixtures were allowed to circulate for at least four air changes. Therefore, the pump was able to hold flammable fuel-air mixtures devoid of likelihood of ignition which could be caused by the pump motor. The pump was controlled by the on/off switch on the ignition panel situated in the Control room.

4.3.3.5 Ignition System

A conventional car spark plug of 16 J was used to ignite the flammable mixture in the test vessel. The spark energy was conveyed via a high-capacitance discharge circuit which goes along with a range of safety links built-in in the ignition power

circuit. As shown in Fig. 4.9, the system warranted that prior to effecting the spark ignition; the following actions which could be confirmed by indicator lights in the Control room were carried out:

- The recirculation pump must be switched off so as to eliminate any increase in explosion severity likely to occur due to ignition of flowing mixture.
- The gate valve separating test vessel from dump vessel must be opened to enable a vented explosion to be carried out and not closed vessel if the valve is not open.
- The linking door between the Control room and Test room must remain closed and locked to save the experimentalist in case of any unforeseen danger during explosion.
- Disconnecting the test vessel from the mixture inlet line in order to guarantee appropriate separation of fuel supply.

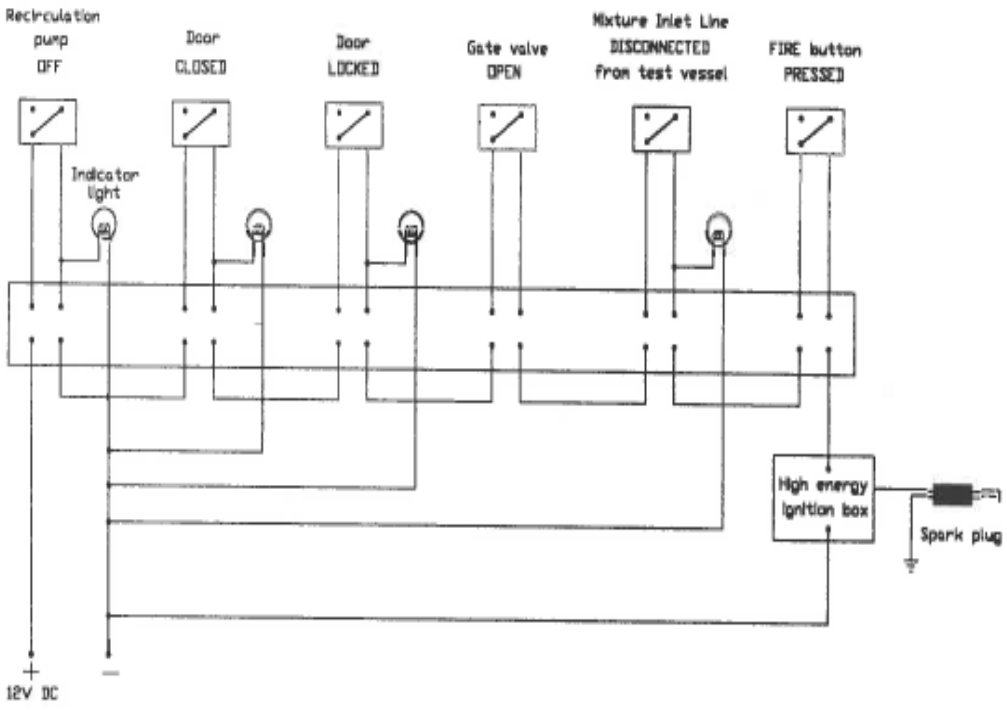

Figure 4.9 Ignition safety interlock circuit (Gardner 1998).

4.3.4 Data Acquistion

The short duration of a transient gas explosions indicated that accurate analysis is required for high speed data collection from a range of instruments positioned all over the test vessel. Processing of the large amount of recorded data was aided by special analysis software. Windspeed Wavecap software package was used to synchronise the initiation of data capture and the time of ignition. This software allowed certain parameters like sampling frequency, pre and post trigger sampling times to be changed.

Pressure transducers and thermocouples were connected to a 34-channel Microlink 4000 system. This was a modular data acquisition system specifically intended for high speed waveform capture with a sampling frequency of about 200 KHz for each channel. The system oversaw the 34 analogue inputs involving thermocouples and pressure transducers. Analogue to digital conversion was through a 12 bit ADC, giving a resolution of one part in 2^{12}. The voltage capacity range of the pressure transducers is 0-100 mV with a resulting transducer resolution of ± 1.2 mbar for pressure measurement range of 0-5 bar. The digital data stored was conveyed to the computer network in the Control room. Subsequent signal conditioning and analysis are performed with the aid of Famos software.

Figure 4.10 shows a schematic diagram of the experimental set-up and the instrumentation techniques.

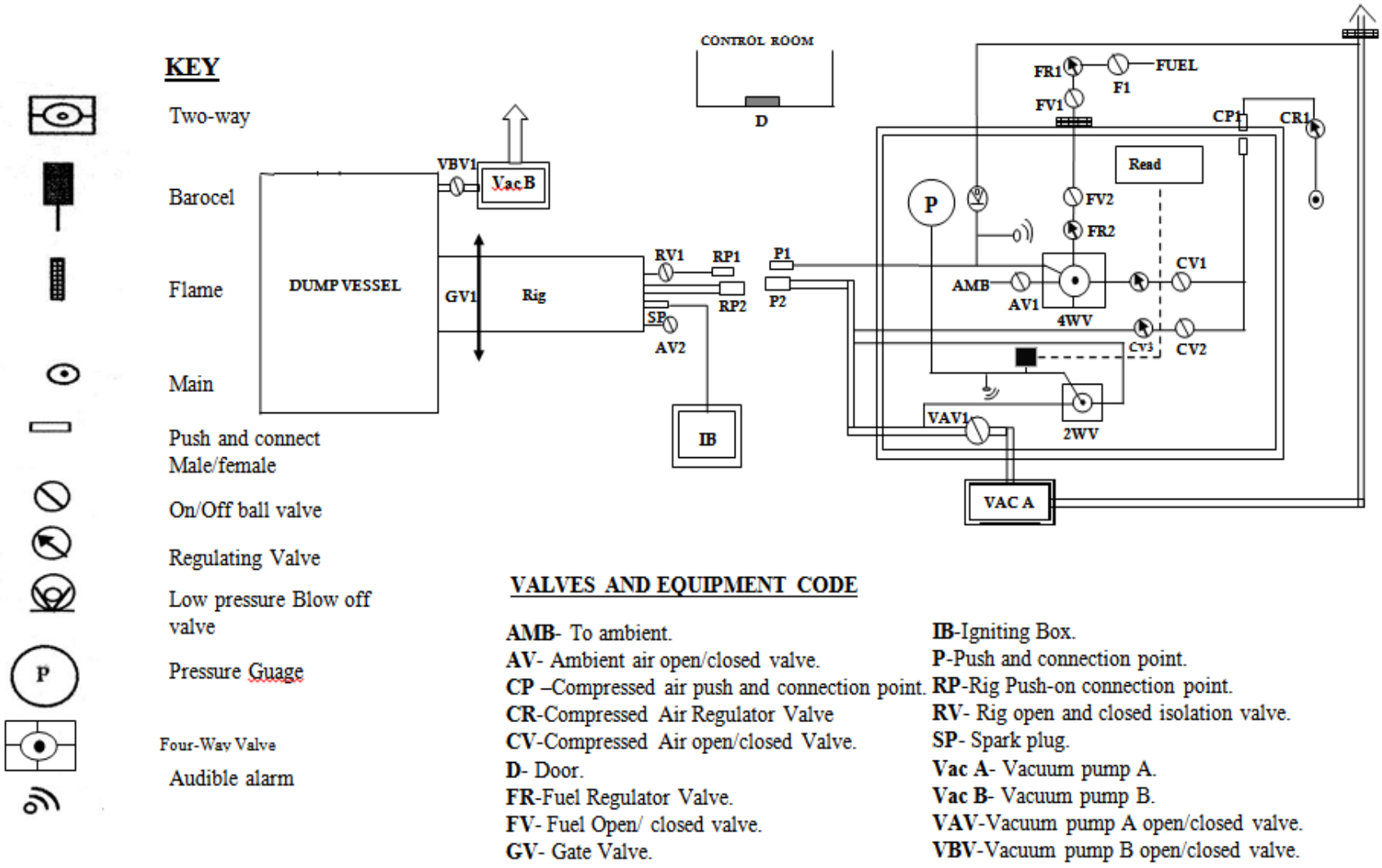

Figure 4. 10 Complete experimental set up with instrumentations.

4.4 Operating Procedures

For each test, there were basically five clear phases that were followed in a consecutive manner. These include: fuel and air entrainment, mixture mixing, ignition procedure, data checking and test rig purging. Every test had followed a strict operating procedure which was clearly detailed in the form of a guide and checklist. For the sake of record keeping for future reference, a standard pro forma was completed for each test conducted. The purpose for this was to enhance safety during the test by ensuring that relevant valves, lines, test-vessel pressure, dump-vessel pressure, ambient temperature, ignition system, type of obstacle, blockage ratio, obstacle position, number of obstacle etc. are properly set and documented. Prior to any test, the test area had to be cleared of any trip or slip hazards. The complete operating procedure of the experiment conducted is given below.

1. Power on the barocel, data logging system, computer and load the Wavecap software.
2. Record the ambient temperature, pressure, humidity from the barocel monitor.
3. Ensure that all the valves in the system are closed. For instance, red light glowing from the Control-room is an indication that the gate valve is closed.
4. Open the valves linking the test vessel to the vacuum pump and recirculation pump.
5. Switch on vacuum pump A and monitor the pressure in the test vessel.
6. Close the valve connecting the pump to the test-vessel as the pressure in the vessel is getting to less than 50 mbar.
7. Repeat step 4 to 6 above at least three times.
8. To guarantee that there is no leakage in the system; ensure that the pressure change in the test-vessel is less than 0.5 mbar per minute.
9. Switch off the vacuum pump A.
10. Open all the valves on the fuel line from the fuel cylinder down to the ones on the control panel.

11. Take note of the vacuum pressure from the test vessel via the barocel panel.

12. The fuel pressure requirement based on the fuel concentration is given as the product of ambient pressure and fuel concentration.

13. The total fill in pressure is obtained as the summation of the vacuum pressure from the test-vessel and fuel pressure requirement as given in steps 11 and 12 respectively.

14. Allow the fuel gas to go into the test-vessel gradually with the aid of a regulating valve until the required partial fuel pressure is attained.

15. Close all the valves on the fuel line.

16. Entrain air into the test-vessel by opening the valve connecting the test-vessel to the atmosphere.

17. With the exception a valve connecting the test-vessel to the recirculation pump, all valves are closed.

18. Switch on the recirculation pump and allow it to operate for about four volume changes (about 5 minutes per air change) in the test-vessel.

19. Close all valves.

20. Connect spark plug to the ignition box and supply power to the ignition box.

21. All personnel in the Test-room to move to Control-room.

22. Close and lock the partition door (the lock would activate the ignition circuit).

23. Arm the data logger using Wavecap software.

24. Press the “FIRE” button firmly.

25. Save the generated data file after the end of the logging time.

26. Unlock the partition door to break the ignition circuit.

27. Purge the system to make it ready for another test.

Special procedures were carried out when any of the two things occurred. First is the entrainment of too much fuel into the test-vessel which forms a non-ignitable mixture in the system. Lastly is the non-ignitability of the fuel-air mixture. This would necessitate the test-vessel been cleared of the mixture.

4.5 Summary of Test Conditions

The test-program involved various ranges of experimental conditions mainly grouped into mixture/fuel influence and obstacle effects. The former comprised the fuel type and its concentrations while the latter had obstacle shape, blockage ratio, number, obstacle scale, integral length scale and obstacle spacing. Table 4.4 shows the list of all the tests carried out in the order in which they were conducted. The number assigned to each test would be used to aid the reader in identifying the conditions of the tests as they are discussed in the subsequent chapters. The majority of the work was carried out with methane-air mixtures followed by propane, hydrogen and ethylene in that order. For the sake of repeatability, each test was repeated at least thrice. In presenting the results of the experimental tests in this research (see Chapter 5,6 and 7), all the repeat tests were shown on the graph where possible. However, for clarity purposes average results are shown in some cases. In total, over 300 tests were carried out demonstrating 84 different test conditions.

Table 4.4 An overview of the experimental test conditions performed in this research.

Mixture			Obstacle									
Test	**Fuel**	**Conc.**	**Shape**	**BR**	**No**	**$N_h/_b$**	**b**	**ℓ**	**x_{s1}**	**x_{s1}/b**	**x_{s2}**	**x_{s2}/b**
(-)	**(-)**	**(%)**	**(-)**	**(-)**	**(-)**	**(-)**	**(m)**	**(m)**	**(m)**	**(-)**	**(m)**	**(-)**
1	CH_4	10	No obstacle									
2	CH_4	10	Hole	0.3	1	1	0.033	0.017	-	-	-	-
3	CH_4	10	Hole	0.3	2	1	0.033	0.017	0.5	15.0	-	-
4	CH_4	10	Hole	0.3	2	1	0.033	0.017	1.0	30.1	-	-
5	CH_4	10	Hole	0.3	2	1	0.033	0.017	1.25	37.6	-	-
6	CH_4	10	Hole	0.3	2	1	0.033	0.017	1.75	52.7	-	-
7	CH_4	10	Hole	0.3	2	1	0.033	0.017	2.25	67.7	-	-
8	CH_4	10	Hole	0.3	2	1	0.033	0.017	2.75	82.7	-	-
9	CH_4	7	No obstacle									
10	CH_4	7	Hole	0.3	1	1	0.033	0.017	-	-	-	-
11	CH_4	7	Hole	0.3	2	1	0.033	0.017	0.5	15.0	-	-
12	CH_4	7	Hole	0.3	2	1	0.033	0.017	1.0	30.1	-	-
13	CH_4	7	Hole	0.3	2	1	0.033	0.017	1.25	37.6	-	-
14	CH_4	7	Hole	0.3	2	1	0.033	0.017	1.75	52.7	-	-
15	CH_4	7	Hole	0.3	2	1	0.033	0.017	2.25	67.7	-	-
16	CH_4	7	Hole	0.3	2	1	0.033	0.017	2.75	82.7	-	-
17	C_3H_8	4.5	No obstacle									
18	C_3H_8	4.5	Hole	0.3	1	1	0.033	0.017	-	-	-	-
19	C_3H_8	4.5	Hole	0.3	2	1	0.033	0.017	1.75	52.7	-	-
20	C_3H_8	3	No obstacle									
21	C_3H_8	3	Hole	0.3	1	1	0.033	0.017	-	-	-	-
22	C_3H_8	3	Hole	0.3	2	1	0.033	0.017	1.75	52.7	-	-
23	C_3H_8	3	Hole	0.3	2	1	0.033	0.017	2.25	67.7	-	-
24	C_3H_8	3	Hole	0.3	2	1	0.033	0.017	2.75	82.7	-	-
25	CH_4	10	Hole	0.4	1	1	0.043	0.021	-	-	-	-
26	CH_4	10	Hole	0.4	2	1	0.043	0.021	1.25	29.2	-	-
27	CH_4	10	Hole	0.4	2	1	0.043	0.021	1.5	34.9	-	-
28	CH_4	10	Hole	0.4	2	1	0.043	0.021	2.25	52.6	-	-
29	CH_4	10	Hole	0.4	1	4	0.022	0.011	-	-	-	-
30	CH_4	10	Hole	0.4	1	16	0.005	0.003	-	-	-	-
31	CH_4	10	Bar	0.2	1	1	0.026	0.013	-	-	-	-
32	CH_4	10	Bar	0.2	2	1	0.026	0.013	1.75	68.4	-	-
33	CH_4	10	Bar	0.2	2	1	0.026	0.013	2.25	87.9	-	-
34	CH_4	10	Bar	0.2	2	1	0.026	0.013	2.75	107.4	-	-

Table 4.4 Cont'd

Mixture			Obstacle									
Test	**Fuel**	**Conc.**	**Shape**	**BR**	**No**	**$N_h/_b$**	**b**	**ℓ**	**x_{s1}**	**x_{s1}/b**	**x_{s2}**	**x_{s2}/b**
(-)	**(-)**	**(%)**	**(-)**	**(-)**	**(-)**	**(-)**	**(m)**	**(m)**	**(m)**	**(-)**	**(m)**	**(-)**
35	CH_4	10	Bar	0.2	1	2	0.013	0.006	-	-	-	-
36	CH_4	10	Bar	0.2	2	2	0.013	0.006	1.0	78.1	-	-
37	CH_4	10	Bar	0.2	2	2	0.013	0.006	1.25	97.7	-	-
38	CH_4	10	Bar	0.2	2	2	0.013	0.006	1.75	136.7	-	-
39	C_3H_8	4.5	Bar	0.2	1	2	0.013	0.006	-	-	-	-
40	C_3H_8	4.5	Bar	0.2	2	2	0.013	0.006	1.0	78.1	-	-
41	C_3H_8	4.5	Bar	0.2	2	2	0.013	0.006	1.25	97.7	-	-
42	C_3H_8	4.5	Bar	0.2	2	2	0.013	0.006	1.75	136.7	-	-
43	C_3H_8	4.5	Bar	0.2	2	2	0.013	0.006	2.25	175.8	-	-
44	C_3H_8	4.5	Bar	0.2	1	4	0.006	0.003	-	-	-	-
45	C_3H_8	4.5	Bar	0.2	2	4	0.006	0.003	0.25	39.1	-	-
46	C_3H_8	4.5	Bar	0.2	2	4	0.006	0.003	0.5	78.1	-	-
47	C_3H_8	4.5	Bar	0.2	2	4	0.006	0.003	1.0	156.3	-	-
48	CH_4	10	Bar	0.2	1	4	0.006	0.003	-	-	-	-
49	CH_4	10	Bar	0.2	2	4	0.006	0.003	0.25	39.1	-	-
50	CH_4	10	Bar	0.2	2	4	0.006	0.003	0.5	78.1	-	-
51	CH_4	10	Bar	0.2	2	4	0.006	0.003	1.0	156.3	-	
52	CH_4	10	Hole	0.2	1	1	0.024	0.012	-	-	-	-
53	CH_4	10	Hole	0.2	2	1	0.024	0.012	1.75	71.9	-	-
54	CH_4	10	Hole	0.2	2	1	0.024	0.012	2.25	92.4	-	
55	CH_4	10	Hole	0.2	2	1	0.024	0.012	2.75	112.9	-	-
56	CH_4	10	Bar	0.3	1	1	0.039	0.019	-	-	-	-
57	CH_4	10	Bar	0.3	2	1	0.039	0.019	1.25	32.5	-	-
58	CH_4	10	Bar	0.3	2	1	0.039	0.019	1.75	45.5	-	-
59	CH_4	10	Bar	0.3	2	1	0.039	0.019	2.25	58.4	-	-
60	H_2	15	No obstacle									
61	H_2	15	Hole	0.3	1	1	0.033	0.017	-	-	-	-
62	H_2	18	Hole	0.3	1	1	0.033	0.017	-	-	-	-
63	H_2	15	Hole	0.3	2	1	0.033	0.017	1.25	37.6	-	-
64	H_2	15	Hole	0.3	2	1	0.033	0.017	1.75	52.7	-	-
65	H_2	15	Hole	0.3	2	1	0.033	0.017	2.25	67.7	-	-
66	H_2	15	Hole	0.3	2	1	0.033	0.017	2.75	82.7	-	-
67	C_2H_4	4.3	No obstacle									
68	C_2H_4	4.3	Hole	0.3	1	1	0.033	0.017			-	-
69	C_2H_4	4.3	Hole	0.3	2	1	0.033	0.017	1.75	52.7	-	-
70	C_2H_4	4.3	Hole	0.3	2	1	0.033	0.017	2.25	67.7	-	-
71	C_2H_4	4.3	Hole	0.3	2	1	0.033	0.017	2.75	82.7	-	-
72	CH_4	10	Disc	0.2	1	-	0.058	0.029	-	-	-	-
73	CH_4	10	Disc	0.2	2	-	0.058	0.029	0.25	4.3	-	-
74*	CH_4	10	Disc	0.2	3	-	0.058	0.029	0.25	4.3	0.25	4.3

Table 4.4 Cont'd

Mixture			Obstacle									
Test	**Fuel**	**Conc.**	**Shape**	**BR**	**No**	**$N_b/_b$**	**b**	**ℓ**	**x_{s1}**	**x_{s1}/b**	**x_{s2}**	**x_{s2}/b**
(-)	**(-)**	**(%)**	**(-)**	**(-)**	**(-)**	**(-)**	**(m)**	**(m)**	**(m)**	**(-)**	**(m)**	**(-)**
75*	H_2	15	Disc	0.2	3	-	0.058	0.029	0.25	4.3	0.25	4.3
76*	H_2	15	Bar	0.2	3	2	0.013	0.006	1.25	97.7	1.25	97.7
77	CH_4	10	Bar	0.2	3	2	0.013	0.006	1.25	97.7	1.0	78.1
78*	CH_4	10	Bar	0.2	3	2	0.013	0.006	1.25	97.7	1.25	97.7
79	CH_4	10	Bar	0.2	3	2	0.013	0.006	1.25	97.7	1.5	117.2
80	CH_4	10	Bar	0.2	3	4	0.006	0.003	0.5	78.1	0.25	39.1
81	CH_4	10	Bar	0.2	3	4	0.006	0.003	0.5	78.1	0.5	78.1
82	CH_4	10	Bar	0.2	3	4	0.006	0.003	0.5	78.1	0.75	117.2
83	CH_4	10	Bar	0.2	3	4	0.006	0.003	0.5	78.1	1.25	195.3
84	H_2	15	Bar	0.2	3	4	0.006	0.003	0.5	78.1	0.5	78.1

* An extra pipe section of about 0.25 m length and 0.162 m diameter was used to have equal spacing within the three obstacles.

4.6 Risk Assessment and Safety Considerations

Issues of safety of the operator and that of others are of paramount importance and were considered at all levels of this research. Risk assessment of the laboratory was carried out in order to identify the potential hazards likely to occur and ways to remedy such hazards. A comprehensive risk assessment of Room B11 based on the Faculty of Engineering standard was written in the Safety Protocol Folder and kept in the laboratory. Most of the safety measures were discussed before in this chapter, and these comprised the partitioning between Control and Test rooms, safety interlocks incorporated into the ignition system etc.

Despite all the safety measures put in place, yet, there are number of hazards that are to be aware of and the necessary safety measures required to prevent or minimise the consequences.

4.6.1 Vessel Failure

The design parameters for the test and dump vessels used in this study were listed in Table 4.1 and 4.2 respectively. The test vessel was designed and certified to withstand the peak adiabatic pressure (8 bar) for most deflagrative combustion of fuel-air mixtures initiated at standard atmospheric pressure (1013.3 mbar). Also, the vessel was designed to resist any possible transition to detonation from deflagration. This is likely to occur in the presence of high reactivity mixtures or obstacles or combination of both as in the case of the present research. The 50 m^3 dump vessel was designed and tested hydraulically. The dump vessel was fitted with pressure relief valves whose openings were set at the required pressure of the dump vessel.

4.6.2 Explosion Transmission into Auxiliary Instruments

Auxiliary instruments such as vacuum pumps and pressure monitoring system were involved in the preparation of flammable fuel-air mixture. As such, the possibility of transmitting explosion into this equipment was certain. A specially designed procedure was adhered to for each explosion test. Various ball-valves were closed and fuel lines disengaged prior to ignition so as to isolate the test vessel. Also prior to ignition, the gas cylinders were isolated from the test vessel.

4.6.3 Gas Leakage

The possibility of gas leakage exist as a result of human error (improper closure of valves) and not so much due to faulty fittings or piping as these were tested for leaks before performing any explosion test. It is therefore recommended that gas detection and warning systems for the fuel gases to be used be installed in the Test room.

4.6.4 Ignition Failure of the Fuel-Air Mixtures

Flammable fuel-air mixtures could not explode due to the fault of an ignition system (for instance fault from spark plug). In order to inspect the reason of the failure, part of the test vessel had to be dismantled. This required the flammable mixtures to be emptied initially with the aid of a vacuum pump. However, the pump is not explosion-proof and as such it would create a hazardous situation. The valves subsequent to the pump and the ones on the control panel both leading to the ambient air are to be opened in order to lessen the risk. The ambient air being sucked into the vessel via the valves would dilute the flammable mixture that is to be purged out with pump. This is the only condition when the vacuum pump is required to handle explosive mixtures.

Chapter 5
Obstacles-Augmented Explosions in a Long Vented Tubular Geometry

5.1 Flame Acceleration in a Tube with Two obstacles

Quantitative analysis of gas explosions were previously conducted in the Leeds Explosion Laboratory using the current test rig. Phylaktou (1993) and Gardner (1998) performed their explosion tests with end plates (totally closed) and vented cylindrical vessels respectively. However, both authors used single obstacles to study a systematic influence of obstacles in gas explosions. In the current work, the influence of two obstacles was explored as a prerequisite of multi-obstacle congestions typically found in industries. More emphasis was given to spacing between obstacles in addition to other parameters such as obstacle blockage, mixture reactivity, obstacle shapes and types that affect the severity of gas.

5.1.1 Comparison with Single and no Obstacle Tests

The effect of double obstacle in an explosion was assessed by comparison to the equivalent single and no obstacle explosions under similar test conditions. In all the tests, slightly rich methane-air at 10% by volume was used. For both single and double obstacle tests, 0.3 BR 1-hole was used as an obstacle. However, the former was positioned at 1 m downstream of the spark while the latter had it first obstacle positioned at same position to single obstacle while the second was 1.75 m downstream of the first. The test numbers (see Table 4.4) for the no, single and two obstacles were given as Test 1, 2 and 6 respectively.

5.1.1.1 Pressure Development

The pressure generation and variation with time is illustrated in Fig. 5.1 and Fig. 5.2 for the case of no obstacle and a double obstacle configuration respectively. Also shown on these plots are the flame arrival times at the thermocouples along the tube axis.

The first observation is the significant increase overpressure in the two obstacle configuration compared to the no obstacle situation. The increase in maximum overpressure was ten-fold, from approximately 0.25 bar to 2.5 bar. This was associated with an overall reduction in the tube travel time from 75 ms to 65 ms. However it should be noted that up to the point of flame interaction with the first obstacle (at around 50ms) the pressure and flame development was very similar in the two cases. This means that the post-first-obstacle flame travel to the tube exit

was completed in less than 15ms compared to the 25 ms in the case of no obstacle at all. This would require an almost doubling of the flame speed in this section of the tube.

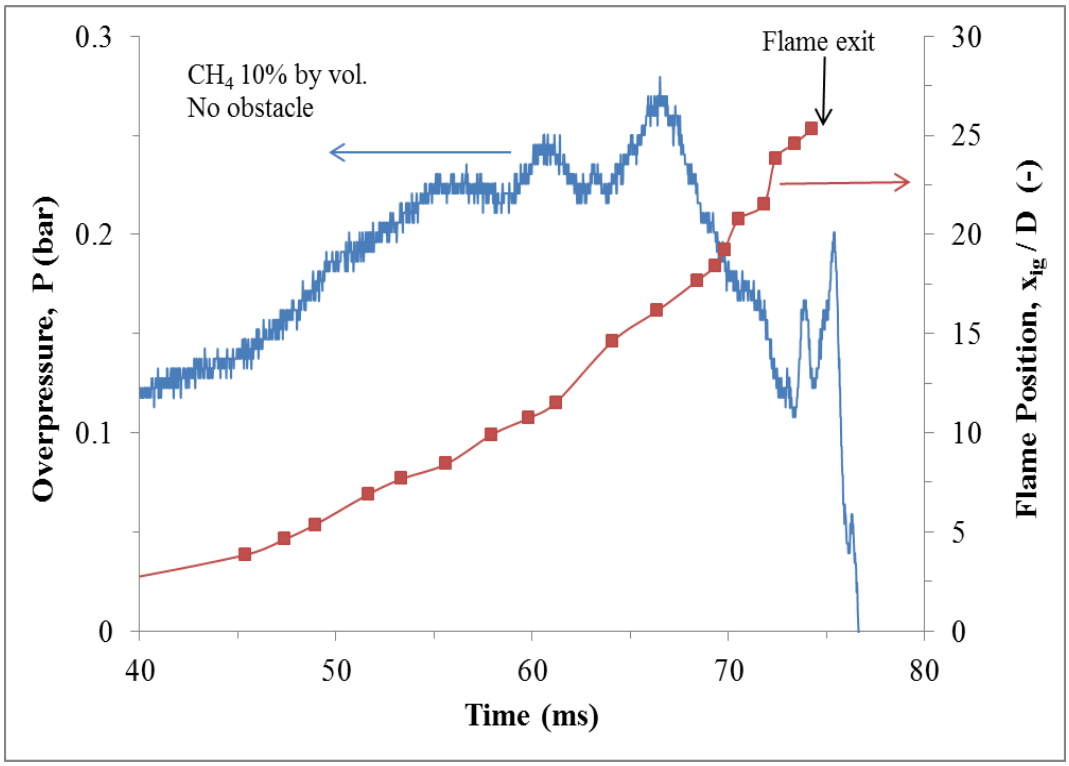

Figure 5.1 Example of pressure trace (transducer PT1), and flame position with time for the empty tube (no obstacles).

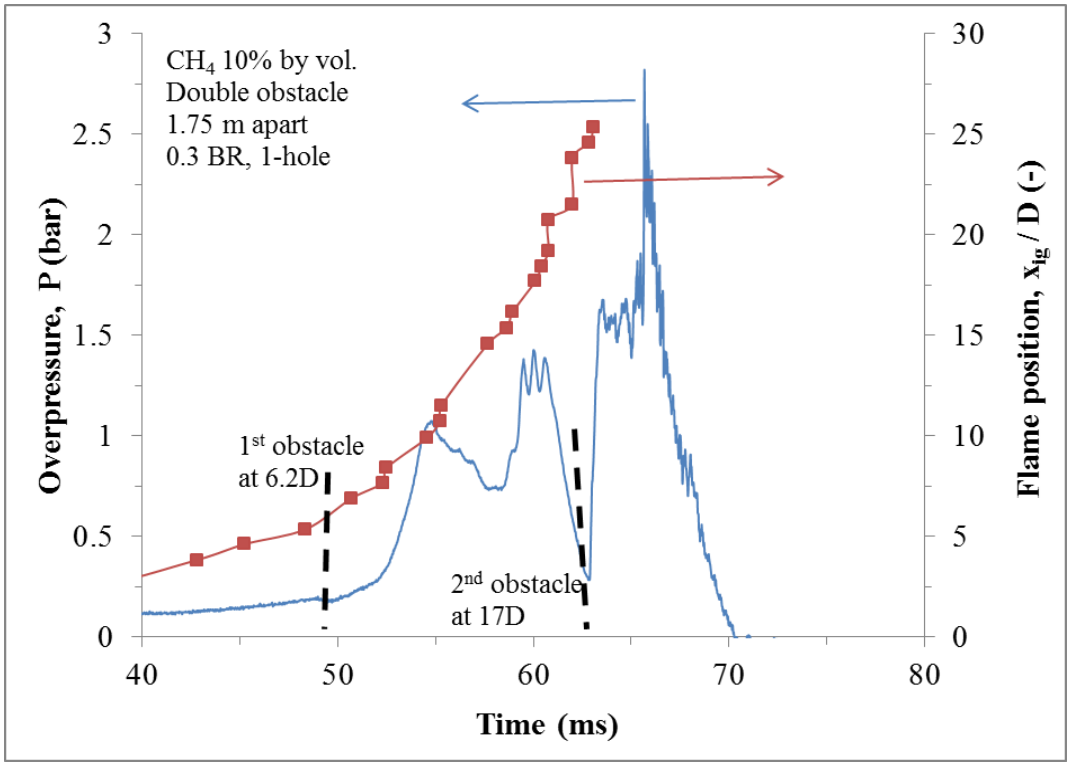

Figure 5.2 Example of pressure trace (transducer PT1), and flame position with time, for a double obstacle case (obstacle separation distance of 1.75m).

Figure 5.2 shows that the maximum pressure was recorded after the flame exited the tube. This is simply an artefact of the distance between the flame front and the recording pressure transducer (in this case PT1 which is located on the ignition flange). Pressure changes associated with the leading flame front take a finite time to before they register on the various pressure transducers along the tube which depends on the separation distance between the "event" location and the recording device and the speed of sound in the intervening medium.

A direct comparison of the two pressure traces is given in Fig.5.3, which additionally includes the case of a single obstacle at 6.2 tube diameters from the spark. Again this plot demonstrates the pre-first obstacle similarity of pressure development in the tube, giving confidence in the repeatability of the tests. Post first-obstacle, good similarity is observed for the effect of first obstacle for both the single and double obstacles cases. The maximum overpressure due to the first obstacle was just over 1 bar in both cases

In the double obstacle configuration the overpressure oscillated stronger in the region downstream of the first obstacle (compared to the single obstacle case) and

after interacting with the second obstacle the overpressure surged to a maximum of over 2.5 bar before the flame vented out of the tube.

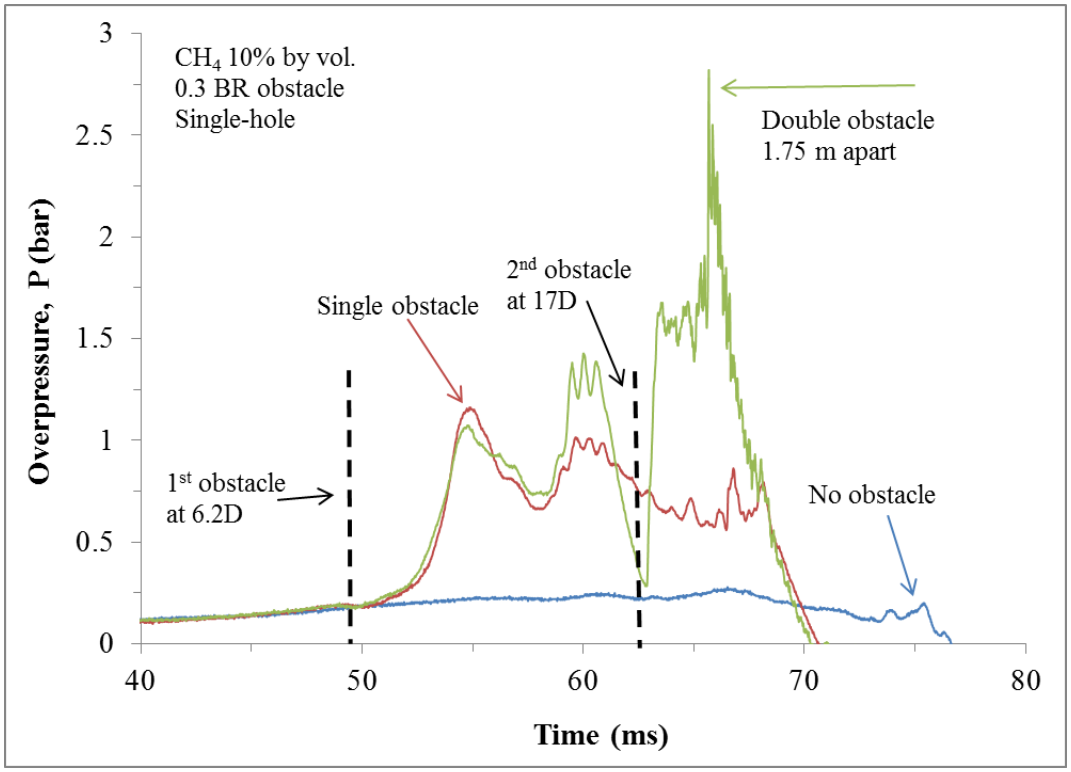

Figure 5.3 Comparison of pressure traces from PT1 for the no obstacle, single obstacle and a double obstacle configuration (separation distance of 1.75m).

5.1.1.2 Flame Speed

Figure 5.4 shows the flame speeds corresponding to tests in Fig. 5.3, as derived from the thermocouple flame arrival times, as a function of the axial position along the tube. A smoothing algorithm was applied to the flame arrival data, as described by Gardner (1998), to avoid negative flame speeds where the flame brush appears to arrive at downstream centreline locations earlier than upstream ones, particularly in the regions of strong acceleration downstream of the obstacles. The flame speeds, in correspondence to the patterns shown by pressure traces, demonstrated similar flame development upstream of the first obstacle location in all 3 tests. In the case of the single and double obstacle cases the flame speeds were similar up to the point of interaction with second obstacle. The maximum flame speeds in the empty tube reached just over 100m/s, while with the single this more than doubled to over 250 m/s, and doubled again to over 500 m/s with the introduction of the second obstacle.

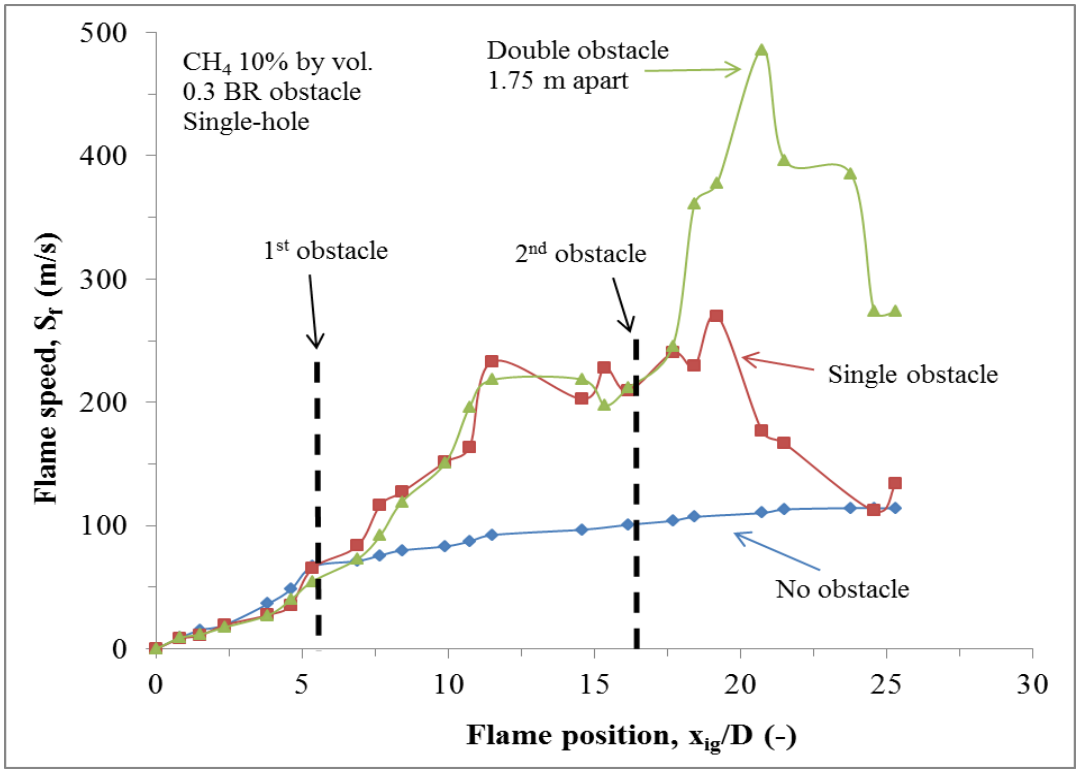

Figure 5.4 Comparison of flame speeds for the no obstacle, single obstacle and a double obstacle configuration (separation distance of 1.75m) as a function of the dimensionless flame position.

The direct evidence on the influence of single and double obstacle in gas explosions was also observed from the pioneer work of Chapman and Wheeler (1926). The details of the experimental conditions were given in Table 3.1. As in the case of the present work, Chapman and Wheeler (1926) performed their tests with no obstacle, single, double and multi obstacle configurations in that order. The no obstacle test produced a maximum flame speed of about 6 m/s whereas the single and double obstacle with 0.75 BR each[1] attained a peak speed of close to 94 m/s and 307 m/s respectively.

[1] The single obstacle was positioned 40 cm from spark. For the double obstacle, the first and second were positioned 40 cm and 110 cm from spark respectively.

5.1.2 Mechanism of Pressure Generation

In vapour cloud explosions it's common to assume that the overpressure is proportional to the square of the flame speed (Taylor and Hirst 1989; Harris and Wickens 1989). A more detailed expression was given by Harrison and Eyre (1987) from Shell Research Ltd. The assumption was based on simplified acoustic theory given by Taylor (1946) in terms of flame speed and Mach number, M. If the ambient pressure is atmospheric, then the overpressure is given as,

$$\mathbf{P} = \frac{2\gamma \mathbf{M}^2}{1 + \mathbf{M}} \tag{5.1}$$

Using an ambient speed of sound of 340 m/s, specific heat constant, γ of 1.4 and the average experimental flame speed measurements for the double obstacle in Fig. 5.4 and (1.75 m apart) an overpressure trace was calculated using Eq. 5.1. This was then compared with the pressure-trace from transducer PT1 and PT6 from one of the tests as a function of time, as shown in Fig. 5.5.

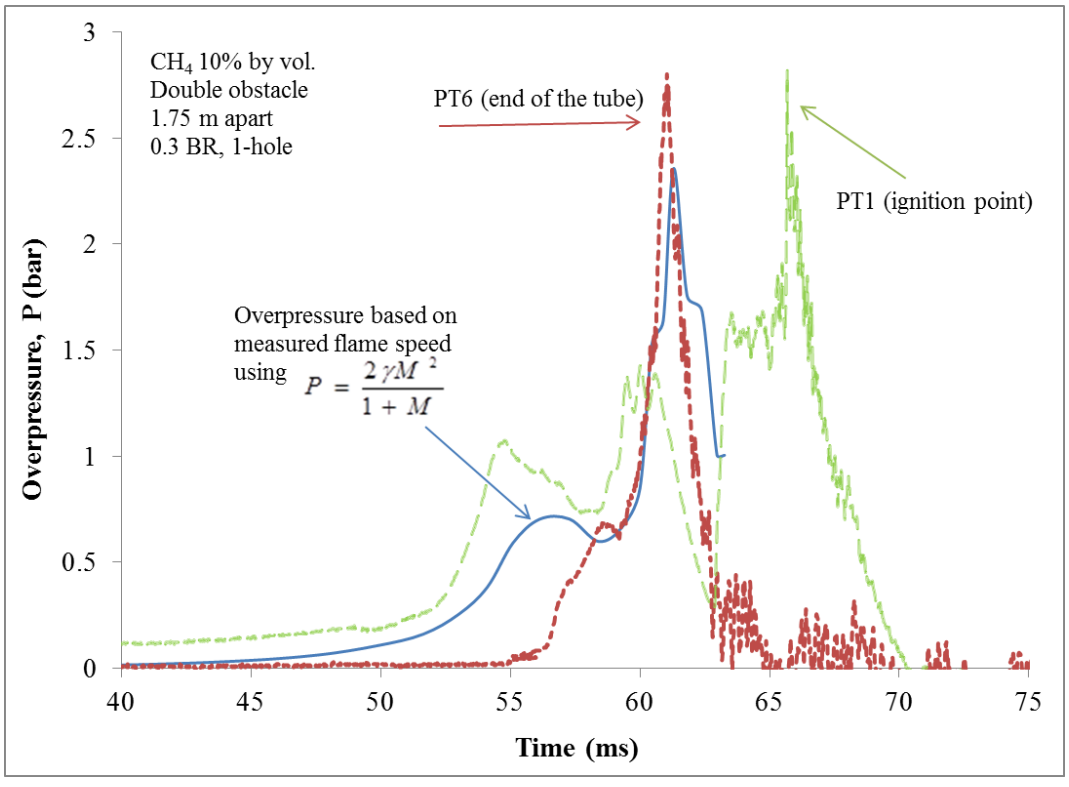

Figure 5.5 Comparison of the flame speed based pressure trace and that from transducer PT1 and PT6 for a double obstacle configuration.

As shown in Fig. 5.5 there was good agreement between the flame-speed based pressure and that measured by transducer PT6 particularly on the profile and timing of the maximum pressure peak. This flame acceleration and pressure peak occur in the region of PT6 and it therefore immediately recorded. The apparent mismatch between the timings of the effect of the first obstacle is again due to the fact that PT6 was some distance away from the region of effects of the first obstacle and there was some time delay in these effects being picked up by PT6. However, this was not the case for PT1 i.e. good agreement with the predicted overpressure for the first obstacle (1 m from spark) and disparity in timings between the PT1 and calculated overpressure at the second obstacle.

The implication of this good agreement was that the mechanism of pressure generation in the present tests is the same as that of vapour-cloud explosions, i.e. the pressure rise was due mainly to the inertia of the gas immediately ahead of the flame, and that it was not significantly influenced by the confinement offered by the tubular geometry. It would however be expected that in a largely-confined system such as the present arrangement (a tube with an open far-end), the maximum pressure would be a function of the net volume increase in the system. This is the balance between volume generation by the combustion process and volume reduction by venting, and therefore the pressure would not simply be a function of the flame speed as in a vapour cloud explosion. However, the pressure records of PT6 (end of tube) and PT7 (dump-vessel) indicated little pressure difference between the two vessels and therefore limited venting was taking place at the time of maximum flame acceleration.

Therefore the overpressures measured in this system were due to the high flame speeds which were caused by the obstacle induced turbulence which itself on the flame speeds associated flow velocities upstream of the obstacle.

5.1.3 Experimental Evidence on the Influence of Obstacle Separation Distance

In order to establish the influence of the obstacle spacing in gas explosions in the current work, two obstacles of 0.3 BR each were spaced in-between at six different positions (see Tests 3,4,5,6,7 and 8 from Table 4.4). The position of the first obstacle was fixed at 1 m from spark while the second obstacle position was

systematically changed in order to determine the obstacle separation distance which would give the maximum overall flame acceleration and overpressure.

5.1.3.1 Pressure Development

Example pressure records from pressure transducer PT6 are shown in Fig. 5.6, for different obstacle separation distances. The data clearly demonstrated a very strong effect of the obstacle separation distance not only in terms of the maximum pressure achieved but also in terms of the profile of the pressure development. For obstacles in close proximity to each other (e.g. 0.5 and 1.0m separation distances) the effect of the obstacles was amalgamated into one pressure rise whilst on the cases where the separation distances are too large (e.g. 2.75 m separation distance) the effects of the individual obstacles become distinct with no significant influence of the first obstacle on the flame behaviour after the second.

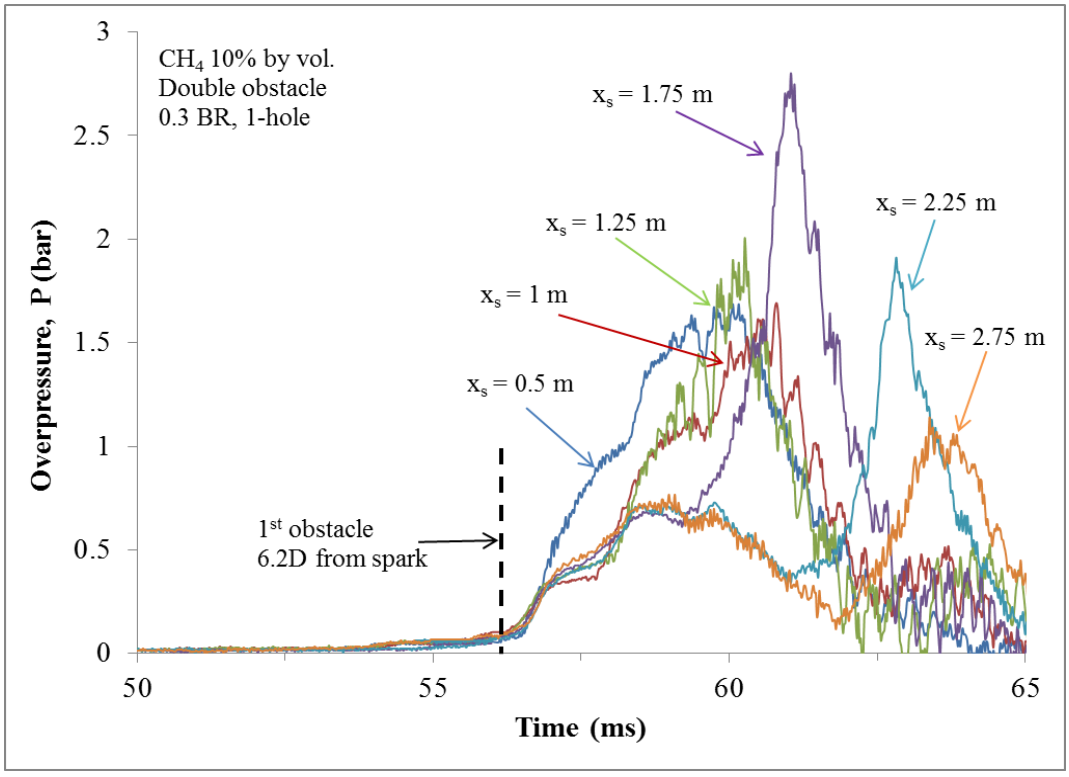

Figure 5.6 Example pressure records from pressure transducer PT6, for different obstacle separation distances.

The maximum synergistic effect of the two obstacles was obtained at a separation distance of 1.75 m where evidently the flame accelerated to its maximum value after the first obstacle before reaching the second. Therefore the highest possible flows

were induced by the accelerating flame through the second obstacle and this would have resulted in the highest turbulence levels after the second and hence to highest overpressures, as shown when the flame reached this region. This concept and behaviour is fully congruent with the turbulence profile downstream of an obstruction presented by Baines Peterson (1951), and discussed earlier (see Fig. 2.4).

5.1.3.2 Flame Speed

The effect of the separation distance on the maximum overpressure (both experimental and predicted from Eq. 5.1) and the maximum flame speed is more clearly illustrated in Fig. 5.7. The obstacle separation distance was presented in terms of a dimensionless distance by dividing the actual distance with the obstacle characteristic scale, b (as defined earlier). It is shown that the maximum effect of the combined obstacles occurred when the separation distance was approximately 53 obstacle scales (or 1.75 m).

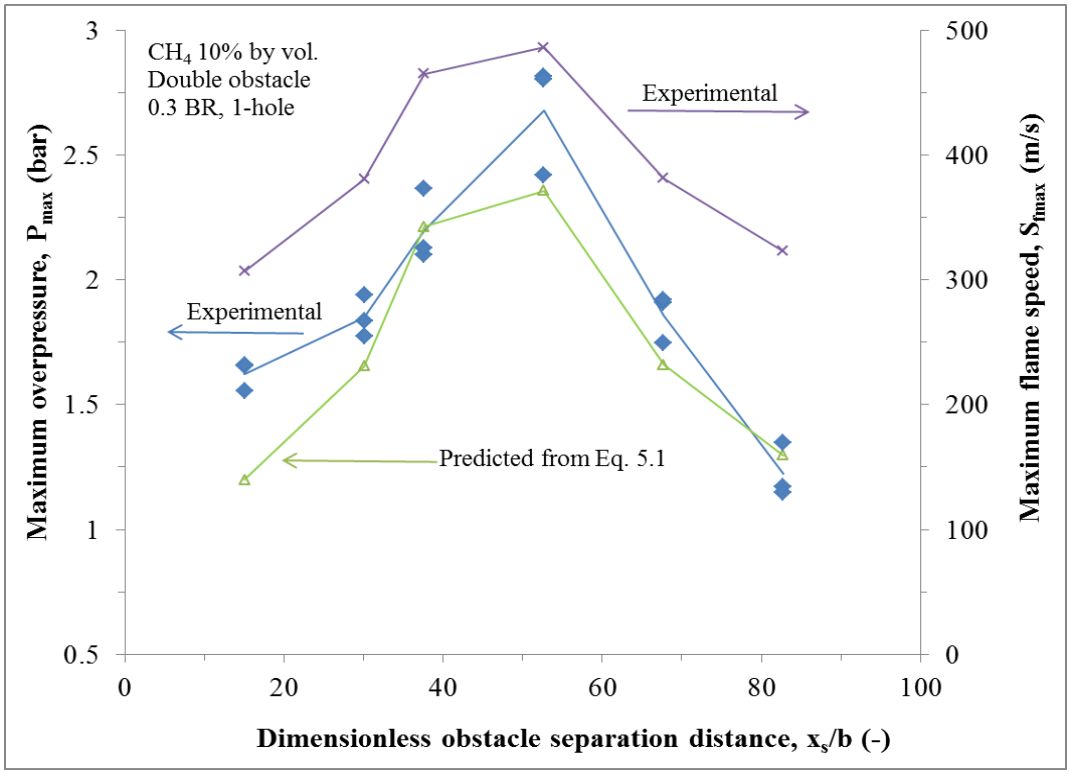

Figure 5.7 The effect of dimensionless separation distance on the maximum overpressure and the maximum flame speed.

5.1.3.3 Comparison with Cold Turbulent Flows

In Fig. 5.8 the effect of the obstacle separation distance on the maximum overpressure is compared with the Baines and Peterson (1951) data on the turbulence profile downstream of an obstruction in non-reacting flows. There was no turbulence data for the same blockage ratio as in the present tests (30%) so the comparison was made to a lower (22%) and a higher (44%) blockage ratio. It is shown that the present tests followed a similar profile to that of turbulence growth and decay, with the maximum however occurring at a further distance from the obstacle than suggested by the Baines and Peterson (1951) data for cold flows.

A possible explanation for the non-correspondence between the cold flow position of maximum turbulence and the worst case obstacle separation distance is that once the flame moves through the obstacle the whole of the generated turbulence profile is detached from the obstruction it is in fact conveyed forward (whilst at the same time being consumed) by the advancing flame front.

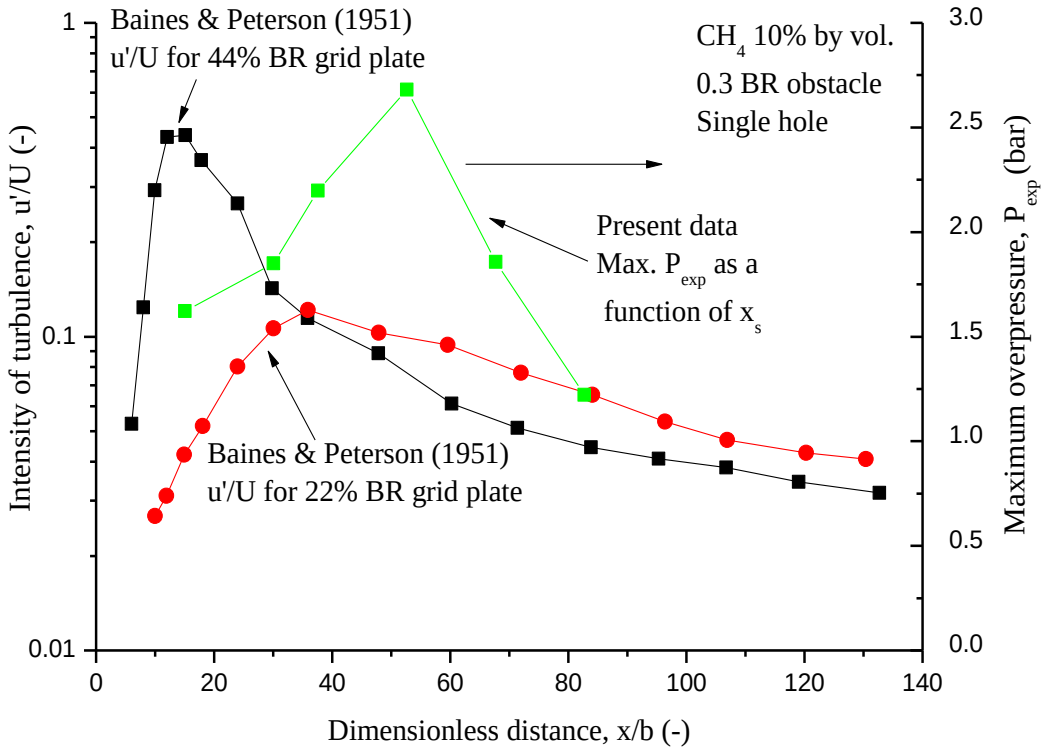

Figure 5.8 Comparison of the present data to the Baines and Peterson (1951) data for a lower and a higher blockage ratio.

As stated in Chapter 2 previously, Eq. 2.23 was used to predict the obstacle separation leading to maximum intensity of turbulence in the current research. The equation was validated with the worst case obstacle spacing of 1.75 m obtained experimentally. The dimensionless optimum spacing $(x/b)_{max}$ from Eq. 2.23 was 17.8 and the obstacle scale, b for 0.3 BR orifice was 0.033 m. This gives the optimum spacing of about 0.587 m which is a factor of three lower than the experimental value.

5.1.4 Influence of Mixture Reactivity

The magnitudes and the likelihood of occurrence of gas explosions will to a large extent depend on fuel type. By keeping experimental conditions constant, different fuel-air mixtures will produce various experimental pressures (Bjerketvedt *et al.* 1997).

Laminar burning velocity is a key parameter of a combustible mixture that comprises the necessary information concerning the mixture reactivity of a given fuel gas. Its precise knowledge is vital for engine design and modelling of turbulent combustion. Also, this parameter is essential for the computations used in fuel tank venting and explosion protection (Buffam *et al.* 2008).

Another important property of a flammable mixture is the Lewis Number, Le, which is the non-dimensional quotient of thermal diffusivity to mass diffusivity. It quantifies differences between the diffusivities of mass and heat that generate the instabilities that lead to the flame transition to cellular flames (Clarke 2002). In case of Le larger than one (signifying weakly diffusing reactants), then the generated heat from the diffusing reactants is lesser than the heat lost by conduction. This resulted to reduction in both flame temperature and burning velocity and hence a reduction of the flame instability. On the contrary, if the Lewis number is smaller than unity (signifying strongly diffusing reactant); then the heat generated from the diffusion of the reactants is higher than the heat lost by conduction. This would lead to an increase in both flame temperature and burning velocity and therefore a growth in the instability. For Lewis number equals to unity, the normal components of the thermal and mass diffusivities from the flame area will be similar. Therefore, the increased heat loss at the convex part of the flame is balanced by an increased diffusion rate of reactants into the flame. This enabled the burning velocity and

flame temperature to remain unchanged (Knudsen 2006). The effect of Lewis number on flame front fragmentation in narrow closed channels was studied using numerical method by Karlin *et al.* (2000). However, this investigation was limited to relatively low Reynolds number flames in a channel with walls that are thermally insulated.

In explosion studies, Markstein number, Ma also influences the reactivity of the mixture. Ma is used to describe the influence of local heat release of a spreading flame on variations in the surface topology along the flame and the connected local flame front curvature. Mathematically, Ma is expressed as the ratio of Markstein length to the flame thickness. The Ma is proportional to the effect of curvature on localized burning velocity. Generally a negative Ma is associated with an unstable flame (Tseng *et al.* 1993).

In the current work, the influence of mixture reactivity was investigated using single 1-hole obstacle of 0.3 BR. In addition to methane, tests were carried out with mixtures of propane, ethylene and hydrogen with air. Two concentrations (slightly rich and lean) of methane (10% and 7% by vol.) and propane (4.5% and 3% by vol.) air mixtures were used. Lean mixtures of ethylene (4.3% by vol.) and hydrogen (18% and 15% by vol.) were also tested. For a given fuel, the choice for the mixture slightly above its stoichiometric concentration would result in higher explosion severity than the lean concentration. This is as a result of the influence of maximum burning velocity. The lean mixtures were carefully chosen to ensure that they have nearly equal value of S_L. A similar approach was used by Goix and Shepherd (1993) to study the effects of turbulent premixed flame structures of lean propane and hydrogen air mixtures with similar laminar burning velocities.

Table 5.1 gives an overview of the basic combustion parameters for the fuel types and concentrations tested. These include the laminar burning velocity, S_L, fuel equivalence ratio[2],$\emptyset$, expansion ratio, E, Lewis number, Le and the Markstein number, Ma.

---

2 It is the ratio of the actual fuel concentration to the theoretical stoichiometric fuel consumption for the same air supply.

The S_L values for methane and hydrogen were obtained from the work of Andrews and Bradley (1972) and (1973) respectively. Harris (1983) gave the value of S_L for propane at slightly above stoichiometric (4.5% by vol.) whereas its lean mixture of 3% by vol. was given by Razus *et al.*(2010). The 4.3% ethylene-air mixtures had it S_L value from Wang and Rogg (1993).

The Lewis number for all the methane, propane and ethylene mixtures used in the present work was sourced from Phylaktou (1993). However, the Le for the hydrogen mixtures i.e. 18% and 15% by vol. were obtained from Bauwens *et al.* (2012) and Abdel-Gayed *et al.* (1985) respectively. For the Markstein number, the values for the methane, propane at various concentrations and lean ethylene mixtures were all obtained from the work of Tseng *et al.* (1993). The lean hydrogen mixtures of both 18% and 15% by vol. were taken from Aung *et al.* (1997).

Table 5.1 Selected properties of different fuel-air mixtures.

Fuel type	**Conc.(v/v)**	**ø**	**S_L**	**E**	**Le**	**Ma**
(-)	(%)	(-)	(m/s)	(-)	(-)	(-)
CH_4	10	1.06	0.45	7.49	1.0	3.5
CH_4	7	0.72	0.24	6.26	1.0	-0.2
C_3H_8	4.5	1.12	0.53	8.10	0.8	2.6
C_3H_8	3	0.74	0.25	6.37	1.8	6.0
C_2H_4	4.3	0.65	0.30	5.82	1.3	3.0
H_2	18	0.52	0.97	5.09	0.5	-0.8
H_2	15	0.42	0.41	4.65	0.7	-1.2

5.1.4.1 Pressure Development

Figure 5.9 shows a pressure-time profile from PT1 for all the fuel types and concentrations tested with 1-hole 0.3 BR single obstacle positioned 6.2D from spark. The designated numbers for these tests were 2, 10, 18, 21, 61, 62 and 68.

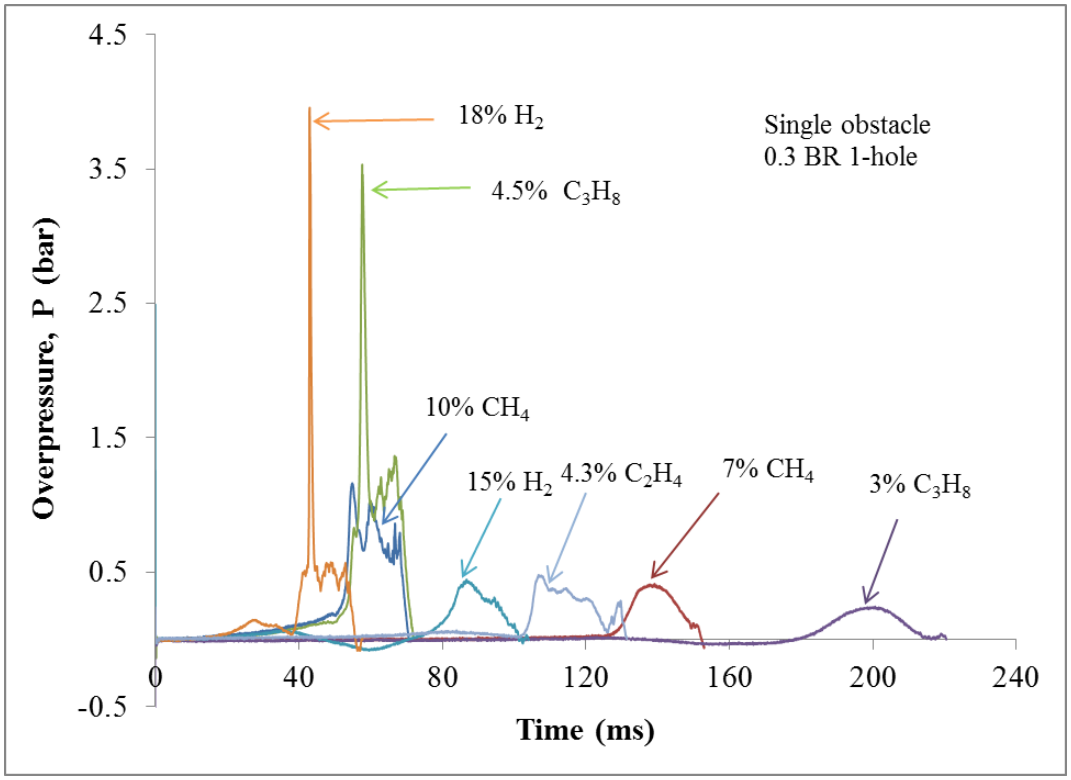

Figure 5.9 Pressure-time profile for various hydrocarbon fuels and hydrogen at different concentrations.

For methane-air mixtures upon ignition, the flame propagated faster in 10% CH_4 test and hit the obstacle at about 48 ms compared to about 124 ms for the 7% CH_4. This indicated a great difference in terms of the approaching flame speed upstream of the first obstacle between the two tests. This gives the 10% concentration test higher upstream flame speeds compared to 7% concentration. The 10% by vol. mixture attained its maximum overpressure of about 1.1 bar downstream of obstacle at about 57 ms. This overpressure was about a factor of 3 higher when compared to 7% by vol. mixture which occurred at 136 ms.

In a more reactive fuel after methane i.e. propane, the slightly rich mixture (4.5% by vol.) accelerated quicker and reached the obstacle at about 3.6 times faster when compared to the lean (3% by vol.) propane at 177 ms. A maximum overpressure of 3.5 bar was achieved after the obstacle for the 4.5% by vol. mixture and this was about 15 folds greater than the lean mixture of 3% by vol. Under similar conditions, slightly rich propane 4.5% proved to be more reactive and hence severe explosion consequences than 10% methane-air mixtures. The overpressure ratio between the two fuels at worst case concentrations was about a factor of 3. The laminar burning

velocity, S_L was mainly responsible to the different overpressures obtained in the two fuels. The propane-air 4.5% by vol. has a value of 0.53 m/s and 0.45 m/s for methane-air 10% by vol.

Also shown in Fig. 5.9 is the pressure-time relation for lean hydrogen-air mixtures of 18% and 15% by vol. These lean concentrations of hydrogen-air mixtures were tested by Lee *et al.* (1984) and recently by Bauweens *et al.* (2012) in a congested 64 m^3 chamber as a wider assessment of the potential of hydrogen energy in the future. The 18% hydrogen-air approached the obstacle at about 35 ms prior to attaining its peak overpressure of nearly 3.9 bar at 43 ms. The overpressure was a factor of 9.8 higher when compared to 15% hydrogen-air with a longer flame propagation timing from the ignition to the obstacle. Lean ethylene-air (4.3% by vol.) is also presented from the same plot with a maximum overpressure of 0.42 bar.

In general, the lean mixtures of various fuel types presented in Fig. 5.9 showed that the maximum overpressures are nearly the same even though the time to such points were different. The near stoichiometric mixtures of these fuels produced violent explosions whose severities increased with increasing mixture reactivity i.e. laminar burning velocity.

The relationship between the laminar burning velocity, S_L and the overpressure i.e. explosion severity for all the gases tested is given in Fig. 5.10. The acronyms M, P, E and H stand for the fuel types as methane, propane, ethylene and hydrogen respectively. The slightly rich and lean mixtures for a given fuel type were designated R and L in that order. It is evident from the plot that gases of different types can produce nearly similar explosion overpressures provided that their laminar burning velocities are fairly the same. A linear correlation had fitted the data well and is given as,

$$P_{max} = 6.048S_L - 1.2493 \tag{5.2}$$

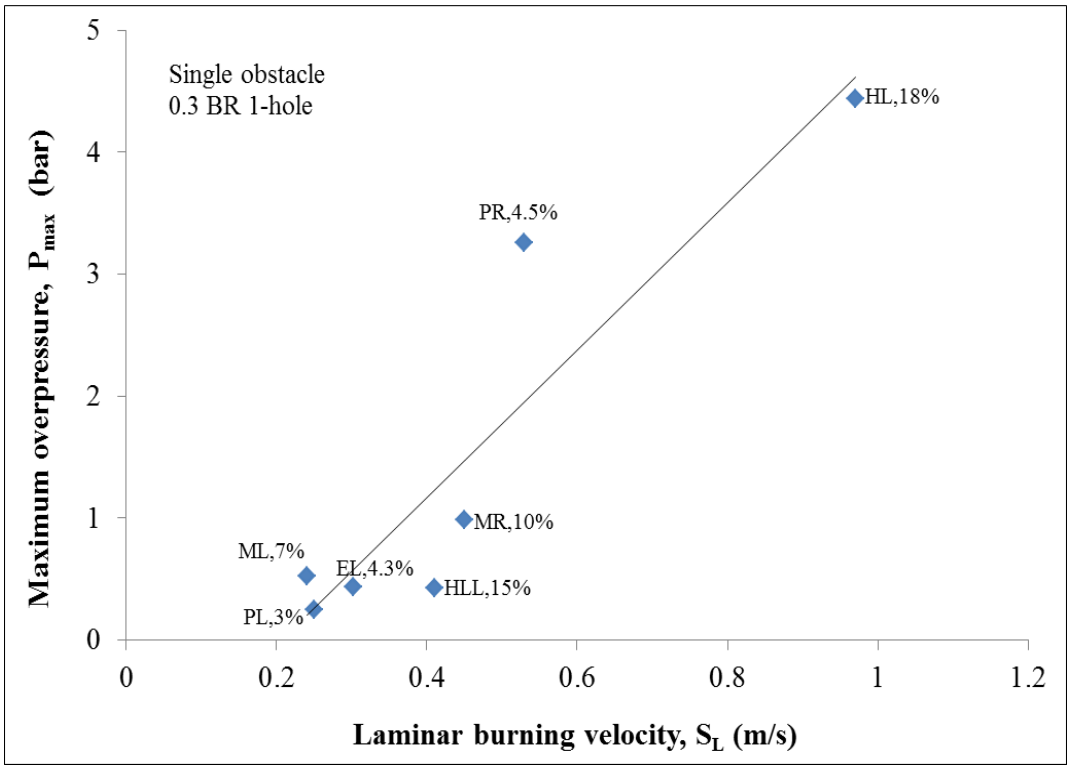

Figure 5.10 Relationship between the maximum overpressure and laminar burning velocities from different fuel types and concentrations.

The effects of dimensionless obstacle separation distance (for two obstacles 0.3 BR 1-hole) in terms of overpressure for all the mixtures tested in this research are presented in Fig. 5.11 with the exception of 18% hydrogen-air mixtures. The influence of obstacle spacing was very evident in terms of both maximum overpressure and pressure development profile for lean methane, propane and ethylene-air mixtures. Unlike the 10% methane mixture the effect of the individual obstacles became distinct with little or no significant influence of the first obstacle on the flame behavior after the second. The full synergistic effect of the two obstacles was recorded at a separation distance of 1.75 m for 10% CH_4, 1.25 m for 7% CH_4 and 2.25 m for 3% C_3H_8, 4.3% C_2H_4 and 15% H_2 air-mixtures.

It was observed that the influence of obstacle separation distance with overpressure was more effective in the slightly rich, 10% methane, compared to 7% methane. The former had an average maximum overpressure of about 2.7 bar which was close to 3.5 times greater than the latter. A worst case obstacle separation distance of 1.75 m and 1.25 m produced the maximum overpressure for both the 10% and 7% methane-air mixtures respectively. For 3% propane-air mixtures, the influence of obstacle spacing with overpressure was discernible with 2.25 m separation being the worst

case. A direct comparison on the effect of mixture reactivity for 4.5% and 3% propane-air mixtures, with double obstacle 1.75 m apart, revealed that the slightly rich mixture test produced 9 bar overpressure and this value was higher than the lean mixture test by a factor of 13. The 15% hydrogen-air mixtures produced an overpressure of about 3.6 bar when the obstacles were spaced at 2.25 m. This value was lower than the 18% hydrogen with one obstacle only which had almost 4 bar maximum overpressure. The 4.3% ethylene-air mixtures had nearly equal optimum overpressure and position with 3% propane-air mixtures i.e. 1 bar at 2.25 m obstacle separation.

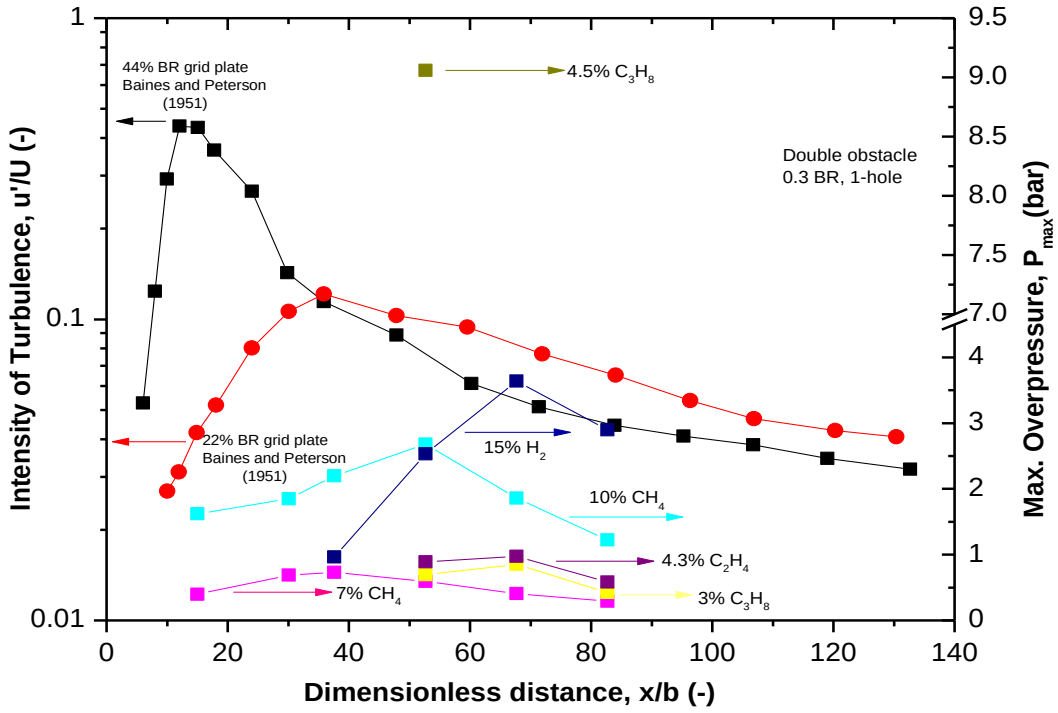

Figure 5.11 Comparisons between the cold flow turbulence and the experimental maximum overpressures from different fuel types and concentrations.

Also shown in Fig. 5.11 is a comparison between the intensity of turbulence downstream of a grid from Baines and Peterson (1951) and average maximum experimental overpressure as a function of dimensionless obstacle separation distance. Even though the cold flow experiments were performed with 0.22 and 0.44 BRs, in the present tests a similar turbulence profile (growth and decay stages) was obtained from the five scenarios. However, the maximum distance happened at a further distance from the obstacle (with 3% propane, 4.3% ethylene and 15% hydrogen greater than the 10% methane and 7% methane) than suggested by Baines and Peterson (1951) cold flows. A probable reason for this non-agreement between

the position of maximum intensity of turbulence and optimum obstacle spacing is that there is a detachment of turbulence profile from the obstacle once the flame moves through it. This body of turbulent fluid would then be conveyed it forward the progressing flame front (and expanding hot gases) and be consumed at the same time.

5.1.4.2 Flame Speed

The flame speeds for the different mixtures were compared with each other along the dimensionless tube length, x_{ig}/D as shown in Fig. 5.12 for single 1-hole obstacle of 0.3 BR. A similar pattern was obtained in terms of severity with the pressure-time profiles in Fig. 5.9. Hydrogen-air mixtures of 18% by vol. produced the highest flame speed of 510 m/s which is nearly a factor of three greater than the least value obtained with 3% propane-air mixtures. It was clearly noticed that the lean limit mixtures with the exception of 18% hydrogen had lower upstream flame speeds (less than 25 m/s) when compared with the slightly rich mixtures. This resulted in high maximum flame speeds downstream of the obstacle in the slightly rich mixture gases.

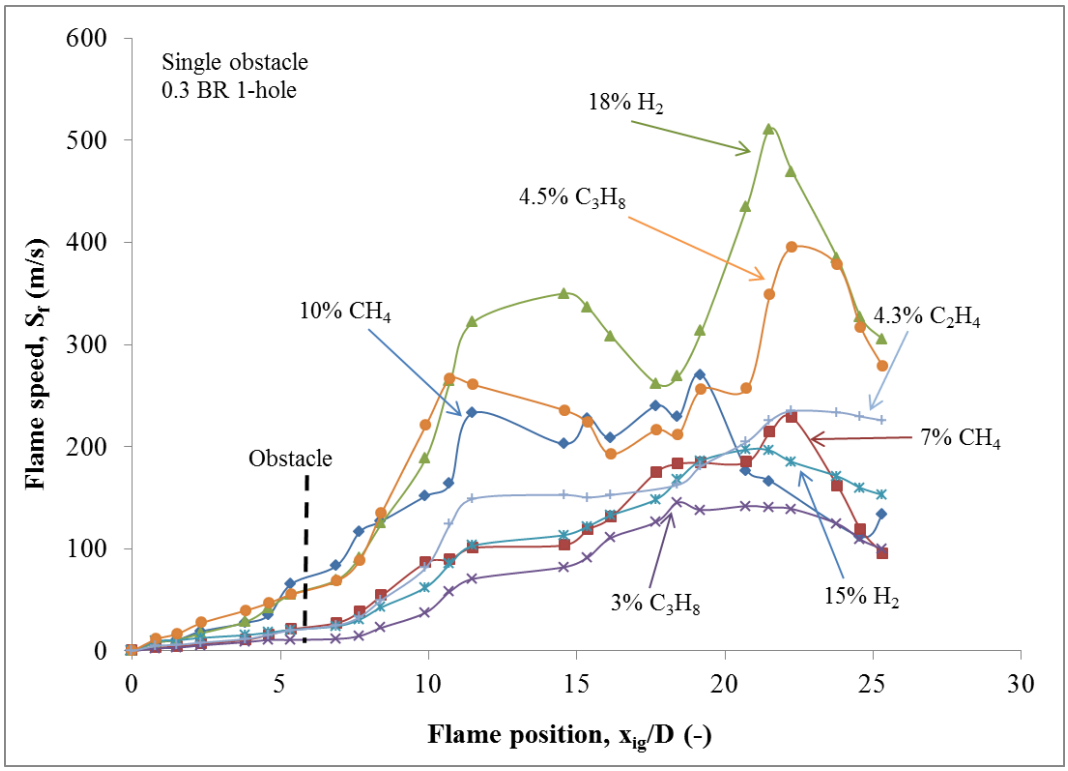

Figure 5.12 Flame speeds across the length of the tube from different mixture reactivities.

A qualitative assessment of the influence of maximum upstream flame speeds, $S_{fu(max)}$ from various fuel types and concentrations for single 0.3 BR 1-hole obstacles was performed. Figure 5.13 shows a range of $S_{fu(max)}$ (11- 60 m/s) against the maximum overpressure. The plot showed that the maximum overpressure increased with increasing $S_{fu(max)}$. A good direct correlation between the two parameters was discernible with a power fit having an R^2 = 0.89 as given in Eq. 5.3. The power exponent, 1.6 (approximately 2 to the nearest whole number) agrees with the overpressure dependence on flame speed in vapour cloud explosions (i.e. $P \propto S_f^2$).

$$P_{max} = 0.004 S_{fu(max)}^{1.6} \tag{5.3}$$

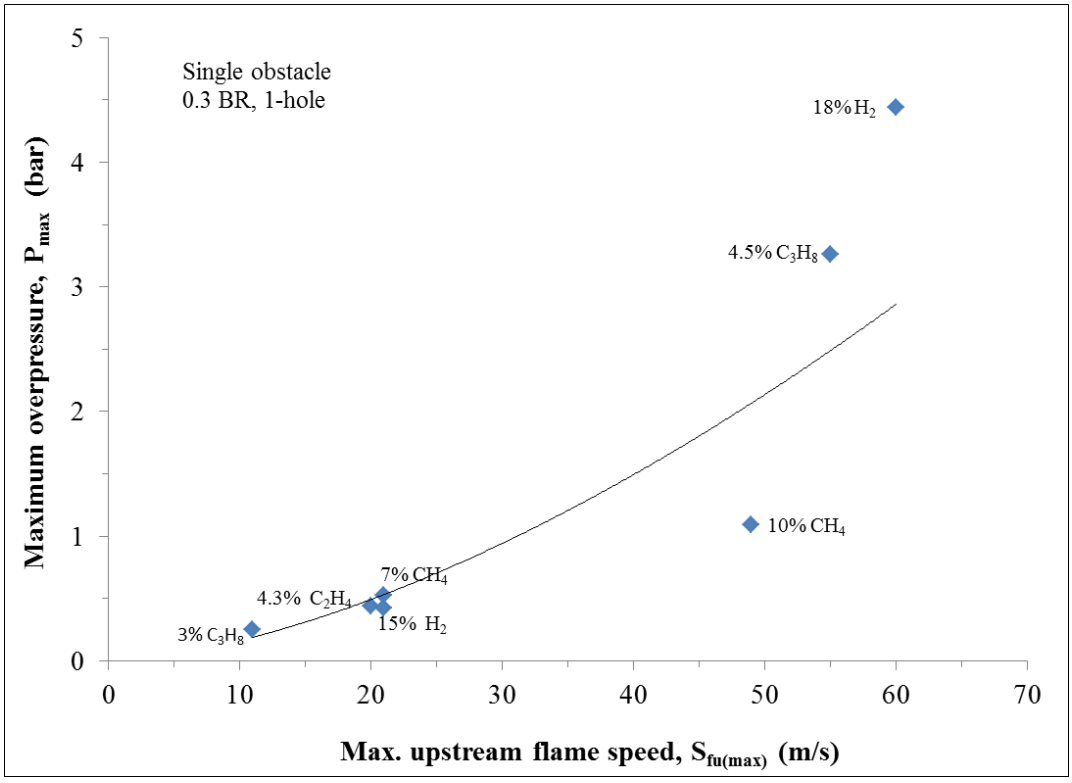

Figure 5.13 Maximum upstream flame speeds versus maximum overpressure from various fuel types and concentrations.

The influence of obstacle spacing on the maximum flame speed is demonstrated in Fig. 5.14. The separation between the obstacles is presented in terms of a non-dimensional distance by dividing the obstacle separation (pitch) with the characteristic obstacle scale, b. It is shown that the maximum effect of the combined obstacles occurred when the separation distance was approximately 38 and 53

obstacle scales for 7% and 10% methane by volume respectively corresponding to flame speeds of 279 m/s and 486 m/s. For the remaining mixtures the maximum effect of the combined obstacles occurred when the separation distance was approximately 68 obstacle scales corresponding to nearly 270 m/s flame speeds for 3% propane and 4.3% ethylene by volume only. However, the 15% by volume hydrogen-air attained a maximum flame speed of about 700 m/s. Also shown in Fig. 5.14 is the flame speed for a single test with slightly rich (4.5%) propane with the obstacles 1.75 m apart and this produced a very high flame speed of about 930 m/s downstream of the second obstacle. The detonation flame speed for propane is about 1,800 m/s and therefore the measured flame speed of 930m/s would suggest it was still a deflagrative event, however it should be noted that the accuracy of the thermocouple flame speed measurement technique at such high flame speeds (for a - most likely-highly fragmented and distributed flame front) and over a relative short distance travel is questionable. The corresponding pressure signal for this test showed that the signal was truncated at 9 bar as it was outside the range of measurement of the transducer suggesting that pressure peak was higher than 9 bar i.e. higher than the adiabatic explosion pressure. Therefore if this was not a detonation it was certainly a DDT event.

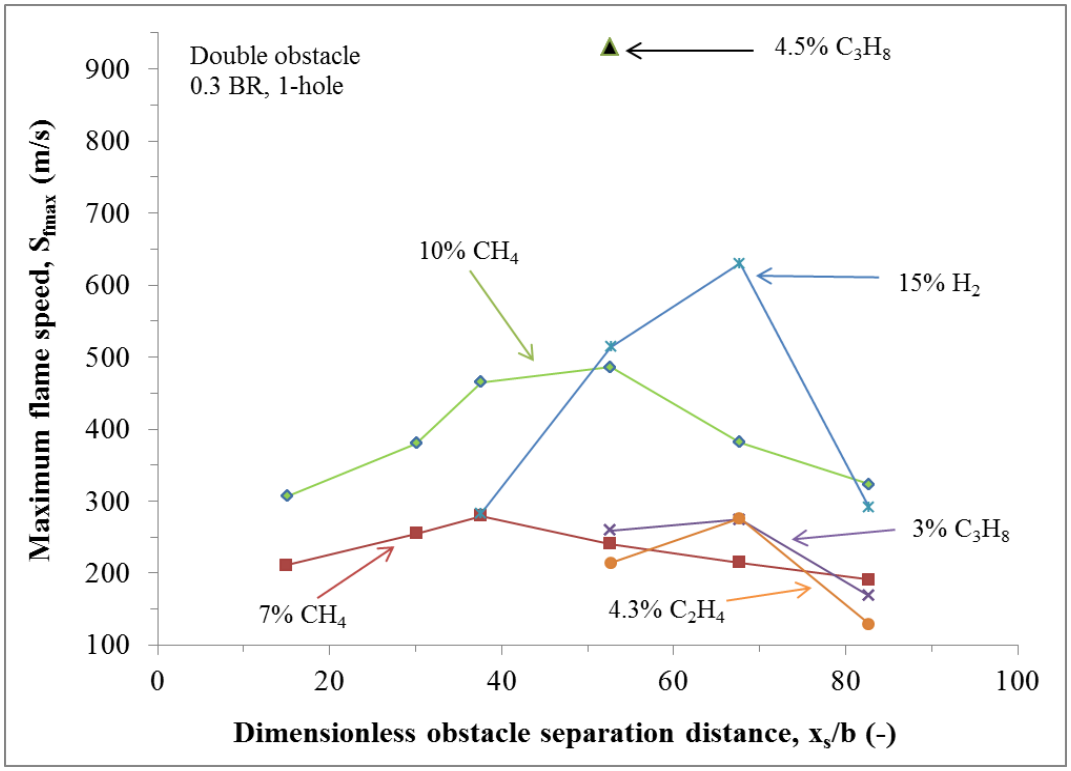

Figure 5.14 Relationships between maximum flame speeds and dimensionless obstacle separation distance for different fuel – air mixtures at various concentrations.

From the preceding analysis on mixture reactivities, it can be concluded tentatively that laminar burning velocities play an important role in determining the severity of gas explosions in terms of overpressure and flame speed. Fuel of different types can produce similar maximum overpressure provided that their laminar burning velocities are equal. The current work also showed that the worst case obstacle separation distance changes with fuel concentration and type. The possible reason for this is the variation of the Lewis and Markstein numbers, which influence the turbulent burning velocities for the same turbulence levels. However, the positions to worst case separations are within a factor of 2 to 4 (a factor of 3 on the average) higher than what was predicted from Eq. 2.23. An average factor of three is obtained for all the fuel types and concentrations tested in the current work.

5.1.5 Influence of Obstacle Blockage Ratio

Systematic studies on the influence of obstacle blockage ratio for single obstacles were previously performed in this laboratory by Phylaktou (1993) and Gardner (1998) using elongated totally closed and vented tubes respectively. The former

author varied the blockage ratio of single-hole obstacles from 0.2 to 0.8 whereas the latter altered the blockage ratio of flat-bar obstacles from 0.2 to 0.8. In all situations, explosion overpressure and flame speeds were found to increase with obstacle blockage ratio. Also, Ibrahim and Masri (2001) studied the influence of obstacle blockage ratio for a range of 10-75% using various obstacles of different shapes. For multi-obstacle tests, the effect of obstacle blockage was explored by Moen *et al.* (1982), Bjorkhaug (1986), Harrison and Eyre (1987), Cicarelli *et al.* (2005) and Yibin *et al.* (2011) among others. A similar trend was also found similar to single obstacle tests.

The actual obstacle blockage ratio is a measure of the blocked area offered to the upstream flow area, thus, this can be changed by varying the dimensions of the obstacle. For 1-hole obstacles this was attained by altering the orifice diameter. This essentially involved a change in the obstacle scale, b, taken as the width of material perpendicular to the flow direction. Thus any explanation of the effect of BR for these obstacle types entailed an associated influence of scale.

In this research, the influence of obstacle blockage ratio for single-hole obstacles from 0.2-0.4 BRs were studied for both single obstacles (Tests 2, 25 and 52) and double obstacles at various obstacle spacing (Tests 3-8, 26-28 and 53-55).

5.1.5.1 Pressure Development

Figure 5.15 shows the relationship between the maximum overpressure against obstacle blockage for single obstacles with 10% CH_4-air mixtures. It was observed that the increase in obstacle BR resulted in increasing maximum overpressure. This could be attributed to the increase in obstacle scale with blockage from 24 mm to 33 mm and 43 mm for 0.2, 0.3 and 0.4 obstacle blockages respectively. A highest overpressure of about 1.7 bar from 0.4 BR obstacle was attained and this value was 1.6, 2.9 and 6.6 folds greater than 0.3 BR, 0.2 BR and no obstacle tests respectively.

A similar trend was noticed from the previous studies mentioned in 5.1.5. However, at high obstacle blockage (from 0.5 BR), the maximum overpressure was found to decrease with increasing blockage (Phylaktou 1993; Gardner 1998). The presence of such high blockages (small orifice diameter) prevented the flame from developing as freely as would have done without the obstacle.

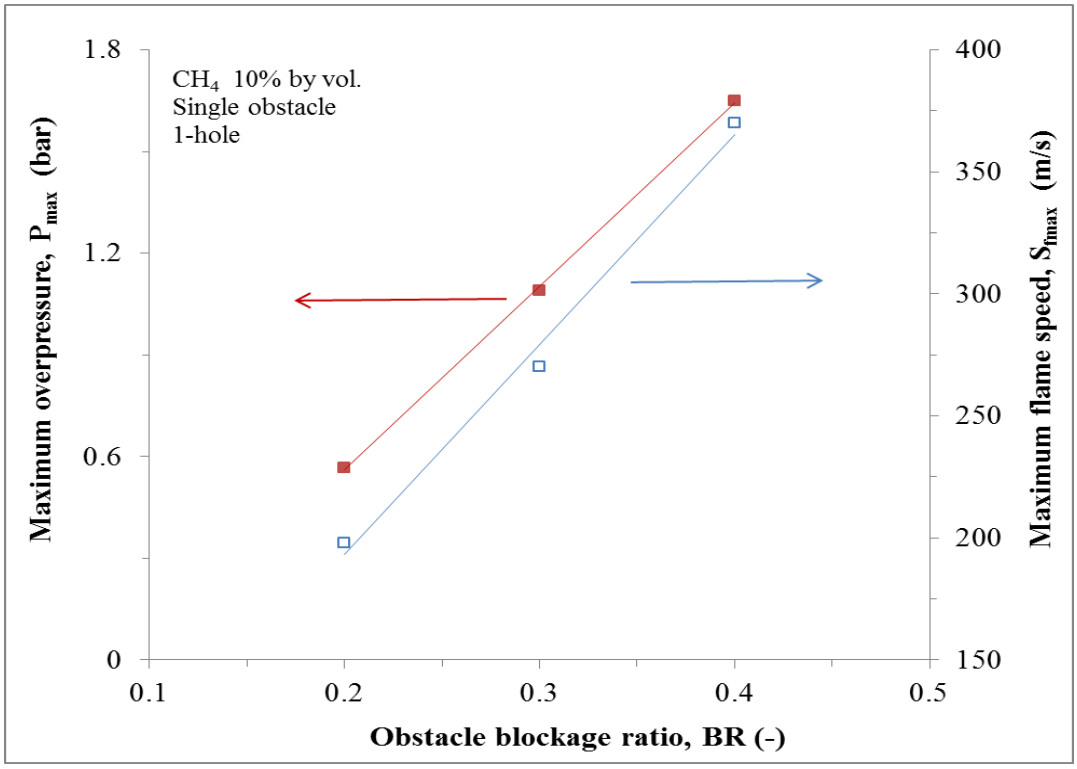

Figure 5.15 Influence of maximum overpressure and flame speeds against obstacle blockage for single 1-hole obstacles.

For the double obstacle configuration tests, the influence of maximum overpressure and flame speed against dimensionless obstacle spacing for various obstacle blockage ratios is shown in Fig. 5.16. A trend comparable to single obstacles was noticed with the double obstacle tests but with a higher magnitude of maximum overpressure. The 0.4 BR produced the highest overpressure of 3.4 bar which was a factor of 1.3 and 2.8 higher than 0.3 and 0.2 obstacle blockage respectively. However, the positions to such maximum overpressures were different with obstacle blockage. The higher obstacle 0.4 BR occurred at a shorter distance (34.9 obstacle scales) in comparison to 0.3 and 0.2 BRs which emerged at 52.7 and 92.4 obstacle scales respectively. This trend was similar to cold flow turbulence intensity of Baines and Peterson (1951) (see Fig. 2.4).

The positions to maximum overpressures and hence intensity of turbulence obtained for the 0.2-0.4 BRs in this work were in agreement with the cold flow prediction correlation of distance to maximum intensity of turbulence as given in Eq. 2.23 with a factor of three. This further validates the predicted correlation of $(x/b)_{max}$.

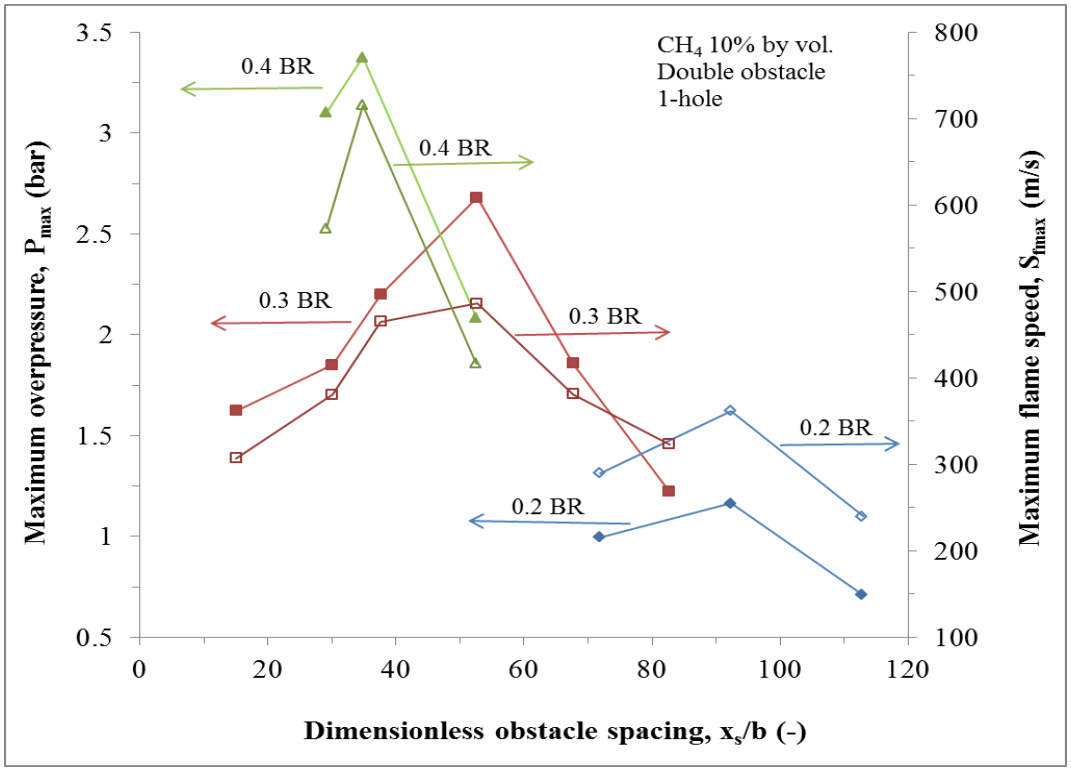

Figure 5.16 Effects of explosion overpressure and flame speed on dimensionless obstacle spacing and obstacle blockage.

The effectiveness of optimum obstacle spacing with just two obstacles with 0.2-0.4 blockage ratios (current work) was compared with the work of Moen *et al.* (1982) using multi obstacles in a large scale vented elongated tube of 50 m^3. The obstacles in the large scale tests were 0.16-0.5 blockage and spaced 2 m apart. Figure 5.17 shows the peak overpressure effect against obstacle blockage for both small and large scale tubes using methane-air combustible mixtures. Even though the obstacle BRs were not the same in both scenarios (with the exception of 0.3 BR), an increase in maximum overpressure and blockage was obtained with the larger scale from Moen *et al.* (1982) been of higher magnitude than the present work. For 0.3 BR, the larger scale (50m^3 tube) produced nearly 4 bar overpressure which is only 1.5 times higher than the small scale in the current work (0.1 m^3 tube). This overpressure would have been greater if the obstacle spacing (2 m) was at its optimum which is going to be larger than 2 m based on Eq. 2.23.

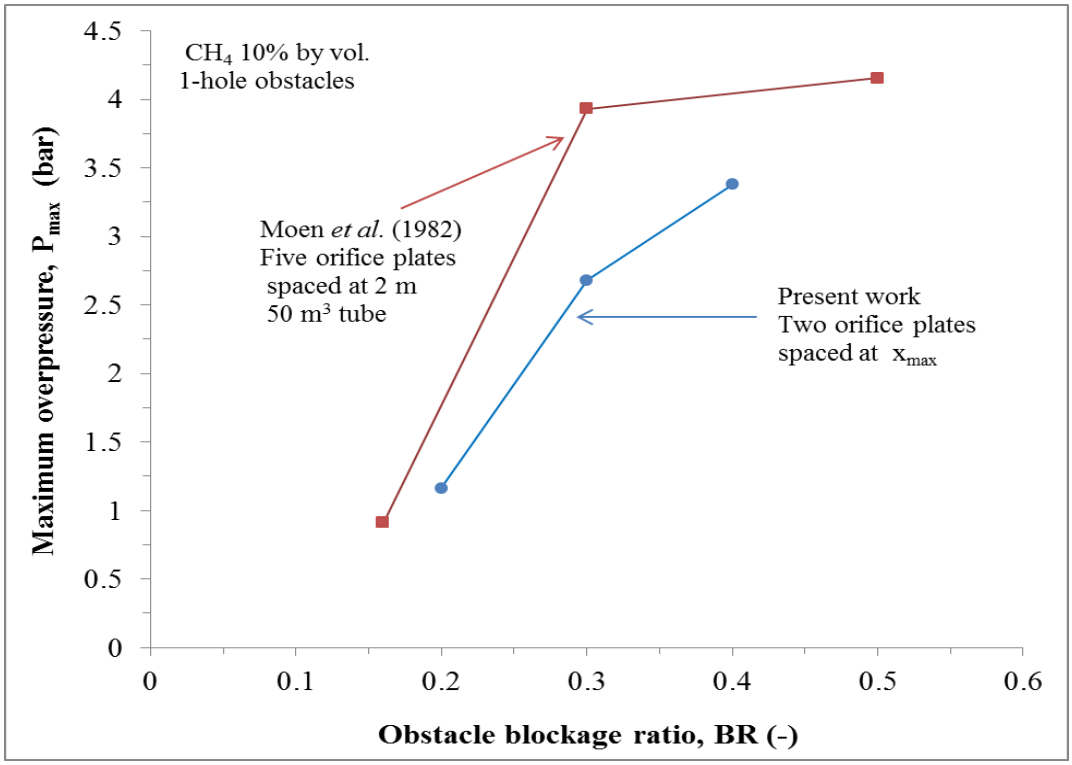

Figure 5.17 Comparison between the maximum overpressure and obstacle blockage from large scale (Moen *et al.* 1982) and present work.

A direct comparison between the intensity of turbulence in cold flow turbulence from Baines and Peterson (1951) and maximum overpressure from the present work at different obstacle blockages is presented in Fig. 5.18. As noticed earlier, similar turbulence profile of growth, peak and decay were noticed in both cases. Also, the position to maximum explosion severity was found to decrease with increase in obstacle blockage. However, such positions occurred at a further distance than suggested in Baines and Peterson (1951).

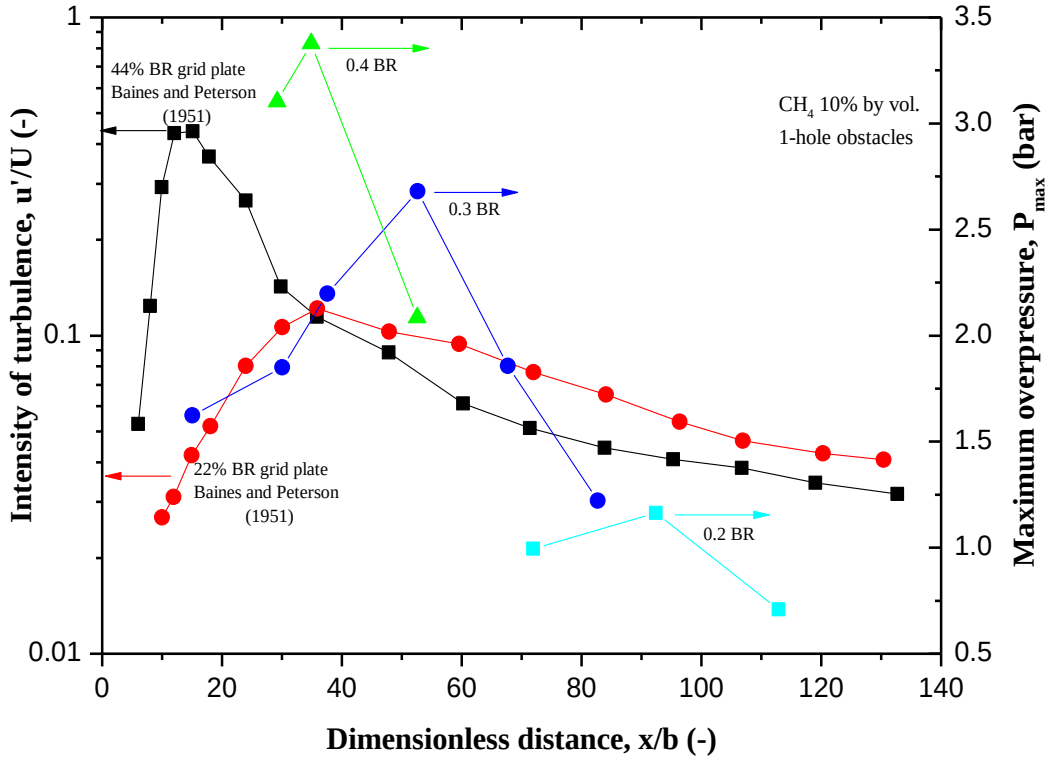

Figure 5.18 Comparison between cold flow turbulence and transient flow experiments with different obstacle blockage ratios.

5.1.5.2 Flame Speed

Also shown in Fig. 5.15 is the relationship between the maximum flame speeds against obstacle blockage with 10% methane-air mixtures. Similar to maximum overpressure, an increase in flame speeds with blockage was obtained. The highest flame speed (370 m/s) attained was with 0.4 BR. This flame speed was a factor of 1.4 and 1.9 higher than 0.3 and 0.2 obstacle blockage ratios respectively.

For the double obstacle tests with variable obstacle spacing, the effect of obstacle blockage with maximum flame speeds is also given in Fig. 5.16. The highest peak flame speeds transpired with a BR of 0.4 followed by 0.3 and 0.2 in that order as 716 m/s, 486 m/s and 362 m/s. However, these values occurred at different obstacle spacing. A similar turbulence profile observed with maximum overpressure with dimensionless spacing was also discernible with the maximum flame speeds.

5.1.6 Influence of Obstacle Shape

Under similar experimental conditions, it was shown in Chapter 2 that thin or sharp-edged obstacles generate higher turbulence levels than thick or round edged obstacles. This could be due to the influence of turbulence generation constant, C_T and hence higher turbulence intensity in the shear layer produced by a sharp obstacle than that produced by a round obstacle. Experiments from a wedge-shaped vessel by Bjorkhaug (1986) showed that the pressure development due to sharp obstacles was nearly doubled of the round obstacles. This corroborated the findings of Hjertager (1993) experiments where an overpressure factor of 2-3 higher was attained for sharp edged obstacles compared to round ones for low to moderate blockage ratios. However, Phylaktou (1993) obtained a factor of 5.5. Van Wingerden *et al.* (1991) demonstrated that the influence of obstacle shape on flame speed was more sensitive to low level of congestions than for high level.

Other experimental works from Lee *et al.* (1984), Moen *et al.* (1989), Lindstedt and Michels (1989), Starke and Roth (1989), Gardner (1998), Ibrahim and Masri (2001), Yu *et al.* (2002), Park *et al.* (2007), Yibin *et al.* (2011) and Zhou *et al.* (2012) have studied the influence of gas explosions with obstacles of various shapes.

In the present work, three obstacles shape namely: orifice plate, flat-bar and disc baffle of 0.2 BR each were used for single obstacle tests only (see tests 31, 52 and 72). For the double obstacle with varying obstacle spacing and blockage, baffle disc was not used.

The orifice plate in the current study represented sharp-edged orifice plates situated perpendicular to the approaching flow. At the plane of an orifice opening, flow separates from the surface of the orifice to a form a discrete jet. Subsequently, recirculation zones are formed. Therefore in the current test geometry, the flow was not instantly influenced by the walls of the test vessel immediately downstream of the orifice but was free to develop radially. Equally, gas flow through 1- flat-bar obstacle was directed between the edges of the obstacle and the wall of the test-vessel. Recirculating regions would then initiate behind the bar towards the vessel centreline. The disc baffle could be regarded as flat, sharp-edged plates placed perpendicular to the oncoming flow. The disc had a larger obstacle scale when compared to both single-hole and flat-bar (Gardner 1998).

5.1.6.1 Pressure Development

Figure 5.19 shows the relationship between maximum overpressure due to single obstacles and obstacle blockage ratio for different obstacle shapes. For 0.2 BR, 1-flat-bar produced the highest overpressure of about 0.67 bar followed by a baffle disc and orifice plate in that order. This trend was observed with the experimental work of Gardner (1998) where 0.2 BR 1-flat-bar produced a higher overpressure nearly equal to the present compared to 1-hole obstacle with about 0. 5 bar. This could be as a result of higher obstacle scale in the flat-bar (26 mm) than orifice plate (24 mm). The influence of obstacle scale was discussed in next section (5.1.7). However, despite the larger scale of the disc plate (58 mm), the overpressure for this obstacle did not generate the highest overpressure. This suggested a strong dependence of obstacle shape on explosion development.

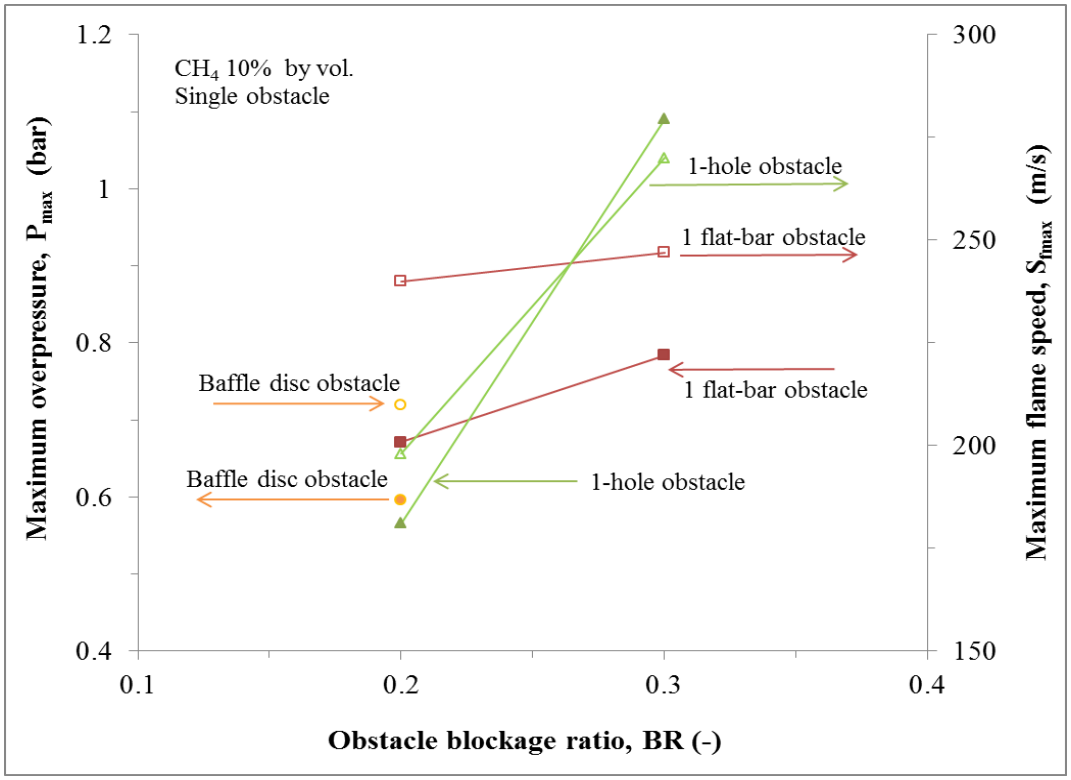

Figure 5.19 Influence of obstacle shapes on maximum overpressure and flame speeds for single obstacles.

By increasing the obstacle blockage ratio to 0.3 (for 1-hole and 1-flat-bar only), the overpressure in 1-hole obstacle was higher (1.1 bar) than the 1-flat-bar by an order of 1.4. However, a general trend of increase in overpressure with blockage ratio was discernible in both obstacle shapes. Gardner (1998) also noticed an increase in

overpressure with blockage ratio up to 0.7 for both hole and flat-bar obstacles with the former higher than the latter from above 0.3 BR.

Flame behaviour during premixed ethylene-air explosions in an enclosed glass cylindrical enclosure of 0.1m diameter and 0.38m length was studied experimentally by Starke and Roth (1989). Orifice plate, circular plate or circular wire grids of 0.75, 0.36 and 0.25 blockage ratios respectively were used as obstacles. The fuel-air mixtures had an equivalent ratio of 0.5 and it was ignited via spark plug centrally from one of the end flange using a special ignition system. Orifice plate obstacles were found to provide the maximum combustion overpressures followed by circular plates and wire grid respectively. The comparison is not systematic since each obstacle shape had different obstacle blockage. However, photographic evidence of similar experiments in a glass tube revealed differences in flame propagation and shape downstream of these obstacles. For the orifice plate, the flame passed through the aperture as a jet which led to fast mixture burning downstream. In case of the disc-shaped obstacle, a toroidial flame shape was formed downstream whereas wire-mesh (assumed to be flat-bar type obstacle) split the flame into several flamelets.

Recently, Yibin *et al.*(2011) performed an experimental work with methane-air mixtures in a semi-open tube with five different types of obstacle shapes (plates, cuboids, triple prisms, quadruple prism and cylinders) and obstacle blockage ratio of 0.2-0.6. The plates and cylinders could be regarded as flat-bar and baffle disc respectively in the present research. The authors observed that for similar blockage ratios, results showed that plates and triple prisms augmented flame speed and overpressure much larger followed by cuboids while effect of quadruple prisms and cylinders were relatively low. An increase in obstacle blockage also resulted in increase in the explosion severity. High speed photography showed that when the flame approached the obstacles, plates and triple prisms formed a vortex while the flame front of cuboids was also clearly distorted. The flame front of quadruple prism was fairly smooth but the combustion intensity of cylinder was the least in all obstacles.

Figure 5.20 shows the effect of maximum overpressure against dimensionless obstacle spacing with double obstacle of various shapes and blockage ratios. As observed with the single obstacle tests, 1-flat-bar of 0.2 BR produced a greater overpressure of 1.29 bar compared to 0.81 bar for 1-hole obstacles. The reverse was

the case for 0.3 BR where 1-hole obstacles generated about 2.67 bar overpressure whereas 1-flat-bar had 2.42 bar. However for both obstacle blockage and shapes, an influence of obstacle separation was discernible with complete turbulence profiles indicating growth, peak and decay. For a given obstacle blockage, the optimum obstacle spacing for the two obstacle shapes was the same. The 0.3 BR obstacles attained its optimum explosion severity with 1.75 m pitch whereas 0.2 BR was at 2.25 m obstacle spacing. However, due to slightly higher scale effects for the flat-bar obstacles compared to hole-obstacles, the former were noticed to realize their maximum explosion overpressure at a relatively shorter dimensionless distance when related to the 1-hole obstacles. The optimum spacing in the experiments (i.e. 1.75 m and 2.25 m) agreed with the predicted correlation of optimum obstacle spacing from cold flow turbulence given in Eq. 2.23 previously.

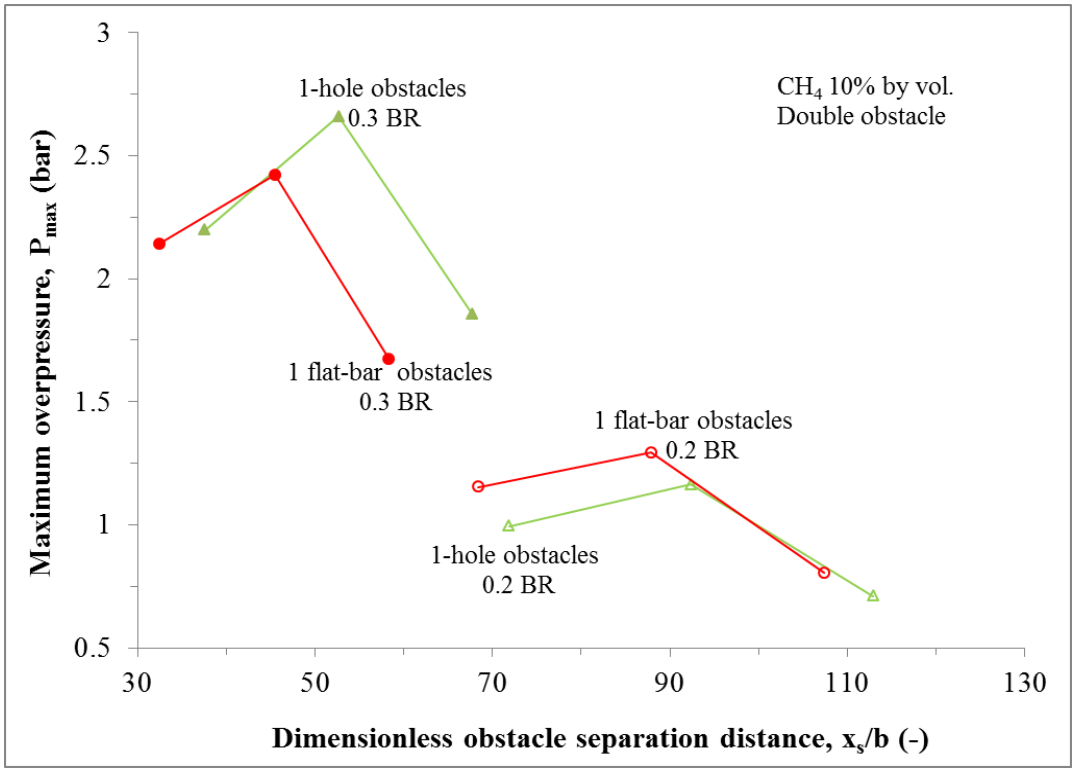

Figure 5.20 Maximum overpressures from double obstacle against dimensionless obstacle spacing for single-hole and flat-bar obstacles.

5.1.6.2 Flame Speed

Also shown in Fig. 5.19 is the maximum flame speeds from a single obstacle against obstacle blockage ratio for different obstacle shapes. For 0.2 BR obstacles, 1-flat-bar obstacle produced the highest maximum flame speeds of about 240 m/s followed by 210 m/s and 198 m/s respectively for disc baffle and 1-hole obstacle. This trend was equally witnessed in overpressure records. As the obstacle blockage ratio was increased to 0.3, 1-hole obstacle attained a flame speed of nearly 270 m/s which is a factor of 1.12 greater than the 1-flat-bar obstacle. It was also seen that the 1-hole obstacle was more sensitive to obstacle blockage when compared to the 1-flat-bar. The former had an increase in flame speed from 198 m/s to 270 m/s respectively for 0.2 and 0.3 BRs whereas the latter had a nearly constant flame speed that ranged from 240 m/s to 247 m/s for 0.2 and 0.3 blockage ratios in that order.

The relationship between the maximum flame speeds and obstacle spacing with two different obstacle shapes and blockage is given in Fig. 5.21. The flame speeds had similar turbulence profile, position to optimum spacing and blockage ratio effect to the maximum overpressure results presented in Fig. 5.20. For maximum flame speeds with 1-hole obstacles, values of 486 m/s (at 1.75 m obstacle spacing) and 362 m/s (at 2.25 m obstacle spacing) were obtained for 0.3 and 0.2 BRs respectively. However, 463 m/s (at 1.75 m obstacle spacing) and 412 m/s (at 2.25 m obstacle spacing) were accomplished for 0.3 and 0.2 BRs in that order from the 1-flat bar obstacles.

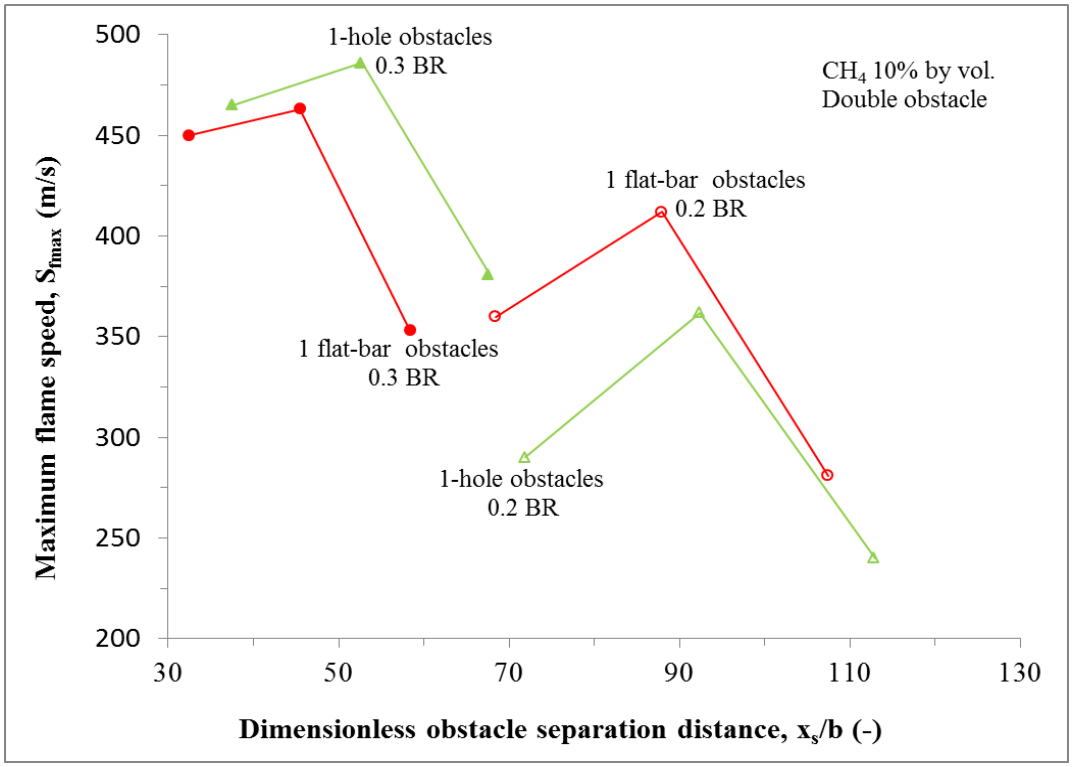

Figure 5.21 Maximum flame speeds for double obstacle of various shapes, blockages and obstacle spacing.

5.1.7 Influence of Obstacle Scale

Most investigators acknowledged that for a meaningful interpretation of results from small scale tests in the laboratory to the large scale ones similar to real industrial size, an explicit influence of scale is required. However, a variation in scale could be achieved by either varying the size of the explosion rig or by varying the characteristics size of the obstacle for a fixed size of rig. Most turbulent combustion models have been carried out in fixed-size equipment. Explicit review on the influence of scale and turbulent combustion models were reviewed previously in Chapter 3.

In the current work, the influence of scale was systematically studied using a fixed geometry and varying the obstacle scale for a given similar blockage ratio. For hole obstacles, this was achieved by increasing the number of smaller, drilled holes ranging from 1-16 (5-43 mm obstacle scale) for 0.4 blockage ratio (Tests 25, 29-30). The flat-bar obstacle scale was varied by reducing the width of the bars as their number was increased from 1-4 (6-26 mm obstacle scale) for 0.2 blockage ratio

(Tests 31-34, 35-38 and 48-51). For both obstacle scales, 10% methane-air by volume was used as the explosible mixtures.

5.1.7.1 Pressure Development

Figure 5.22 shows a plot of maximum overpressure from single obstacles against obstacle scale for multi-flat-bar and multi-hole obstacles of 0.2 and 0.4 blockage ratios respectively. Also shown is the maximum overpressure for single multi-flat-bar obstacles of 0.3 blockage from Gardner (1998). In overall, a strong power dependence of maximum overpressure with obstacle scale, b was indicated as shown by the fitted lines for all the obstacles. However, the magnitude of overpressures was found to increase with obstacle blockage.

P_{max} scales with $b^{0.33}$ and the flame speed scales with $b^{0.15}$, which agrees with a roughly square relationship between overpressure and flame speed. These are similar to the dependences previously found by Phylaktou *et al.* (1994,1995 and 1998). These length scale exponents are lower than those from the MERGE data in an overpressure correlation analysed by Gardner *et al.* (2001).

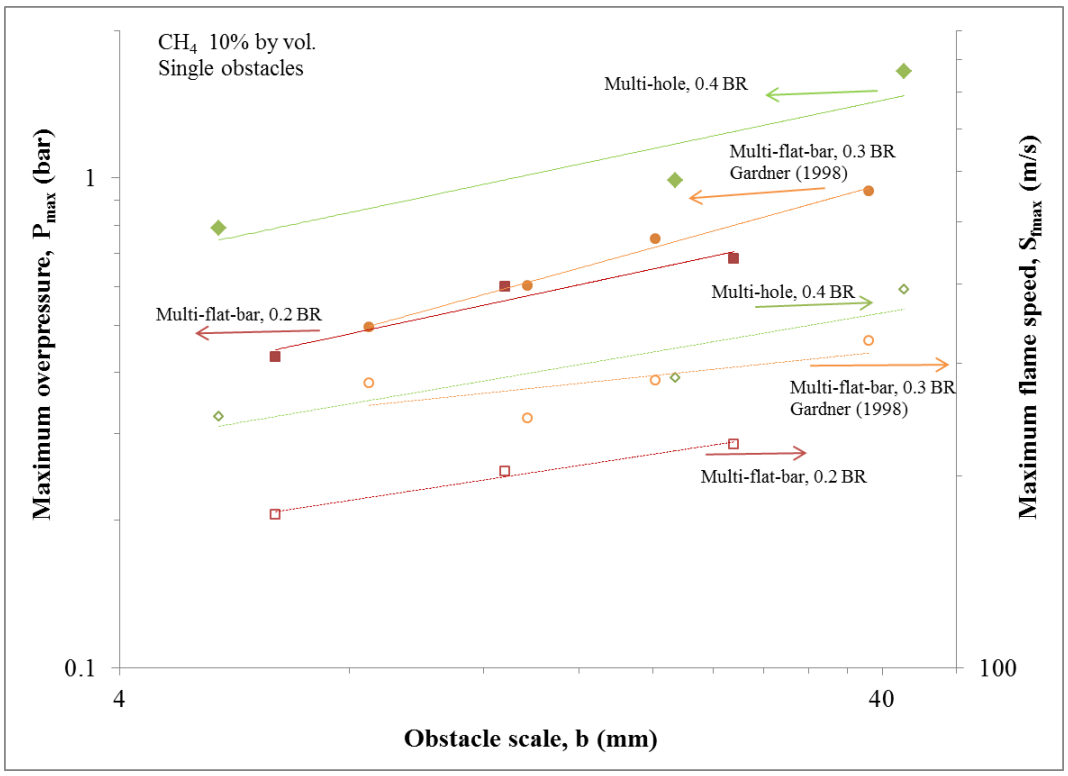

Figure 5.22 Maximum overpressure and flame speeds from single obstacles versus obstacle scale.

For double obstacle configurations with variable obstacle spacing, the influence of obstacle scale was explored with multi-flat-bar only. Figure 5.23 presents the maximum overpressure and dimensionless obstacle spacing for 1-4 flat-bar obstacles. Also shown is the intensity of turbulence profile against dimensionless distance downstream of a bar-grid obstacle of 0.22 BR from Baines and Peterson (1951). It was observed that the maximum overpressure increased with the reduction in number of flat-bars. This was as a result of the increase in obstacle scale, b with decrease in number of flat-bars. A maximum overpressure of about 1.29 bar at 2.25 m (87 obstacle scales) obstacle spacing was achieved with 1-flat-bar followed by 1.18 bar and 1.10 bar for 2 and 4-flat-bars respectively at 1.25 m (98 obstacle scales) and 0.5 m (78 obstacle scales) obstacle separation. This shows as the obstacle scale increased the optimum obstacle spacing also increased in absolute terms. However the optimum obstacle separation distance in terms of number of obstacle scale was roughly constant between 80 and 100 within the resolution of the data due the limited spacing distances possible in the experiments. The positions to worst case obstacle spacing (in absolute terms) in all the obstacles agreed with the prediction correlation of Eq. 2.23 if multiplied by a factor of three.

The overall pattern of the maximum overpressure with dimensionless obstacle spacing for all the obstacles was similar to turbulence intensity profile from Baines and Peterson (1951). For nearly equal obstacle blockage ratio (0.2 BR) between the cold flow and the present work, the latter attained its maximum values at a further distance from the obstacle than suggested by the former. This shift was also noticed with orifice plates in the current experimental work.

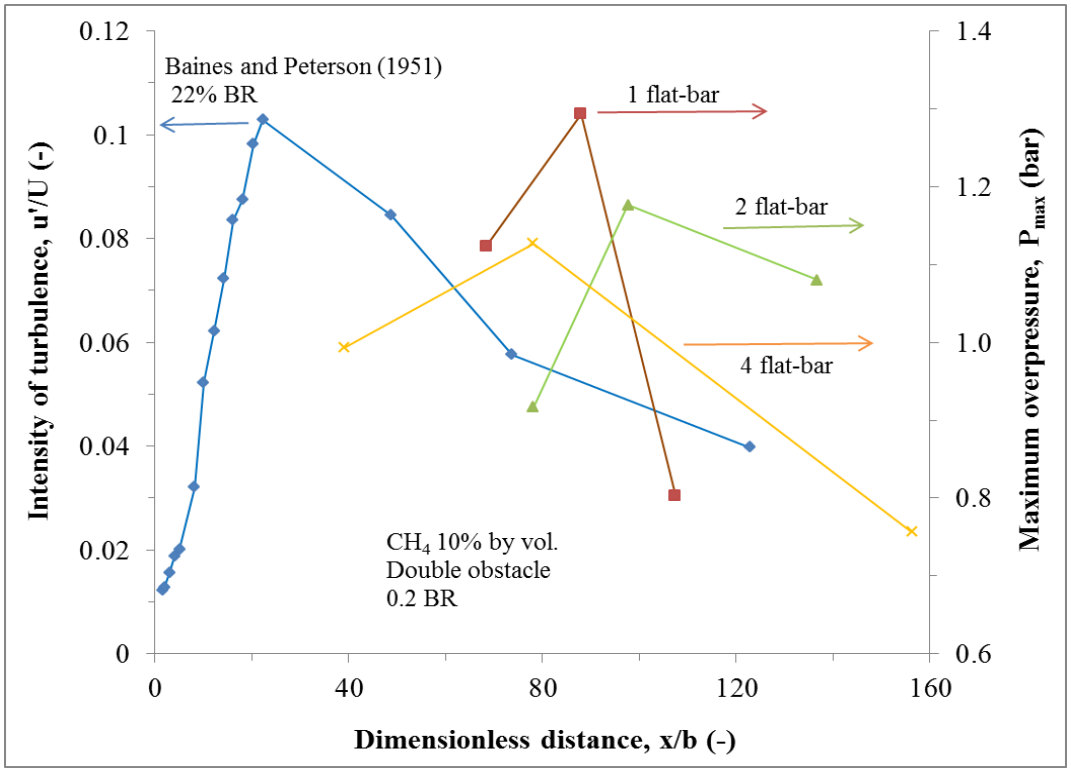

Figure 5.23 Comparison between intensity of turbulence from cold flow turbulence and transient experimental work with flat-bar obstacles.

5.1.7.2 Flame Speed

Also presented in Fig. 5.22 is the maximum flame speeds against obstacle scale, b of different obstacle shapes and blockage for single obstacles. As noticed with maximum overpressure, there was a strong dependence of maximum flame speeds with obstacle scale for all blockages. A maximum flame speed of close to 400 m/s was obtained with 43 mm obstacle scale (1-hole 0.4 BR); this value was about two times greater than that with 26 mm obstacle scale (1-flat-bar 0.2 BR).

The effect of maximum flame speeds on dimensionless obstacle spacing between two obstacles for 1-4 flat-bar obstacles is shown in Fig. 5.24. The profiles, dependence of obstacle scale and positions to optimum obstacle spacing in flame speeds were similar to those in maximum overpressure results.

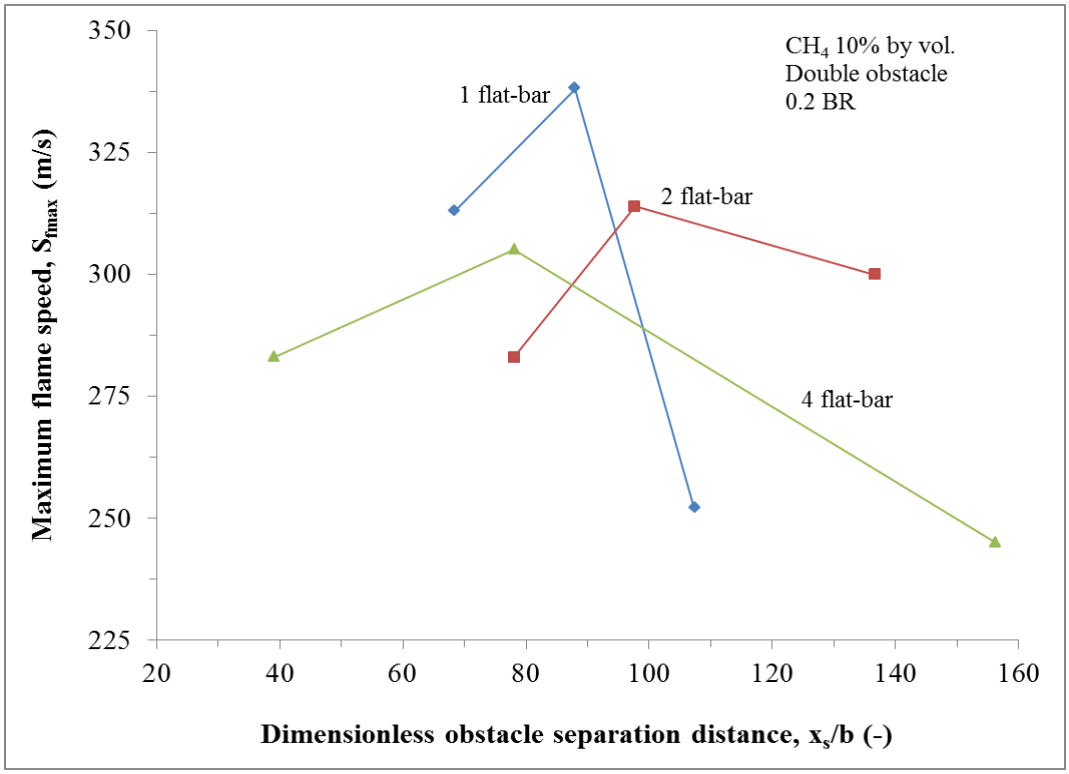

Figure 5.24 Influence of obstacle scale on maximum flame speeds and dimensionless obstacle spacing.

5.1.8 Influence of Optimum Spacing: Comparison with the Literature

In the present work, the influence of obstacle separation was studied on various obstacle blockage ratios, obstacle shapes, fuel types and fuel concentration mixtures. In each case, an optimum spacing corresponding to the worst case explosion scenario was found. These spacing were then compared with multi-obstacle tests with fixed pitch from the literature so as to quantify the effectiveness of obstacle spacing. Figure 5.25 and 5.26 show the relationship between dimensionless obstacle separation against maximum overpressure and flame speeds respectively for the present work and literature. The symbols used in both figures i.e. M, P, E and H represent the different fuel types as methane, propane, ethylene and hydrogen in that order. The lean and rich mixtures in the two figures were denoted as L and R respectively.

Table 5.2 shows an overview of the present test with optimum obstacle spacing and multi-obstacles from the present work and literature.

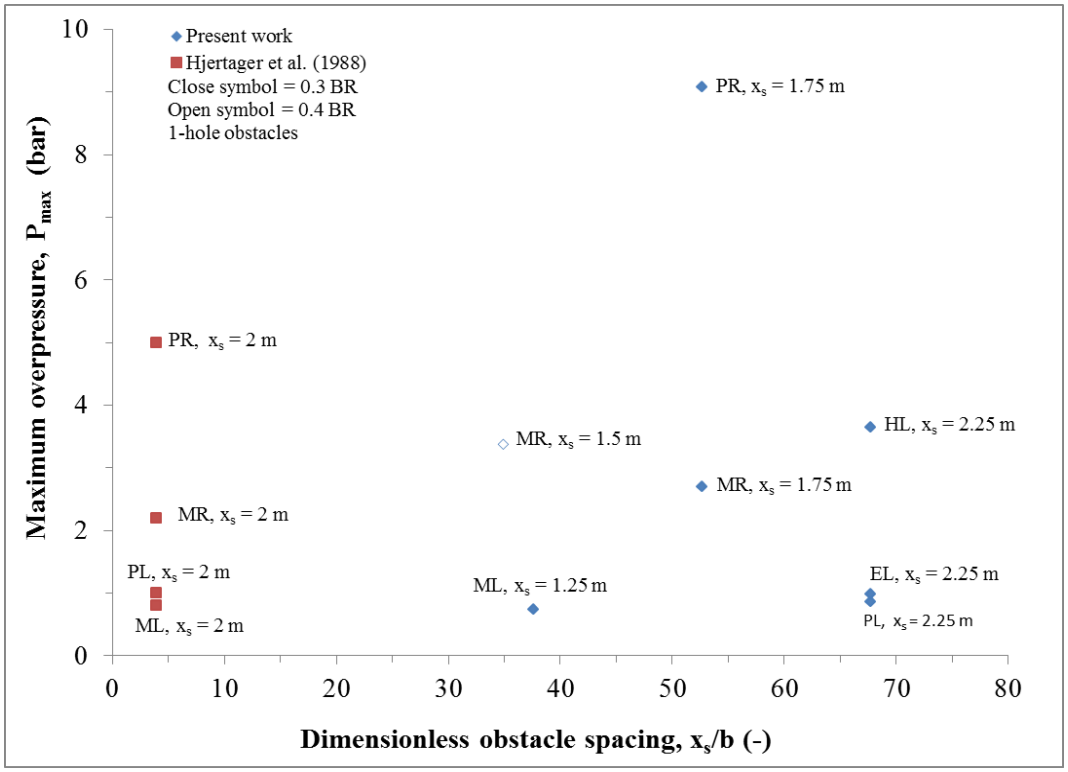

Figure 5.25 Comparison between the present work with two obstacles at worst case separation and the literature on maximum overpressures and dimensionless obstacle spacing.

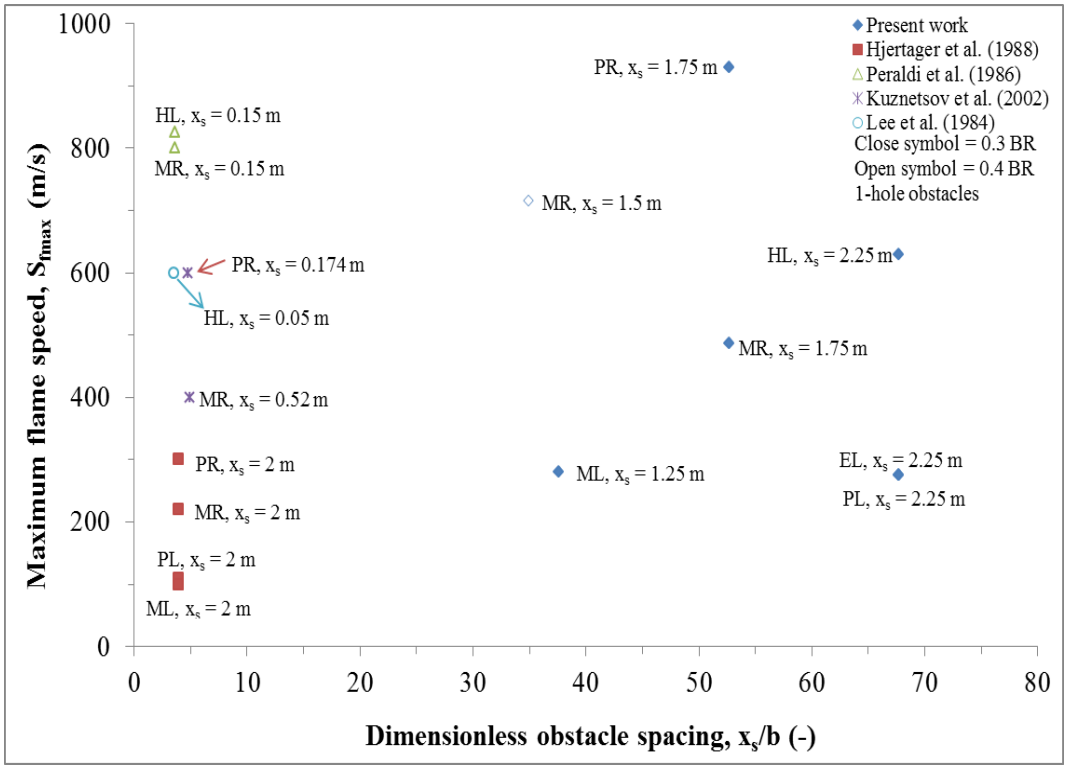

Figure 5.26 Comparison between the present work with two obstacles at worst case separation and the literature on maximum flame speeds and dimensionless obstacle spacing.

Lee *et al.* (1984) performed an experimental investigation on flame acceleration and DDT on hydrogen-air mixtures of various fuel concentrations. An explosion tube of 11 m long and 50 mm cross-sectional diameter, D was used. Obstacles in the form of a spiral coil (0.44 BR) and repeated orifice plates obstacles spaced at D with 0.44 and 0.6 BR were used. The first 3 m length of the tube was filled with the obstacles (estimated to be about 60) while the remaining tube length was obstacle free. For a concentration similar to the present work i.e. 15% H_2-air tests, Lee *et al.* (1984) obtained a maximum flame speed of close to 600 m/s with 0.44 BR orifice plate obstacles. However, a higher flame speed of 630 m/s was achieved in the present work with just two obstacles of lower blockage ratio i.e. 0.3 BR.

Wide-ranging series of experimental tests were carried out by Peraldi *et al.* (1988) using three long tubes of 18 m long with the intention to establish quantitative limiting criteria for the onset of DDT. The internal diameter of each tube was taken to be 0.05, 0.15 and 0.3 m respectively. Fuels such as methane, propane, ethylene, acetylene and hydrogen of various concentrations ignited at the one end of the tube were used. The entire tube length was filled with orifice ring obstacles separated at one tube diameter apart. In comparison with the present work, 0.15 cm diameter tube was used. The authors attained a maximum flame speed of about 800 m/s for 10% methane-air by vol. with 0.4 BR. The flame speed value was just 1.12 times greater than that with two obstacles spaced at 1.5 m apart in the present work. For 15% hydrogen-air mixtures, 825 m/s flame speed was obtained as the optimum speed by the authors with 0.4 BR. This flame speed was just a factor of 1.3 higher in the present work with double obstacle of 0.3 BR spaced at 2.25 m separation.

The present maximum flame speeds and overpressures with two 30% blockage obstacles were compared with those of Hjertager *et al.* (1988a). These authors conducted their research in a vented large scale cylindrical tube of 50 m^3 by volume (10 m long and 2.5 m in diameter). Five 30% blockage steel rings were used as obstacles, regularly spaced at 2 m each apart. Various concentrations of either methane-air or propane-air homogeneously mixed were ignited with either planar or point source the closed end of the tube. For point ignition which is similar to the current work, the authors got a maximum overpressure and flame speed of slightly above 2 bar and 200 m/s respectively for 10% by vol. methane-air mixtures, compared to the significantly higher pressure of 2.7 bar and 486 m/s flame speed

with just 2 obstacles of the same blockage but optimally spaced, in the present work. For 4.5% by vol. propane-air mixtures Hjertager *et al*. (1988a) reported a maximum overpressure and flame speed close to 5 bar and 300 m/s respectively for point-ignition. This is about half the overpressure and 1/3 of the flame speed achieved with just 2 obstacles in the present work. In case of the lean mixture fuels i.e. 7% methane-air and 3% propane-air, a nearly equal overpressure of about unity was achieved in the two scenarios. However, a disparity was noticed in the flame speeds. The present work had a maximum value of flame speeds of about 280 m/s for the two lean mixtures. This was about 2.8 times higher than that obtained from Hjertager *et al*.(1988a).

The flame speeds from the current work were also compared with that of the extensive set of experimental data in obstacle laden tubes by Kuznetsov *et al*. (2002a) and (2002b). In Kuznetsov *et al.* (2002a), the authors used a tube 12 m long with an internal diameter of 174 mm which accommodated 30% BR orifice-plate obstacles spaced at one tube diameter. For 3% propane-air mixtures ignited at the end of the tube, a flame speed of about 600 m/s was attained at about 4.25 m (equivalent tube length of the present test) from ignition with over 20 orifice plates. This flame speed is only double the one obtained in the current test (3% propane-air) with two 30% BR orifice plates 2.25 m apart. In the same year, the authors Kuznetsov *et al.* (2002b) used a large scale tubular geometry of 34.5 m long and inner diameter of 520 mm equipped with 30% blockage orifice-plates spaced at one tube diameter. A flame speed of close to 400 m/s was attained for a slightly rich methane-air mixture at a distance similar to the length of the current explosion tube. This is nearly 100 m/s lower when compared to the 10% methane-air tests with just two obstacles spaced at 1.75 m in the present work.

The above comparisons clearly demonstrate the important effect the obstacle separation distance can have on the severity of the explosion and highlights the possibility that many previous studies with multi-obstacles may have under-demonstrated the effect of repeat obstacles. It was evident that the obstacle spacing from the literature are quite closer (less than five obstacle scales) when compared to the present work. It can now be deduced that large congestions in a given medium do not necessarily signify potential maximum explosion severity as traditionally assumed. But, small congestions optimally separated apart could lead to devastating overpressure.

Table 5.2 An overview of explosions results on optimum obstacle spacing from the present work and multi-obstacle from the literature.

Reference	Geometry		Gas	Conc.	BR	No*	x_s	x_s/b	x to 1st obst.	P_{max}	S_{fmax}
	L	D									
(-)	(m)	(m)	(-)	(%)	(-)	(-)	(m)	(-)	(m)	(bar)	(m/s)
Present work	4.5	0.162	CH_4	10	0.3	2	1.75	52.7	1	2.68	486
Present work	4.5	0.162	CH_4	7	0.3	2	1.25	37.6	1	0.73	280
Present work	4.5	0.162	CH_4	10	0.4	2	1.5	34.9	1	3.38	716
Present work	4.5	0.162	C_3H_8	4.5	0.3	2	1.75	52.7	1	9.06	930
Present work	4.5	0.162	C_3H_8	3	0.3	2	2.25	67.7	1	0.85	275
Present work	4.5	0.162	H_2	15	0.3	2	2.25	67.7	1	3.64	630
Present work	4.5	0.162	C_2H_4	4.3	0.3	2	2.25	67.7	1	0.98	276
Lee *et al.* (1984)	11	0.05	H_2	15	0.44	60	0.05	3.5	-	-	600
Peraldi *et al.* (1988)	18	0.15	$H_{2`}$	15	0.4	120	0.15	3.6	-	-	825
Peraldi *et al.* (1988)	18	0.15	CH_4	10	0.4	120	0.15	3.6	-	-	800
Hjertager *et al.* (1988)	10	2.5	CH_4	10	0.3	5	2	3.96	1.65	2.2	220
Hjertager *et al.* (1988)	10	2.5	CH_4	7	0.3	5	2	3.96	1.65	0.8	100
Hjertager *et al.* (1988)	10	2.5	C_3H_8	4.5	0.3	5	2	3.96	1.65	5	300
Hjertager *et al.* (1988)	10	2.5	C_3H_8	3	0.3	5	2	3.96	1.65	1	110
Kuznetsov *et al.* (2002a)	12	0.174	C_3H_8	3	0.3	20	0.17	4.8	-	-	600
Kuznetsov *et al.* (2002b)	34.5	0.52	CH_4	10	0.3	8	0.52	4.8	-	-	400

* With the exception of the present work and Hjertager *et al.* (1988), all the number of obstacles were based on estimates.

5.2 Flame Acceleration in a Tube with Three obstacles

The influence of number of obstacles as a wider assessment of multi-obstacle congestions typically found in industries have been studied previously by Chapman and Wheeler (1926), Moen *et al.* (1982), Hjertager *et al.* (1988a) and Ning *et al.* (2005). All the authors observed that the severity of explosions in terms of overpressure and flame speeds were affected as the number of obstacles increased. However, in all the previous works, only orifice plate obstacles were used to generate turbulence in the system.

In the present work, the effect of number of obstacles was investigated using flat-bar and baffle-disc obstacles spaced at optimum distance established previously in 5.1.

The test conditions for 2 flat-bar, 4-flat-bar and baffle disc were test number (35, 37, 78), (48, 50, 81), and (72-74) respectively. Also in the current work, the influence of obstacle spacing was studied on 2 flat-bar and 4 flat-bar obstacles only corresponding to test number (77-79) and (80-83) in that order. In all the tests, 10% methane-air was used as the flammable mixture.

5.2.1 Influence of Obstacle Separation Distance

The influence of obstacle separation on the three obstacles was achieved by keeping the spacing of the first two obstacles fixed (at optimum distance established in 5.1) and varying only the spacing between the second and the third obstacles. Figure 5.27 shows an overpressure profile of three obstacles against dimensionless obstacle spacing between the second and third obstacles. The profile is similar to that of cold flow turbulence from Baines and Peterson (1951). For 2 flat-bar obstacles, peak overpressure of 2.2 bar was attained at a separation of 97 obstacle scales (1.25 m separation distance). This distance corresponds to the optimum spacing obtained with two obstacles. In case of 4-flat-bar obstacles, a maximum overpressure of 2 bar was realised at an obstacle spacing of 78 obstacle scales from the second i.e. again at the same relative positioning as the optimum distance of the second obstacle from the first in the two obstacle configuration.

Also shown in Fig. 5.27 are the flame speed results for the 2 and 4 flat-bar obstacles in the triple obstacle configuration. The flame speeds showed similar turbulence profile and position to peak intensity as the overpressures with maximum flame speed of 569 m/s for the 2-flat-bar and 498 m/s for the 4-flat-bar.

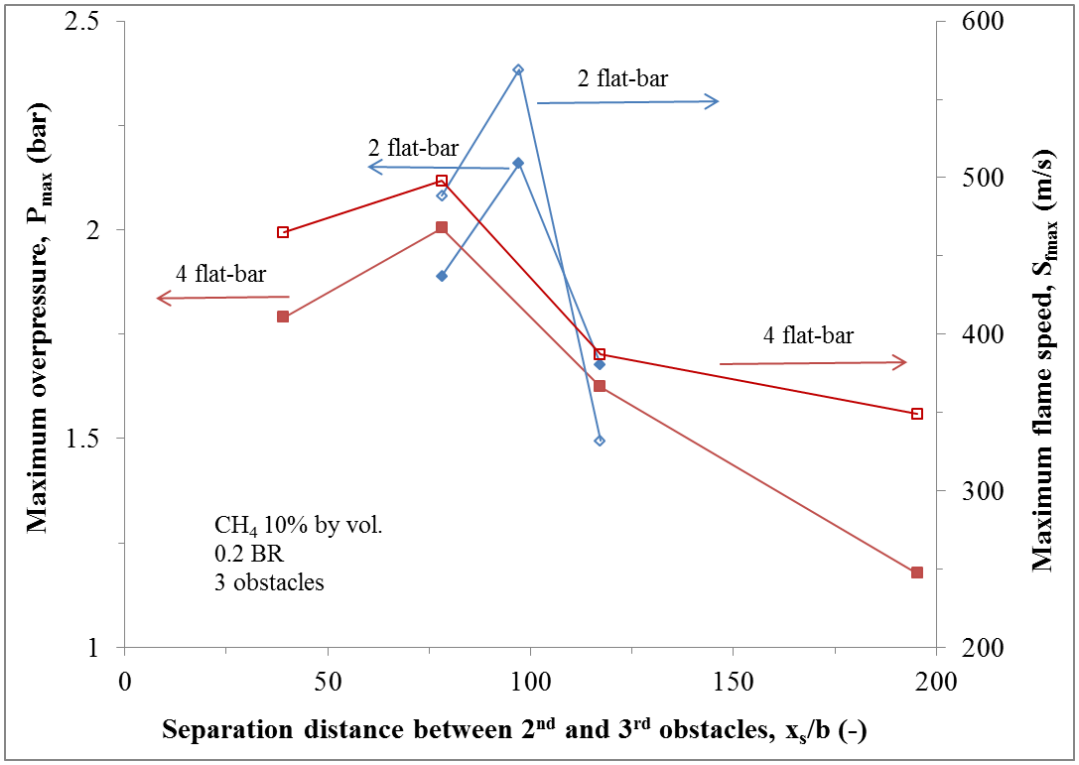

Figure 5.27 Influence of obstacle separation between 2nd and 3rd obstacles on maximum overpressures and flame speeds.

This work shows that for both obstacle types the optimum spacing between the second and third obstacles corresponded to the same optimum spacing found for the first two obstacles. This suggests that the optimum absolute separation distance does not change with number of obstacles nor with the severity of the explosion, but it does change with the obstacle scale. Therefore this suggests that in multi-obstacle explosions, the spacing between obstacles must be kept at optimum value throughout in order to attain the worst case explosion severity.

5.2.2 Influence of the Number of Obstacles

Figure 5.28 shows an overpressure-time profile of 1 to 3 obstacles (2-flat-bar types) of 0.2 BR with 10% methane-air mixtures by vol. The obstacles were spaced at 1.25 m each which was established in 5.1 to give the worst case obstacle separation distance. Upon ignition, the overpressure-time profile was fairly constant in all the obstacle configurations up to the position of the first obstacle positioned at 6.2D from spark. For all the obstacle tests, a sharp rise in overpressure was noticed downstream of the first obstacle and attained a maximum value of about 0.6 bar. The time to this value was slightly delayed in the three obstacle test. Subsequently, the

overpressure in the first obstacle test attenuated and exited the vent at about 72 ms. Another rise in overpressure behind the second obstacle (14D from spark) was observed for the double and triple obstacle tests and a peak value of close to 1.1 bar was achieved with the former while the latter had about 1.3 bar. However, the time to such maximum overpressures were nearly the same in both scenarios. The maximum overpressures doubled that of the single obstacle test. The overpressure in the double obstacle test later decayed and left the vent at the same time with that of single obstacle test. As the flame approached the third obstacle (21.6D from spark), an increase in overpressure was discerned followed by attaining a maximum overpressure of close to 2.2 bar downstream of the obstacle. This value was nearly two and four times greater than that of double and single obstacle tests respectively.

As noticed from the work in Moen *et al.*(1982), multiple peak structures were witnessed in some of the pressure records in the current work, this could be attributed to strong pressure pulses related to intense burning or localised explosions at the other positions in the tube also contribute to the pressure development.

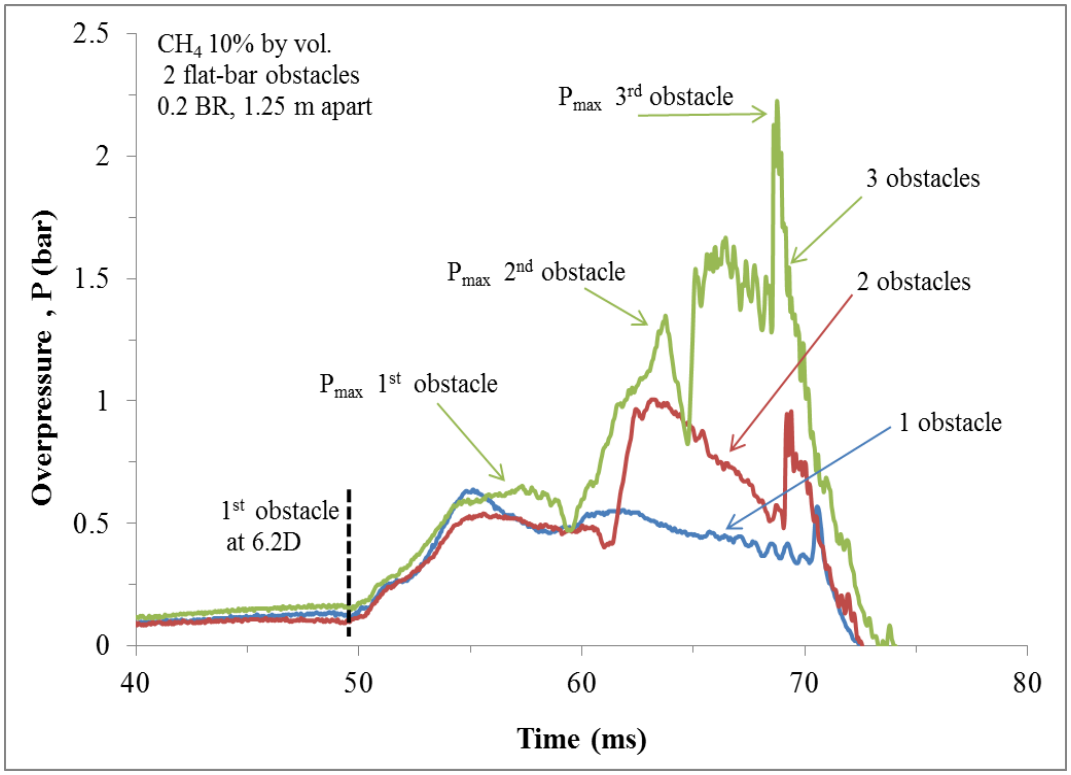

Figure 5.28 Pressure-time profile for 1, 2 and 3 obstacles spaced at optimum obstacle separation distance.

The influence of number of obstacles in terms of flame speeds against a dimensionless distance from spark is shown in Fig. 5.29. The flame speeds in comparison to the patterns shown by pressure-time profile (see Fig. 5.28) demonstrated similar flame development upstream and downstream of the first obstacle location in all the three tests. Similar maximum flame speed of about 43 m/s upstream and 200 m/s downstream of the first obstacle was achieved. The double obstacle test attained a maximum value of 386 m/s downstream of the second obstacle. This value nearly doubled that of a single obstacle test (a similar factor obtained with overpressure effect). For the three obstacle configuration, a maximum flame speed value of about one and a half times higher than that of the double obstacle was achieved.

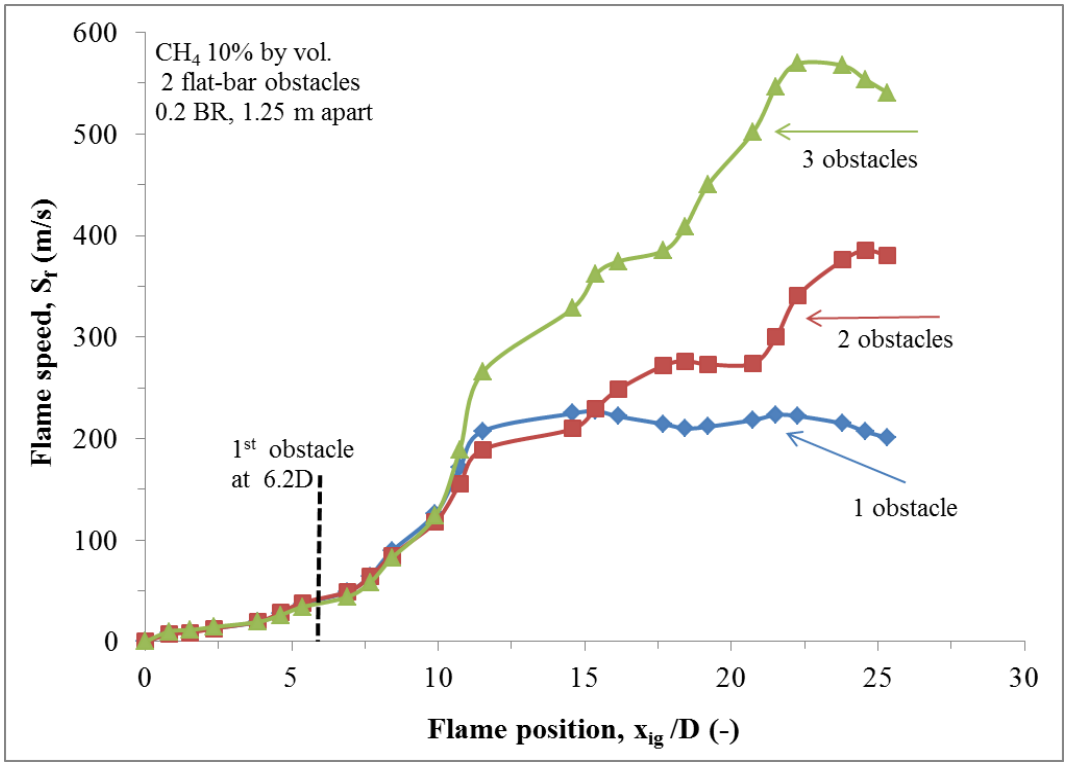

Figure 5.29 Flame speeds against flame position for 1, 2 and 3 obstacles spaced at optimum obstacle separation distance.

The effect of number of obstacles on overpressure for all the obstacles tested in the present research spaced at maximum obstacle separation distance is given in Fig. 5.30. Up to three number of obstacles was achieved for 2 and 4 flat-bars and baffle disc only due to smaller obstacle scale for the former and large obstacle scale for the latter and both necessitated for short obstacle spacing. In overall, an increase in overpressure was noticed with increase in the number of obstacles. However for the

three obstacle configurations, the magnitude of overpressure with 2 flat-bar obstacle (2.2 bar) was slightly higher than that of the 4 flat-bar (2 bar) due to the influence of obstacle scale. As a result of the influence of obstacle shape, (see 5.1.6), the baffle disc obstacle had the least overpressure of about 1.5 bar.

In comparison with the literature, Moen *et al.* (1982) studied the influence of number of obstacles on explosion overpressures. The experimental details of their work were previously mentioned in 5.1.5. For 16% BR obstacles, an overpressure of about 1 bar was achieved with nine plates 1 m apart. This value was 2.2 times lower than that obtained with just three 2 flat-bar obstacles of 0.2 BR in the current work. Also, the authors observed a lower value of overpressure (compared to the present work) of close to 2 bar with three obstacles of 0.3 BR. The likely possibility of the lower overpressure in the work of Moen *et al.* (1982) compared to the present one was that the obstacle spacing in the former was not at optimum value as in the case of the present work. However, a general trend of increase in overpressure with number of obstacles was similar in both two tests.

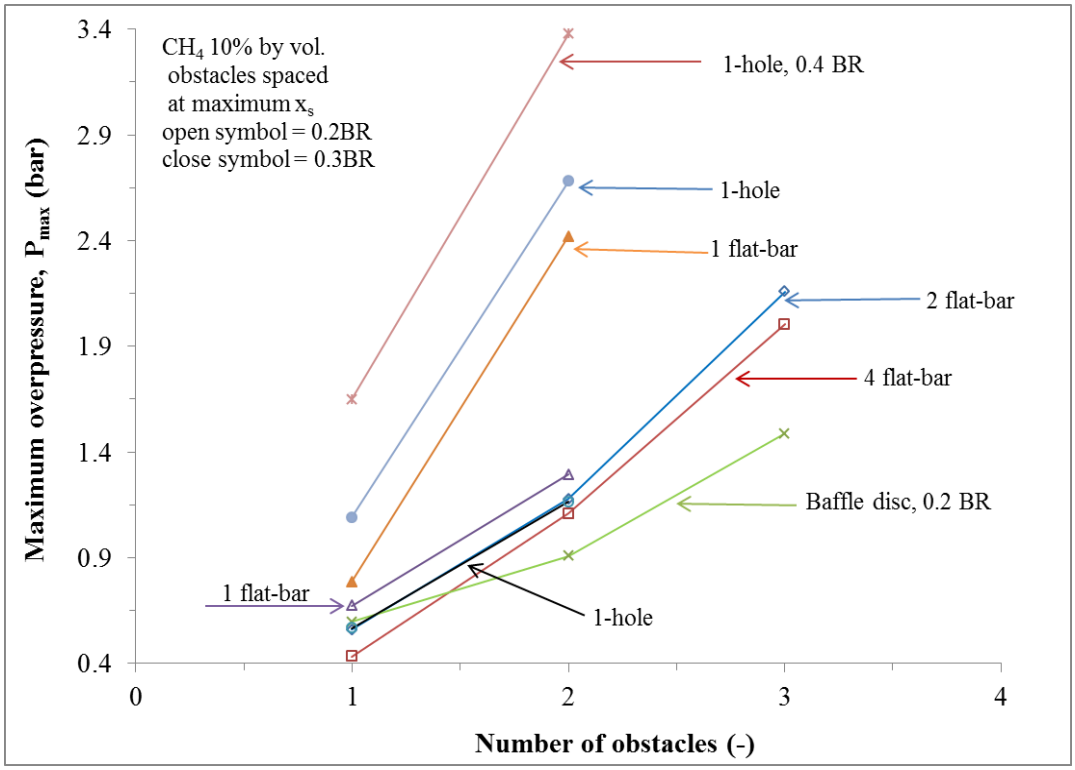

Figure 5.30 Effect of number of obstacles spaced at optimum position on maximum overpressure for all the obstacles tested in the present research.

Figure 5.31 shows the influence of number of obstacles on maximum flame speed for all the obstacles used in the present research spaced at worst case obstacle separation distance. Patterns similar to overpressures (see Fig. 5.30) were equally observed with the flame speeds. Also for the three obstacle configurations, maximum flame speeds of 569 m/s, 498 m/s and 401 m/s were obtained for 2 flat-bar, 4 flat-bar and baffle disc respectively downstream of the third obstacle.

The highest flame speed from 2-flat-bar obstacles was about 1.4 times higher than that obtained from the pioneer work of Chapman and Wheeler (1926) with up to 20 obstacles spaced at 5 cm to each other. The maximum flame speed value was achieved at the 12th obstacle, after which an increase in the number of obstacles caused no change. That value was sustained constant throughout the rest of the tube. This behaviour was equally observed with overpressure from the work of Moen *et al.* (1982). But, a reduction in overpressure was observed after the 6th obstacle with 0.3 BR.

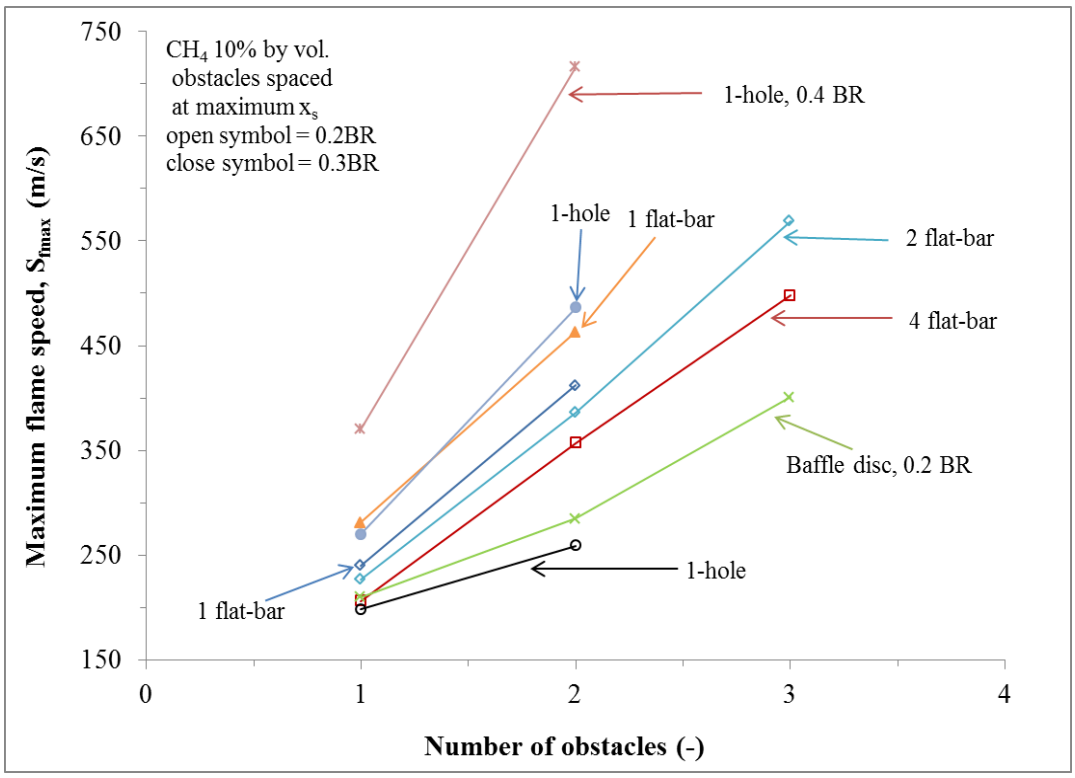

Figure 5.31 Effect of number of obstacles spaced at optimum position on maximum flame speeds for all the obstacles tested in the present research

5.3 Results Table

The summary of the experimental results (overpressure and flame speed) for all the tests carried out in the present research are presented in Table 5.3. The experimental maximum overpressure, P_{max} was the maximum value recorded by any of the pressure transducers of the test vessel (PT1-PT6). However, the predicted maximum overpressure, $P_{calc.}$ was calculated from Eq. 5.1. The maximum experimental flame speed, S_{fmax} was obtained from the smoothened flame speed data.

Table 5.3 Summary of the experimental results in terms of overpressure and flame speeds.

Mixture			Obstacle							Results		
Test	**Fuel**	**Conc.**	**Shape**	**BR**	**$N_h/_b$**	**No**	**b**	**x_{s1}/b**	**x_{s2}/b**	**P_{max} (exp.)**	**S_{fmax} (exp.)**	**P_{max} (calc.)**
(-)	**(-)**	**(%)**	**(-)**	**(-)**	**(-)**	**(-)**	**(m)**	**(-)**	**(-)**	**(bar)**	**(m/s)**	**(bar)**
1	CH_4	10	No obstacle							0.256	122	-
2	CH_4	10	Hole	0.3	1	1	0.033		-	1.091	270	0.984
3	CH_4	10	Hole	0.3	1	2	0.033	15.0	-	1.623	307	1.200
4	CH_4	10	Hole	0.3	1	2	0.033	30.1	-	1.850	381	1.655
5	CH_4	10	Hole	0.3	1	2	0.033	37.6	-	2.198	465	2.212
6	CH_4	10	Hole	0.3	1	2	0.033	52.7	-	2.680	486	2.356
7	CH_4	10	Hole	0.3	1	2	0.033	67.7	-	1.858	381	1.661
8	CH_4	10	Hole	0.3	1	2	0.033	82.7	-	1.222	323	1.296
9	CH_4	7	No obstacle							0.054	30	-
10	CH_4	7	Hole	0.3	1	1	0.033	-	-	0.395	229	0.756
11	CH_4	7	Hole	0.3	1	2	0.033	15.0	-	0.782	232	0.775
12	CH_4	7	Hole	0.3	1	2	0.033	30.1	-	0.686	255	0.899
13	CH_4	7	Hole	0.3	1	2	0.033	37.6	-	0.730	280	1.038
14	CH_4	7	Hole	0.3	1	2	0.033	52.7	-	0.595	241	0.821
15	CH_4	7	Hole	0.3	1	2	0.033	67.7	-	0.406	215	0.684
16	CH_4	7	Hole	0.3	1	2	0.033	82.7	-	0.572	206	0.640
17	C_3H_8	4.5	No obstacle							0.617	273	-
18	C_3H_8	4.5	Hole	0.3	1	1	0.033	-	-	3.259	606	3.197
19	C_3H_8	4.5	Hole	0.3	1	2	0.033	52.7	-	9.060	930	5.608
20	C_3H_8	3	No obstacle							0.054	48	-
21	C_3H_8	3	Hole	0.3	1	1	0.033	-	-	0.212	142	0.344
22	C_3H_8	3	Hole	0.3	1	2	0.033	52.7	-	0.692	259	0.923
23	C_3H_8	3	Hole	0.3	1	2	0.033	67.7	-	0.851	275	1.010
24	C_3H_8	3	Hole	0.3	1	2	0.033	82.7	-	0.425	168	0.459
25	CH_4	10	Hole	0.4	1	1	0.043	-	-	1.649	370	1.586
26	CH_4	10	Hole	0.4	1	2	0.043	29.2	-	3.103	573	2.961
27	CH_4	10	Hole	0.4	1	2	0.043	34.9	-	3.378	716	3.999
28	CH_4	10	Hole	0.4	1	2	0.043	52.6	-	2.085	522	2.603
29	CH_4	10	Hole	0.4	4	1	0.022	-	-	0.989	307	1.198
30	CH_4	10	Hole	0.4	16	1	0.005	-	-	0.791	237	0.802
31	CH_4	10	Bar	0.2	1	1	0.026	-	-	0.671	240	0.820
32	CH_4	10	Bar	0.2	1	2	0.026	68.4	-	1.154	360	1.525
33	CH_4	10	Bar	0.2	1	2	0.026	87.9	-	1.294	412	1.859
34	CH_4	10	Bar	0.2	1	2	0.026	107.4	-	0.805	281	1.049

Table 5.3 Cont'd

Mixture			Obstacle							Results		
Test	**Fuel**	**Conc.**	**Shape**	**BR**	**$N_h/_b$**	**No**	**b**	**x_{s1}/b**	**x_{s2}/b**	**P_{max} (exp.)**	**S_{fmax} (exp.)**	**P_{max} (calc.)**
(-)	**(-)**	**(%)**	**(-)**	**(-)**	**(-)**	**(-)**	**(m)**	**(-)**	**(-)**	**(bar)**	**(m/s)**	**(bar)**
35	CH_4	10	Bar	0.2	2	1	0.013	-	-	0.559	227	0.748
36	CH_4	10	Bar	0.2	2	2	0.013	78.1	-	0.982	333	1.357
37	CH_4	10	Bar	0.2	2	2	0.013	97.7	-	1.177	386	1.688
38	CH_4	10	Bar	0.2	2	2	0.013	136.7	-	1.081	360	1.525
39	C_3H_8	4.5	Bar	0.2	2	1	0.013	-	-	1.073	342	1.412
40	C_3H_8	4.5	Bar	0.2	2	2	0.013	78.1	-	3.364	600	3.154
41	C_3H_8	4.5	Bar	0.2	2	2	0.013	97.7	-	4.759	845	4.962
42	C_3H_8	4.5	Bar	0.2	2	2	0.013	136.7	-	6.041	910	5.456
43	C_3H_8	4.5	Bar	0.2	2	2	0.013	175.8	-	4.323	439	2.037
44	C_3H_8	4.5	Bar	0.2	4	1	0.006	-	-	1.767	386	1.690
45	C_3H_8	4.5	Bar	0.2	4	2	0.006	39.1	-	5.157	605	3.190
46	C_3H_8	4.5	Bar	0.2	4	2	0.006	78.1	-	4.477	578	2.997
47	C_3H_8	4.5	Bar	0.2	4	2	0.006	156.3	-	2.779	526	2.631
48	CH_4	10	Bar	0.2	4	1	0.006	-	-	0.431	206	0.642
49	CH_4	10	Bar	0.2	4	2	0.006	39.1	-	0.976	276	1.017
50	CH_4	10	Bar	0.2	4	2	0.006	78.1	-	1.108	357	1.506
51	CH_4	10	Bar	0.2	4	2	0.006	156.3		0.771	348	1.450
52	CH_4	10	Hole	0.2	1	1	0.024	-	-	0.566	198	0.600
53	CH_4	10	Hole	0.2	1	2	0.024	71.9	-	0.995	290	1.097
54	CH_4	10	Hole	0.2	1	2	0.024	92.4		1.164	362	1.535
55	CH_4	10	Hole	0.2	1	2	0.024	112.9	-	0.710	240	0.818
56	CH_4	10	Bar	0.3	1	1	0.039	-	-	0.784	281	1.047
57	CH_4	10	Bar	0.3	1	2	0.039	32.5	-	2.141	450	2.111
58	CH_4	10	Bar	0.3	1	2	0.039	45.5	-	2.420	463	2.198
59	CH_4	10	Bar	0.3	1	2	0.039	58.4	-	1.671	353	1.481
60	H_2	15	No obstacle							0.083	83	-
61	H_2	15	Hole	0.3	1	1	0.033	-	-	0.422	197	0.595
62	H_2	18	Hole	0.3	1	1	0.033	-	-	4.440	509	2.513
63	H_2	15	Hole	0.3	1	2	0.033	37.6	-	0.966	283	1.059
64	H_2	15	Hole	0.3	1	2	0.033	52.7	-	2.534	514	2.548
65	H_2	15	Hole	0.3	1	2	0.033	67.7	-	3.639	630	3.370
66	H_2	15	Hole	0.3	1	2	0.033	82.7	-	2.899	291	1.105
67	C_2H_4	4.3	No obstacle							0.068	31	-
68	C_2H_4	4.3	Hole	0.3	1	1	0.033		-	0.436	233	0.780
69	C_2H_4	4.3	Hole	0.3	1	2	0.033	52.7	-	0.889	214	0.681
70	C_2H_4	4.3	Hole	0.3	1	2	0.033	67.7	-	0.976	276	1.018
71	C_2H_4	4.3	Hole	0.3	1	2	0.033	82.7	-	0.581	129	0.292
72	CH_4	10	Disc	0.2	-	1	0.058	-	-	0.600	210	0.660
73	CH_4	10	Disc	0.2	-	2	0.058	4.3	-	0.907	285	1.070
74	CH_4	10	Disc	0.2	-	3	0.058	4.3	4.3	1.486	401	1.787

Table 5.3 Cont'd

Mixture			Obstacle							Results		
Test	**Fuel**	**Conc.**	**Shape**	**BR**	**$N_h/_b$**	**No**	**b**	**x_{s1}/b**	**x_{s2}/b**	**P_{max} (exp.)**	**S_{fmax} (exp.)**	**P_{max} (calc.)**
(-)	**(-)**	**(%)**	**(-)**	**(-)**	**(-)**	**(-)**	**(m)**	**(-)**	**(-)**	**(bar)**	**(m/s)**	**(bar)**
75	H_2	15	Disc	0.2	-	3	0.058	4.3	4.3	3.289	681	3.741
76	H_2	15	Bar	0.2	2	3	0.013	97.7	97.7	2.479	369	1.582
77	CH_4	10	Bar	0.2	2	3	0.013	97.7	78.1	1.889	489	2.372
78	CH_4	10	Bar	0.2	2	3	0.013	97.7	97.7	2.159	569	2.933
79	CH_4	10	Bar	0.2	2	3	0.013	97.7	117.2	1.677	332	1.351
80	CH_4	10	Bar	0.2	4	3	0.006	78.1	39.1	1.791	465	2.212
81	CH_4	10	Bar	0.2	4	3	0.006	78.1	78.1	2.004	498	2.437
82	CH_4	10	Bar	0.2	4	3	0.006	78.1	117.2	1.625	387	1.697
83	CH_4	10	Bar	0.2	4	3	0.006	78.1	195.3	1.177	349	1.456
84	H_2	15	Bar	0.2	4	3	0.006	78.1	78.1	2.878	347	1.443

5.4 Summary of the Major Findings

From the experimental data described in this chapter, the following important findings are made:

- There was significant increase in overpressure in the two obstacle configuration compared to the no obstacle and single obstacle situations. The increase in maximum overpressure was ten-fold and three-fold respectively. The maximum flame speeds in the empty tube reached just over 100m/s, while with the single and double obstacle tests, this was more than double and four folds respectively of the no obstacle test.
- The mechanism of pressure generation in the present tests is the same as that of vapour-cloud explosions, i.e. the pressure rise was due mainly to the inertia of the gas immediately ahead of the flame, and that it was not significantly influenced by the confinement offered by the tubular geometry.
- The effects of obstacle separation distance in a double obstacle configuration study was clearly demonstrated in this chapter. There is a defined separation distance which gave the most severe explosions in terms of both maximum flame speed and overpressure. This trend was obtained for obstacles of

different blockage ratio, shapes, number, scale and different mixture reactivities.

- The profile of effects with separation distance was shown to agree with the cold flow turbulence profile determined in cold flows by other researchers. However, the present results showed that the maximum effect in explosions is experienced further downstream than the position of maximum turbulence determined in the cold flow studies. It is suggested that this may be due to the convection of the turbulence profile by the propagating flame.
- The predicted equation (Eq. 2.23) on position to maximum intensity of turbulence from cold flow data agreed with the worst case obstacle separation distance in the current research if multiplied by a factor of three.
- An increase in obstacle BR resulted in increasing maximum overpressure and flame speeds for both single and double obstacles. The worst case obstacle spacing leading to maximum overpressures and flame speeds decreased with increasing obstacle blockage ratio. However, for a fixed obstacle blockage ratio, both the severity of explosions and worst case obstacle spacing increased with obstacle scale (number of flat-bars /holes).
- It was evident that the obstacle spacing from the literature is quite closer when compared to the present work. It can now be deduced that large congestions in a given medium do not necessarily signify potential maximum explosion severity as traditionally assumed. But, small congestions optimally separated apart could lead to very high overpressure.
- An increase in explosions overpressures and flame speeds was noticed with increase in number of obstacles up to three for 2 and 4-flat-bars and baffle disc obstacles spaced at established optimum obstacle separation distance.
- For three obstacle tests, the optimum spacing between the second and third obstacles corresponded to the same optimum spacing found for the first two obstacles demonstrating that the optimum separation distance does not change with number of obstacles nor the severity of the explosion, but it does change with the obstacle scale.

Chapter 6

Estimation of Turbulent Combustion Parameters

6.1 Introduction

Most of the congested gas explosions studies (i.e. turbulent in nature) have focussed on quantifying global flame acceleration and maximum overpressure through obstacle groupings rather than detailed analysis of the flame propagation through the individual elements of the congested region. Also, the turbulent parameters such as intensity of turbulence, turbulent Reynolds number, Karlovitz number, turbulent flame speed etc. would aid better understanding in gas explosion phenomena in the presence of obstacles in addition to the traditional flame speed and overpressures been reported in most cases.

The transient nature of obstacle induced explosion flow coupling with harshness and costs of measuring equipment have restricted the experimental measurements of turbulent flows in the present experiment. As such, the majority of these measurements were dependent on steady state flows. Phylaktou (1993) and Gardner (1998) used this approach to estimate some turbulence combustion parameters induced by single obstacle in a closed and vented elongated cylindrical vessel respectively. Also, Phylaktou and Andrews (1994) used data from cold flow turbulence induced by grid plates to predict the maximum intensity of turbulence where the maximum explosion severity occurs.

6.2 Explosion Induced Gas Velocities

By considering the obstacle as an orifice plate and using the procedures described in the British Standard, BS 5167-2 (2003), the maximum unburnt gas flow velocity ahead of the flame was calculated from the experimental measured static pressure difference across the obstacle using static pressure tappings at 1D and 0.5D upstream and downstream of the obstacle respectively. It is worth noting that the Standard is meant for flow calculations in steady state conditions and not for a transient as in the present application. In order to justify the application of the orifice flow theory to the current research, it is imperative to address the following factors:

- The pressure loss theory in the BS 5167-2 (2003) was for isotropic, steady-state flow whereas the present explosion tests were characterised by highly transient flows that propagated towards the obstacle owing to gas explosion behind the flame front. However, it was shown in Chapter 2 that some

researchers e.g. Phylaktou and Andrews (1994) established the applicability of steady-state flow to congested gas explosions.

- The orifice flow metering in the British Standard applies to single-hole orifice plates only. Most of the obstacles used in the present work were single-hole obstacles. However, multi-hole, flat-bar and baffle discs were used. Turbulence measurements downstream of grid plate obstacles in wind tunnel by Baines and Peterson (1951) comprised of obstacles of various shapes i.e. round and square bar-grid plates as well as multi-hole types. The turbulence intensity generated was found to have no discernible dependence on the obstacle geometry but does on the obstacle blockage ratio.
- The Standard is applicable to orifice plates with blockage ratios above 44%. However, the various obstacles used in the current research were within a range of 20-40% obstacle blockage.

For all the obstacle types used in the current work, the pressure drop across the obstacle, ΔP_d was used in the calculation of mass flow rate, $\dot{m}$ using the calculation procedure in the British Standard which is effectively Eq. 2.12. The induced gas velocity ahead of the flame, S_g is thus given as,

$$S_g = \frac{\dot{m}}{\rho A_2} \tag{6.1}$$

The measurement of ΔP_d due to single 1-hole obstacle of 0.4 BR with 10% CH_4 by vol. was obtained from the recorded differential pressure trace as shown in Fig. 6.1. Also shown is the flame position up to its arrival at the last thermocouple prior to the obstacle. The differential pressure increased as the flame propagated towards the obstacle. As the flame reached the obstacle, the forced flow through the obstacle (and therefore the turbulence generation) terminated. This led to an abrupt drop in pressure, ΔP_d, across the obstacle. This happened at a point just after flame arrival was recorded at the last thermocouple (TC6) before the obstacle. The location of the maximum differential pressure therefore signified the time of flame arrival at the obstacle and was the period of maximum flow velocity through the obstacle. This shows that the significance of pressure loss caused by friction was negligible

compared to that due to flow interaction with the obstacle, as the measurement point for ΔP_d behind the obstacle was in close proximity to the obstacle.

A similar trend was obtained for the differential pressure across the second and third obstacles with higher pressure drop compared to that of first obstacle. The pressure loss in this case was obtained by finding the difference between the pressure trace from pressure transducer PT3 and PT4 for the second obstacle and PT2 and PT5 for the third obstacle. The positioning of the pressure transducers upstream and downstream of the obstacles respectively was in accordance to BS 5167-2 (2003).

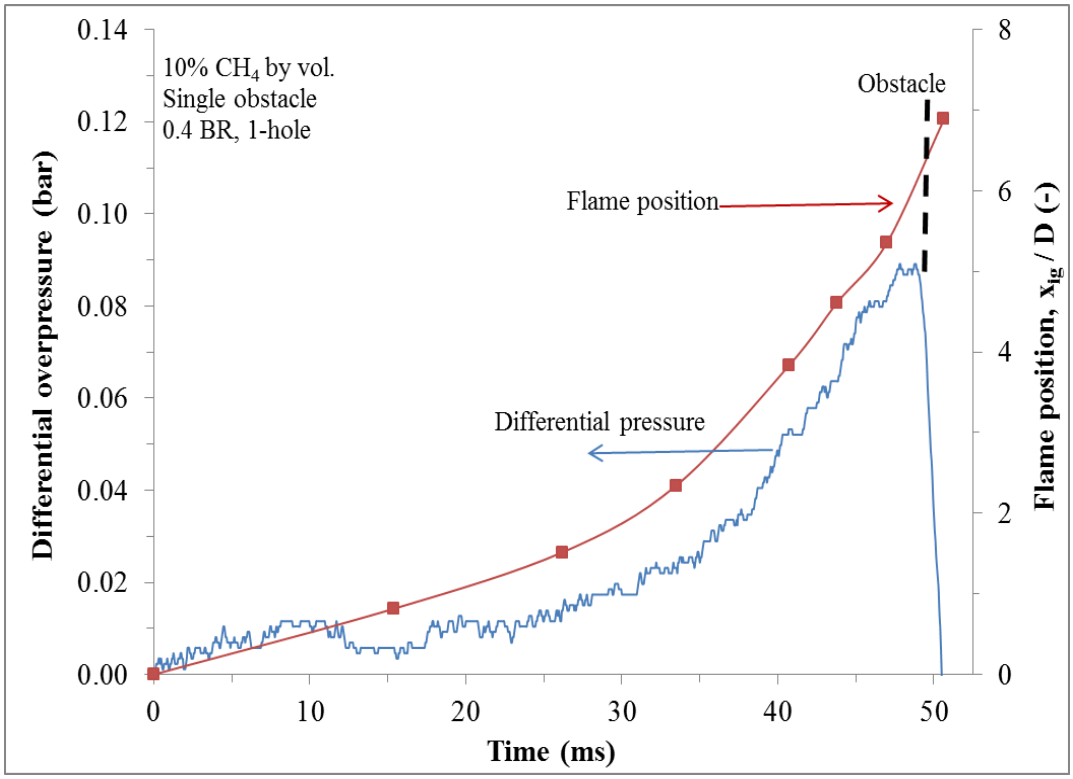

Figure 6.1 Pressure drop measurement across an orifice plate of 0.4 BR and 10% CH_4 by vol.

Figure 6.2 shows a comparison between the maximum induced gas velocities ahead of the flame and obstacle separation distance with 10% CH_4 by vol. mixtures. The obstacle used was 1- hole 0.3 BR. The gas velocity due to first obstacle was found to be almost constant (close to 40 m/s) for all the tests performed. The value of the induced gas velocity due to first obstacle was closely similar to that obtained by Phylaktou (1993) and Gardner (1998) using the same blockage and test rig as the present work. However, the gas velocity as a result of the second obstacle was found to increase with obstacle separation and attained a maximum value of slightly above

150 m/s at 53 obstacle scales (1.75 m separation) before it started decreasing with the obstacle separation of 68 and 83 obstacle scales. In comparison with the most closely separated obstacles (15 obstacle scales), the maximum induced gas velocity was about two times higher in magnitude. Interestingly, a complete turbulence profile was formed with the gas velocities at the obstacle separation distance similar to that of overpressure and flame speed profiles reported in Chapter 5.

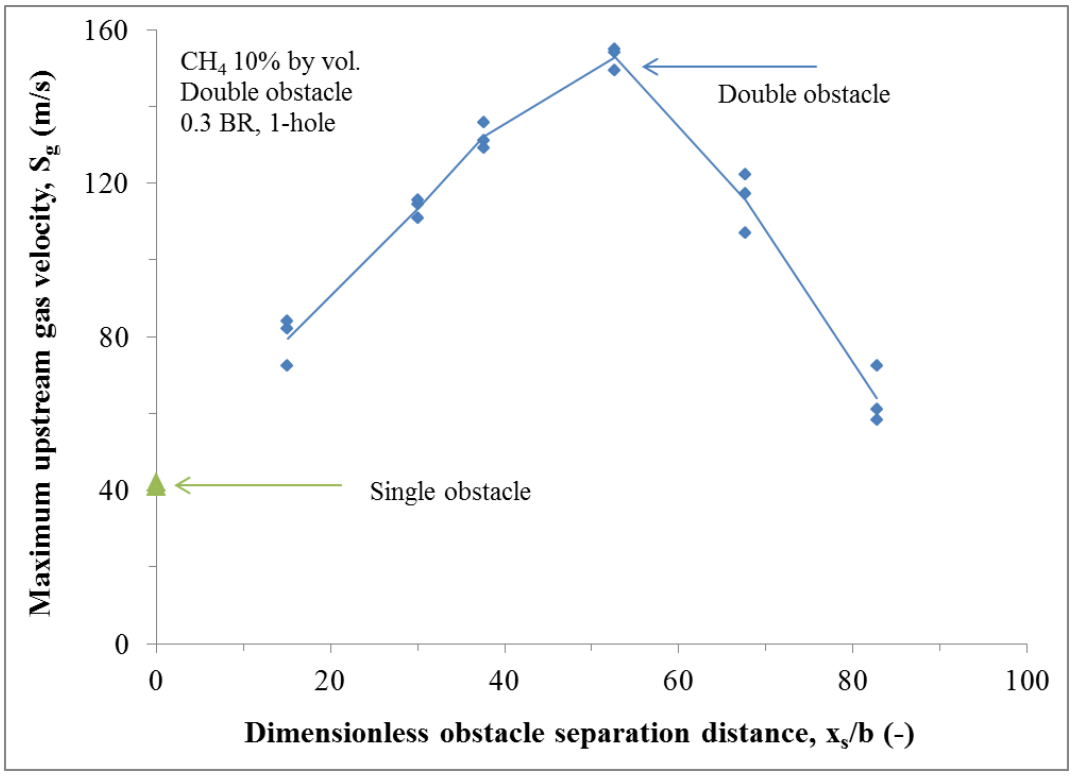

Figure 6.2 Maximum upstream induced gas velocities for single and double obstacle against the obstacle separation distance.

For 0.2 to 0.4 BR 1-hole obstacles with slightly rich methane-air mixtures (10% by vol.), an overview of the gas induced velocities, S_g, upstream flame speeds just prior to the obstacle, S_{fu} and the ratios of the two velocities for the first and second obstacle is shown in Table 6.1.

Under adiabatic conditions for laminar spherical flames, the induced gas velocity, S_g was found to be about 86% of the flame speed, S_f (See Eq.1.5). Though, the S_g can be affected by conditions that are non-laminar and distortions of the flame shape by the flow geometry such as flow channelling (Gardner 1998). In the present work, the flame propagation was in a cylindrical geometry but yet the calculated gas velocity for the first obstacles was nearer to that of spherical flame as shown in Table 6.1.

The S_{g1}/S_{fu1} was roughly 0.80 and this is comparable to the ratio of 0.86 expected from the laminar spherical explosions. However, there is no good agreement with the flame speed ratios (S_{g2}/S_{fu2}) for the second obstacles. This could be attributed to the influence of the turbulence generated downstream of the first obstacles which distort the flame (making it non-laminar) prior to reaching the second obstacle. It can therefore be deduced that in the present test, the initial flame propagation upstream of the first obstacle was similar to that of spherical flame.

Table 6.1 Relationship between induced gas velocity and upsream flame speeds.

Test No	**S_{g1}**	**S_{fu1}**	**S_{g1}/S_{fu1}**	**S_{g2}**	**S_{fu2}**	**S_{g2}/S_{fu2}**
(-)	(m/s)	(m/s)	(-)	(m/s)	(m/s)	(-)
2	41	49	0.84	-	-	-
3	34	66	0.53	80	131	0.61
4	36	61	0.59	114	247	0.46
5	41	56	0.73	132	263	0.50
6	42	55	0.77	153	212	0.72
7	41	52	0.79	116	271	0.43
8	38	50	0.76	64	204	0.31
25	34	48	0.71	-	-	-
26	32	57	0.57	138	337	0.41
27	35	42	0.84	160	294	0.54
28	35	63	0.55	128	307	0.42
52	44	58	0.77	-	-	-
53	41	51	0.81	98	236	0.42
54	45	53	0.85	124	259	0.48
55	42	52	0.80	79	200	0.40

6.3 Maximum r.m.s Turbulent Velocity

In the present research, the maximum intensity of turbulence, u'/U_{max} leading to maximum severity in explosions was calculated using Eq. 2.20 for C_T of 0.225 given by Phylaktou and Andrews (1994). Figure 6.3 shows the calculated values u' for a given mean flow velocity, U (assumed to be gas velocity, S_g in the current work) for both first and second obstacles of 0.3 BR, 1-hole at different obstacle pitch. A fixed relationship in turbulence intensity was attained for single obstacle tests with an average value of about 8 m/s. This value was closer to that obtained by Gardner (1998) under similar experimental condition. On the other hand, the intensity of turbulence varied significantly with obstacle separations for the double obstacle tests. The u'_{max} for the double obstacle tests was 30 m/s at a spacing of 53

obstacle scales. This value doubled that obtained with obstacles separated at 15 and 83 obstacle scales. Also, the maximum u' obtained (30 m/s) was similar to that in real gas turbine combustion as reported by Andrews (2011).

Table 6.2 gives an overview of all the maximum u' calculated in the current research. Also presented are the other turbulent combustion parameters (to be discussed later) such as turbulent Reynolds number, R_ℓ, turbulent burning velocity, S_T and Karlovitz number, Ka.

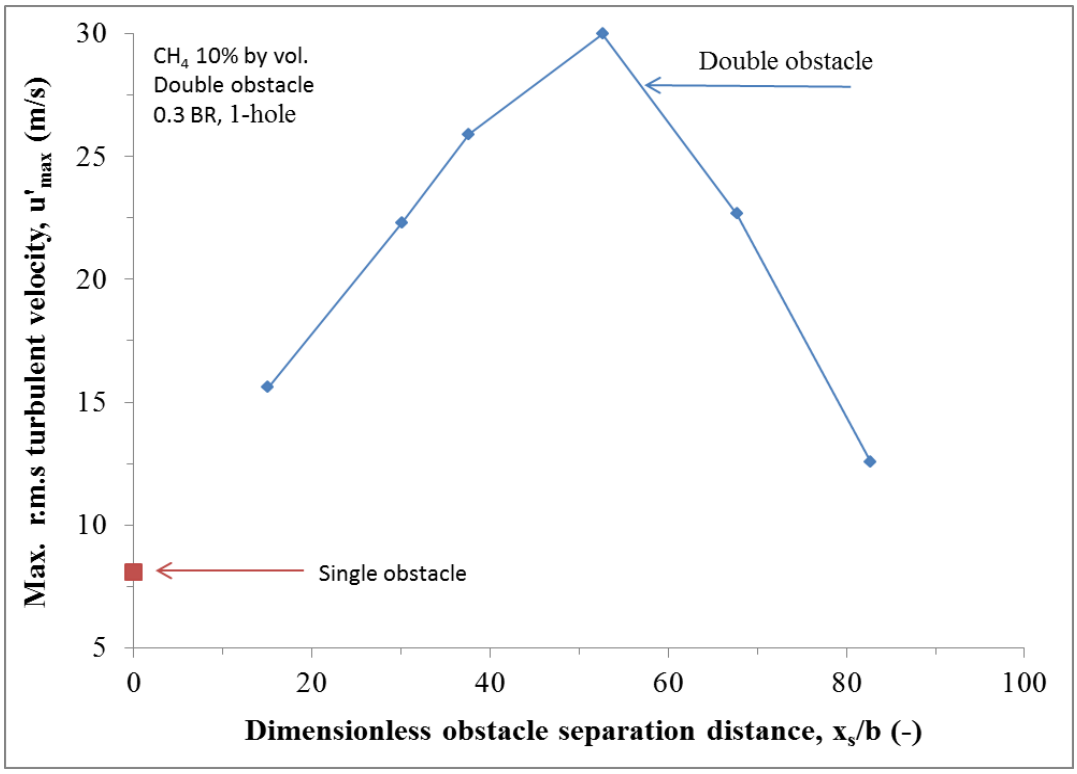

Figure 6.3 Maximum r.m.s turbulent velocity from single and double obstacles as a function of obstacle separation distance.

As shown in Fig. 6.4, a linear relationship exists between the r.m.s velocity, u' versus the unburned gas flow velocity, S_g for two obstacles with different obstacle spacing. A similar relationship between the two parameters was reported by Phylaktou and Andrews (1994). Also shown in Fig. 6.4 is the experimental work from a large scale (50 m^3) experimental work of Hjertager *et al.*(1988a). The experimental details of the authors were mentioned previously in Chapter 3 and 5. In addition to reporting the usual flame speeds and overpressures, the authors studied the influence of turbulent flow velocities (gas velocities). To the author's

knowledge, this was the only available data that measured turbulent flow velocities in transient gas explosions.

The pressure loss coefficient, K from the 0.3 BR obstacle used by Hjertager *et al.* (1988a) was calculated using Eq. 2.16 to be 0.76. With the given experimental measurement of the turbulent flow velocities, the r.m.s turbulent velocity, u' up to 6 m length tube (three orifice plates) was obtained from Eq. 2.20.

In comparison with the work of Hjertager *et al.* (1988a) i.e. large scale, and the present work (small scale), higher u' and S_g were obtained in small scale tests. This contradicts the expectation that large scale tests produced greater overpressure and flame speed when related to smaller scale. The only probable reason to this situation is as a result of close spacing between the obstacles in the large scale work (less than one-hole diameter). Therefore, the termination of the potential core (where the maximum intensity of turbulence is attained) of the generated jets was never reached within the tube from the work of Hjertager *et al.* (1988a).

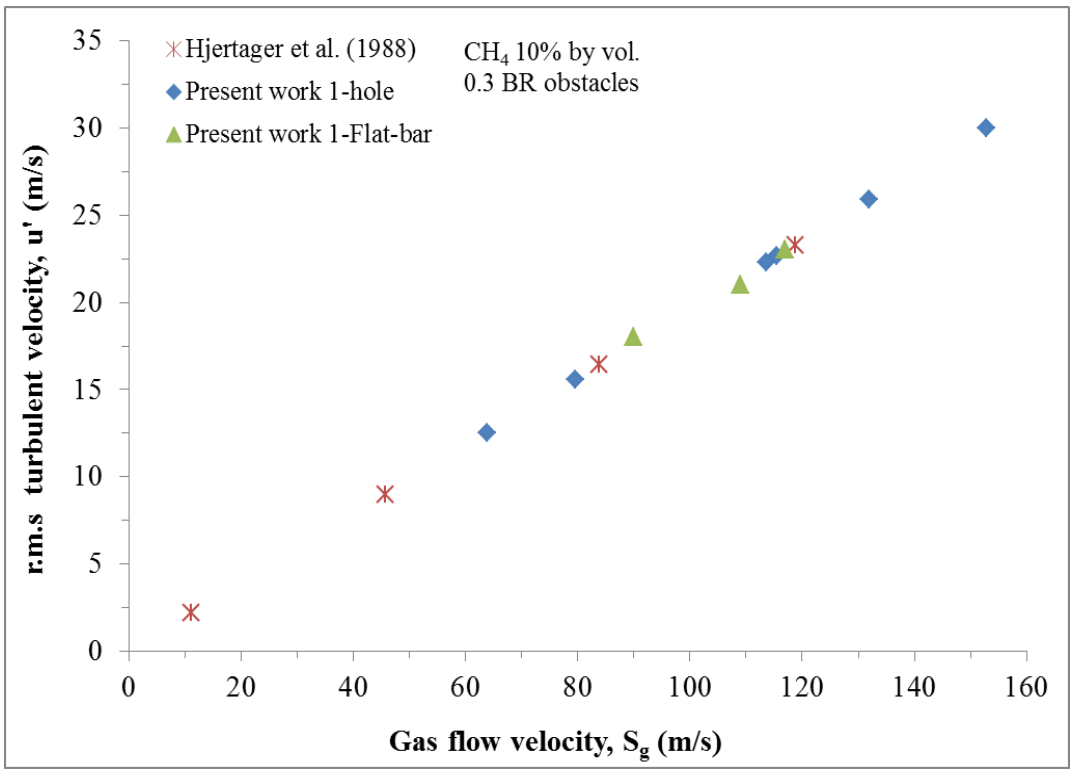

Figure 6.4 Linear relationship between r.m.s turbulent velocity and gas flow velocity from small scale (present work) and large scale (Hjertager *et al.* 1988a).

6.4 Turbulent Reynolds Number

Most of the real combustion systems operate in turbulent regimes with values of R_ℓ ranging from 250 to 25,000 (Andrews *et al.* 1975). For instance, the estimated R_ℓ value for a bunsen burner was found to be 1,500 whereas a gas turbine combustion chamber operating at maximum power has R_ℓ higher than that of the bunsen burner by 13.3 folds. Ironically, most studies on experimental flame structure do not characterize systems of practical concern, because they have been performed in regimes with R_ℓ well below 250 and this is more accurately referred to as trivial turbulence levels. The problem is that most models on turbulent combustions are intended at predicting these trivial turbulent flames (Phylaktou 1993). In vapour cloud explosions with pipe arrays, Catlin and Johnson (1992) estimated R_ℓ in the order of 70,000. AbdelGayed and Bradley (1982) estimated that atmospheric explosions can be related with R_ℓ values in the range of 10^6 to 10^7.

In the present experiment, turbulent Reynolds number R_ℓ was calculated using Eq. 2.4. Figure 6.5 shows a profile of calculated R_ℓ as a function of obstacle separation distance for 10% CH_4 by vol. with 0.3 BR obstacles. As observed from other turbulent combustion parameters, R_ℓ for the single obstacles were similar for all separations with a value of close to 10,000. This is well within turbulent flow regime. For the double obstacle tests, R_ℓ was found to change with pitch. The maximum value of R_ℓ with the double obstacle at 1.75 m apart was close to 50,000. This value was nearly five folds higher than the single obstacle and doubled that of two obstacles separated at 0.5 m and 2.75 m.

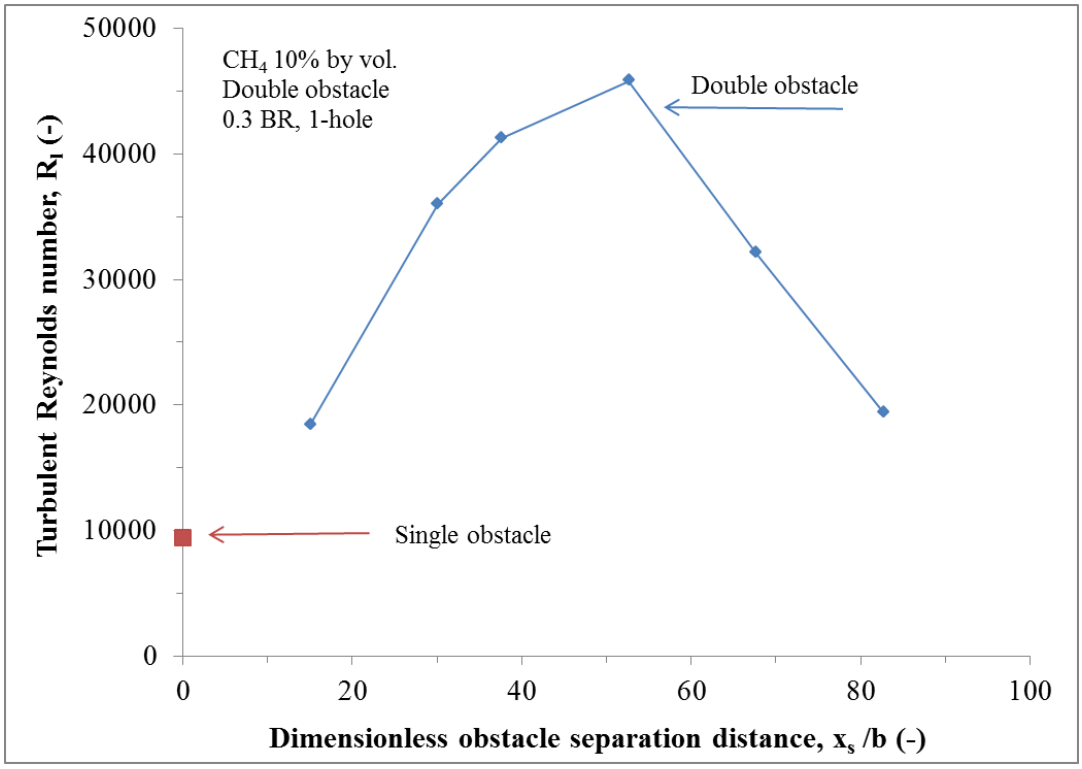

Figure 6.5 Relationship between turbulent Reynolds numbers and obstacle separation distance.

Most of the R_ℓ obtained in the present research (see Table 6.2) were above 4000 i.e. cut off value for turbulence. A maximum value of over 90,000 was realised for test 27. This was due to the influence of high u' induced by fast combustion-generated flow through the obstacles and the integral length scale, ℓ which is dependent on obstacle scale, b. Therefore this suggests that the current experiments are of direct application to real systems.

6.5 Turbulent Burning Velocity

The interaction of a flame with an obstacle results in an increase of the flame area. The flame shape distorts as it follows the turbulent flow patterns downstream of the obstacle. As reviewed in Chapter 3, there are several models in the literature to measure the turbulent burning velocity, S_T. The S_T that results is therefore greater than the laminar value, S_L.

In Chapter 1, it was described that the expansion of gas behind the flame front was the driving force of the downstream flow field and Eq. 1.1 showed that the flame speed could be obtained from the product of the adiabatic expansion ratio, E and the

burning velocity, S_u. In the present study, the turbulent burning velocity, S_T at the time of maximum flame speed, $S_{f(max)}$ was calculated as,

$$S_T = \frac{S_{f(max)}}{E} \tag{6.2}$$

The presence of the adiabatic factor in Eq. 6.2 assumes that the reaction was instantaneous with no heat loss to the vessel walls.

Figure 6.6 shows the calculated turbulent burning velocity from Eq. 6.2 against obstacle spacing for 0.3 BR obstacles with 10% CH_4 by vol. A profile similar to the ones obtained for S_g, u' and R_ℓ was obtained with the S_T. The worst case obstacle spacing i.e. 1.75 m (53 obstacle scales) produced the maximum S_T of 65 m/s. This value was about 1.6 times greater than those obtained at the most closest and widest obstacle spacing. In comparison with the single obstacle, the maximum S_T for the double obstacle nearly doubled that of the single.

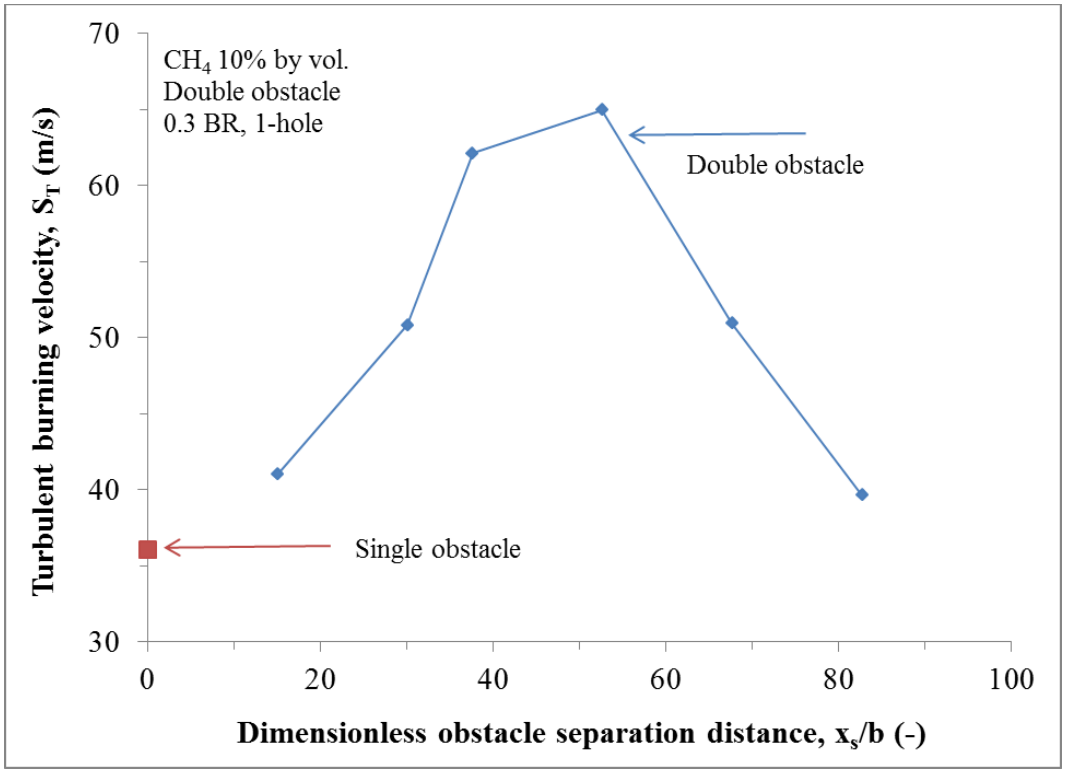

Figure 6.6 Turbulent burning velocity as a function of the obstacle separation distance.

Figure 6.7 shows a plot of turbulent burning velocity dimensionalised with S_L as a function of u'/S_L for multi-flat-bar and single-hole obstacles of 20% and 30%

blockage ratios with varying separation distance and for different mixture reactivities. Also shown is the correlation of Bradley *et al.* (1992) and the data range from the review of turbulent to laminar burning velocity ratio of Phylaktou and Andrews (1995), which extends to S_T/S_L of 120. The mean line through this experimental data fitted Eq. 6.3.

$$S_T/S_L = 1 + C\ u'/S_L \qquad (6.3)$$

where C is a constant that has a value of 2 for the mean of the data range in the literature, but varies between 4 and 0.5 to encompass most of the data. The value of 2 is typical of data for hydrocarbon fuels and lower values are more typical of hydrogen. The correlation of Abdel-Gayed *et al.* (1985) can be expressed in the form of Eq. 6.3, when C becomes $0.88/(KaLe)^{0.3}$ and for KaLe values from 10 to 0.01 C varies from 0.4 to 3.5 which is a very similar range to that in the experimental data. C is < 2 if Ka is high, which occurs if S_L, R_ℓ or u' is high, such as for hydrogen or large turbulent length scales, conversely C is > 2 if Ka is low, which occurs if S_L, R_ℓ or u' is low such as for lean methane mixtures or for small turbulent length scales.

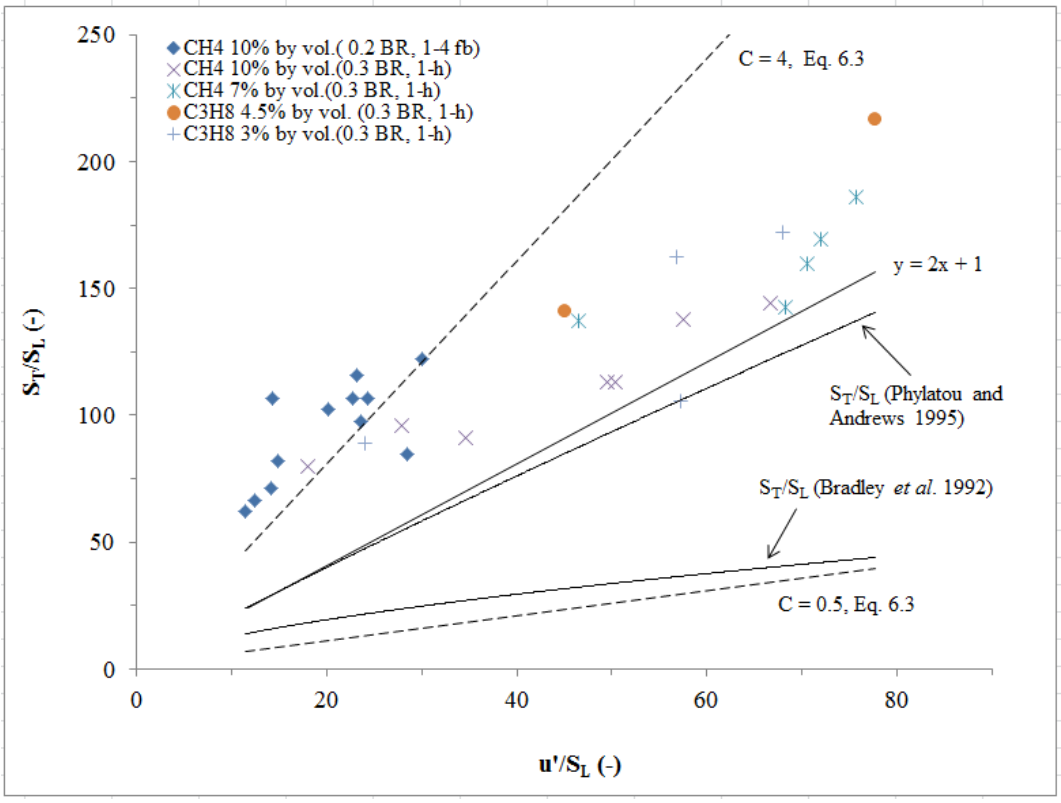

Figure 6.7 Turbulent burning velocity as a function of the u'/S_L.

The flat-bar obstacles results in Fig. 6.7 lie close to the line with C = 4 in Eq. 6.3, but for single-hole obstacles, the data points were closer to C = 2 at the higher u'/S_L. S_T/S_L ratios of 55 to 120 were found for two interacting bar type grid plates with BR of 20%. However, for BR of 30% with two single hole orifice had S_T/S_L from 60 to 220. Both of these sets of results show the turbulent enhancements necessary to explain the fast flames in unconfined vapour cloud explosions in the presence of obstacles. In incidents such as Flixborough, Buncefield and Texas City, overpressures were of the order of 1 bar. It may be shown that this requires a flame speed of about 300 m/s (Gardner *et al.* 2001; Phylaktou and Andrews, 1991; 1994; 1995 and Phylaktou *et al.* 1998). For a typical adiabatic hot gas expansion ratio of 8 this requires turbulent burning velocities of about 37 m/s and for a laminar burning velocity of 0.4 m/s this gives S_T/S_L of 92, which increases to around 200 if the mixture was very lean or rich rather than stoichiometric.

6.6 Karlovitz number and Flame Quenching

Abdel-Gayed *et al.* (1984) studied the influence of S_T at higher level of turbulence than that usually realized on burners with the aid of an explosion bomb equipped with four high speed fans. The authors observed that at first, the r.m.s turbulent velocity, u' increased with increase in fully developed S_T. However, as u' increased further, the rate of S_T with u' decreased, until a maximum value u' is reached after which S_T decreased thereby leading to the flame in the gas phase been quenched by the turbulence.

Most theories of turbulent burning assume that locally the propagation of flame is similar to laminar and observed reductions in the expected values of S_T have been explained by the effect of strain upon the laminar burning velocity (Abdel-Gayed *et al.* 1985).

Karlovitz (1954) quantified that for turbulent flames, the flame straining is expressed by the Karlovitz stretch factor otherwise known as Karlovitz number, Ka as the ratio of the chemical lifetime, τ_c to the turbulent lifetime, τ_ℓ. Mathematically, Ka is given as,

$$\mathrm{Ka} = \frac{\text{Chemical lifetime}}{\text{Turbulent lifetime}} = \frac{\tau_c}{\tau_\ell} = \frac{\left(\delta_L/S_L\right)}{\left(\ell/u'\right)} \tag{6.4}$$

Abdel-Gayed *et al.* (1984) further defined Ka from Eq. 6.4 based on turbulent Reynolds number, R_ℓ with dependence on ℓ as,

$$Ka = 0.157 \left(\frac{u'}{S_L}\right)^2 R_\ell^{-0.5} \tag{6.5}$$

At sufficiently high turbulence levels, flame front fragmentation can result in partial or full quenching of the flame (Abdel-Gayed and Bradley 1985). Global quenching of premixed flames is of both fundamental and practical importance. As the premixed flame encounters external perturbations like heat loses or aerodynamic stretch, quenching of the flame may take place provided the perturbations are strong enough to diminish the reaction rate in the flame to an insignificant value (Yang and Shy 2002).

Using an explosion bomb with fans, Abdel-Gayed *et al.* (1985) established that the Ka at global quenching of premixed turbulent flames must satisfy the criterion given as,

$$KaLe \geq 1.5 \tag{6.6}$$

For a stoichiometric methane-air mixture, Le is nearly unity and therefore flame quenching was estimated for values of Ka above 1.5. Later correlations presented by Abdel-Gayed *et al.* (1987) proposed flame quench for $Ka \geq 1$. Further study on flame extinction by Bradley *et al.* (1992) showed that Eq. 6.5 corresponded to the lower boundary of the quenching process; hence the new quench limit was extended to $Ka \geq 6$.

Even though the explosion bomb used by the above authors has an advantage of having high turbulent intensities with insignificant mean velocities, the method has some drawbacks that flame development and quenching were affected by the ignition source and by non-uniform distributions of mean reactant temperature and pressure during the explosion. This enables the determination of the actual global quenching conditions rather problematic (Yang and Shy 2002).

Using a cruciform burner, the authors (Yang and Shy 2002) presented a new approach with the aim of avoiding the ignition problem and to further consider the effect of radiative heat loss using N_2 and CO_2 as diluents. In order to determine isotropic turbulence, counter-rotating fans and perforated plates were fitted. Flame

quenching was determined using two methods namely: high speed camcorder and gas chromatography.

For pure premixed methane-air flames at very rich (ϕ1.45) and very lean (ϕ 0.6) concentrations, flame quenching occurred at a critical value of Ka greater than 1 and 6.2 respectively. This shows that lean methane flames are more difficult to extinct than the rich methane flames.

Dorofeev (2007) reported that the previous studies of flame quenching by turbulence were established on flame stretch only. In spite of the substantial progress made in understanding the phenomena of flame quenching as a result of stretch, there are several questions and, especially on how these occurrences can be associated to the observed sharp boundary between cases of weak and strong flame acceleration, where mixed products/reactants pockets are believed to have a significant effect. As a result of turbulence, flames are expected to be broken to form mixed pockets of products and reactants. In order to fill in the gap of the previous studies, the author came up with the critical conditions of quenching of products/reactants pockets mixed by turbulence based on the analysis of thermal regimes of the pockets but not from the flame stretch viewpoint. The critical Karlovitz number, Ka, for the flame extinction was reported to increase with gas expansion factor, E and decrease with Lewis number, Le

Figure 6.8 shows a plot of the calculated Ka from Eq. 6.5 against the obstacle separation distance with 0.3 BR 1-hole and 10% methane-air mixtures by vol. The Ka values for single obstacle with obstacle separations were fairly constant with a value of about 0.5 signifying no flame extinction. However, the Ka for the second obstacles increased with obstacle pitch and attained a maximum value of 3.3 at 53 obstacle scales prior to decrease in Ka at farther obstacle separations. With the exception of 83 obstacle scales (large spaced test configuration i.e. 2.75 m) test, the Ka values for all the obstacle separations were well above unity. Theoretically, this indicated global flame extinction however, the entire flame quench was not observed in any of the present tests. In all cases the explosion propagated strongly, leading to significant overpressures. The values of Ka in this study would therefore suggest a measure of the prevailing flame straining conditions downstream of an obstacle, as opposed to an indication of flame extinction.

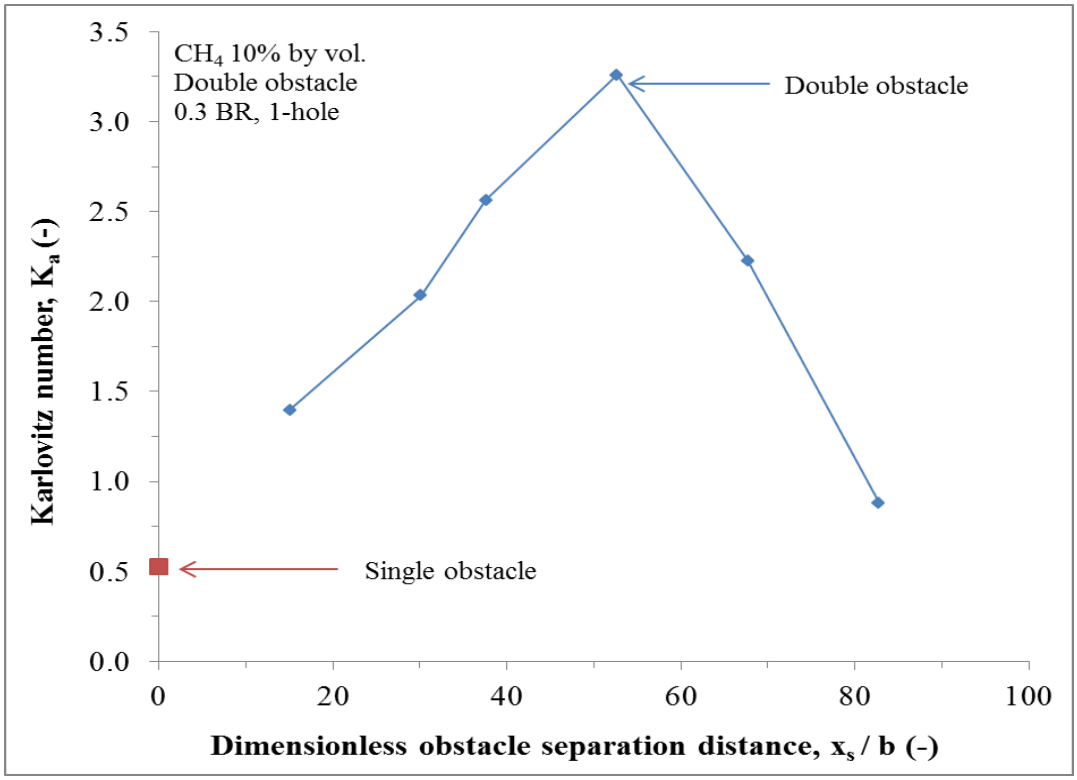

Figure 6.8 Calculated Karlovitz number as a function of the obstacle separation distances for single and double obstacles.

The relationship between experimental maximum overpressure, P_{max} and calculated Ka for one and two obstacles (optimally spaced) is presented in Fig. 6.9. The single obstacle data are from Tests 2, 25, 31, 52 and 56 whereas the double obstacle data are from Tests 6, 27, 33, 54 and 58. In both cases, Ka was found to increase with P_{max} with the double obstacle tests having higher magnitude compared to the single obstacle tests. The single obstacle tests have a Ka of well below unity and this shows no sign of flame quenching. However, Ka value of greater than unity was realised with the double obstacle tests.

A strong relationship between the laminar burning velocities, S_L and Ka was equally reported two decades ago by Tseng *et al.* (1993). It should be noted that S_L is a strong determining factor in maximum explosion overpressure. The authors reported this trend for four different gases used at various equivalence ratios, ϕ. These are: propane, methane, ethylene and ethane.

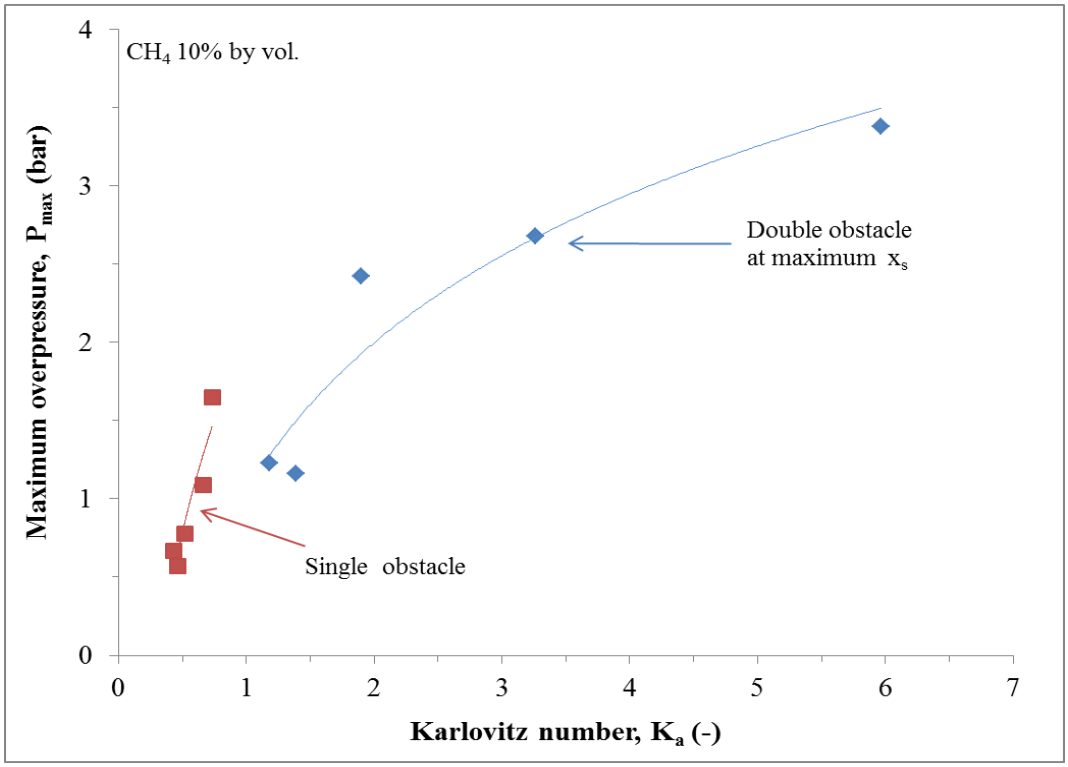

Figure 6.9 Calculated Karlovitz number as a function of the experimental maximum overpressure for single and double obstacles.

6.7 Turbulent Premixed Combustion Regimes

Premixed turbulent combustion regimes could be related to turbulence and chemical characteristic length and time scales. This investigation leads to combustion diagrams where different regimes are given as function of non-dimensional numbers (Williams 1985; Borghi 1988; Peters 1988; Borghi and Destriau 1998; Peters 1999). The diagrams could serve as a guide to choose and develop the appropriate combustion model for a specified situation.

The chemical time scale,τ_c, for a given premixed turbulent flames can be estimated as the ratio of the laminar flame thickness, δ_ℓ (given as ν/S_L) to the laminar burning velocity, S_L. The turbulent time scale,τ_t, is given as the ratio of the integral length scale, ℓ, to r.m.s turbulent velocity, u'. The dimensionless ratio of the two time scales gives rise to Damkohler number, Da where velocity and length scale ratios (u'/S_L and ℓ/δ_ℓ respectively) are shown as,

$$\mathrm{Da} = \frac{\tau_t}{\tau_c} = \frac{\ell S_L}{\delta_\ell u'} \tag{6.7}$$

The Damkohler number, Da can also be regarded as the inverse of Karlovitz number, Ka defined in Eq. 6.4 as the ratio of the chemical lifetime to turbulent lifetime. According to Veynante and Vervisch (2002), the turbulent Reynolds number, R_ℓ, is related to the two parameters as,

$$\mathrm{R}_\ell = \mathrm{Da}^2\ \mathrm{Ka}^2 \tag{6.8}$$

A set of two parameters of (R_ℓ, Ka), (Ka, Da) or (R_ℓ, Da) are necessary to discuss the combustion regimes.

For Da greater than unity, Da >> 1, the flame front becomes thin. In this case, turbulence motions wrinkle the flame surface only and not affecting its inner structure. This *flamelet regime or thin wrinkled flame regime* occurs due to the influence of the smallest turbulence scales i.e. Kolmogorov length scale, η. The turbulent motions in this regime are too slow to disturb the flame structure.

The Karlovitz number, Ka is used to define the *Klimov-Williams criterion*, resulting to Ka equals to unity, demarcating between two combustion regimes. This criterion was initially taken as the transition between the flamelet regimes with Ka < 1 earlier described, and the *distributed combustion regime* where the inner structure of the flame is intensely changed by turbulent motions. An analysis from Peters (1999) has revealed that for Ka > 1, turbulent motions disturb the inner structure of the flame but not the reaction zone.

Peters (1999) proposed the following turbulent premixed regimes as,

- *Ka < 1: Flamelet regime or thin wrinkled flame regime*. Based on the velocity ratio, u'/S_L, this regime is subdivided into two namely:
  - *$(u'/S_L) < 1$: wrinkled flame*. The turbulent structures are incapable of wrinkling the flame surface up to flame front interactions. The laminar propagation is higher than the turbulence/combustion interactions which remain inadequate.

- *$(u'/S_L) > 1$: wrinkled flame with pockets otherwise called corrugated flames*. In this division, larger structures are capable of inducing flame fronts interactions leading to pockets.

- *$1 < Ka \leq 100$: Thickened wrinkled flame regime or thin reaction zone.* The turbulent motions in this regime are capable of affecting and thickening the flame preheat zone, but not able to change the reaction zone which still remains thin and near to a laminar reaction zone.
- *$Ka > 100$: Thickened flame regime or well –stirred reactor*. In this condition, the turbulent motions strongly affect both preheat and reaction zones. No laminar flame structure could be identified in this regime.

Figure 6.10 shows the various regimes of turbulent premixed combustion as specified by Peters(1999) and Borghi and Destriau (1998) using the length scale (ℓ/δ_ℓ) and the velocity (u'/S_L) ratios. The Klimov-Williams criterion for Karlovitz number, Ka equals to unity is attained when the flame thickness is equivalent to the Kolmogorov length scale. Below this line, the flame is thinner than any turbulent length scales. Below the line delineating the Peters criterion i.e. Ka = 100, the thickness of the reaction zone is thinner than any turbulent length scales and is not influenced by turbulent motions.

In the present experiments, the dimensionless ratios (ℓ/δ_ℓ and u'/S_L) were calculated and listed in Table 6.2 and plotted on Fig. 6.10. It can be seen that the bulk of the data points fall in the *thickened-wrinkled flames regime*.

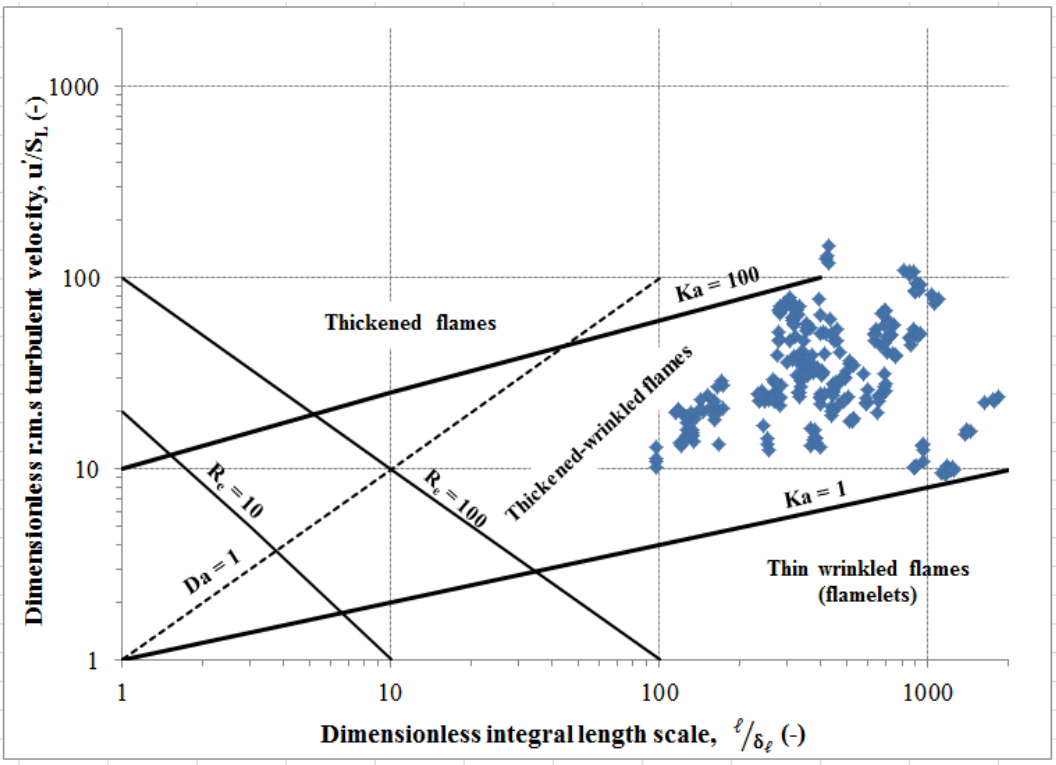

Figure 6.10 Present research data on premixed turbulent combustion regimes diagram as specified by Peters (1999) and Borghi and Destriau (1998).

6.8 Overview of Turbulent Combustion Parameters from the Present Research

The summary of all the turbulent combustion parameters calculated in the present research are given in Table 6.2.

Table 6.2 Summary of the calculated turbulent combustion parameters.

Test	$\ell = 0.5b$	u'/S_L	R_ℓ	S_T	Ka	ℓ/δ_ℓ
(-)	(m)	(-)	(-)	(m/s)	(-)	(-)
1	No obstacle					
2	0.017	18	9390	36	0.52	522
3	0.017	35	18416	41	1.40	533
4	0.017	50	35981	51	2.03	726
5	0.017	58	41236	62	2.56	716
6	0.017	67	45793	65	3.26	687
7	0.017	50	32078	51	2.23	636
8	0.017	28	19330	40	0.88	693
9	No obstacle					
10	0.017	26	7144	36	1.29	271
11	0.017	34	10542	37	1.79	308
12	0.017	72	22596	41	5.42	314
13	0.017	76	23116	45	5.92	305
14	0.017	71	20522	38	5.46	291
15	0.017	68	19166	34	5.28	281
16	0.017	47	12911	33	3.00	278
17	No obstacle					
18	0.017	45	31085	75	1.81	691
19	0.017	78	82528	115	3.31	1062
20	No obstacle					
21	0.017	24	6726	22	1.11	280
22	0.017	57	17963	41	3.80	316
23	0.017	68	22195	43	4.87	326
24	0.017	57	18176	26	3.84	316
25	0.021	23	14952	49	0.66	660
26	0.021	93	85532	77	4.63	922
27	0.021	107	90888	96	5.97	849
28	0.021	86	77637	70	4.14	905
29	0.011	4.9	1666	41	0.09	337
30	0.003	1.2	103	31	0.02	83
31	0.013	14	5314	32	0.43	377
32	0.013	23	11024	48	0.77	485
33	0.013	30	14722	55	1.18	488
34	0.013	28	12893	38	1.11	454
35	0.006	12	2464	30	0.49	198
36	0.006	24	6086	44	1.12	258
37	0.006	23	6127	52	1.07	238
38	0.006	24	5824	48	1.21	240
39	0.006	12	2872	42	0.42	241
40	0.006	31	11111	74	1.47	354
41	0.006	36	13139	104	1.77	366
42	0.006	31	10872	112	1.46	349
43	0.006	25	5889	54	1.23	233
44	0.003	15	1983	48	0.83	129
45	0.003	20	3298	75	1.10	165

Table 6.2 Cont'd

Test	$\ell = 0.5b$	u'/S_L	R_ℓ	S_T	Ka	ℓ/δ_ℓ
(-)	(m)	(-)	(-)	(m/s)	(-)	(-)
46	0.003	19	3034	71	1.05	161
47	0.003	27	4447	65	1.70	165
48	0.003	11	1108	28	0.61	97
49	0.003	15	1965	37	0.78	132
50	0.003	14	1785	48	0.72	124
51	0.003	20	2348	46	0.70	117
52	0.012	15	5606	26	0.46	380
53	0.012	25	11115	39	0.94	442
54	0.012	20	8866	48	0.68	440
55	0.012	32	12827	32	1.39	405
56	0.019	23	13814	38	0.73	592
57	0.019	47	40871	60	1.75	862
58	0.019	51	46620	62	1.90	913
59	0.019	39	29529	47	1.40	754
60	No obstacle					
61	0.017	23	9302	42	0.89	398
62	0.017	13	12018	100	0.23	960
63	0.017	47	21708	61	2.39	460
64	0.017	131	55404	111	11.4	424
65	0.017	25	14836	135	1.75	412
66	0.017	51	21372	63	2.83	416
67	No obstacle					
68	0.017	41	14104	40	2.26	341
69	0.017	64	25605	37	4.10	398
70	0.017	55	19425	47	3.41	353
71	0.017	25	8369	22	1.09	333
72	0.029	10	9130	28	0.17	893
73	0.029	10	11642	38	0.15	1164
74	0.029	16	21949	54	0.26	1407
75	0.029	23	39956	146	0.41	1738
76	0.006	38	11814	79	1.96	314
77	0.006	21	5343	65	1.10	252
78	0.006	28	8205	76	1.40	288
79	0.006	38	10427	44	2.25	273
80	0.003	20	2604	62	1.22	131
81	0.003	23	3493	67	1.36	154
82	0.003	27	3859	52	1.89	141
83	0.003	25	3191	47	1.74	127
84	0.003	71	7195	75	9.37	101

6.9 Summary of the Major Findings

The following important findings on the prediction of turbulent combustion parameters in this chapter are:

- Turbulence parameters were estimated from pressure differential measurements and geometrical obstacle dimensions. This enabled the calculation of the explosions induced gas velocities, r.m.s turbulent velocity, turbulent Reynolds number and Karlovitz number. A complete turbulence profile similar to that of overpressure and flame speeds profiles was formed with all the turbulent combustion parameters predicted in this research as a function of the obstacle separation distance.
- An increase in the r.m.s velocity, u' resulted to an increase in the unburned gas flow velocity, S_g. In comparing the effectiveness of obstacle spacing with the work of Hjertager *et al.* (1988a) using 50 m^3 vented tube with six obstacles closely spaced, the present work (0.1 m^3 vented tube with just two obstacles) produced higher turbulence intensity than the large scale geometry at an equivalent length similar to that of the current research.
- A strong dependence of maximum overpressure on Ka for 10% CH_4 mixtures was found in the present research. The single obstacle tests had a Ka of well below unity and this shows no sign of flame quenching. However, Ka value of greater than unity was realised with the double obstacle tests. Theoretically, Ka above unity indicates global flame extinction however, the entire flame quench was not observed in any of the present tests. In all cases the explosion propagated strongly, leading to significant overpressures. The values of Ka in this study would therefore suggest a measure of the prevailing flame straining conditions downstream of an obstacle, as opposed to an indication of flame extinction.
- The current research data were presented on premixed turbulent combustion regimes diagram as specified by Peters(1999) and Borghi and Destriau (1998). The bulk of the data points fall in the thickened-wrinkled flames regime.

Chapter 7

Turbulent Combustion Models and Scaling

7.1 Introduction

As discussed in Chapter 3, gas explosion scaling techniques has to do with carrying out an experiment in a geometrically-similar, reduced rig. However, to realize accurate scaling of an explosion the overpressures (taken as proportional to the square of flame speeds) that occur at large scale must be replicated in the small scale experiment. In the existing practice, precise scaling is attained by enhancing the reactivity of the mixture used at small scale either by using a more reactive fuel-gas e.g. ethylene as related to methane (Taylor and Hirst 1989) or by oxygen enrichment of the gas-air mixtures (Catlin and Johnson 1992). It is worth noting that these scaling techniques are greatly dependent on the fundamental turbulent combustion models on which it is established. Critical review of S_T models with dependence on integral length scale, ℓ was performed also in Chapter 3. This review revealed that there are great differences on the dependence on ℓ, laminar burning velocity, S_L and r.m.s. flow velocity, u'.

In this chapter, the experimental evidence on the influence of scale by either changing the size of the experimental rig or by varying the size of the obstacle scale, b for fixed explosion geometry will be reviewed. Also, in this chapter, a new turbulent burning velocity, S_T model based on the present research will be formulated and compared with other models in the literature. The implication of turbulent combustion models on gas explosions scaling and CFD will be highlighted. From the newly derived S_T model in the present research and others in the literature, new scaling relationships for overpressures will be derived and validated against the limited experimental data.

7.2 Experimental Evidence on the Influence of Scale

A variation of scale could be achieved in two ways. Firstly, by varying the size of the explosion rig and secondly, by varying the characteristics size of the obstacle for a fixed size of rig.

Most of the reported experimental studies on scale were based on varying the size of the explosion geometries. These include the works on: Bjorkhaug(1986); Hjertager *et al.* (1988b); Johnson *et al.* (1991); Mercx (1992); Bimson *et al.* (1993) and van Wingerden *et al.* (1994). Table 7.1 shows an overview of the experimental

conditions from the above experimental work on varying the explosion vessel. Also shown are the scale factors between the small and large geometries, obstacle blockage ratios and explosions severities in terms of flame speeds and overpressures.

The limited experimental works based on varying the size of the obstacle for a given geometry were performed by Phylaktou (1993) and Gardner (1998). The authors used perforated grid plates as turbulent generating obstacles in elongated cylindrical vessels of 76 mm, 162 mm and 500 mm diameters. For a fixed geometry and constant obstacle blockage, the obstacle scale was varied by changing the number of holes or bars for perforated-hole grid plate or bar grid plate respectively. The authors found that peak overpressures and turbulent burning velocity, S_T had strong dependence on obstacle scale which relied on the obstacle blockage ratio. In the present research, this approach was used to vary the obstacle scale for a constant obstacle blockage and geometry (see Chapter 5).

Table 7.1 Experimental investigation on the influence of scale for variable explosion geometries.

Reference	Experimental condition	Scale factor	Obstacle	BR	S_{fmax}	P_{max}	Comments
(-)	(-)	(-)	(-)	(-)	(m/s)	(bar)	(-)
Bjorkhaug (1986)	Geometry: Small scale radial vessel of 0.5 m long and variable height. A large scale 20 times greater than the small scale was used. Mixture: Propane and methane-air mixtures. Ignition: Central.	20	Five thin metal obstacles	0.3-0.75	-	2.75	The maximum overpressure for the large scale (2.75 bar) was attained with propane-air mixtures and 0.5 BR obstacle. The equivalent overpressure for small scale was 7 folds lower than that of the large scale.
Hjertager *et al.* (1988b)	Geometry: Two scaled down versions of realistic separator and compressor modules with variable vent sizes and locations. The test scales were 1:33 and 1:5 with the latter having a dimension of 8 m by 2.5 m by 2.5 m. Mixture: Propane and methane-air mixtures Ignition: Variable positions.	33	Equipment and pipes	0.1-0.3	800	1.9	For the most confined tests, a maximum pressure in 1:5 scale was approximately 5-10 times higher than 1:33 scale separator and compressor modules tests respectively.

Table 7.1 Cont'd

Reference	Experimental condition	Scale factor	Obstacle	BR	S_{fmax}	P_{max}	Comments
(-)	(-)	(-)	(-)	(-)	(m/s)	(bar)	
Johnson *et al.* (1991)	Geometry: A confined enclosure of 9 m long and 3 m square cross section with 36 m long polythene covered region of external congestion pipes. A $1/5^{th}$ scale replica of the large scale geometry was also used. Mixture: Natural gas-air Ignition: From the confined enclosure.	5	0.18 m diameter pipe	0.42	500	-	The resultant flame speed of 40 m/s from the small scale enclosure indicated a reduction by a factor 12.5 compared to that of large scale test.
Mercx (1992)	Geometry: An enclosure of 25.4 m x 12.7 m x 1.0 m. Also, a reduced scaled factor of 6.35 to the large scale geometry was used. Mixture: Stoichiometric ethylene-air mixtures Ignition: Central ignition	6.35	0.5 m diameter pipes	0.5	1323	4.85	The highest overpressure in the large scale (4.85 bar) was 4 folds higher when compared to small scale geometry. Also, for the large scale geometry, the detonative flame speeds obtained (1323 m/s) was a factor of 5.7 greater than that of the small scale experiment.

Table 7.1 Cont'd

Reference	Experimental condition	Scale factor	Obstacle	BR	S_{fmax}	P_{max}	Comments
(-)	(-)	(-)	(-)	(-)	(m/s)	(bar)	
Bimson *et al.* (1993)	Geometry: An enclosure of 10 m by 8.75 m by 6.25 m with centrally placed vent opening occupying 50% of one of the end walls. A $1/6^{th}$ linear dimension of the full scale enclosure was used. Mixture: Propane-air mixture Ignition: Spark plug of 30 mJ situated opposite the vent.	6	0.5 m diameter pipe	0.4	75	0.3	The maximum overpressure (0.3 bar) was a factor of 2.5 higher compared to the $1/6^{th}$ geometry of the large scale.
Van Wingerden *et al.* (1994)	Geometry: Two wedge-shaped explosion vessels of small and large scales with a scale factor of 1:10 and 1:1 respectively. The undersized scale geometry had a dimension of 1m long and 0.125 m high. Mixture: Pure methane-air mixtures. Ignition: Spark plug.	10	Five baffle-like obstacles	0.33	350	-	The flame speed obtained in large scale vessel (350 m/s) was five times higher than that achieved in small scale vessel for methane-air tests.

7.3 Derivation of New S_T Models with Dependence on Scale, ℓ

Turbulent burning velocity models with dependence on obstacle scale, ℓ were reviewed previously in Chapter 3. It was observed that most of the models were derived based on data with little or no variation in scale and with fairly low turbulence levels. Therefore it becomes necessary in the present research to formulate an empirical correlation of turbulent burning velocity with dependence on obstacle scale in order to be compared with the other models and be applied to realistic geometries as found in the industries.

As described in Chapter 6, the turbulent burning velocity, S_T was calculated as the ratio of the maximum flame speed, S_{fmax} to the adiabatic expansion factor, E. In order to obtain an S_T model with dependence on obstacle scale, ℓ, turbulent Reynolds number, R_ℓ, has to be incorporated. Figure 7.1 shows a plot of dimensionless turbulent burning velocity, S_T/S_L against the turbulent Reynolds number, R_ℓ, for single-hole and single flat-bar obstacles of 10% methane-air mixtures each. The single-hole obstacles comprised of Tests 2-8, 25-28 and 52-55 whereas the single flat-bar obstacles had Tests 31-34 and 56-59.

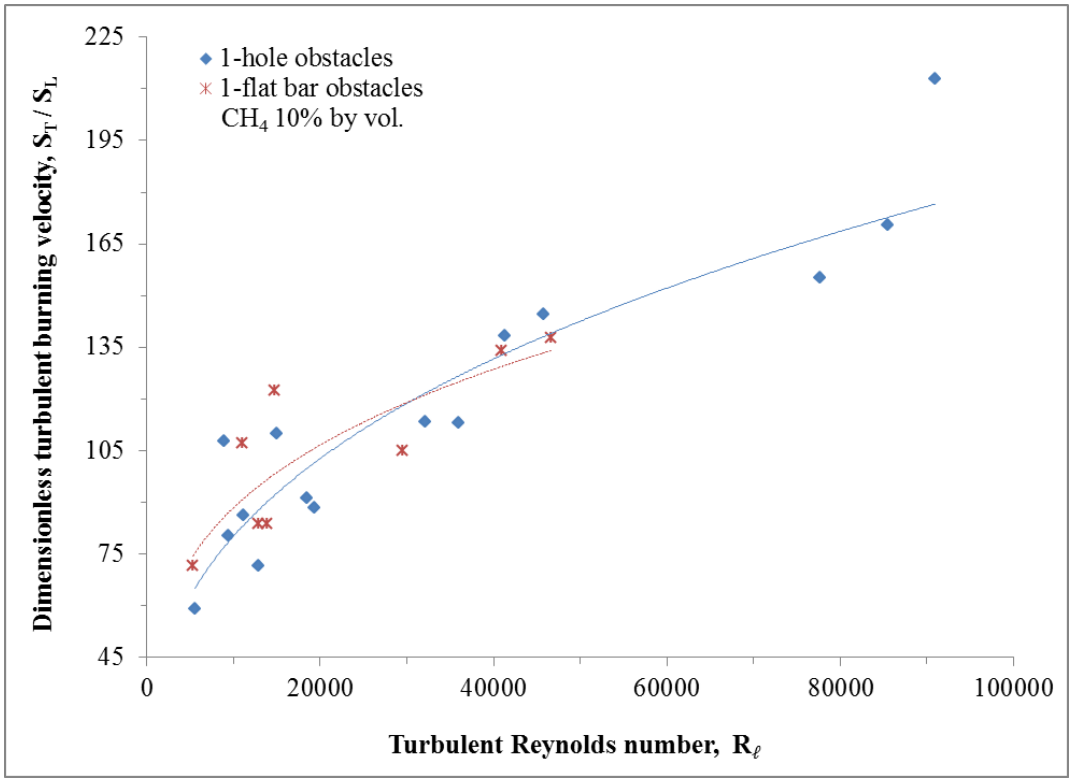

Figure 7.1 Relationship between turbulent burning velocity and turbulent Reynolds number.

The equations of the fitted curves for the single-hole and single flat-bar obstacles respectively had the form of,

$$\frac{S_T}{S_L} = 2.99 R_\ell^{0.36} \quad (7.1)$$

$$\frac{S_T}{S_L} = 7.36 R_\ell^{0.27} \quad (7.2)$$

The empirical correlations shown above have demonstrated a dependence on the length scale with single-hole obstacles i.e. Eq. 7.1 higher than that of the single flat-bar obstacles Eq. 7.2. The dependence on Eq. 7.1 is significantly higher than most of the models reviewed but it is closer to that of Phylaktou and Andrews (1995).

7.4 Implication of Turbulent Combustion Models on Gas Explosion Scaling and CFD Modelling

A simple comparison between the turbulent combustion models revised previously in Chapter 3 can be made by obtaining the predicted overpressure ratios for an increase in scale factor. This is shown in Table 7.2 in which predicted flame speed and overpressure factors were presented for increase in scale by factors of 10 and 30. The flame speed was presumed to increase in proportion to the turbulent burning velocity, S_T, while the overpressure was taken as dependent on the square of the flame speed (Harris and Wickens 1989). The results demonstrated that though the variance in the dependency on scale designated by the different models is trivial in absolute terms, the resultant estimates, mostly of overpressure, are considerably different and could make a barrier between safe and unsafe design.

An overview of available CFD codes used to model gas explosions was given by Lea and Ledin (2002). Most of the codes have been embedded with a turbulent burning velocity different from each other as shown in Table 7.2. By doing so, the influence of scale dependence will play a major role in determining the explosion overpressure and flame speed. For instance, FLACS model has an S_T model from Brays' correlation as stated earlier in Eq. 3.3 whereas FLUENT used Zimont *et al.* (1998) correlation (see Eq. 3.7). By considering a scale factor of 10, the difference

in scale exponent of 0.196 and 0.25 for the former and latter will result to flame speed difference by a factor of 1.57 and 1.78 respectively. This in turn will lead to an overpressure prediction by a factor of 2.47 and 3.16 in that order.

Currently, Shell Global Solutions, UK make use of Gouldin S_T model (see Eq. 3.2) for explosion scaling between small and large explosion rigs (Taylor and Hirst 1989). EXSIM is one the CFD codes developed by Shell and is "most likely" to use S_T correlation based on fractal approach by Gouldin (1987). On the other hand, British Gas Limited, BG developed a code called COBRA. The BG incorporates the S_T correlation of Bradley *et al.* (1992) (see Eq. 3.4) to perform its explosion scaling technique (Catlin and Johnson 1992). Considering a scale factor of 30 from the two scenarios (Shell – EXSIM and BG – COBRA), the variance in scale exponent of 0.26 and 0.15 for the former and latter will lead to flame speed difference by a factor of 2.42 and 1.67 respectively. This in turn will cause an overpressure prediction by a factor of 5.86 and 2.77 in that order.

However, there have been some efforts to determine the precision of frequently used explosion models individually. These comprise the MERGE and EMERGE project, EU co-funded projects, and the Joint Industry Project on Blast and Fire Engineering for Topside Structures Phase 2 (Lea and Ledin 2002). The CFD codes used to model the gas explosions were COBRA, FLACS, EXSIM and AutoReaGas. The authors testified reasonable scatter in the predicted overpressure results within the codes. This poor result is likely to be due to difference in turbulent burning velocity model in each code with respect to scale,ℓ. The EXSIM model with the highest exponent in scale, 0.26 produced the highest overpressure when compared to others.

Table 7.2 Comparative increase in flame speed and overpressure estimated by different S_T models for a 10-fold and a 30-fold increase in scale.

S/N	Reference	CFD code/Industry	u' exponent	ℓ exponent	Scale factor 1	Scale factor 2	S_f factor 1	S_f factor 2	P factor 1	P Factor 2
1	[1]	SHELL	0.26	0.26	10	30	1.82	2.42	3.31	5.86
2	[2]	FLACS/CMR	0.412	0.196	10	30	1.57	1.95	2.47	3.79
3	[3]	BRITISH GAS	0.55	0.15	10	30	1.41	1.67	1.20	2.77
4	[4]	-	0.78	0.31	10	30	2.04	2.87	4.17	8.24
5	[5]	-	0.75	0.5	10	30	3.16	5.48	10.0	30.0
6	[6]	FLUENT	0.75	0.25	10	30	1.78	2.34	3.16	5.48
7	[7]	-	0.5	0.5	10	30	3.16	5.48	10.0	30.0
8	[8]	-	0.39	0.61	10	30	4.07	7.96	16.6	63.4
9	[9]	-	0.5	0.5	10	30	3.16	5.48	10.0	30.0
10	[10]	-	0.5	0.5	10	30	3.16	5.48	10.0	30.0
11	[11]	-	0.5	0.167	10	30	1.47	1.76	2.16	3.11
12	[12]	-	0.55	0.25	10	30	1.78	2.34	3.16	5.48
13	[13]	-	0.63	0.58	10	30	3.80	7.19	14.5	51.7
14	[14]	-	0.36	0.36	10	30	2.30	3.40	5.25	11.6
15	[15]	-	0.27	0.27	10	30	1.86	2.51	3.47	6.28

[1] Gouldin 1987 [2] Bray 1990 [3] Bradley *et al.* 1992 [4] Phylaktou 1993 [5] Kobayashi 1997 [6] Zimont *et al.* 1998 [7] Peters 1999
[9] Filatyev *et al.* 2005 [10] Driscoll 2008 [11] Dorofeev 2008 [12] Mupala *et al.* 2009 [13] Daniele and Jansohn 2012 [14] Present model eq. 7.1
[15] Present model eq. 7.2

7.5 Derivation and Validation of Scaling Relationships for Overpressures

Phylaktou and Andrews (1995) formulated a pioneer equation (see Eq. 7.3) in the explosion protection literature that gave an explicit dependence of the blast overpressure on the geometric configuration, pressure loss characteristics (effectively the blockage ratio of the obstacles) and mixture properties. The correlation was derived from their S_T correlation and validated against the limited suitable experimental data and showed a good agreement.

$$P \propto \left[\left(C_T\sqrt{K}\right)^{1.56}\ell^{0.62}\right][E^{3.56}S_L^{2.62}L_e^{-0.92}(v/v_a)^{1.28}] \text{ Phylaktou's model} \quad (7.3)$$

The S_T obtained in the present research (Eq. 7.2) and those currently in use to model gas explosions using CFD were used to derive the scaling relationships for overpressure based on the approach of Phylaktou and Andrews (1995). The respective overpressure equations are given as,

$$P \propto \left[\left(C_T\sqrt{K}\right)^{0.54}\ell^{0.54}\right]\left[E^{2.54}S_L^{2.54}v^{-0.54}\right] \quad \text{Present model} \quad (7.4)$$

$$P \propto \left[\left(C_T\sqrt{K}\right)^{0.52}\ell^{0.52}\right]\left[E^{2.52}S_L^{2.52}v^{-0.52}\right] \quad \text{Gouldin's model} \quad (7.5)$$

$$P \propto \left[\left(C_T\sqrt{K}\right)^{0.82}\ell^{0.39}\right][E^{2.82}S_L^{2.39}v^{-0.39}] \quad \text{Bray's model} \quad (7.6)$$

$$P \propto \left[\left(C_T\sqrt{K}\right)^{1.1}\ell^{0.3}\right][E^{3.1}S_L^{2.3}L_e^{-0.6}v^{-0.3}] \quad \text{Bradley's model} \quad (7.7)$$

$$P \propto \left[\left(C_T\sqrt{K}\right)^{1.5}\ell^{0.5}\right]\left[E^{3.5}S_L^{2.5}v^{-0.5}\right] \quad \text{Zimonts's model} \quad (7.8)$$

The relevant experimental work performed both at laboratory and large scales by Bjorkhaug (1986) were used to validate the newly derived overpressure equations. A radial vessel with 17^o (pie) sector of a full cylindrical disk with solid walls at top, bottom, sides, and open to outer radius was used in these experiments. Ignition was effected at the apex of the vessel which is the centre of the imaginary full disk. Five obstacles of variable blockage ratios were used to generate turbulence in the experiments. The evenly spaced obstacles along the length of the vessel were either thin metal strips or round tubes. The influence of sharp/thin and thick/round obstacles on intensity of turbulence and hence overpressure was discussed previously in Chapter 2. In the present validation, the results from the sharp/thin obstacles were considered. Stoichiometric methane and propane air mixtures were used to perform the explosions in both small and large scale geometries.

In the small scale (laboratory) tests, a vessel of 0.5 m long was used. The pitch and the height of the obstacles were kept at 0.1 m and 0.016 m respectively. However, the height of the vessel was adjustable and this permitted the study of the blockage ratios to be altered from 0.3 to 0.75.

Figure 7.2 and 7.3 show the experimental overpressures as a function of obstacle blockage for methane and propane in that order. Also shown in those figures are the respective predicted overpressures based on the newly derived models (Eqs. 7.3-7.8). The constant of proportionality in each equation was obtained from fitting that equation to the methane test with the 0.54 blockage ratio obstacle labelled as "reference point" in Fig. 7.2 only. However, it should be noted that the constant is not universal but only applicable to this geometry. With the constant calculated in each equation, the equations became absolute (for this specific geometry) and were used to determine the overpressures at the various obstacle blockages for both gas/air mixtures. The turbulence generation constant, C_T was taken as 0.225 (for sharp/thin obstacles) whereas the pressure loss coefficient, K was calculated from Eq. 2.16 as given in Chapter 2. The integral scale, ℓ was taken as half the obstacle height and the mixture properties listed in Table 5.1, from Phylaktou and Andrews (1995) and GasEq (for kinematic viscosity, v only) were used. The predicted overpressures shown as data points were in good agreement with the experimental overpressures shown as dashed lines for both fuels and range of obstacle blockage used.

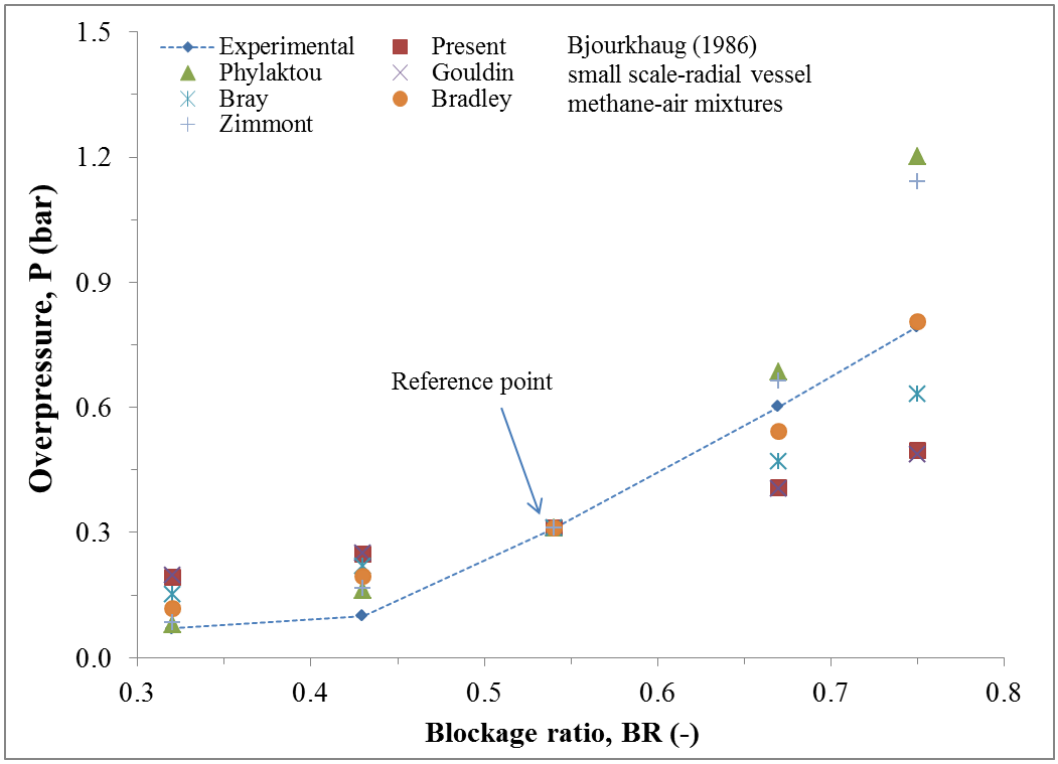

Figure 7.2 Comparison between laboratory-scale experimental (Bjourkhaug 1986) and predicted overpressures for stoichiometric methane-air mixtures at different blockages.

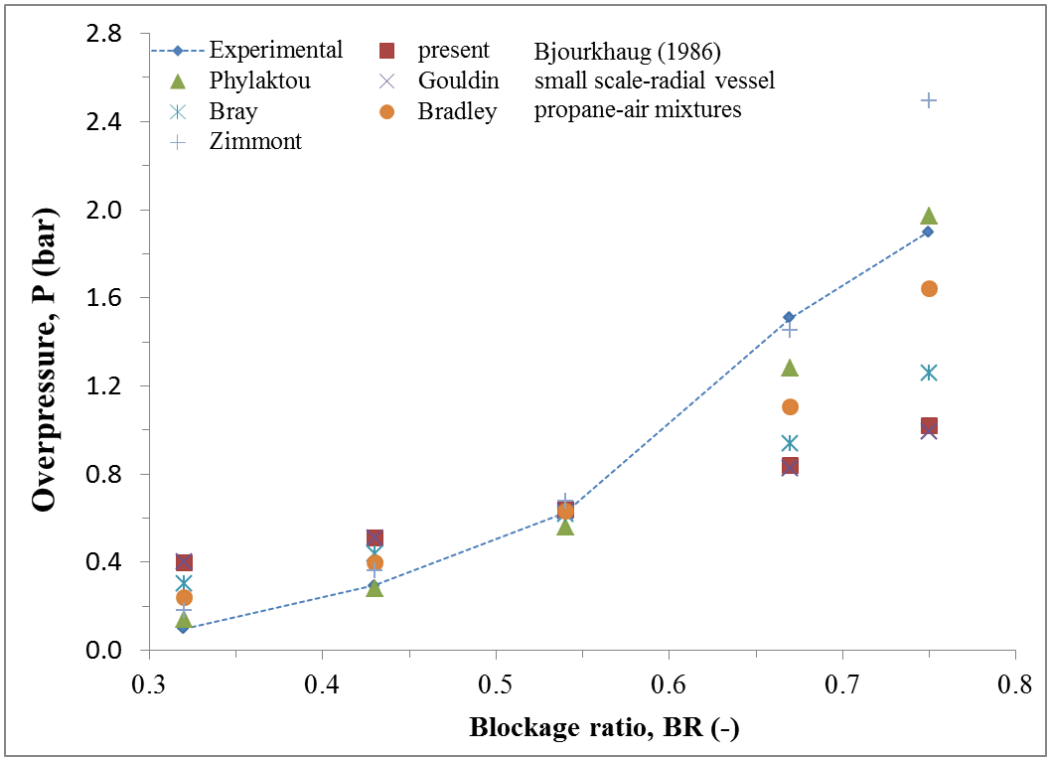

Figure 7.3 Comparison between laboratory-scale experimental (Bjourkhaug 1986) and predicted overpressures for stoichiometric propane-air mixtures at different blockages.

The author also reported the overpressure results from a large-scale rig akin to the small scale geometry described above. The large scale vessel had the identical disc-sector shape, 10 m long and the spacing between obstacles was 2 m. This corresponded to a scale increase by a factor of 20. For tests with methane-air mixtures, three obstacle blockage ratios of 0.16, 0.3 and 0.5 were used while propane-air mixtures had only 0.16 and 0.5 blockages.

Figure 7.4 and 7.5 presented the experimental measured overpressures in the large scale tests for methane and propane-air mixtures respectively. Also shown are the predicted overpressures from Eqs. 7.3-7.8 with similar proportionality constant as obtained from the single methane-air test with 0.54 obstacle blockage at the small-scale experiments and assuming complete geometric comparison between the laboratory (small) and large-scale tests with a scale ratio of 20. For both methane and propane-air mixtures, the calculated overpressures were in a close agreement with the experimental data especially for models with high integral length scale, ℓ exponent.

This agreement is very promising as it reveals that from using geometry at laboratory scale in the present research to calibrate the present equations (Eqs. 7.1 and 7.2), then the effects of different blockage ratios, gases and scales for the same overall geometry could be successfully predicted.

None of the current gas explosion scaling techniques by Taylor and Hirst (1989) and Catlin and Johnson (1992) has been utilized for such an extensive predictive application based on data from a single test performed at laboratory scale. However, by incorporating certain parameters dependence on overpressures as pioneered by Phylaktou and Andrews (1995), the predictive ability of the models used in scaling techniques and those in gas explosions CFD codes (FLACS and FLUENT) has improved.

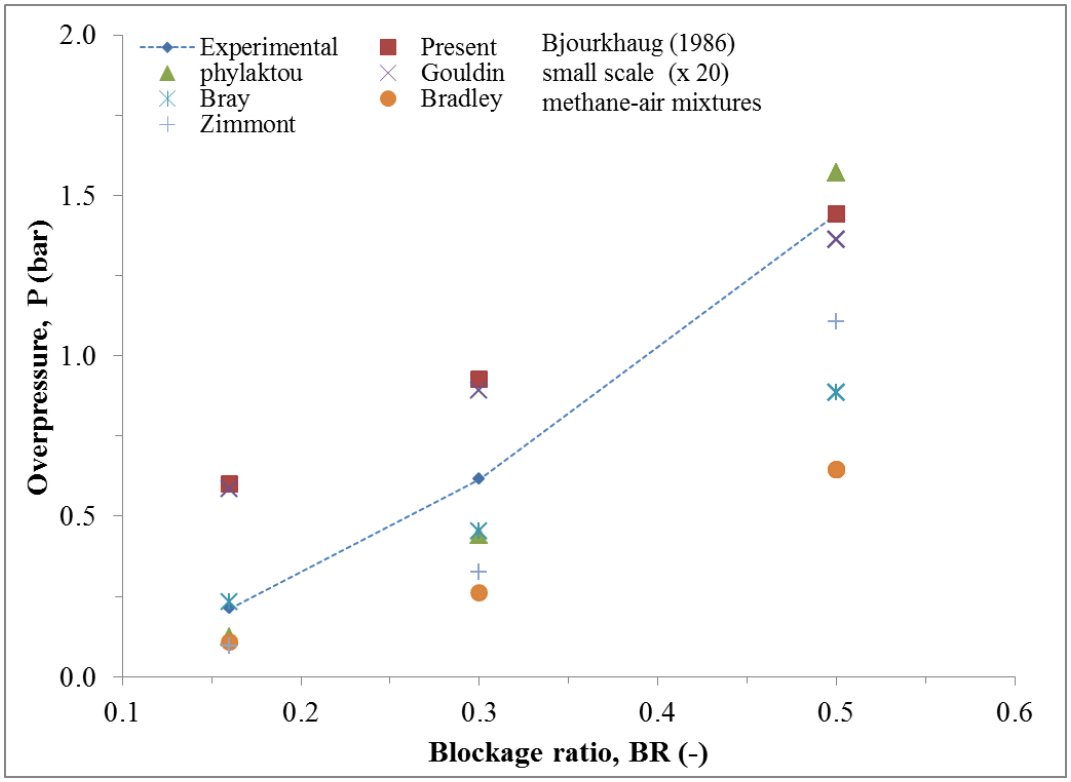

Figure 7.4 Comparison between large- scale experimental (Bjourkhaug 1986) and predicted overpressures for stoichiometric methane-air mixtures at different blockages.

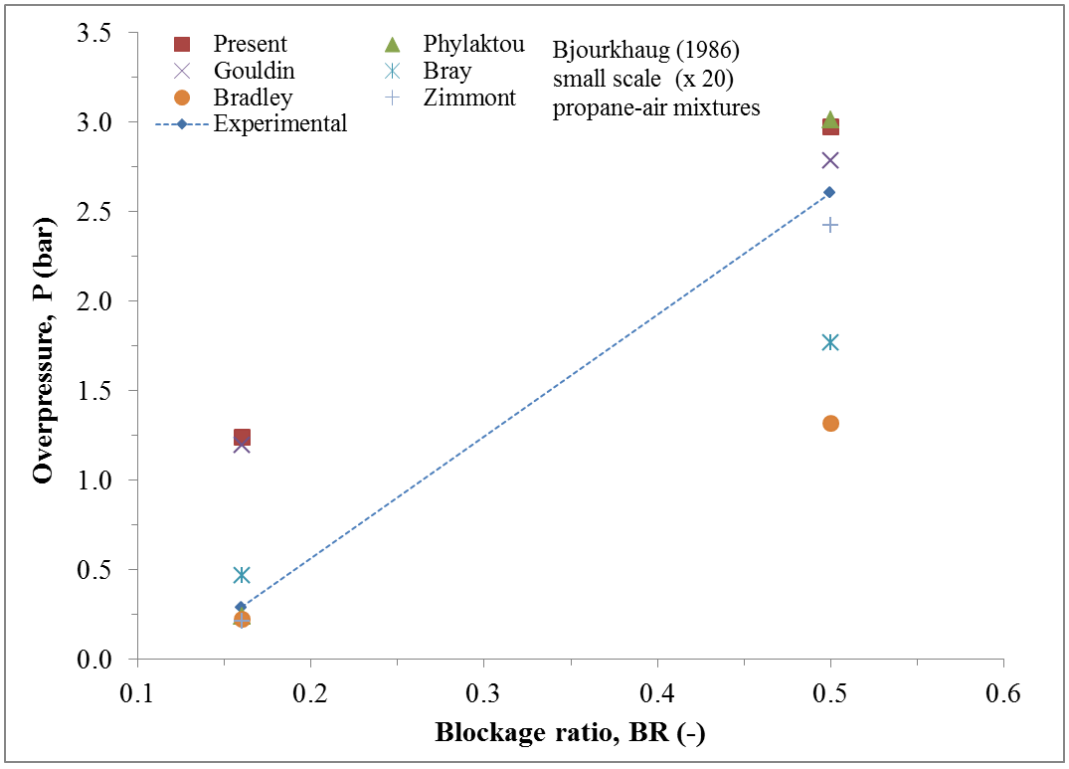

Figure 7.5 Comparison between large- scale experimental (Bjourkhaug 1986) and predicted overpressures for stoichiometric propane-air mixtures at different blockages.

7.6 Summary of the Major Findings

The main findings of this chapter are as follows:

- Turbulent burning velocity models with dependence on obstacle scale, ℓ were derived from the experimental results of the current research with double obstacle and 10% CH_4 mixtures. The equations of the fitted curves for the single-hole and single flat-bar obstacles respectively had the form of,

$$\frac{S_T}{S_L} = 2.99 R_\ell^{0.36}$$

$$\frac{S_T}{S_L} = 7.36 R_\ell^{0.27}$$

- A simple comparison between the turbulent combustion models with dependence on scale, ℓ was made by obtaining the predicted overpressure ratios for an increase in scale factor. The predicted flame speed and overpressure factors were presented for increase in scale by factors of 10 and 30. The results revealed that though the difference in the dependency on scale designated by the different models is less in absolute terms, the resultant estimates, mostly of overpressure, are considerably different and could make a barrier between safe and unsafe design.
- From the newly obtained S_T correlations, an equation with explicit dependence of the blast overpressure on the geometric configuration, pressure loss characteristics (effectively the blockage ratio of the obstacles) and mixture properties was derived as,

$$P \propto \left[\left(C_T\sqrt{K}\right)^{0.54} \ell^{0.54}\right]\left[E^{2.54} S_L^{2.54} v^{-0.54}\right]$$

- The overpressure equation was validated against the limited suitable experimental data from both small and large scales and different fuel mixtures and showed a good agreement.

Chapter 8
An Initial CFD Modelling Approach using FLACS

8.1 Introduction

The Flame Acceleration Simulator (FLACS) code has been developed at Gexcon AS Norway. FLACS is a finite volume code based on a 3-D Cartesian grid. The CFD tool is used broadly for simulating problems applicable to process safety. It has been designed specifically for modelling the consequences of flammable gas release and explosions in a semi-confined and/or congested region. The sub-grid scale obstacles are modelled using the Porosity/Distributed Resistance Approach. In turbulent processes, the transport of scalars and momentum is modelled using $\kappa - \varepsilon$ turbulence.

The combustion model used in FLACS is the β-flame model which is based on correlations of turbulent burning velocities, S_T from Bray (1990) as given in Eq. 3.3 with turbulence parameters such as u' and S_L (Arntzen 1998). The β-flame model assumes that the flame propagates at a given burning velocity and with a given constant flame thickness (Arntzen 1998) . In order to account for flame thickness as a result of diffusion, flame curvature and burning towards the wall, the flame model uses correction functions. The turbulent viscosity and the reaction rate are set in the transport equation for the reaction progress variable in order to ensure that the burning velocity corresponds to that specified by a correlation (Lea and Ledin 2002).

In FLACS, an advanced user interface comprising of the Computer Aided Scenario Design, CASD, and Flowvis has been developed. The former is used to generate the scenario definition by simplifying the geometry while the latter shows the results from the FLACS simulations.

The grid resolution in FLACS is based on a certain number of cells across the gas cloud. The grid resolution has to be selected to acquire a simulation result within a satisfactory time frame in most cases less than an hour for a coarse grid. Grid guidelines as applicable to gas explosion simulations in FLACS have been stated in the user manual (GexCon 2010).

FLACS has been validated against a wide range of experiments (Lea and Ledin 2002). The criterion that makes comparison generally acceptable in FLACS is when the predicted pressure is within a factor of two of the experimental work. In recent times, Middha and Hansen (2008) applied FLACS to predict the deflagration to

detonation transition in hydrogen explosions. Also, the code was used by Middha *et al.* (2011) to determine the effect of adding hydrogen to natural gas in order to ascertain the level of explosion risk. In addition to industrial explosions, FLACS was used to model large-scale vented gas explosions in a twin-compartment enclosure (Pedersen *et al.* 2013).

In line with the aim of this project, FLACS will be used in this chapter to model the influence of obstacle separation distance using two orifice plate obstacles of 0.3 BR and 10% CH_4-air mixtures in a vented elongated cylindrical vessel. The results obtained will be compared with the experimental values to ascertain the agreement between the two setups. To the author's knowledge, this is the narrowest geometry ever to be modelled in FLACS as it is mainly built to perform gas explosions on real industrial scale application.

8.2 FLACS Pre-processor

FLACS, version 9.1 (GexCon 2010) was used to simulate the experimental evidence on the influence of obstacle separation distance on gas explosions as described in Chapter 5.1.3. The model's capacity to capture the effect of obstacles and flow interactions between two obstacles spaced at various distances and consequently its prediction of overpressure is of basic concern.

The cylindrical vessel used in the experiment was modelled in FLACS by inserting it into a 3D rectangular geometry of similar length. This was as a result of the conservative nature of FLACS to model 3D geometries only. Three monitor points (M1-M3) at positions similar to those in the experimental tests were used to record the model's overpressure at those points. Figure 8.1 shows the diagram of an explosion geometry accommodating a single obstacle of 0.3 BR, 1-hole.

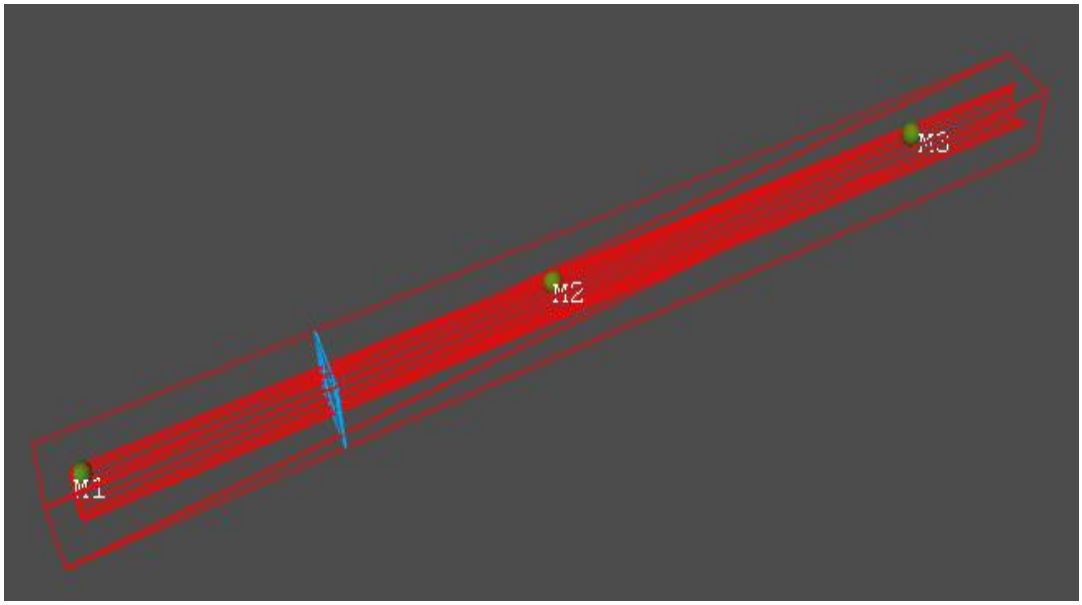

Figure 8.1 Gas explosion geometry used in FLACS simulations showing an obstacle and the monitor points M1-M3.

Due to the narrowness of the present tube and the thin nature of the obstacle, a grid resolution of 25 mm seemed to be essential to resolve the involved mechanisms suitably. As a result of the connection between the propagating reaction zone and the flow equations in the model, it is not continually promising to refine the mesh until a grid independent solution is established. For resolutions close to or below 10 mm, the thickened flame may lead to severe grid dependency (Pedersen *et al.* 2013).

8.3 FLACS Post-processor

8.3.1 Single and Double Obstacle

The comparison between modelled overpressure-time profile and that of experiment for a single 0.3 BR obstacle with 1-hole is shown in Fig. 8.2. It should be noted that the time at which the flame hit the obstacle in the experimental result was normalized with that of the FLACS model. In the CFD model, the overpressure was nearly constant upon ignition until the flame approached the obstacle at about 18 ms. Thereafter, a sudden rise in overpressure transpired leading to a maximum value of 1.4 bar at 43 ms. Subsequent decrease in overpressure followed after attaining the maximum value. In case of the experimental, an increment in overpressure occurred since from the ignition of the fuel to air mixtures until the propagating flame reached

the obstacle. A higher overpressure attaining a peak value of about 1.1 bar was experienced downstream of the obstacles.

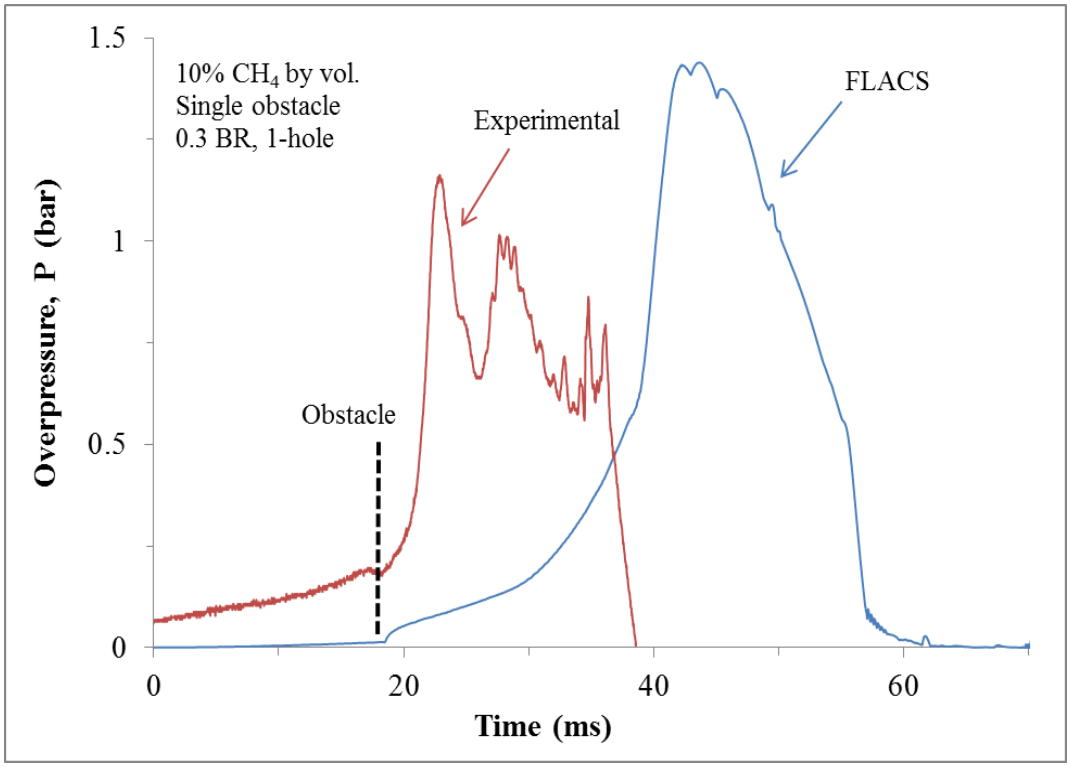

Figure 8.2 Comparison of overpressures between experimental and FLACS for single obstacle 0.3 BR with 10% CH_4-air mixtures.

The discrepancies between the two scenarios could be due to the fact that it is expected FLACS will give conservative overpressures when a grid resolution of 2.5 cm is used in a small geometry such as this. As such, the pipe will not have the same efficient cross-section as the real pipe, since the code imposes a Cartesian grid on a circular pipe. The grid resolution of the orifice obstacle should also ideally be higher. This might explain some of the discrepancies.

In addition, the obstacle (3.2 mm thick) was not resolved with a sufficient number of grid cells according to FLACS guidelines (dominant obstructions should not be resolved with one grid cell as this may not give the expected turbulence contribution), so the subsequent turbulence build-up might be slow compared to the experiment. The turbulence production in the narrow pipe will not represent that of the experiment, as the sub-grid models will dominate (circular pipe on Cartesian grid). The sub-grid models in FLACS will not be able to give the exact results for such a small geometry. They will be conservative with the default settings applied.

For the careful analysis performed, it is ideally expected to apply a finer grid resolution than the one in use. However, finer resolution would lead to even more conservative results. The conservative trend observed when the grid is refined to a resolution of 1-2 cm in FLACS is a known artefact of the combustion sub-model. Notwithstanding, the agreement between FLACS and the experimental results (based on the magnitude of overpressure only and not time) in general was good. Usually, a good result from a model lies within a factor of two from the experiment.

Figure 8.3 shows a plot of an overpressure-time profile for double obstacle tests of 0.3 BR and 1.75 m apart from both the experimental and FLACS works. Similar to the single obstacle tests, the upstream pressure-time curve was shifted to match the time of the model where the first obstacle was hit by the flame. The FLACS result attained its maximum overpressure of 4.1 bar downstream of the second obstacle. This maximum value was a factor of one and a half higher than that of the experiment. The apparent mismatch between the two setups was as a result of the reasons given to that noticed with single obstacle.

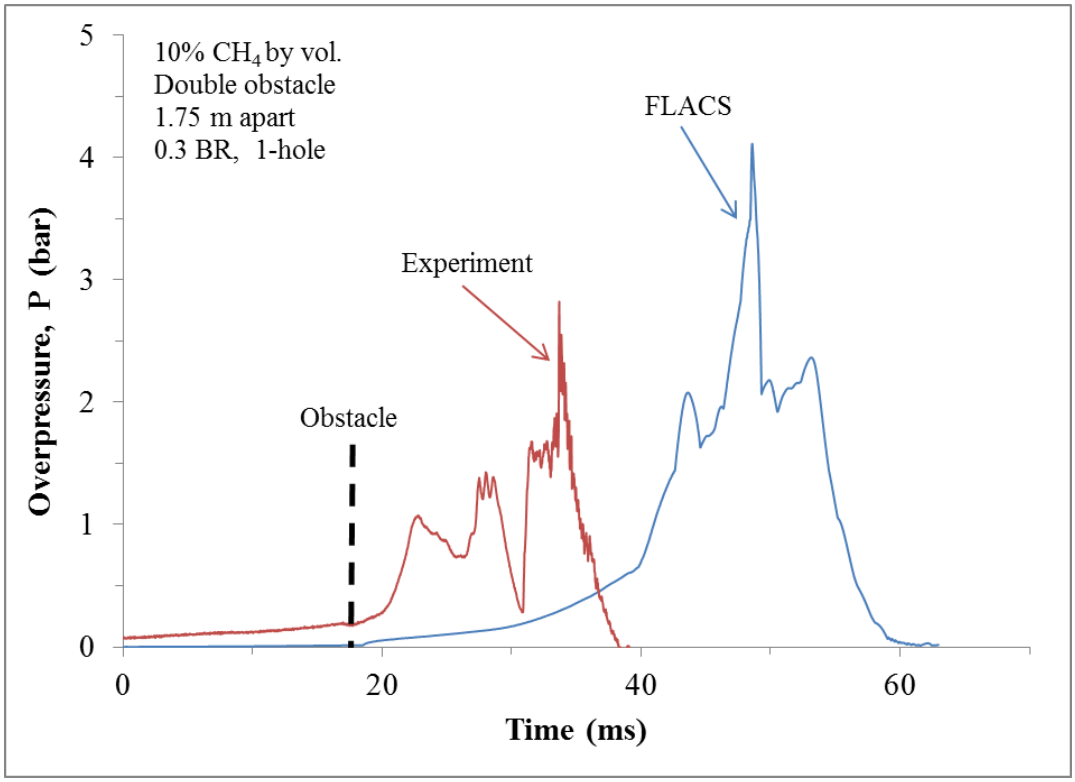

Figure 8.3 Comparison of overpressures between experimental and FLACS for double obstacle (0.3 BR each) 1.75 m apart with 10% CH_4-air mixtures.

8.3.2 Evidence of the Obstacle Separation Distance

The experimental evidence on the influence of obstacle separation distance was shown in Chapter 5.1.3 to have effects on explosions severity. This influence of obstacle spacing was explored using FLACS simulations and the maximum overpressures obtained were compared with that of the experimental results as shown in Fig. 8.4.

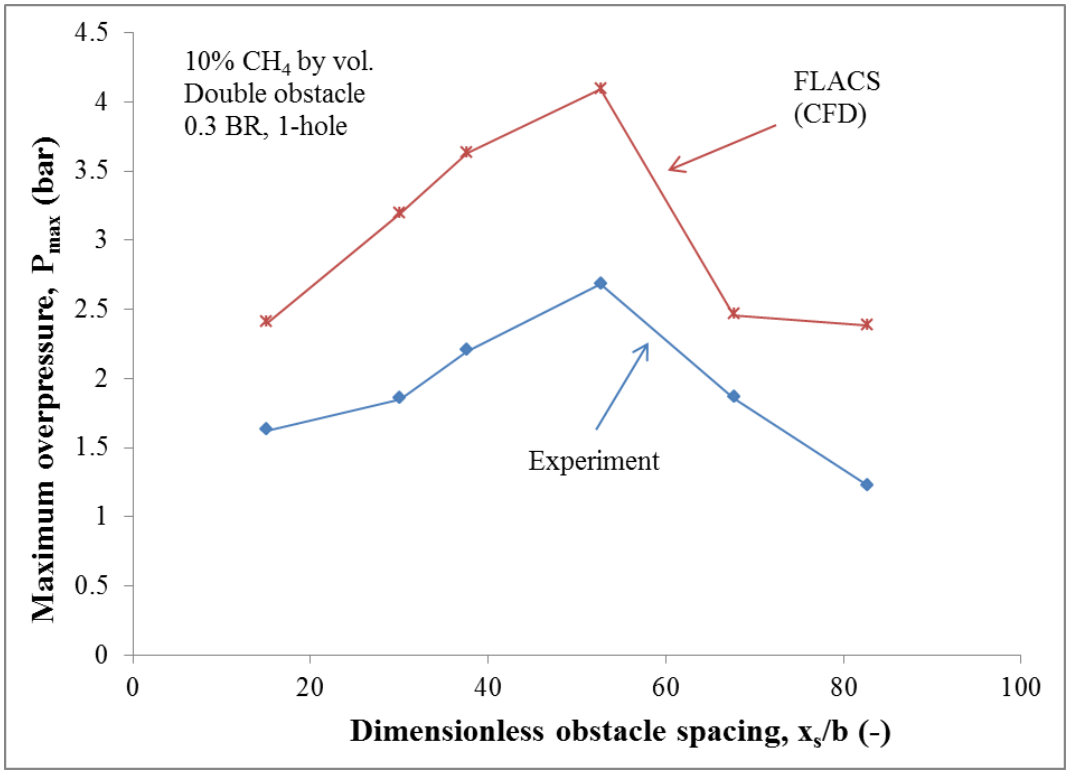

Figure 8.4 Experimental and FLACS overpressure profiles against obstacle separation distance.

Similar overpressure profiles were obtained in both scenarios, the profiles correspond to that of cold flow turbulence intensity behind a grid in the literature. The position to worst case obstacle spacing (1.75 m, about 53 obstacle scale, b) was also the same. However, the magnitude of the overpressure was higher in the FLACS simulation by a factor of about 1.5 when compared to the experimental work. This deviation in overpressure is within an acceptable range of a factor of two which is basically considered in validating FLACS with the experiments.

This work shows the influence of obstacle separation distance in gas explosions using a CFD tool, FLACS. The model agreed with the experimental work well. Therefore this suggests that FLACS can be used to study the influence of obstacle

pitch on gas explosions. This is in order to improve flexibility in gas explosions in terms of cost and time and wider options of analyzing other parameters (e.g. turbulent kinetic energy) that cannot be quantified in the experiments.

Figure 8.5 shows a 2D plot of maximum overpressure for single (a) and double obstacle for closely (b), optimum (c) and widely (d) spaced obstacles. Also, the time at which the maximum overpressure occurred were indicated in the plot (a-d).

For the single obstacle tests, (a), a maximum overpressure of close to 1.4 bar was achieved in 44 ms. This maximum value occurred at about 1.8 m downstream of the obstacle. This downstream position nearly equalled that of the optimum spacing established in the experiment where the maximum explosion severity was experienced. Afterwards, the magnitude of the overpressure started diminishing as a result of turbulence decay until it reached zero value at the end of the tube. Throughout the propagation of the flame in the tube, the overpressure was noticed to be changing with positions and this is as a result of the compressibility nature of the flow. This change was equally observed with the double obstacle configurations, (b-d).

In case of closely spaced obstacles, (b), a maximum overpressure and its corresponding time experienced downstream of the second obstacle was slightly above 2 bar and 45 ms respectively. Also, the positions to peak overpressure downstream of the second obstacle and the overpressure upstream were similar to the position (1.8 m) and value (1.4 bar) respectively for the single obstacle test.

Maximum explosion severity in terms of overpressure (about 4.1 bar) was realised when the obstacles were spaced optimally i.e. 1.75 m as shown in (c). This maximum overpressure value was attained downstream of the second obstacle at 50 ms and it nearly doubled that of 0.5 m obstacle spacing test, (b). At optimum spacing, the flame accelerated to its maximum value after the first obstacle before reaching the second. Therefore the highest possible flows were induced by the accelerating flame through the second obstacle and this would have resulted in the highest turbulence levels after the second and hence to highest overpressures. However, it is discernible that the overpressure generated downstream of the second obstacles was not fully developed due to short tube length which was lesser than the

optimum spacing. It was previously shown in Chapter 5.2.2 that the optimum spacing does not change with number of obstacles.

The widely spaced obstacle test (d) had it maximum overpressure of over 2 bar downstream of the first obstacle at about 47 ms. The non-influence of the second obstacle on the explosion overpressure is attributed to the large separation distance between the two obstacles. The turbulence intensity attained its maximum value after the first obstacle and subsequently decayed prior to reaching the second. Therefore the lower possible flows were induced by the accelerating flame through the second obstacle and coupling with the shorter tube length downstream of the second obstacle (0.75 m) would have resulted in the lower turbulence levels after the obstacle and hence lower overpressures.

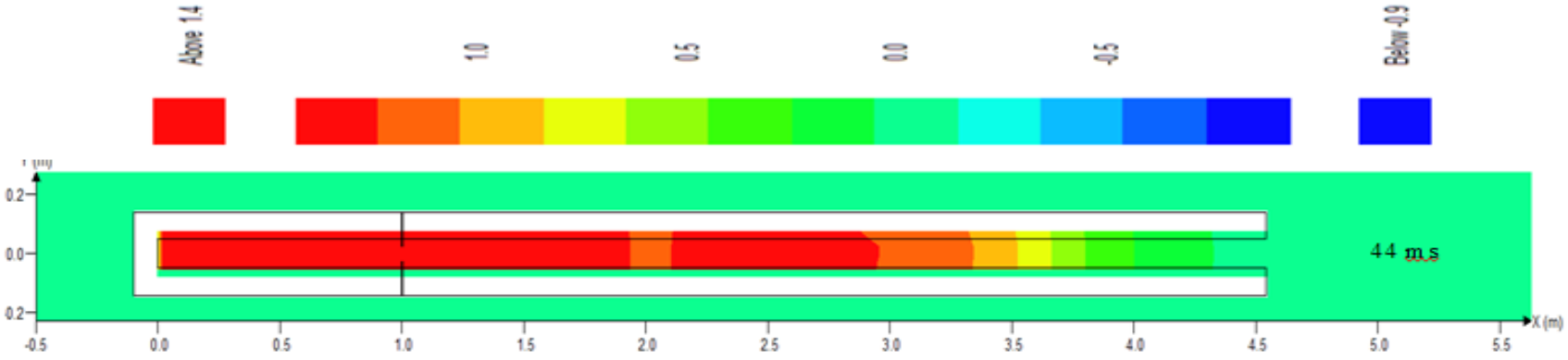
Above 1.4
1.0
0.5
0.0
-0.5
Below -0.9
44 m.s
X (m)

(a)

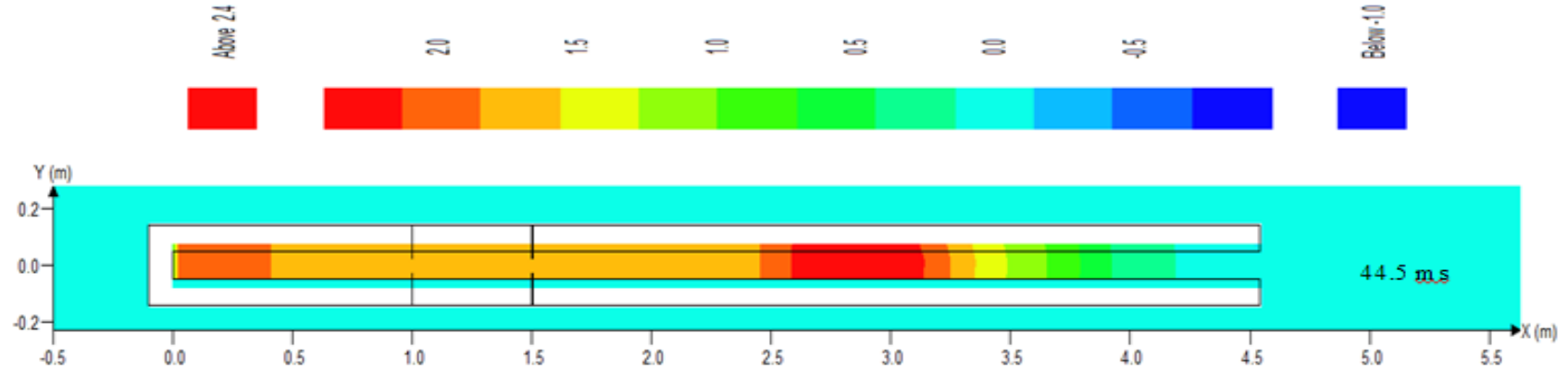
Above 2.4
2.0
1.5
1.0
0.5
0.0
-0.5
Below -1.0
Y (m)
44.5 m.s
X (m)

(b)

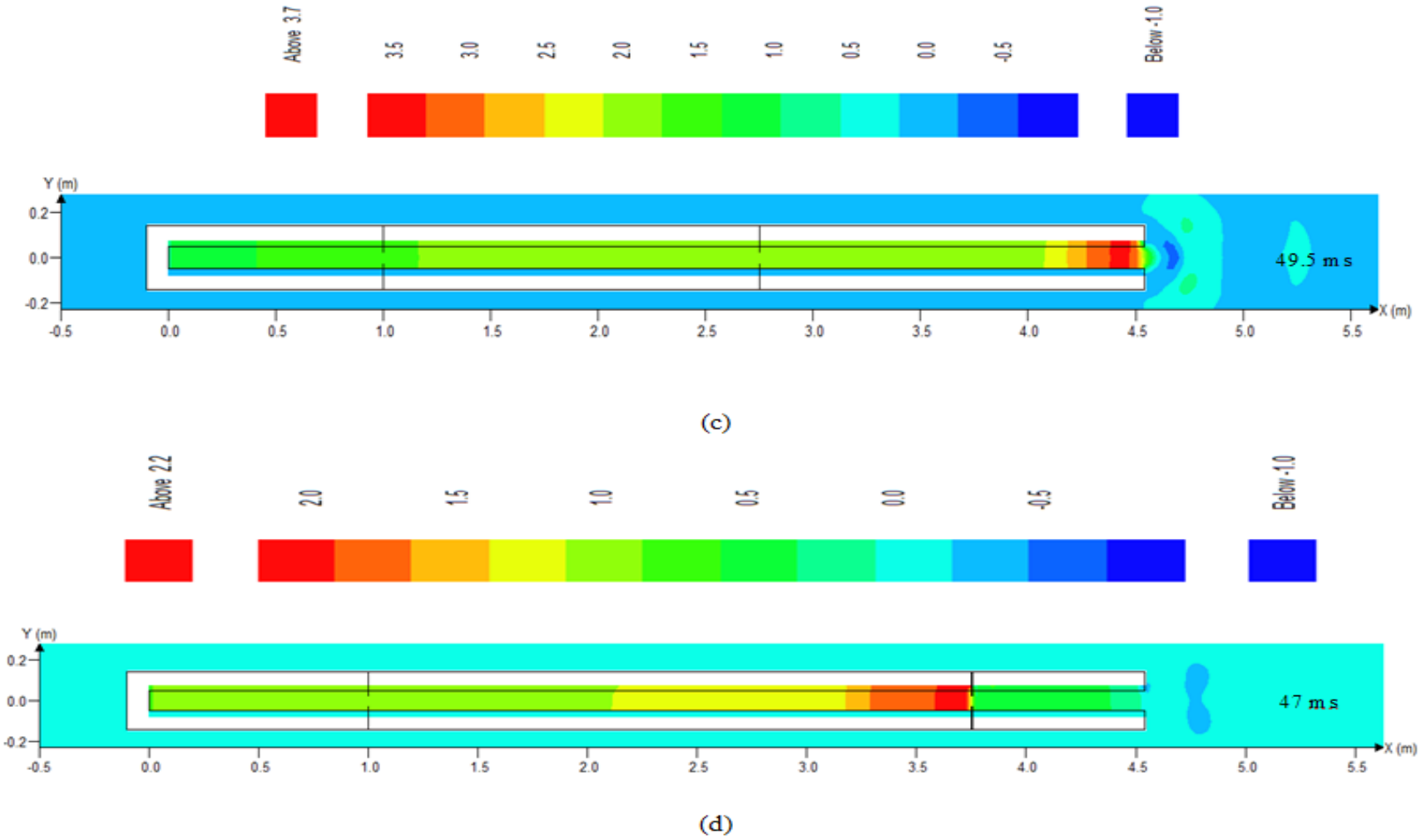

Figure 8.5 2D plots of explosions overpressure for single (a) and double obstacle separated at different spacing (b-d).

Equally, the influence of tube length downstream of the second obstacle on pressure development from the experimental work is shown in Fig. 8.6. It is a plot of the explosion tube length against the obstacle separation distance all dimensionalised by obstacle scale, b. The time to maximum overpressure was obtained from the pressure-time profile whereas its corresponding position was taken from the flame position -time traces given by thermocouple records. For single and the entire first obstacle (for double obstacle) tests positioned at one meter from spark, the distance to maximum overpressure downstream was nearly similar. However, the reverse was the case for the second obstacle in the double obstacle configuration tests due to the influence of spacing. The distance to the maximum overpressure increased with decrease in obstacle spacing. This experimental analysis clearly showed that the widely spaced obstacles tests (2.25 m and 2.75 m) had not fully attained their maximum explosion severities downstream of the second obstacle due to short tube length.

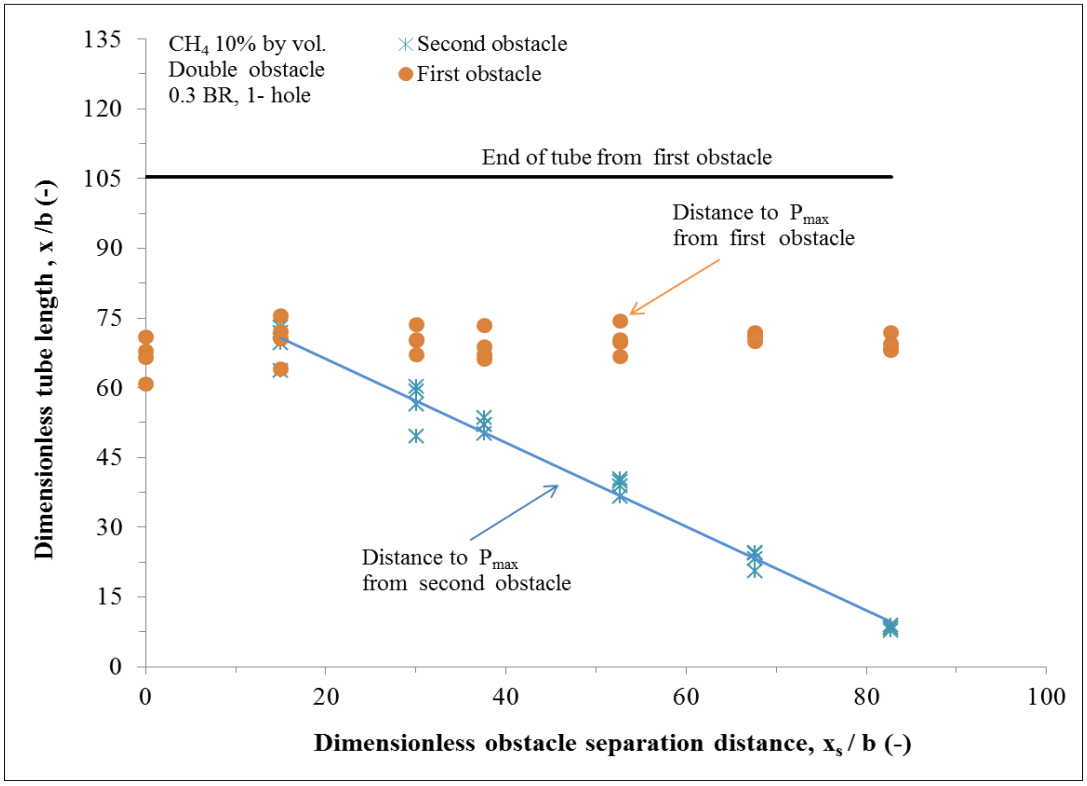

Figure 8.6 Positions to maximum overpressures from first and second obstacles in relations to dimensionless tube length and obstacle separation distance.

8.4 Summary of the Main Findings

This work shows the influence of obstacle separation distance in gas explosions using a CFD tool, FLACS. The current experimental work validated the FLACS model fairly well (based on the magnitude of explosion overpressure only). Therefore this suggests that FLACS can be used to study the influence of obstacle pitch on gas explosions.

Chapter 9
Conclusions and Recommendations for Future Work

9.1 Conclusions

The turbulence intensity and its spatial distribution downstream of the obstacle are the responsible factors of the severity of the explosion and speed of flame acceleration. However, most measurements in obstacle induced turbulent flow fields have been made far behind the obstacle, in the turbulent decay region. This is well away from the region of concern in the explosion hazards field since the maximum combustion rate generally takes place within a distance of 3 to 20 obstacle-hole diameters after the obstacle. Scarce measurements of the turbulence intensity, $(u'/U)_{max}$ in the region immediately downstream of the grid were related with the grid blockage ratios with the data separated into thin/sharp and thick/round geometries. In both cases, the intensity of turbulence was found to be strongly dependent on the blockage ratio. The correlations obtained from this relationship are given as,

$$(u'/U)_{max} = 0.042e^{4.22BR} \quad \text{for } t/d < 0.6 \text{ (thin/sharp obstacles)} \tag{9.1}$$

$$(u'/U)_{max} = 0.018e^{3.90BR} \quad \text{for } t/d > 1 \text{ (thick/round obstacles)} \tag{9.2}$$

The position to maximum intensity of turbulence, x_{max} non-dimensionalised with obstacle scale, b as a function of obstacle blockage was correlated using steady state experiments from the limited available data in the literature as,

$$(x/b)_{max} = 2.77BR^{-1.55} \quad \text{for } t/d < 0.6 \text{ (thin/sharp obstacles)} \tag{9.3}$$

$$(x/b)_{max} = 3.10BR^{-2.40} \quad \text{for } t/d > 1 \text{ (thick/round obstacles)} \tag{9.4}$$

Unlike the maximum intensity of turbulence, the dimensionless position $(x/b)_{max}$ increased with decrease in obstacle blockage. The above correlation (Eq. 9.3) was used as a guide in the present research to predict the worst case obstacle spacing leading to maximum flame speeds and overpressures. The correlation was found to

agree with the free jet theory which suggested that the maximum intensity of turbulence would occur after the completion of the length of the potential core (expressed normally as 4-5 jet diameters).

It was shown in Chapter 2 that either too large or too small separation distance between the obstacles would lead to lower maximum intensity of turbulence and hence lower explosion severity. Sustained flame acceleration could not be attained for large pitch due to decay of turbulence in between obstacles while for small pitch the pocket of unburned gas between the obstacles would be too small to allow for the flame to accelerate before reaching the next obstacle. In compliance with the ATEX directive (ATEX 1994), the worst case scenarios need to be used in assessing the severity of the hazard posed by gas explosions in process plant. Therefore an optimum obstacle spacing corresponding to maximum explosion overpressure should be used in the general assessment of these phenomena.

In Chapter 3 a critical review of gas explosions studies with repeat of obstacles mostly used in formulating safety guidelines and standards was carried out and split into studies with fixed obstacle spacing and studies with variable spacing. In both cases, the bulk of spacing between the obstacles was close as it was not more than 10 obstacle scales. This is not within the range of characteristic obstacle scales downstream of the grid where the maximum combustion rate usually occurs as given by Phylaktou and Andrews (1991). Also, the justification of the obstacle spacing was not given by most of the researchers.

The results from an extensive experimental study of the effects of obstacles and the separation distance were presented in Chapter 5. The manifestations of the obstacle separation distance were recognized to be mainly increase in flame speeds and maximum overpressures. These parameters were obtained over a broad range of experimental set-ups and conditions.

Preliminary investigation of the pressure records indicated that limited venting was taking place at the tube exit, at the time of maximum burning rate caused by obstacle enhanced explosions. This suggested that the mechanism of pressure generation in the present tests is the same as that of vapour-cloud explosions, i.e. the pressure rise was due mainly to the inertia of the gas immediately ahead of the flame, and that it was not significantly influenced by the confinement offered by the tubular geometry.

Subsequent comparison of experimental overpressure and that predicted by simple acoustic theory gave support for these experimental findings.

A significant increase in overpressures and flame speeds was obtained in the two obstacle configuration compared to the no obstacle and single obstacle situations. A strong increase in explosion overpressures and flame speeds was noticed with increase in number of obstacles up to three for 2 and 4-flat-bars and baffle disc obstacles spaced at established optimum obstacle separation distance.

The importance of the obstacle separation distance in a double obstacle configuration study was that there is a defined separation distance which gave the most severe explosions in terms of both maximum flame speed and overpressure. This trend was obtained for obstacles of different blockage ratio, shapes, number, scale and different mixture reactivities. The profile of effects with separation distance in the present research agreed with the cold flow turbulence profile determined in cold flows by other researchers. However, in the present results the maximum effect in explosions is experienced further downstream than the position of maximum turbulence determined in the cold flow studies. It is suggested that this may be due to the convection of the turbulence profile by the propagating flame. The predicted equation (Eq. 9.3) on position to maximum intensity of turbulence from cold flow data agreed with the worst case obstacle separation distance in the current research, if multiplied by a factor of three.

An increase in obstacle BR resulted in increasing maximum overpressure and flame speeds for both single and double obstacles. The worst case obstacle spacing leading to maximum overpressures and flame speeds decreased with increasing obstacle blockage ratio. However, for a fixed obstacle blockage ratio, both the severity of explosions and worst case obstacle spacing increased with obstacle scale (number of flat-bars /holes).

It was evident that the obstacle spacing from the literature is quite closer when compared to the present work. It can now be deduced that high congestion in a given medium does not necessarily imply maximum explosion severity as traditionally assumed. Less congested but optimally separated obstructions could lead to higher overpressures.

For three obstacle tests, the optimum spacing between the second and third obstacles corresponded to the same optimum spacing found for the first two obstacles demonstrating that the optimum separation distance does not change with number of obstacles nor the severity of the explosion, but it does change with obstacle scale.

Turbulence parameters were estimated from pressure differential measurements and geometrical obstacle dimensions. This enabled the calculation of the explosions induced gas velocities, r.m.s turbulent velocity, turbulent Reynolds number and Karlovitz number. A complete turbulence profile similar to that of overpressure and flame speeds profiles was formed with all the turbulent combustion parameters predicted in this research as a function of the obstacle separation distance. By expressing these parameters in terms of turbulent combustion regimes, the bulk of the tests in this study was shown to be within the thickened-wrinkled flames regime.

A strong dependence of Ka on maximum overpressure for 10% CH_4 mixtures was found. The single obstacle tests have a Ka of well below unity and this shows no sign of flame quenching. However, Ka value of greater than unity and up to a value of six was realised with the double obstacle tests. Theoretically, Ka above unity indicates global flame extinction however, the entire flame quench was not observed in any of the present tests. In all cases the explosion propagated strongly, leading to significant overpressures. The values of Ka in this study would therefore suggest a measure of the prevailing flame straining conditions downstream of an obstacle, as opposed to an indication of flame extinction.

Turbulent burning velocity models with dependence on obstacle scale, ℓ was derived from the experimental results of the double obstacle tests with different obstacle spacing and 10% CH_4 –air mixtures by volume. The equations of the fitted curves for the single-hole and single flat-bar obstacles respectively had the form of,

$$\frac{S_T}{S_L} = 2.99 R_\ell^{0.36} \qquad \text{for single-hole obstacles} \qquad (9.5)$$

$$\frac{S_T}{S_L} = 7.36 R_\ell^{0.27} \qquad \text{for single-flat-bar obstacles} \qquad (9.6)$$

The dependence on scale, ℓ as indicated by the R_ℓ exponent in both Eqs. 9.5 and 9.6, was higher than that of turbulent combustion models that have been applied to the

scaling of gas explosions. These combustion models are from Bradley *et al.* (1992) with ℓ exponent of 0.15 and Gouldin (1987) with ℓ exponent of 0.26. It was demonstrated that though the variance in the dependency on scale designated by the different models is trivial in absolute terms, the resultant estimates in gas explosions scaling, mostly of overpressure, are considerably different and could make a difference between safe and unsafe design.

From the newly obtained S_T correlations for single-flat-bar obstacles (Eq. 9.6), an equation with explicit dependence of the blast overpressure on the geometric configuration, pressure loss characteristics (effectively the blockage ratio of the obstacles) and mixture properties was derived as,

$$P \propto \left[\left(C_T\sqrt{K}\right)^{0.54}\ell^{0.54}\right]\left[E^{2.54}S_L^{2.54}v^{-0.54}\right] \tag{9.7}$$

The overpressure equation was validated against the limited suitable experimental data from both small and large scales and different fuel mixtures and showed a good agreement.

The influence of obstacle separation distance in gas explosions was studied using a CFD tool, FLACS. The present experimental work validated the FLACS model well based on the magnitude of explosion overpressure only. Therefore this suggests that FLACS can be used to study the influence of obstacle spacing on gas explosions. This is in order to improve flexibility in gas explosions in terms of cost and time and wider options of analyzing some parameters like turbulent kinetic energy that cannot be quantified in the experiments.

9.2 Recommendations for Future Work

In the current research, there were a number of assumptions and generalisations in analysing the experimental data and that necessitate more investigation and more careful consideration. The following suggestions for future work based on the present study are:

- To source for more data from steady state flows measuring the intensity of turbulence immediately downstream of the obstacles where the maximum

turbulence intensity and hence overpressures occur. This is particularly for thick/round grid plates and baffle plate obstacles.

- To look into the influence of Karlovitz, Lewis and Markstein numbers, as these influence the turbulent burning velocities for the same turbulence levels. It was shown in Chapter 5 that fuels of different types but similar burning velocities can produce similar maximum overpressure. However, the current work also showed that the worst case obstacle separation distance changes with fuel concentration and type.
- In the present experimental set up there is a need to increase the length of the tube downstream of the last obstacle by ensuring that at least the distance to optimum spacing for such obstacle is attained. This would lead to achieving the maximum intensity of turbulence and hence overpressures and flame speeds. In the present study, it was shown in Chapter 8 that full effects of the second obstacle of 0.3 BR 1-hole at worst case spacing (1.75 m) would not have been reached due to the short length of the tube (approximately 1.5 m) downstream of the obstacle.
- To provide shorter pipe sections than the existing ones used in this research. This would facilitate the study of the influence of obstacle spacing on smaller scale obstacles.
- To apply the correlation of distance to maximum intensity of turbulence (Eq. 2.23) on obstacles that are arranged in a non-serial layout e.g. staggered arrangement.
- To further validate the overpressure scaling model with comprehensive experimental data from large scale explosions as typically found in industry.

9.3 Final Remarks

In planning the layout of new installations, it is appropriate to identify the relevant worst case obstacle separation in order to avoid it. In assessing the risk to existing installations and taking appropriate mitigation measures it is important to evaluate such risk on the basis of a clear understanding of the effects of separation distance and congestion. The present results would suggest that in many previous studies of repeated obstacles the separation distance investigated might not have included the worst case set up, and therefore existing explosion protection guidelines may not correspond to worst case scenarios.

It is suggested that the various new correlations obtained from this research be subjected to further rigorous validation prior to been applied as design tools. Finally, it is expected that this research has contributed positively to the field of explosion prediction and mitigation.

References

ABDEL-GAYED, R. G., K. J. AL-KHISHALI and D. BRADLEY. 1984. Turbulent Burning Velocities and Flame Straining in Explosions. *Proceedings of the Royal Society of London. A. Mathematical and Physical Sciences,* **391**(1801), pp.393-414.

ABDEL-GAYED, R. G. and D. BRADLEY. 1981. A Two-Eddy Theory of Premixed Turbulent Flame Propagation. *Proc R Soc Lond, A,* **301**(1).

ABDEL-GAYED, R. G. and D. BRADLEY. 1982. *The influence of turbulence upon the rate of turbulent burning, In Fuel Air Explosions. (J. Lee, C.M. Guirao and D.E. Grierson, Eds.),* [manuscript]. *At:* University of Waterloo Press, Montreal, p.51.

ABDEL-GAYED, R. G. and D. BRADLEY. 1985. Criteria for turbulent propagation limits of premixed flames. *Combustion and Flame,* **62**(1), pp.61-68.

ABDEL-GAYED, R. G., D. BRADLEY, M. N. HAMID and M. LAWES. 1985. Lewis number effects on turbulent burning velocity. *Symposium (International) on Combustion,* **20**(1), pp.505-512.

ABDEL-GAYED, R. G., D. BRADLEY and M. LAWES. 1987. Turbulent Burning Velocities: A General Correlation in Terms of Straining Rates. *Proceedings of the Royal Society of London, Series A: Mathematical, Physical and Engineering Sciences,* **414**(1847), pp.389-413

AL-DABBAGH, N. A. and G. E. ANDREWS. 1984. *Combust. Flame,* **55**(33).

ALEKSEEV, V. I., M. S. KUZNETSOV, Y. G. YANKIN and S. B. DOROFEEV. 2001. Experimental study of flame acceleration and the deflagration-to-detonation transition under conditions of transverse venting. *Journal of Loss Prevention in the Process Industries,* **14**(6), pp.591-596.

ANDREWS, G. E. 2011. *Explosion prediction and mitigation lecture note (CPD)* [manuscript]. *At:* University of Leeds.

ANDREWS, G. E. and D. BRADLEY. 1972. The burning velocity of methane-air mixtures. *Combustion and Flame,* **19**(2), pp.275-288.

ANDREWS, G. E. and D. BRADLEY. 1973. Determination of burning velocity by double ignition in a closed vessel. *Combustion and Flame,* **20**(1), pp.77-89.

ANDREWS, G. E., D. BRADLEY and S. B. LWAKABAMBA. 1975. Turbulence and turbulent flame propagation—A critical appraisal. *Combustion and Flame,* **24**(0), pp.285-304.

ARIA. 2006. *Explosion followed by fire in a hydrocarbon tank farm : Saint Herblain, France* [online]. [Accessed 5 July 2013]. Available from: http://www.aria.developpement-durable.gouv.fr/ressources/2914_st_herblain_sj_ang.pdf.

ARNTZEN, B. J. 1998. *Modelling of turbulence and combustion for simulation of gas explosions in complex geometries*. PhD thesis, The Norwegian University of Science and Technology.

ATEX. 1994. *ATEX (Explosive Atmosphere) Directives 94/9/EC*. European Commission.

AUNG, K. T., M. I. HASSAN and G. M. FAETH. 1997. Flame stretch interactions of laminar premixed hydrogen/air flames at normal temperature and pressure. *Combustion and Flame,* **109**(1–2), pp.1-24.

BAINES, W. D. and E. G. PETERSON. 1951. An investigation of flow through screens. *Trans. American Society of Mechanical Engineering,* **73**, p167.

BAKKER, A. 2006. *Lecture 3 on Conservation Equations: Applied Computational Fluid Dynamics* [online]. [Accessed 19 Sept. 2012]. Available from: http://www.bakker.org/dartmouth06/engs150/10-rans.pdf.

BALLAL, D. R. and A. H. LEFEBVRE. 1975. The Structure and Propagation of Turbulent Flames. *Proceedings of the Royal Society of London. A. Mathematical and Physical Sciences,* **344**(1637), pp.217-234.

BAUWENS, C. R., J. CHAO and S. B. DOROFEEV. 2012. Effect of hydrogen concentration on vented explosion overpressures from lean hydrogen–air deflagrations. *International Journal of Hydrogen Energy,* **37**(22), pp.17599-17605.

BEARMAN, P. W. and T. MOREL. 1983. Effect of free stream turbulence on the flow around bluff bodies. *Progress in Aerospace Sciences,* **20**(2–3), pp.97-123.

BEAUVAIS, R., F. MAYINGER and G. STRUBE. 1993. Severe Accident in a light water reactor: Influence of elevated initial temperature on hydrogen combustion. *ASME/JSME Nuclear Engineering Conference*, **1**, pp.425-433.

BEER, J. M. and N. A. CHIGIER. eds. 1983. *Combustion aerodynamics.* Essex, UK: Applied science publishers.

BIMSON, S. J., D. C. BULL, T. M. CRESSWELL, P. R. MARKS, A. P. MASTERS, A. PROTHERO, J. S. PUTTOCK and B. SAMUELS. 1993. An experimental study of the physics of gaseous deflagration in a very large vented enclosure. *In: International Colloquium on the Dynamics of Explosions and Reactive Systems, Coimbra, Portugal*.

BJERKETVEDT, D., J. R. BAKKE and K. VAN WINGERDEN. 1997. Gas explosion handbook. *Journal of Hazardous Materials*, **52**(1), pp.1-150.

BJORKHAUG, M. 1986. *Flame acceleration in obstructed radial geometries*. PhD thesis, City University London.

BOC EDWARDS. 2013. *Model 600 Barocel Absolute Vacuum/Pressure Transducer*. [Accessed 17 July 2013]. Available from: http://saba.kntu.ac.ir/eecd/Ecourses/instrumentation/projects/reports/Poly%20Vaccum/BEdwards/Barocel_600.pdf.

BOECK, L. R., J. HASSLBERGER, F. ETTNER and T. SATTELMAYER. 2013. Investigation of Peak Pressures during Explosive Combustion of Inhomogeneous Hydrogen-Air Mixtures. *In: Proc. of the Seventh International Seminar on Fire & Explosion Hazards (ISFEH7)*, Providence, Rhodes Island. Research Publishing, pp. 959–965.

BORGHI, R. 1988. Turbulent combustion modelling. *Progress in Energy and Combustion Science*, **14**(4), pp.245-292.

BORGHI, R. and M. DESTRIAU. eds. 1998. *Combustion and flames, chemical and physical principles.* Paris: Editions Technip.

BP. 2010. *Deepwater Horizon accident and response*. [Accessed 28 July 2013]. Available from: http://www.bp.com/en/global/corporate/gulf-of-mexico-restoration/deepwater-horizon-accident-and-response.html.

BRADBURY, L. J. S. 1976. Measurements with a pulsed-wire and a hot-wire anemometer in the highly turbulent wake of a normal flat plate. *Journal of Fluid Mechanics*, **77**(03), pp.473-497.

BRADLEY, D., A. K. C. LAU and M. LAWES. 1992. Flame Stretch Rate as a Determinant of Turbulent Burning Velocity. *Philosophical Transactions of the Royal Society of London. Series A: Physical and Engineering Sciences,* **338**(1650), pp.359-387.

BRADLEY, D., M. LAWES and M. S. MANSOUR. 2011. Measurement of turbulent burning velocities in implosions at high pressures. *Proceedings of the Combustion Institute,* **33**(1), pp.1269-1275.

BRAY, K. N. C. 1990. Studies of the Turbulent Burning Velocity. *Proceedings of the Royal Society of London. Series A: Mathematical and Physical Sciences,* **431**(1882), pp.315-335.

BS5167-2. 2003. *Measurement of fluid flow by means of pressure differential devices inserted in circular cross-section conduits running full - Part 2: Orifice plates (ISO 5167-2:2003).* Brussels: European Committee for Standardization.

BUFFAM, J., K. COX and H. SCHIESS. 2008. *Measurement of Laminar Burning Velocity of Methane-Air Mixtures Using a Slot and Bunsen Burner*. BSc thesis, Worchester Polytechnic Institute.

CAROL, S., J. A. VILCHEZ and J. CASAL. 2002. Study of the severity of industrial accidents with hazardous substances by historical analysis. *Journal of Loss Prevention in the Process Industries,* **15**(6), pp.517-524.

CATES, A. and B. SAMUELS. 1991. A simple assessment methodology for vented explosions. *Journal of Loss Prevention in the Process Industries,* **4**(5), pp.287-296.

CATLIN, C. A. and D. M. JOHNSON. 1992. Experimental scaling of the flame acceleration phase of an explosion by changing fuel gas reactivity. *Combustion and Flame,* **88**(1), pp.15-27.

CENGEL, Y. A. and J. M. CIMBALA. eds. 2010. *Fluid Mechanics: Fundamentals and Applications.* Second ed. New York: McGraw-Hill.

CHAN, C., I. O. MOEN and J. H. S. LEE. 1983. Influence of confinement on flame acceleration due to repeated obstacles. *Combustion and Flame,* **49**(1–3), pp.27-39.

CHAN, C. K. and W. A. DEWIT. 1996. Deflagration-to-detonation transition in end gases. *Symposium (International) on Combustion,* **26**(2), pp.2679-2684.

CHAN, C. K. and D. R. GREIG. 1989. The structures of fast deflagrations and quasi-detonations. *Symposium (International) on Combustion,* **22**(1), pp.1733-1739.

CHAPMAN, W. R. and R. V. WHEELER. 1926. The propagation of flame in mixtures of methane and air. Part IV. The effect of restrictions in the path of the flame. *Journal of the Chemical Society (Resumed),* pp.2139-2147.

CHECKEL, M. D. 1981. *Turbulence enhanced combustion of lean mixtures*. PhD thesis, University of Cambridge.

CHUN, K. B. and H. J. SUNG. 1996. Control of turbulent separated flow over a backward-facing step by local forcing. *Experiments in Fluids,* **21**(6), pp.417-426.

CICCARELLI, G., C. J. FOWLER and M. BARDON. 2005. Effect of obstacle size and spacing on the initial stage of flame acceleration in a rough tube. *Shock Waves,* **14**(3), pp.161-166.

CLANCEY, V. J. 1975. The phenomenology of vapour cloud explosions in free space. *In: Europ. Symp. Comb., French Section, Comb. Inst.,* Paris. p.p.238.

CLARKE, A. 2002. Calculation and Consideration of the Lewis Number for Explosion Studies. *Process Safety and Environmental Protection,* **80**(3), pp.135-140.

COMTE-BELLOT, G., EACUTE, VE and S. CORRSIN. 1966. The use of a contraction to improve the isotropy of grid-generated turbulence. *Journal of Fluid Mechanics,* **25**(04), pp.657-682.

CSB. 2007. *Investigation report: refinery explosion and fire report number 2005-04-I-TX*. [Accessed 15 June 2013]. Available from: http://www.csb.gov/assets/1/19/CSBFinalReportBP.pdf.

CSB. 2010. *US Chemical Safety and Hazard Investigation Board: Urgent Recommendations*. [Accessed 12 July 2013]. Available from: http://www.csb.gov/assets/1/19/KleenUrgentRec.pdf.

DANIELE, S. and P. JANSOHN. 2012. Correlations for turbulent flame speed of different syngas mixtures at high pressure and temperature. *In: Proceedings of ASME Turbo Expo,* Copenhagen. pp.1-7.

DEOTTE JR, R. E., G. L. MORRISON, D. L. PANAK and G. H. NAIL. 1991. 3-D laser Doppler anemometry measurements of the axisymmetric flow field

near an orifice plate. *Flow Measurement and Instrumentation,* **2**(2), pp.115-123.

DONG, C., M. BI and Y. ZHOU. 2012. Effects of obstacles and deposited coal dust on characteristics of premixed methane–air explosions in a long closed pipe. *Safety Science,* **50**(9), pp.1786-1791.

DOROFEEV, S. 2007. Thermal quenching and re-ignition of mixed pockets of reactants and products in gas explosions. *Proceedings of the Combustion Institute,* **31**(2), pp.2371-2379.

DOROFEEV, S. B. 2008. Flame Acceleration and Transition to Detonation: a Framework for Estimating Potential Explosion Hazards in Hydrogen Mixtures. *In: Third European Summer School on Hydrogen Safety,* Belfast.

DOROFEEV, S. B., V. P. SIDOROV, A. E. DVOINISHNIKOV and W. BREITUNG. 1996. Deflagration to detonation transition in large confined volume of lean hydrogen-air mixtures. *Combustion and Flame,* **104**(1–2), pp.95-110.

DRISCOLL, J. F. 2008. Turbulent premixed combustion: Flamelet structure and its effect on turbulent burning velocities. *Progress in Energy and Combustion Science,* **34**(1), pp.91-134.

DURÃO, D. F. G., M. FOUNTI and J. H. WHITELAW. 1979. Velocity characteristics of three-dimensional disc-stabilised diffusion flames. *Letters in Heat and Mass Transfer,* **6**(1), pp.1-12.

E-SCOTLAND. 2013. *Piper Alpha disaster*. [Accessed 10 May 2013]. Available from: http://www.educationscotland.gov.uk/scotlandshistory/20thand21stcenturies/piperalpha/index.asp.

ECKHOFF, R. K., K. FUHRE, C. M. GUIRAO and J. H. S. LEE. 1984. Venting of turbulent gas explosions in a 50 m3 chamber. *Fire Safety Journal,* **7**(2), pp.191-197.

ERM. 2010. LNG Explosion Levels One Square Mile (Cleveland 1944). [online]. Available from: http://www.ircrisk.com/blognet/post/2010/03/29/LNG-Explosion-Levels-One-Square-Mile-(Cleveland-1944).aspx.

ETHERIDGE, D. W. and P. H. KEMP. 1978. Measurements of turbulent flow downstream of a rearward-facing step. *Journal of Fluid Mechanics,* **86**(03), pp.545-566.

FILATYEV, S. A., J. F. DRISCOLL, C. D. CARTER and J. M. DONBAR. 2005. Measured properties of turbulent premixed flames for model assessment, including burning velocities, stretch rates, and surface densities. *Combustion and Flame,* **141**(1–2), pp.1-21.

FUJI, S., M. GOMI and K. EGUCHI. 1978. Cold flow tests of a bluff-body flame stabilizer. *Journal of Fluids Engineering,* **100**, pp.323-332.

GAMEZO, V. N., R. K. ZIPF, K. M. MOHAMED, E. S. ORAN and D. A. KESSLER. 2013. DDT Experiments with Natural Gas-Air Mixtures. *In: Proc. of the Seventh International Seminar on Fire & Explosion Hazards (ISFEH7),* 5-10 May, Providence, Rhodes Island. Research Publishing, pp.729-738.

GARDNER, C. L. 1998. *Turbulent combustion in obstacle-accelerated gas explosions – The influence of scale*. PhD thesis, University of Leeds.

GARDNER, C.L., H.N. PHYLAKTOU, and G.E. ANDREWS. 2001. Turbulent Explosion Scaling: An Assessment of Experimental Data. In: *Third International Seminar on Fire and Explosion Hazards,* Windermere, UK, pp. 665-676.

GEXCON. 2010. *FLACS v9.1 user's manual*. Bergen: CMR.

GOIX, P. J. and I. G. SHEPHERD. 1993. Lewis Number Effects on Turbulent Premixed Flame Structure. *Combustion science and technology*, **91**(4-6), pp.191-206.

GOULDIN, F. C. 1987. An application of fractals to modeling premixed turbulent flames. *Combustion and Flame*, **68**(3), pp.249-266.

GROTH, J. and A. V. JOHANSSON. 1988. Turbulence reduction by screens. *Journal of Fluid Mechanics,* **197**, pp.139-155.

HARRIS, R. J. 1983. *The investigation and control of gas explosions in buildings and heating plant.* London and New York: E. & F.N. Spon in association with the British Gas Corp.

HARRIS, R. J. and M. J. WICKENS. 1989. Understanding vapour cloud explosions-an experimental study. *In: 55th Autumn Meeting: The Institution of Gas Engineers,* Kensington Town Hall. The Institution of Gas Engineers

HARRISON, A. J. and J. A. EYRE. 1987. The Effect of Obstacle Arrays on the Combustion of Large Premixed Gas/Air Clouds. *Combustion science and technology,* **52**(1-3), pp.121-137.

HERATH, P. 1986. *Closed vessel explosions: the influence of baffles*. PhD thesis, University of Leeds.

HJERTAGER, B. H. 1984. Influence of turbulence on gas explosions. *Journal of Hazardous Materials,* **9**(3), pp.315-346.

HJERTAGER, B. H. 1993. *Gas explosions in obstructed vessels* [manuscript]. *At*, Short Course on Explosion Prediction and Mitigation, Deparment of Fuel and Energy, University of Leeds.

HJERTAGER, B. H., K. FUHRE and M. BJØRKHAUG. 1988a. Concentration Effects on Flame Acceleration by Obstacles in Large-Scale Methane-Air and Propane-Air Vented Explosions. *Combustion science and technology,* **62**(4-6), pp.239-256.

HJERTAGER, B. H., K. FUHRE and M. BJØRKHAUG. 1988b. Gas explosion experiments in 1:33 and 1:5 scale offshore separator and compressor modules using stoichiometric homogeneous fuel/air clouds. *Journal of Loss Prevention in the Process Industries,* **1**(4), pp.197-205.

HSE. 1974. *Flixborough (Nypro UK) Explosion 1st June 1974*. [Accessed 14 May 2013]. Available from: http://www.hse.gov.uk/comah/sragtech/caseflixboroug74.htm.

IBRAHIM, S. S. and A. R. MASRI. 2001. The effects of obstructions on overpressure resulting from premixed flame deflagration. *Journal of Loss Prevention in the Process Industries,* **14**(3), pp.213-221.

JOHNSON, D. M., P. SUTTON and M. J. WICKENS. 1991. Scaled experiments to study vapour cloud explosions. *Institution of Chemical Engineers,* **69 Part B**, pp.76-84.

KARLIN, V., G. MAKHVILADZE, J. ROBERTS and V. I. MELIKHOV. 2000. Effect of Lewis number on flame front fragmentation in narrow closed channels. *Combustion and Flame,* **120**(1–2), pp.173-187.

KARLOVITZ, B. 1954. Selected Combustion Problems p.248. London: Butterworths.

KIDO, H., M. NAKAHARA, K. NAKASHIMA and J. HASHIMOTO. 2002. Influence of local flame displacement velocity on turbulent burning velocity. *Proceedings of the Combustion Institute,* **29**(2), pp.1855-1861.

KIRKBY, W. A. and R. V. WHEELER. 1931. Explosions in closed cylinders. Part V. The effect of restrictions. *Journal of the Chemical Society (Resumed),* **Part V**, pp.2303-2306.

KNUDSEN, V. 2006. *Hydrogen gas explosions in pipelines - modeling and experimental investigations*. PhD thesis, Norwegian University of Science and Technology.

KOBAYASHI, H., T. NAKASHIMA, T. TAMURA, K. MARUTA and T. NIIOKA. 1997. Turbulence measurements and observations of turbulent premixed flames at elevated pressures up to 3.0 MPa. *Combustion and Flame,* **108**(1–2), pp.104-117.

KUMAR, R. K., W. A. DEWIT and D. R. GREIG. 1989. Vented Explosion of Hydrogen-Air Mixtures in a Large Volume. *Combustion science and technology,* **66**(4-6), pp.251-266.

KUZNETSOV, M., V. ALEKSEEV, Y. YANKIN and S. DOROFEEV. 2002a. Slow and fast deflagrations in Hydrocarbon-air mixtures. *Combustion science and technology,* **174**(5-6), pp.157-172.

KUZNETSOV, M., G. CICCARELLI, S. DOROFEEV, V. ALEKSEEV, Y. YANKIN and T. H. KIM. 2002b. DDT in methane-air mixtures. *Shock Waves,* **12**(3), pp.215-220.

LEA, C. J. and H. S. LEDIN. 2002. *A Review of the State-of-the-Art in Gas Explosion Modelling*. Buxton: Health and Safety Laboratory.

LEE, J. H. S., R. KNYSTAUTAS and A. FREIMAN. 1984. High speed turbulent deflagrations and transition to detonation in H_2O- air mixtures. *Combustion and Flame,* **56**(2), pp.227-239.

LEE, J. H. S. and I. O. MOEN. 1980. The mechans of transition from deflagration to detonation in vapor cloud explosions. *Progress in Energy and Combustion Science,* **6**(4), pp.359-389.

LINDSTEDT, R. P. and H. J. MICHELS. 1989. Deflagration to detonation transitions and strong deflagrations in alkane and alkene air mixtures. *Combustion and Flame,* **76**(2), pp.169-181.

LOWESMITH, B. J., G. HANKINSON and D. M. JOHNSON. 2011. Vapour cloud explosions in a long congested region involving methane/hydrogen mixtures. *Process Safety and Environmental Protection,* **89**(4), pp.234-247.

MACKAY, D. J., S. B. MURRAY, I. O. MOEN and P. A. THIBAULT. 1989. Flame-jet ignition of large fuel-air clouds. *Symposium (International) on Combustion,* **22**(1), pp.1339-1353.

MAKHVILADZE, G. M. and S. E. YAKUSH. 2002. Large-scale unconfined fires and explosions. *Proceedings of the Combustion Institute,* **29**(1), pp.195-210.

MERCX, W. P. M. 1992. Large-scale experimental investigation into vapour cloud explosions: comparison with the small-scale Discoe trials. *Institution of Chemical Engineers,* **70 Part B**, pp.197-204.

MIDDHA, P., D. ENGEL and O. R. HANSEN. 2011. Can the addition of hydrogen to natural gas reduce the explosion risk? *International Journal of Hydrogen Energy,* **36**(3), pp.2628-2636.

MIDDHA, P. and O. R. HANSEN. 2008. Predicting deflagration to detonation transition in hydrogen explosions. *Process Safety Progress,* **27**(3), pp.192-204.

MOEN, I. O., D. BJERKETVEDT, T. ENGEBRETSEN, A. JENSSEN, B. H. HJERTAGER and J. R. BAKKE. 1989. Transition to detonation in a flame jet. *Combustion and Flame,* **75**(3–4), pp.297-308.

MOEN, I. O., M. DONATO, R. KNYSTAUTAS and J. H. LEE. 1980. Flame acceleration due to turbulence produced by obstacles. *Combustion and Flame,* **39**(1), pp.21-32.

MOEN, I. O., J. H. S. LEE, B. H. HJERTAGER, K. FUHRE and R. K. ECKHOFF. 1982. Pressure development due to turbulent flame propagation in large-scale methane□air explosions. *Combustion and Flame,* **47**(0), pp.31-52.

MOEN, I. O., A. SULMISTRAS, B. H. HJERTAGER and J. R. BAKKE. 1988. Turbulent flame propagation and transition to detonation in large fuel-air clouds. *Symposium (International) on Combustion,* **21**(1), pp.1617-1627.

MOL'KOV, V. V., V. V. AGAFONOV and S. V. ALEKSANDROV. 1997. Deflagration in a vented vessel with internal obstacles. *Combustion, Explosion and Shock Waves,* **33**(4), pp.418-424.

MUPPALA, S. P. R., M. NAKAHARA, N. K. ALURI, H. KIDO, J. X. WEN and M. V. PAPALEXANDRIS. 2009. Experimental and analytical investigation of the turbulent burning velocity of two-component fuel mixtures of hydrogen, methane and propane. *International Journal of Hydrogen Energy,* **34**(22), pp.9258-9265.

NEWTON, L. 2008. *The Buncefield Incident 11 December 2005: The final report of the Major Incident Investigation Board*. [Accessed 23 July 2013]. Available from: http://www.buncefieldinvestigation.gov.uk/reports/volume1.pdf.

NICHOLS, R. H. 2012. *Turbulence Models and Their Application to Complex Flows* [online]. [Accessed 19 Sept.]. Available from: http://people.nas.nasa.gov/~pulliam/Turbulence/Turbulence_Guide_v4.01.pdf.

NING, J., C. WANG and J. LU. 2005. Influence of obstacles on flame propagation of multi-combustion mixture gas. *Modern Physics Letters B,* **19**(28 and 29), p1687−1690.

NOLAN, D. P. ed. 2011. *Characteristics of Hydrocarbon Releases, Fires, and Explosions. Handbook of Fire and Explosion Protection Engineering Principles (Second Edition).* Oxford: William Andrew Publishing.

OBARA, T., S. YAJIMA, T. YOSHIHASHI and S. OHYAGI. 1996. A high-speed photographic study of the transition from deflagration to detonation wave. *Shock Waves,* **6**(4), pp.205-210.

PANG, L., Q. ZHANG, T. WANG, D. C. LIN and L. CHENG. 2012. Influence of laneway support spacing on methane/air explosion shock wave. *Safety Science,* **50**(1), pp.83-89.

PARK, D. J., A. R. GREEN, Y. S. LEE and Y.-C. CHEN. 2007. Experimental studies on interactions between a freely propagating flame and single obstacles in a rectangular confinement. *Combustion and Flame,* **150**(1–2), pp.27-39.

PEDERSEN, H. H., G. TOMLIN, P. MIDDHA, H. N. PHYLAKTOU and G. E. ANDREWS. 2013. Modelling large-scale vented gas explosions in a twin-compartment enclosure. *Journal of Loss Prevention in the Process Industries,* **http://dx.doi.org/10.1016/j.jlp.2013.08.001**(0).

PERALDI, O., R. KNYSTAUTAS and J. H. LEE. 1988. Criteria for transition to detonation in tubes. *Symposium (International) on Combustion,* **21**(1), pp.1629-1637.

PETERS, N. 1988. Laminar flamelet concepts in turbulent combustion. *Symposium (International) on Combustion,* **21**(1), pp.1231-1250.

PETERS, N. 1999. The turbulent burning velocity for large-scale and small-scale turbulence. *Journal of Fluid Mechanics,* **384**, pp.107-132.

PHYLAKTOU, H. and G. E. ANDREWS. 1991. The acceleration of flame propagation in a tube by an obstacle. *Combustion and Flame,* **85**(3–4), pp.363-379.

PHYLAKTOU, H. and G. E. ANDREWS. 1995. Application of turbulent combustion models to explosion scaling *Process Safety and Environmental Protection,* **73**(1), pp.3-10.

PHYLAKTOU, H. N. 1993. *Gas explosions in long closed vessels with obstacles : a turbulent combustion study applicable to industrial explosions*. PhD thesis, University of Leeds.

PHYLAKTOU, H. N. and G. E. ANDREWS. 1994. Prediction of the maximum turbulence intensities generated by grid-plate obstacles in explosion-induced flows. *Symposium (International) on Combustion,* **25**(1), pp.103-110.

PHYLAKTOU, H.N., Y. LIU and G.E. ANDREWS. 1994. *IChemE Symp*. **134,** pp. 269-284.

PHYLAKTOU, H.N., G.E. ANDREWS and J. LEDGER. 1998. *IChemE Symp*. **144**, pp. 279-292.

POROWSKI, R. and A. TEODORCZYK. 2013. Experimental study on DDT for hydrogen–methane–air mixtures in tube with obstacles. *Journal of Loss Prevention in the Process Industries,* **26**(2), pp.374-379.

PUTTOCK, J. 1999. Improvements in Guidelines for Prediction of Vapour - cloud Explosions. *In: Intl. Conf. and Workshop on Modeling the Consequences of Accidental Releases of Mazardous Materials, San Francisco*. American Institute of Chemical Engineers.

RAZUS, D., D. OANCEA, V. BRINZEA, M. MITU and C. MOVILEANU. 2010. Experimental and computed burning velocities of propane–air mixtures. *Energy Conversion and Management,* **51**(12), pp.2979-2984.

ROBINSON, G. F. and A. A. KOVITZ. 1975. *AAIA J.,* **13**.

ROBINSON, H. and R. V. WHEELER. 1933. Explosions of methane and air: propagation through a restricted tube. *Journal of the Chemical Society (Resumed)*, pp.758-760.

RUDY, W., R. POROWSKI and A. TEODORCZYK. 2011. Propagation of hydrogen-air detonation in tube with obstacles. *Journal of Power Technologies,* **91**(3), pp.122-129.

SAKTHITHARAN, V. 1995. *Time-Resolved Measurements of Flame Propagation over Baffle-type Obstacles*. PhD thesis, University of London.

SHCHELKIN, K. I. 1940. *J. Exper. Theoret. Phys.*, **10**, p823.

SHY, S. S., W. J. LIN and K. Z. PENG. 2000. High-intensity turbulent premixed combustion: General correlations of turbulent burning velocities in a new cruciform burner. *Proceedings of the Combustion Institute,* **28**(1), pp.561-568.

SIDHU, J. 2010. Sunrise blast caused by illegal 'tank-to-tank transfer. *The Star Newspaper:* *http://www.thestar.com/news/gta/2010/08/03/sunrise_blast_caused_by_illegal_tanktotank_transfer_report_says.html*.

SIEWERT, P. 2006. *Flame front characteristics of turbulent lean premixed methane /air flame at high-pressure*. PhD thesis, Swiss Federal Institute of Technology Zurich.

STARKE, R. and P. ROTH. 1989. An experimental investigation of flame behavior during explosions in cylindrical enclosures with obstacles. *Combustion and Flame,* **75**(2), pp.111-121.

SWITHENBANK, J. ed. 1974. *Combustion Technology-Some Modern Developments.* New York: Academic Press.

TAN-ATICHAT, J., H. M. NAGIB and R. I. LOEHRKE. 1982. Interaction of free-stream turbulence with screens and grids: a balance between turbulence scales. *Journal of Fluid Mechanics,* **114**, pp.501-528.

TAYLOR, A. M. K. P. and J. H. WHITELAW. 1984. Velocity characteristics in the turbulent near wakes of confined axisymmetric bluff bodies. *Journal of Fluid Mechanics,* **139**, pp.391-416.

TAYLOR, G. I. 1946. The Air Wave Surrounding an Expanding Sphere. *Proceedings of the Royal Society of London. Series A, Mathematical and Physical Sciences,* **186**(1006), pp.273-292.

TAYLOR, P. H. and W. J. S. HIRST. 1989. The scaling of vapour cloud explosions: A fractal model for size and fuel type. *In: Twenty Second International*

Symposium on Combustion (Poster Presentation), Seattle, USA. Combustion Institute.

TEODORCZYK, A., P. DROBNIAK and A. DABKOWSKI. 2009. Fast turbulent deflagration and DDT of hydrogen–air mixtures in small obstructed channel. *International Journal of Hydrogen Energy,* **34**(14), pp.5887-5893.

TEODORCZYK, A., J. H. S. LEE and R. KNYSTAUTAS. 1989. Propagation mechanism of quasi-detonations. *Symposium (International) on Combustion,* **22**(1), pp.1723-1731.

TONY, F. 2011. The fire and explosion at Indian Oil Corporation, Jaipur, a summary of events and outcomes. *Loss Prevention Bulletin,* (222), p9.

TSENG, L. K., M. A. ISMAIL and G. M. FAETH. 1993. Laminar burning velocities and Markstein numbers of hydrocarbonair flames. *Combustion and Flame,* **95**(4), pp.410-426.

TURNS, S. R. ed. 1996. *Introduction to Combustion: Concepts and Applications.* New York: McGraw-Hill.

VAN WINGERDEN, C. J. M., J. G. VISSER and H. J. PASMAN. 1991. Combustion in obstructed diverging and non-diverging flow fields. *In: Combustion and Reaction Kinetics, 22nd International Annual Conference of ICT, July 1991, Karlsruhe*.

VAN WINGERDEN, K., G. H. PEDERSON and B. A. WILKINS. 1994. Turbulent flame propagation in gas mixtures. *Hazards XII European Advances in Process Safety,* pp.249-261.

VERSTEEG, H. K. and W. MALALASEKERA. eds. 2007. *An Introduction to Computational Fluid Dynamics the Finite Volume Method.* Second ed. Essex: Pearson Education Limited.

VEYNANTE, D. and L. VERVISCH. 2002. Turbulent combustion modeling. *Progress in Energy and Combustion Science,* **28**(3), pp.193-266.

VOLLMER, K. G., F. ETTNER and T. SATTELMAYER. 2011. Deflagration-to-detonation transition in hydrogen-air mixtures with concentration gradients. *In: 23rd International Colloquium on Dynamics of Explosions and Reactive Systems (ICDERS),* 24-29 July, Irvine.

WANG, W. and B. ROGG. 1993. Premixed Ethylene/Air and Ethane/Air Flames: Reduced Mechanisms Based on Inner Iteration. *In:* N. PETERS and B.

ROGG, eds. *Reduced Kinetic Mechanisms for Applications in Combustion Systems.* Springer Berlin Heidelberg, pp.76-101.

WARD SMITH, A. J. ed. 1971. *Pressure Losses in Ducted Flows.* London: Butterworths.

WARD SMITH, A. J. ed. 1980. *Internal fluid flow.* Oxford, UK: Clarendon press.

WILLIAMS, F. E. ed. 1985. *Combustion theory.* Addison-Wesley.

XINHUA. 2010. Lax safety standards caused Nanjing factory blast: http://www.chinadaily.com.cn/china/2010-08/01/content_11077794.htm. *China Daily*.

YANG, S. I. and S. S. SHY. 2002. Global quenching of premixed CH4/air flames: Effects of turbulent straining, equivalence ratio, and radiative heat loss. *Proceedings of the Combustion Institute,* **29**(2), pp.1841-1847.

YIBIN, D., X. FUQUAN, X. XIAOYAN, C. XIN and D. HONGBIN. 2011. Investigation of solid structure obstacles influence on flame propagation in semi-open tube. *Procedia Engineering,* **26**(0), pp.538-544.

YU, L. X., W. C. SUN and C. K. WU. 2002. Flame acceleration and overpressure development in a semiopen tube with repeated obstacles. *Proceedings of the Combustion Institute,* **29**(1), pp.321-327.

ZHOU, D. W. and S.-J. LEE. 2004. Heat transfer enhancement of impinging jets using mesh screens. *International Journal of Heat and Mass Transfer,* **47**(10–11), pp.2097-2108.

ZHOU, Y.-H., M.-S. BI and F. QI. 2012. Experimental research into effects of obstacle on methane–coal dust hybrid explosion. *Journal of Loss Prevention in the Process Industries,* **25**(1), pp.127-130.

ZIMONT, V., W. POLIFKE, M. BETTELINI and W. WEISENSTEIN. 1998. An Efficient Computational Model for Premixed Turbulent Combustion at High Reynolds Numbers Based on a Turbulent Flame Speed Closure. *Journal of Engineering for Gas Turbines and Power,* **120**(3), pp.526-532.

List of Abbreviations

Abbreviations/symbols are described in more detail as they are presented in the text. The following list is not comprehensive.

A_{vc} area of the vena contracta

A_1 area of the obstacle opening

A_2 area of the pipe

b obstacle scale

BR obstacle blockage ratio

β flame factor

C_c coefficient of contraction

C_d discharge coefficient

C_T turbulent generation constant

D internal tube diameter

d diameter of the obstacle opening

d_{jet} jet diameter

δ_ℓ flame thickness

E expansion ratio

ε turbulent dissipation

K turbulent kinetic energy

Ka Karlovitz number

L length of the tube

Le Lewis number

ℓ integral length scale

M Mach number

Ma Markstein number

max.	maximum
$\dot{m}$	mass flow rate
n	eddies wavelength
η	Kolmogorov length scale
P	overpressure
p	porosity ratio
P_T	total pressure loss
ΔP_d	pressure differential
ρ	fluid density
Re	Reynolds number
R_ℓ	turbulent Reynolds number based on integral length scale
R_η	turbulent Reynolds number based on Komogorov length scale
R_λ	turbulent Reynolds number based on Taylor length scale
S_f	flame speed
S_g	induced gas velocity
S_L	laminar burning velocity
S_T	turbulent burning velocity
S_u	burning velocity
T	time scale for integral length scale
T_b	burnt gas temperature
T_u	unburnt gas temperature
t	thickness of an obstacle
t/d	aspect ratio
τ	time scale for Kolmogorov length scale
τ_c	chemical lifetime
τ_ℓ	turbulent lifetime
U	mean flow velocity

u'	r.m.s velocity
u'/U	intensity of turbulence
u(t)	turbulent velocity as a function of time
u'(t)	velocity fluctuation as a function of time
υ	kinematic viscosity
x	distance downstream of an obstacle
x_{ig}	distance from ignition
x_s	obstacle separation distance
$(x/b)_{max}$	dimensionless distance to maximum intensity of turbulence
γ	specific heat constant
ϕ	equivalence ratio